AD-A085 312 CORNELL UNIV ITHACA NY LAB OF PLASMA STUDIES F/6 20/7
COLLECTIVE ION ACCELERATION.(U)
1980 J A NATION F44620-75-C-0054
UNCLASSIFIED AFOSR-TR-80-0440 NL

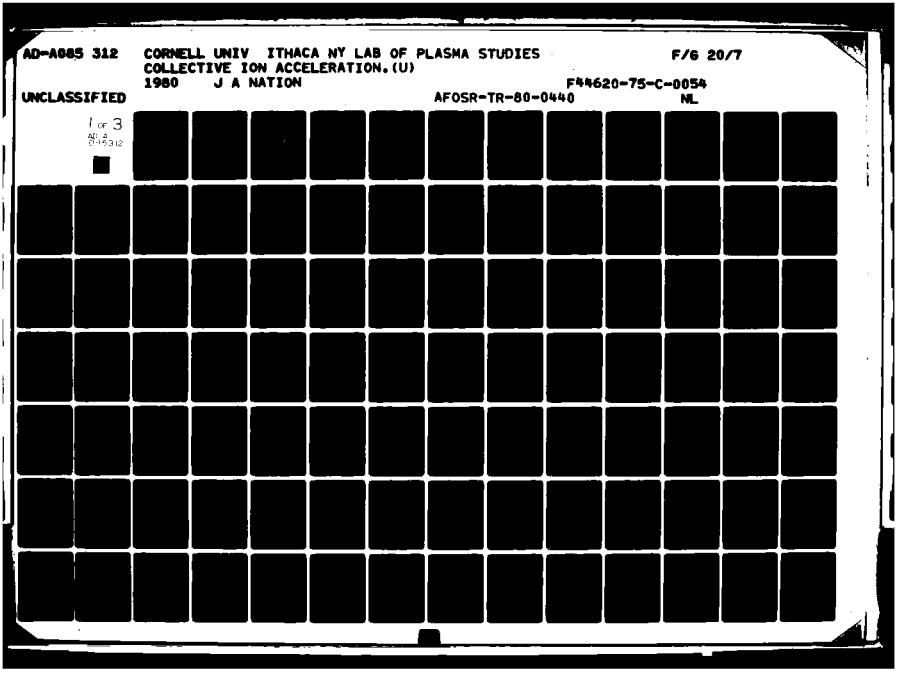

AFOSR-TR- 80-0440

Collective Ion Acceleration

(13)

Final Scientific Report to

AIR FORCE OFFICE OF SCIENTIFIC RESEARCH

LEVEL II

Research Contract Number F44620-75-C-0054

Period Covered: 15 January 1975 - 14 January 1980

Principal Investigator: John A. Nation
Laboratory of Plasma Studies
School of Electrical Engineering
Cornell University
Ithaca, New York 14853

UNCLASSIFIED

SECURITY CLASSIFICATION OF THIS PAGE (When Data Entered)

REPORT DOCUMENTATION PAGE	READ INSTRUCTIONS BEFORE COMPLETING FORM
1. REPORT NUMBER: AFOSR TR-80-0440	2. GOVT ACCESSION NO.: AD-A085312
3. RECIPIENT'S CATALOG NUMBER	
4. TITLE (and Subtitle): COLLECTIVE ION ACCELERATION .	5. TYPE OF REPORT & PERIOD COVERED: Final rept. 15 Jan 75 — 14 Jan 80
6. PERFORMING ORG. REPORT NUMBER	
7. AUTHOR(s): John A. Nation	8. CONTRACT OR GRANT NUMBER(s): F44620-75-C-0054
9. PERFORMING ORGANIZATION NAME AND ADDRESS: School of Electrical Engineering, Cornell University, Ithaca, NY 14853	10. PROGRAM ELEMENT, PROJECT, TASK AREA & WORK UNIT NUMBERS: 2301 A7 61102F
11. CONTROLLING OFFICE NAME AND ADDRESS: AFOSR/NP, Bolling AFB, Bldg.410, Wash DC 20332	12. REPORT DATE: 1980
	13. NUMBER OF PAGES: 191
14. MONITORING AGENCY NAME & ADDRESS (if different from Controlling Office)	15. SECURITY CLASS. (of this report): unclassified
	15a. DECLASSIFICATION/DOWNGRADING SCHEDULE

16. DISTRIBUTION STATEMENT (of this Report)

Approved for public release;
distribution unlimited.

17. DISTRIBUTION STATEMENT (of the abstract entered in Block 20, if different from Report)

18. SUPPLEMENTARY NOTES

19. KEY WORDS (Continue on reverse side if necessary and identify by block number)

403 200

20. ABSTRACT (Continue on reverse side if necessary and identify by block number)

Work was conducted on the excitation of slow cyclotron and slow space charge waves in a plasma beam. Observations were made when a planar electron beam was propagated through a strip line. The beam was guided by a homogeneous magnetic field and the excitation achieved with a zero frequency pump wave. Both the space charge and cyclotron waves were excited in the 20-30 GHz interaction and the cyclotron wave in the 70 GHz range. For the first time, independent measurements were made of the effects on growth rate of the homogeneous guide field and the rippled field. Experiments were conducted on the proof-of-

DD FORM 1 JAN 73 1473 EDITION OF 1 NOV 65 IS OBSOLETE

UNCLASSIFIED

principle for a space charge wave accelerator. A large amplitude space charge wave was grown on an electron beam. Phase velocities of 0.25 c, and accelerating fields of 60kV/cm were obtained.

Introduction

The research supported under Contract Number F44620-75-C-0054 has addressed two distinct topics, namely, high power microwave generation and collective ion acceleration. A more recent effort has been initiated to investigate proton acceleration in Induction Linacs. The original contract supported the study of microwave generation using slow wave structures and study of a free electron laser configuration. About halfway through the contract, this program was converted to a study of the collective acceleration of ions in high current relativistic electron beams. This is still the main area on which the continuation grant is centered although some work has been initiated on an Induction Linac for protons. Each of these topics will be reviewed in this report, although the bulk of the technical data will be presented as reprints or preprints of published work. These are appended to this report.

Laboratory Equipment

During the course of this program the laboratory facilities have been continually upgraded. We now operate two reliable Blumlein pulsed power sources from a single Marx generator. The former supplies are both 7 Ω lines, however, one feeds a diode through a step up transformer and, hence, has an output impedance of about 18 Ω. Both lines are equipped with prepulse switches which result in very low diode voltages during the charging phase. These lines and the Marx generator have been operated for over 10,000 shots.

Diagnostic techniques and equipment have also been developed during the contract duration. The facilities available also include a transient digitizer and microprocessor system (purchased with an NSF special equipment grant). This system greatly enhances our diagnostic capabilities extending our operation to high (~1 GHz) frequency response at high sensitivities and further providing a modest on line computing capability. Built-in waveform processing techniques include integration, differentiation, and fast Fourier transforms. Specific processing techniques for other signals have been developed as required. These include proton spectroscopy using activation of foils, proton spectroscopy using neutron time-of-flight, and a variety of other techniques largely centered on phase velocity measurement methods.

The laboratory is adequately equipped for low energy nuclear measurements, fast beam measurements, and microwave measurements from D.C. to 3 GHz and 8 GHz to 40 GHz. Some additional equipment is available outside this range.

Microwave Measurements

The work carried out during the initial phase of this program is described in some detail in the Appendix, Articles 1, 2, and 3. Of these, the most significant are the results reported on the excitation of slow cyclotron and slow space charge waves in a planar beam. The operation reported is in the coherent stimulated scattering regime, of interest in Free Electron Laser work.

The observations were made when a planar electron beam was propagated through a strip line. The beam was guided by a homogeneous magnetic field and the excitation achieved with a zero frequency pump wave. Both the space charge and cyclotron waves were excited in the 20-30 GHz interaction and the cyclotron wave in the 70 GHz range. This experiment provided for an active excitation of the rippled B field and gave, for the first time, independent measurements of the effects of the homogeneous guide field and the rippled field on the growth rate.

Collective Acceleration

Results from our Collective Accelerator Program are attached as articles 4 to 13 in the Appendix.

The investigation has two distinct features: i) a study of the so-called "Luce" diode as a collective accelerator; and ii) a study of slow space charge waves.

The overall program has, as its objective, a proof-of-principle experiment for a space charge wave accelerator. In this experiment, a large amplitude space charge wave is grown on an electron beam and

ions trapped in the wave troughs. An increase in the wave phase velocity then results in an ion acceleration.

For this purpose, we have investigated slow space charge wave propagation on electron beams to determine both the phase velocities and electric fields achievable. We have readily obtained accelerating fields of about 60 kV/cm at wave phase velocities of about 0.25 c. There does not appear to be an obstacle to prevent the achieving of larger fields. The minimum wave phase velocity obtained is high and we have devoted considerable time and effort to reducing the velocity to a lower value. We have met with some measure of success, albeit on a single shot basis and with poor repeatability. To achieve low phase velocities requires operation at beam currents close to the vacuum limit. Operation in this range gives rise to rapid changes in velocity with small changes in beam current, necessitating single shot measurement techniques. The acquisition of a transient digitizer provides us with the needed tool to make the single shot measurement. We are currently working to confirm these preliminary results ($\beta \sim 0.1$ c). In addition, we are using dielectric media surrounding the beam to produce a low phase velocity at moderate beam currents. This effect is due to the difference between the dielectric constant of the material at the beam 'frequency' and at the wave frequency. These results should also be available during the summer of 1980.

In summary, we now have evidence of adequate accelerating fields at useful phase velocities to carry out the proof-of-principle

experiment. The low phase velocity measurements do, however, require confirmation on a single shot basis.

An encouraging feature of this aspect of the program is the result reported in article 7. The achievable phase velocity at a given beam to limiting current is amplitude dependent. There is now solid theoretical basis for expecting sufficiently low phase velocities for practical use. Further theoretical work on stabilization of beam instabilities at high currents has also been carried out (article 8). Some of the wave results are described in detail in papers 4 through 8. Additional information also appears in papers 11 and 12, which like 6 also report work on the proton acceleration in Luce diodes.

Collective Acceleration in Vacuum

This aspect of our program has two objectives: i) a study of the "Luce" diode per se; and ii) an optimization of the proton yield from the diode.

The latter objective is to meet the requirement of a suitable source for the injector and the former to study the acceleration process so that one might hope to improve the accelerator performance over its present level.

Proton acceleration has been consistently obtained with ion energy spectra extending up to 22 times the electron beam energy. This repeatable performance is, to the best of our knowledge, unique among these devices.

A detailed study of the acceleration length, beam parameters during acceleration, ion losses, and electron beam losses has been carried out and a paper describing these in detail is now in preparation. A letter summarizing the mechanisms and most important features is included as a preprint (number 10 in the appendix). Based on this work we now believe that we have a fairly good understanding of the acceleration mechanisms and ion loss rates. We are now trying to enhance the acceleration, based on our observations. Articles 9 and 10 review the observations and 6 and 11 provide additional data together with information on the wave aspects of the program.

Wave Growth in the Presence of Ions

Papers 11 and 12 summarize the results of an initial study of proton injection into the wave growth and propagation section. These results, which are very encouraging, show that it is possible to propagate a substantial number of ions through the wave section without serious degradation of the wave. The injection method described will be essentially that which we shall use in the proof-of-principle experiment.

Acceleration of Heavy Ions

Article 13 presents, in letter form, the results of an investigation of heavy ion acceleration. The technique employed uses a reflexing electron beam to generate a plasma in the foil material of the E-beam diode. Ions from this plasma are collectively accelerated

by the electron beam. The preliminary results reported show that this technique may be used to generate and accelerate "heavy" ion beams. The beam ion species, yield, and acceleration can undoubtedly be optimized further. We do not intend to pursue this area any further.

Induction Linac

An Induction Linac module has been designed and partially fabricated. The system, which consists of an electrostatic proton beam generator and an inductive accelerator section, has been designed to give a 1.0 MeV proton beam of about 1 kA for 50 nsecs. The purpose of this system, which may be extended, is to study Induction Linac design and beam transport for moderate ion (~1 kA) currents. The central problem in this device is beam transport between successive accelerating modules. The problem is most severe at low energy where the ion velocity is low.

We anticipate operation of the module in the spring of 1980. Such a device, apart from interest in the device in its own right, could serve as an injector into a collective accelerator. Positive ion induction linacs have not been previously fabricated.

Pulse Power Technology

A review paper, number 14 in the appendix, has been prepared and was recently published in Particle Accelerators. This paper is the first comprehensive summary of contemporary pulse power technology to appear in the open literature.

Conference Presentations Arising from this Contract

"Microwave Generation Experiments Using Rippled Magnetic Field Configurations", Bull Am. Phys. Soc. 20, 10, 1289 (1976).

"Collective Ion Acceleration in Relativistic Electron Beams", IEEE International Conference on Plasma Science - Conference Record (1976), p. 177.

Production of Microwaves with an Intense Relativistic Sheet Beam, 2nd Int. Conf. Summer School on Submillimeter Waves and Their Applications - San Juan, December 1976. Conference Digest p. 142.

Microwave Generation Processes in Rotating Relativistic Electron Beams, Bull. Am. Phys. Soc. 21, 9, 1059 (1976).

Measurements of Ion Acceleration in Relativistic Electron Beams, Bull. Am. Phys. Soc. 21, 9, 1059 (1976).

Space Charge Waves Generated on a Relativistic Electron Beam for Use in the Collective Accelerations of Ions, CA, 1976, Bull. Am. Phys. Soc. 21, 9, 1184 (1976).

"Collective Ion Acceleration in High Current Electron Beams", APS Annual Meeting - Chicago, February 1977.

High Power Millimeter Wave Generation from Planes and Annular Relativistic Electron Beams, IEEE meeting on Plasma Science, May 1977. Conference Record, P. 34.

Collective Ion Acceleration in Intense Relativistic Electron Beams, IEEE Meeting on Plasma Science, May 1977. (Conference Record P. 172.)

Generation of an Intense Slow Space Charge Wave on a Relativistic Electron Beam and its Application to Collective Ion Acceleration, IEEE Meeting on Plasma Science, May 1977. Conference Record P. 173.

"Magnetic Shear Stabilization of the Diocotron Instability on a Relativistic Electron Beam", Bull. Am. Phys. Soc. 23(7), 853 (1978).

"Wave Accelerators for Collective Ion Acceleration", Bull Am. Phys. Soc. 23(7), 907 (1978).

"Collective Ion Acceleration in Ion Source Diodes", Bull. Am. Phys. Soc. 23(7), 9074 (1978).

"An Experimental Study of Luce Diode Phenomena", IEEE Meeting on Plasma Sci., May 1978, Conf. Record p. 232.

"Microwave Generation Due to Electron Beam Interactions in a Rippled Magnetic Field", IEEE Meeting on Plasma Sci., May 1978, Conf. Record p. 285.

"Collective Acceleration of Heavy Ions from Metal Foils". Bull. Am. Phys. Soc. 24 (8), 1013, 1979.

"Investigation and Control of Collective Ion Acceleration in Vacuum". Bull. Am. Phys. Soc. 24 (8), 1013, 1979.

"Phase Velocity Measurements of a Space Charge Wave on a Relativistic Electron Beam". Bull. Am. Phys. Soc. 24 (8), 1013, 1979.

Published Papers Arising from this Contract

1. "Excitation of the Slow Cyclotron and Space-Charge Waves in a Relativistic Electron Beam", G. Providakes and J. A. Nation, J. Appl. Phys. 50, 3026 (1979).

2. "Microwave Generation Using Sheet Relativistic Electron Beams", G. Providakes, J. A. Nation, and M. E. Read, IEEE Trans. Microwave Theory and Techniques MTT-25, 563 (1977).

3. "Observations on Microwave Radiation Generation in the Fundamental Circular Waveguide Mode by a Relativistic Electron Beam", A. J. Dudas, J. A. Nation, and M. E. Read, Laboratory of Plasma Studies Report No. 215 (Jan. 1977).

4. "A Wave Accelerator for Collective Ion Acceleration", R. Adler, G. Gammel, J. A. Nation, M. E. Read, and R. Williams, P. Sprangle, A. Drobot, Proceedings of the 2nd Int. Top. Conf. on High Power Electron and Ion Beam Research and Technology, J. A. Nation and R. N. Sudan, Eds. (Cornell University, 1977) Vol. II, p. 509.

5. "Slow Space-Charge Wave Propagation on a Relativistic Electron Beam", G. Gammel, J. A. Nation, and M. E. Read, J. Appl. Phys. 50, 5603 (1979).

6. "Space Charge Waves and Collective Ion Acceleration", R. Adler, G. Gammel, J. A. Nation, G. Providakes, and R. Williams, Proceedings Third International Conference on Collective Methods of Acceleration (Laguna Beach, 1978), p. 249.

7. "Nonlinear Space Charge Waves on Cylindrical Electron Beams and Plasmas", T. P. Hughes and E. Ott, Plasma Preprint PL #80-031 (submitted for publication).

8. "Magnetic Shear Stabilization of the Diocotron Modes of a Relativistic Electron Beam", E. Ott and J.-M. Wersinger, Phys. Fluids 23, 324 (1980).

9. "Ion-Acceleration Mechanisms in Vacuum Diodes", R. J. Adler and J. A. Nation, J. Appl. Phys. 50, 5025 (1979).

10. "Mechanisms for Collective Ion Acceleration in Vacuum", R. J. Adler, J. A. Nation, and V. Serlin, (submitted for publication).

11. "Proton Injection Into a Large Amplitude Space Charge Wave", R. J. Adler, G. Gammel, J. A. Nation, J. D. Ivers, G. Providakes, and V. Serlin, IEEE Trans. on Nucl. Sci. NS-26, 4223 (1979).

12. "Studies of a Slow Space Charge Wave Collective Ion Accelerator", R. J. Adler, G. Gammel, T. Hughes, J. Ivers, J. A. Nation, and E. Ott, G. Providakes, and V. Serlin, Proceedings 3rd Int. Top. Conf. on High Power Electron and Ion Beam Research and Technology, (Novosibirsk, 1979).

13. "Collective Acceleration of Metallic Ions", R. J. Adler and J. A. Nation, (accepted for publication in Appl. Phys. Lett.).

14. "High-Power Electron and Ion Beam Generation", J. A. Nation, Particle Accelerators 10, 1 (1979).

Appendix

Excitation of the slow cyclotron and space-charge waves in a relativistic electron beam

G. Providakes and J. A. Nation

Laboratory of Plasma Studies and School of Electrical Engineering, Cornell University, Ithaca, New York 14853

(Received 11 September 1978; accepted for publication 10 November 1978)

Experiments are reported in which a relativistic electron beam, having an energy of 650 keV and carrying a beam current of about 0.8 kA, was used to excite slow (negative energy) space-charge and cyclotron waves. The waves, which yielded megawatt powers in the *Ka* and *V* bands, were generated as a result of the unstable interaction between a beam wave, a static rippled magnetic field, and a waveguide mode. The instability growth was observed to increase with both increasing guide and ripple magetic field strengths, and saturated when the ripple field was about 10% of the guide field. The observations are mainly consistent with theoretical predictions, although selection rules for excited modes violate predictions.

PACS numbers: 41.80.Dd, 41.70. + t, 84.40.Ts

I. INTRODUCTION

An electron beam propagating within a waveguide with a guiding magnetic field and a small periodic ripple magnetic field has been shown to generate coherent high-power microwave radiation.[1-3] For a short-wavelength ripple the source of this radiation is the interaction between the negative-energy cyclotron and space-charge waves on the electron beam with waveguide modes.[4-6] In this paper we describe the results of experiments investigating this interaction.

The original theoretical basis for the interaction was provided by Manheimer and Ott[7] who analyzed the case of a weak thin cold-sheet electron beam propagating in a parallel-plate waveguide. They showed that the slow cyclotron and space-charge waves can interact with the waveguide modes in the presence of a sufficiently short-wavelength ripple in the magnetic field, and that the instability growth rate was of the order 10^8–10^{10} sec^{-1} for ripple amplitudes of about 5% of the guide-field strength. Since the Manheimer and Ott analysis, a number of other theoretical studies of the interaction have been developed.[8-10] These theories are based on the equivalent view in which the instability is treated as a three-wave interaction with the rippled field acting as a zero-frequency pump wave which scatters from fluctuations on the beam. These analyses consider the problem of Raman scattering from a warm beam and find nonlinear limits on the interaction efficiency. They do not, however, include magnetic field effects or waveguide-boundary processes. In these experiments the waveguide effects are important and to a large extent control the frequency of the radiation generated in the interaction. We compare our observations with the predictions of Manheimer and Ott whose analysis closely approximates the experimental conditions used.

Earlier experimental attempts to excite the negative-energy cyclotron wave have met with limited success due to the difficulty of obtaining a sufficiently large ripple field at the beam location. The experiments reported in this paper were carried out utilizing a current-driven ripple field which could be varied independently of the guiding magnetic field. The experiments show growth rates substantially larger than predicted by the Manheimer and Ott theory and demonstrate that significant interactions occur with relatively weak ($\sim 1\%$ ripple) fields. The qualitative features of the scaling of power with the ripple-and guide-field strengths agree with the theory. The observed frequency of the radiation was consistent with the generation of negative-energy space change and cyclotron waves.

II. REVIEW OF THEORETICAL ANALYSIS

The microwave oscillation resulting when a beam propagates along a rippled magnetic field can be modeled as a three-wave interaction between a zero-frequency pump wave, a beam wave, and a scattered wave. The interaction must satisfy both the frequency and wave-number conditions imposed by the dispersion relations of the waveguide radiation, and the modified beam mode.

Space charge:

$$\omega^2 = \omega_{co}{}^2 + k^2c^2; \quad \omega = (k + \kappa)v - \omega_p/\gamma^{3/2}. \tag{1}$$

Cyclotron:

$$\omega^2 = \omega_{co}^2 + k^2c^2; \quad \omega = (k + \kappa)v - \Omega/\gamma. \tag{2}$$

Figure 1 gives a typical dispersion diagram illustrating the interaction regime. The slow space-charge wave dispersion relation is displaced from its usual position by an amount κv, where v is the beam velocity, κ is the wave number of the zero frequency pump, k is the radiation wave number, ω_{co} is the mode cutoff frequency, c is the velocity of light, and ω_p is the plasma frequency. The interaction of the modified space-charge wave dispersion relation with the TM or TE waveguide modes of a plane-parallel wall waveguide yields the frequency of the microwave radiation. The interaction strength is dependent on the parameters of the experiment; however, the interaction frequency where the space-charge instability occurs is independent of the ripple- and guide field strengths.

 0021-8979/79/053026-05$01.10

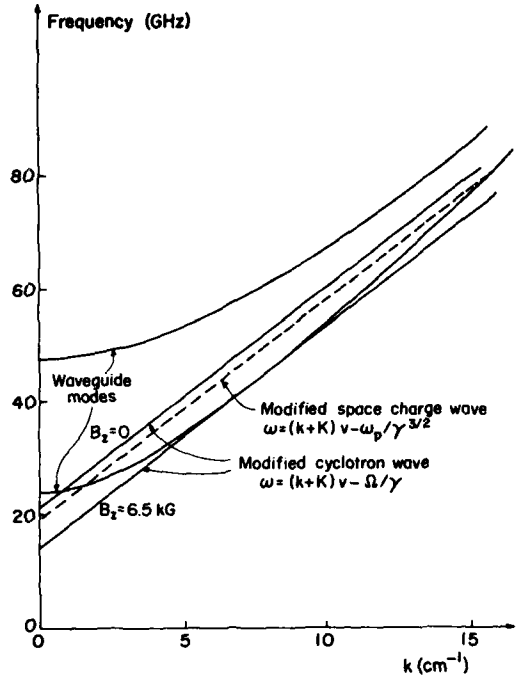

FIG. 1. Dispersion curves for the waveguide, cyclotron, and space-charge waves. The beam modes are modified due to the effects of the periodic rippled magnetic field.

The dispersion relation used to calculate the interaction frequency for the cyclotron-wave interaction is also shown in Fig. 1. In this case the slow cyclotron wave on the beam has its dispersion relation modified by the zero-frequency pump (ripple field) wave. The cyclotron-wave interaction will occur at the frequency which satisfies the matching conditions of Eq.(2). This frequency is the intercept of the displaced cyclotron slow-beam wave and the waveguide mode. The cyclotron-wave dispersion relation has a cyclotron frequency term in it which is magnetic field dependent. This permits tuning of the interaction by changing the guide magnetic field. It is possible to choose a magnetic field such that there is no intersection of the cyclotron-wave dispersion relation with the waveguide modes and, therefore, no interaction.

As mentioned in Sec. I, the Manheimer and Ott theory predicts the frequency of the interaction and the gain expected in the small-signal limit. The linear theory predicts that the interaction of the space charge and cyclotron waves with TM and TE modes are limited by the boundary conditions on the sheet electron beam. Listed in Table I is a compilation of the possible permitted interactions. Permitted interactions are designated by an X, and the O denotes a nonallowed interaction. The relations derived for the instability growth rates are complicated and the results obtained depend fairly critically on the parameters assumed. Numerical evaluation of the cyclotron-instability growth rate in the *Ka* band indicates a growth rate of about 10^8 sec^{-1} for a ripple amplitude of 5% of the guide field. The calculations indicate that there is a shallow resonance in the growth rate at a field

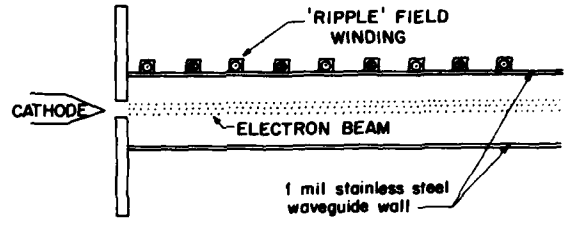

FIG. 2. Cross-sectional view of the experimental interaction region.

of about 7.5 kG. This peaking which is also apparent in the experimental observations, is consistent with the resonance condition found empirically by Schlesinger and Efthimion, namely,

$$\kappa v - \Omega/\gamma = \omega_{co}. \tag{3}$$

In contrast with the cyclotron modes, the space-charge wave instability growth rate scales with the two-thirds power of the ripple-field strength and linearly with the guide magnetic field. These results follow from numerical evaluation of the dispersion relation and adequately describe the variations found over a fairly wide set of assumed values of the experimental parameters. As stated above, interactions are expected with the odd symmetry modes of the waveguide.

III. APPARATUS

Figure 2 shows schematically the experimental apparatus. The electron beam was generated from a pulse line feeding a carbon cathode with an emitting surface 50 mm × 2 mm. The beam was injected through a slot 60 mm × 4 mm in the anode into a stripline waveguide. The waveguide consisted of two parallel plates of stainless steel (0.001 in.) mounted on Lucite backplates. The stainless steel acted as the waveguide boundary and path for the beam return current. Within the Lucite and adjacent to the stainless steel was a wire folded in a long tight "S" through which was passed a current which generated the ripple magnetic field. The waveguide was immersed in a vacuum and a guiding magnetic field. The strength of the ripple and guide magnetic fields were independent of each other and were the basic parameters varied during the experiment. Previous experiments using iron to perturb the guide magnetic field have been unable to vary the ripple field independently of the guide-field amplitude.

The beam diagnostics used included diode current and voltage monitors, a Rogowski beam curent monitor, a resistive shunt monitor to measure the driving current for the

TABLE I. Selection rules for wave excitation.

	Space charge	Cyclotron
TE odd	X	O
TE even	O	O
TM odd	X	O
TM even	O	X

TABLE II Experimental parameters.

Diode voltage	650 kV
Beam current	800 A
Electron-beam duration	90 nsec
Plasma frequency	2.27 GHz
Guide cutoff	23.5 GHz
Period ripple	1.27cm

ripple field, and magnetic pickup loops to measure the guiding magnetic field. The microwave diagnostics consisted of high-pass waveguides with octave band detectors for the frequency bands *X*, *Ku*, *K*, *Ka* and *V*. The *X* and the *Ka* band had 300′ and 100′ dispersive lines, respectively, for the frequency measurements. The frequencies distinguishable on these lines were 8–12 GHz and 23–30 GHz. The detectors were approximately 3 m from the output of the waveguide. The total emitted power was determined from a spatial intensity profile on a shot-to-shot basis. An additional array of high-pass filters was built at 5-GHz intervals from 30–60 GHz to measure the power in these bands.

IV. EXPERIMENT

Experiments were done using a variety of waveguide cutoff frequencies, ripple periods, and interaction lengths. The experiment which will receive the primary attention in this section was performed under the conditions listed in Table II. The beam was generated using a Blumlein; oscilloscope records show that both the diode voltage and beam current were constant in time through the 90-nsec plus to within $\pm$ 10%.

The expected interactions of a beam in a waveguide with a primary cutoff frequency of 23.5 GHz can be seen in Fig. 1. The only modes that are intercepted by the space-charge wave and the cyclotron wave are the TM_{10} and the TE_{10}. These waves will only interact when the ripple field is present to couple the waveguide and beam waves. Only the cyclotron-wave interaction would be expected from the selection rules due to symmetry arguments. The cyclotron-interaction radiation should occur approximately at 24 and 80 GHz for a very weak guiding magnetic field. As the guiding magnetic field increased, the frequency of the interaction should increase from the lower intercept point at 24 GHz to 35 GHz, and the 80-GHz intercept should drop to 35 GHz. The magnetic field should be approximately 6.5 kG when the lower intercept and the higher intercept meet at 35 GHz. Any further increase in the field would drive the modified cyclotron dispersion relation off the waveguide mode and therefore turn off the instability.

From the arguments presented earlier, no interaction is expected with the space-charge waves since the lowest mode leading to an unstable interaction should be either the TE_{20} or TM_{20} waveguide modes. The cutoff frequencies for these modes, in the parallel-plate geometry, occur at about 47 GHz. As shown in Fig. 1, no interaction is expected since the beam modes are well away from the waveguide mode. As will be seen later in the experimental results, an interaction was observed with the lowest waveguide modes. This result is contrary to predictions of the theory. Due to the wide separation of the guide modes, the interaction is unambiguous.

Figure 3 shows the radiation detected by the *Ka*-band antenna. The guide field was fixed and a series of increasing ripple-field strengths applied. The guide-field strength was then increased and the experiment repeated. The behavior of the radiation was the same in the *V* band (Fig.4). A striking feature was the low-percentage ripple required to excite the instability; less than 1%. The radiation was strongly affected by the guide-field strength. An increase in the guide-field

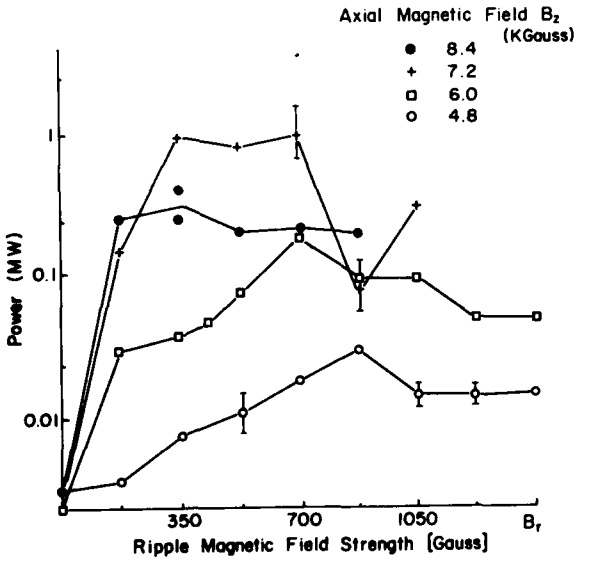

FIG. 3. Experimentally measured radiated *Ka*-band power as a function of the rippled magnetic field strength. The several curves are appropriate to different values of the magnetic field guide.

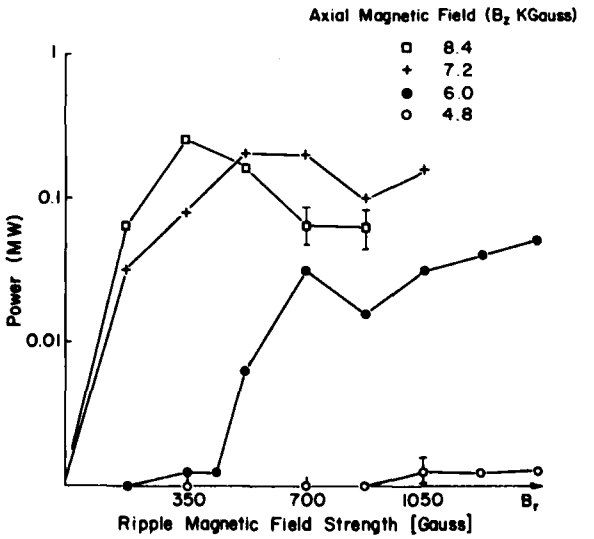

FIG. 4. Radiated power in *V* band as a function of the rippled-field strength.

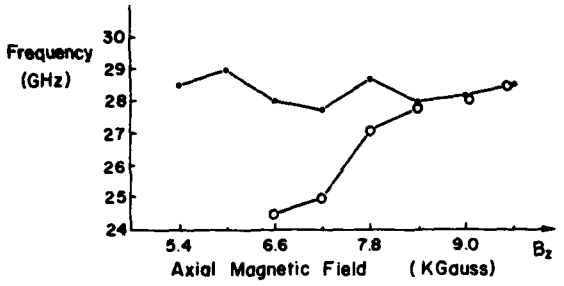

FIG. 5. Dispersive line measurements giving the frequency spectrum in the *Ka*-band.

strength resulted in a lower-percentage ripple necessary to achieve the same radiated power.

Experiments performed by other groups using a passive system to create a rippled magnetic field were constrained to use an approximately fixed-percentage ripple. These experiments reported a 2-kG resonance in the *Ka* band attributed to the cyclotron interaction and a linear growth in the *V*-band power radiated with an increasing magnetic field. The *V*-band radiation was attributed to a space-charge wave interaction. A comparison of the experiment done here with the above-mentioned experiments shows qualitatively similar features. It is apparent that the *V*-band radiation intensity increases linearly with increasing guide magnetic field if a fixed-percentage ripple is used. However, Figs. 3 and 4 show that for a sufficiently strong ripple magnetic field ($6 < B_r/B_z < 12\%$) the radiation drops in intensity and appears to saturate. The *Ka*-band radiation shows a resonance with the axial guide field at fixed ripple-field strength. This phenomena, which is also seen in Fig. 6, occurs at a magnetic field satisfying Eq. (3) and is consistent with the observations of Schlesinger and Efthimion.

The total power observed in the experiments are similar. Based on an intensity profile, we estimate 1 MW peak power and the Columbia group reported 5 MW of peak power, albeit using a more powerful beam.

Figure 5 shows the calculated frequencies of the radiation determined from the transit time of the microwaves through the *Ka*-band dispersive line. The dispersive line could distinguish frequencies between 23 and 30 GHz.. The dispersive lines showed a two-peak radiation output consistent with a fixed frequency of approximately 28.5 GHz for a guide-field variation from 5.4 to 9.6 kG. This peak is consistent with a space-charge interaction. The frequency is 20% higher than predicted by simple-dispersion-relation phase-matching conditions, but well within the tolerances of possible values of plasma frequency and beam energy. An additional important observation was that the second pulse tuned with magnetic field. The second pulse had a frequency of 24.5 GHz at 6 kG rising to 28 GHz at 8.4 kG at which point the two pulses were no longer resolvable. The ripple field used was chosen to give maximum total radiation. The radiated frequency for magnetic fields above 8.4 kG showed only a single-frequency-radiation pulse at 28 GHz.

The two signals had approximately the same power but different frequencies. One of these remained fixed in frequency and could be identified with the space-charge interaction, while the second rose in frequency and is probably the cyclotron-wave interaction. The shift in frequency with magnetic field is not unambiguous since the dispersion of the line is not much greater than the pulse duration.

The *V*-band radiation exhibited power curves similar to those found for the *Ka* band; and since no shift in frequency of the radiation was observed using the array of high-pass filters, the radiation was identified as arising from a space-charge wave interaction. The *V*-band radiation retained a strong signal even with a strong magnetic field, confirming the space-charge interaction. Again, as with the *Ka*-band radiation, the power increased with the guide magnetic field until it saturated. The percentage ripple required to reach saturation or a turn on of the radiation dropped with increasing magnetic guide field.

An examination of the dependence of the signal level on the rippled-field strength indicates that the *V*-band power output is consistent with a growth rate scaling with the rippled-field strength to the two-thirds power. At higher signal levels there is some evidence of scaling with the square root of the ripple-field strength. The *Ka*-band power output is, at weak magnetic fields, consistent with a linear dependence of the growth rate on the rippled-field strength. At higher fields the growth rate scales more slowly with B_r. Both of these results are reasonable and consistent with theoretical predictions.

An alternative possible explanation of the radiation at the lower frequencies was the cyclotron-maser[11-13] interaction, where the velocity anistropy/inversion created by the ripple magnetic field can drive an instability in an a homo-

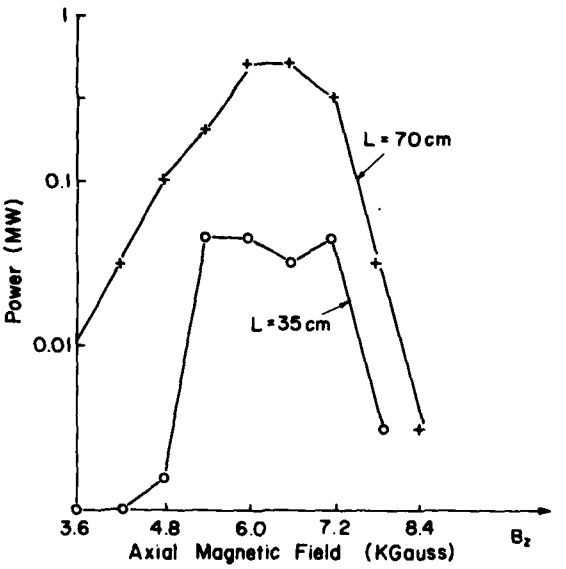

FIG. 6. *Ka*-band radiated power measurements as a function of the length of the rippled-field structure. These measurements used a 1-kG ripple field with a period of 1.9 cm. The guide cutoff frequency was about 10 GHz.

geneous section following the rippled field. In order to create the velocity anistropy/inversion, a short length of rippled magnetic field (10–20 cm) is required. Instability growth occurs in the remaining length of homogeneous magnetic field where the electron distribution relaxes to its equlibrium state. The intensity of the radiation from the cyclotron maser is proportional to the length of the homogeneous section. In the present experiment, the homogeneous section is 10 cm long and the ripple section 65 cm long. If the homogeneous section were enlarged at the expense of the rippled section, the cyclotron-maser interaction should yield the same or greater radiated power. The negative-energy-wave interaction[3] has the gain proportional to the rippled magnetic field length. A reduction in the ripple-field length should, therefore, reduce the power proportionately. An experiment was performed with a long period structure, 1.9 cm, in which the ripple field was kept constant and the guide field was swept from 3.6 to 8 kG. The ripple-field strength was 1000 G. Figure 6 shows the power versus guide magnetic field. The ripple interaction length was 65 cm for curve A of Fig. 6. When the interaction length was cut down to 30 cm, but the total waveguide length remained the same, the power dropped approximately 13 dB. This experiment provides a strong argument for the three-wave interaction.

V. CONCLUSIONS

Experiments have been carried out to observe the excitation of the negative-energy space-charge and cyclotron waves in a rippled magnetic field. These interactions have been observed and their growth monitored as a function of the experimental conditions. The wave growth was observed with ripple fields as weak as 1% of the guide field and saturation found at about the 1-MW power level with ripple amplitudes of less than 12% of the guide field. The observation of the frequency variation of the radiation with the applied magnetic field showed that both the negative-energy space charge and cyclotron waves were excited at comparable power levels. The experimentally observed decrease in power radiated with a decrease in the length of the rippled-field section indicated that the cyclotron-maser interaction was not the dominant source of the observed radiation. Finally, we note that the space-charge wave interaction was present in both the *Ka* and *V* bands with the interaction occuring coupling to the 10 modes of the guide. This interaction mode is inconsistent with the predictions of theoretical analysis.

ACKNOWLEDGMENT

Work supported by the U.S. Air Force Office of Scientific Research under Contract No.F44620-75-C-0054.

[1]M. Friedman and M. Herndon, Phys. Fluids **16**, 1982 (1973).
[2]Y. Carmel and J.A. Nation, J. Appl. Phys. **44**, 5268 (1973).
[3]V. Granatstein, M. Herndon, P. Sprangle, Y. Carmel, and J.A. Nation, Plasma Phys. **17**, 23 (1975).
[4]V.L. Granatstein, R.K. Parker, J.A. Pasour, P. Sprangle, and A.T. Drobot, *Proceedings 2nd International Tropical Conference on High Power Electron and Ion Beam Research and Technology* (Cornell University, Ithica 1977), p 675.
[5]S.P. Schlesinger and P.C. Efthimion, in Ref. 4, p 691.
[6]T.C. Marshall, F.L. Sandel, and R.M. Gilgenbach, in Ref. 4, p 697.
[7]W.M. Manheimer and E. Ott, Phys. Fluids **17**, 463 (1974).
[8]P. Sprangle, V.L. Granatstein, and L. Baker, Phys. Rev. A **12**, 1697 (1975).
[9]P. Sprangle and A.T. Drobot, NRL Memorandum Report 3587, (1978) unpublished.
[10]T. Kwan, J.M. Dawson, and A.T. Lin, Phys. Fluids **20**, 581 (1977).
[11]E. Ott and W.M. Manheimer, IEEE Trans. Plasma Sci. **PS-3**, 1 (1975).
[12]P. Sprangle and A.T. Drobot, IEEE Trans. Microwave Theory Tech. **MTT-25**, 528 (1977).
[13]P. Sprangle, V.L. Granatstein, and A.T. Drobot, J. Phys. C6-135 (1977).

Microwave Generation Using Sheet Relativistic Electron Beams

G. PROVIDAKES, J. A. NATION, AND M. E. READ

Abstract—**Potential advantages in the use of a sheet electron beam for generation of high-power microwave signals are discussed and preliminary experiments to establish their applicability are reported. An examination indicates that sheet beams probably have greatest utility in the frequency, range 10–100 GHz.**

THE use of intense relativistic electron beams for the generation of high-power microwave signals has resulted in the development of gigawatt sources at frequencies of less than 10 GHz and megawatt sources at about 100 GHz [1]–[7]. These sources enhance by better than two orders of magnitude [8] the powers available from single source systems. Techniques for the generation of these high-power sources fall into two broad categories; axial bunching devices [1]–[3] such as slow wave systems, and transverse bunching systems such as the cyclotron [4]–[7] maser. The available power from these systems scales approximately as $1/f^{5/2}$ with the wave frequency [8]. At this meeting power levels [9] of about 1 MW at a wavelength of 0.5 mm have been reported and the generation mechanism identified as Raman scattering [10] from fluctuations in the electron beam. Since this generation technique depends on the scattering of a pump wave from an electron beam, the guide dimensions are determined by the beam pump requirements.

Manuscript received January 20, 1977. This work was supported by the Air Force Office of Scientific Research, United States Air Force, under Contract F44620-75-C-0054. The United States Government is authorized to reproduce and distribute reprints for governmental purposes notwithstanding any copyright notation heron.

The authors are with the Laboratory of Plasma Studies, School of Electrical Engineering, Cornell University, Ithaca, NY 14853.

We therefore do not expect that the scattered wave will be subject to the same scaling limitations as indicated above for the various bunching devices. In this instance the interaction efficiency depends on the "quiver" velocity of the electrons in the pump wave fields. To obtain coherent scattering requires threshold pump levels [11] of the order of 50 MW/1 cm^2. The frequency of the scattered wave is related to the pump wave frequency f_p by the relation $f_{sc} \approx 4\gamma^2 f_p$. With an electron beam capability of up to a few megavolts, we require pump waves in the range of tens of gigahertz to generate submillimeter waves.

The generation of millimeter or submillimeter waves therefore requires either the direct generation of the wave or the availability of very powerful sources of radiation in the tens of gigahertz range. We discuss in this article some of the limitations on power production and indicate the possible advantages inherent in the use of striplines for increasing power availability at intermediate frequencies. Initial results of microwave generation experiments using a slow wave system excited by a strip electron beam are also reported.

The scaling of microwave power inversely with the square (or with losses $1/f^{2.5}$) of the frequency arises in conventional tubes from limits set on the electron beam. The E-beam power is, for a thermionic cathode, limited by the current density and hence scales as the area of the guide. This limitation becomes relaxed in the cold cathode devices used for intense E-beam generation. The beam current is determined by the beam-waveguide geometry in the interaction region. For an infinitely thin annular beam of radius a in a drift tube of radius b we find that the space charge limited current is [12], [13]

$$I_{sc} = \frac{8500(\gamma_{inj}^{2/3} - 1)^{3/2}}{\ln (b/a)}.$$

A finite thickness annular beam carries a somewhat smaller current than that given above. Such a beam is also subject to shear and can be liable to diocotron instability. Diocotron instability [14] can be minimized by using a sufficiently strong magnetic field to guide the electron beam. This may result in the limitation of modes which can be excited. Specifically, the negative energy cyclotron wave excitation, in configurations such as the ubitron, would be impossible with magnetic fields large enough to control the diocotron instability in high shear beams. The effects of reducing the beam current below the space charge limit have been analyzed [13] and show that relatively small reductions in the beam current can lead to substantial reductions in the beam shear. Ideally, the beam current does not depend on the size of the drift tube but only on the ratio of the beam-to-waveguide radius. In practice, some limitations arise, principally due to the finite thickness of the beam, which is difficult to reduce below 1–2 mm. Limiting currents of about one-third of the value given above are common in small tubes, whereas one can approach the full limiting current in larger tubes where the beamwidth is small compared to its radius. The beam current can be made large if a thin beam is generated close to the waveguide wall, and for a fixed thickness beam scales linearly with the tube radius. Unfortunately, the beam location is frequently fixed at a given fraction of the tube radius in order that efficient coupling to the wave can occur. For example, in the coupling to a TE_{01} mode it is desirable to have the beam located at about half the tube radius.

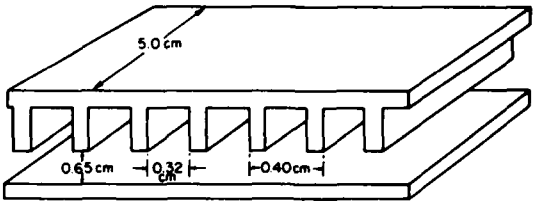

Fig. 1. Schematic of ridged waveguide structure.

It is clear that current density limitations are not the cause of the rapid decrease of RF power with increasing frequency. In addition, the intermediate frequency signals have been mainly generated using the interaction of an harmonic of the cyclotron wave with a higher order TE_{0n} waveguide mode or by the interaction of a "rigid rotor" beam rotating synchronously (or at a rate shifted by the relativistic cyclotron frequency) with the wave fields. The interactions in both cases are rich in harmonic content. Finally, it should be pointed out that the limitations are probably not arising from nonlinear effects except perhaps for the lower voltage (submegavolt) or low frequency (< 10 GHz) regimes. Assuming propagation in the TE_{01} mode at a frequency of about $1.6f_{c0}$, we find the electric field of the wave is about $3(P)^{1/2}/a$ where P is the wave power and a the tube radius. For a significant nonlinear effect one might expect $\frac{1}{2}E\lambda \simeq (\gamma_d - 1)mc^2/e$ where γ_d is the drift energy of the electrons which is related at the space charge limit to the injection energy by $\gamma_d = \gamma_{inj}^{1/3}$. This only appears likely at powers in excess of 1 GW which have been observed for wave frequencies of less than about 10 GHz, or for submegavolt beams. From a phenomenological point of view, the wave power availability does exhibit a $1/f^{5/2}$ scaling and power is limited below desired levels in both the millimeter and submillimeter regimes.

We now address the issue of using sheet beams for microwave generation and point out some of the differences between the sheet configuration and an annular beam in a waveguide. For a thin beam of width W located between two symmetrically placed conducting boundaries separated by a distance S, the limiting current is

$$I_{sc} = \frac{8500(\gamma^{2/3} - 1)^{3/2} W}{2\pi S}.$$

For a length of beam about one-half of the circumference of the annular beam, one may achieve comparable impedance operation. The factor of 2 ($b - a \simeq s$) arises from the fact that the beam fields extend equally to either waveguide plate. This factor of 2 in the current density may be of significance when bunching is important. More immediately significant, however, is the point that high beam currents

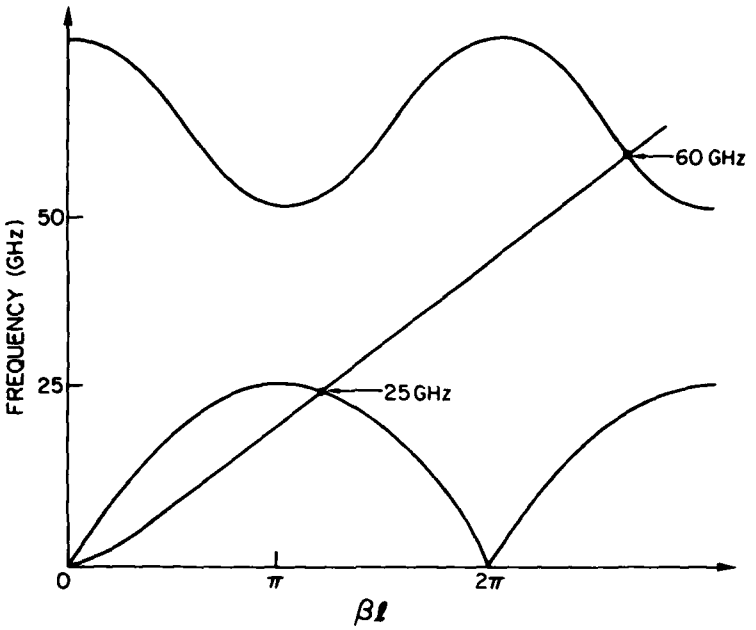

Fig. 2. Brillouin diagram for ridged waveguide structure.

are achieved with the beam located on the axis of symmetry of the system, that is, at the peak axial field location for a TM_{10} mode and the peak transverse field for a TE_{10} mode. It seems possible to produce sheet beams with thicknesses of 1–2 mm and widths of up to 50 cm provided that instabilities can be controlled. The diocotron instability is still expected to be present in this configuration but should be stabilized by a sufficiently intense magnetic field. At comparable beam current densities and with equal microwave power densities, a sheet beam should be capable of enhancing RF power capabilities by one to two orders of magnitude over cylindrical beams, with the greatest effects at the higher frequencies.

Some initial experiments have been carried out to assess the utility of sheet beams for high-power generation. The configuration is shown in Fig. 1 where we illustrate a backward wave oscillator (BWO) designed to operate at about 25 GHz. The BWO configuration was chosen solely for ease of construction and comparison with theory. Other devices such as the cyclotron maser and the ubitron may have better field geometries and permit higher power level operation. The beam was 5 cm wide and had a thickness of about 2 mm. The slow wave structure was formed by a ridge-loaded parallel plate waveguide and had a length of 40 cm. The beam entrance to the structure was tapered to ensure reflection of the backward wave for coupling out of the system. The Brillouin diagram [15] for the structure and a slow space charge wave is shown in Fig. 2. The period and transverse dimensions were chosen for BWO operation. Two systems were used: one with a tooth depth of 2.8 mm and the second with a tooth depth of 1.9 mm. Operation of these two systems should be at frequencies of about 20 and 26 GHz, respectively. The parallel plate structure was mounted in a cylindrical waveguide of 7.5-cm diameter. The tube also provided a return path for the beam current. A gradual taper was used to match the planar guide to the oversize cylindrical system which in turn fed a 10° half-angle cylindrical antenna to couple to free space. The beam was fed from a Marx–Blumlein system at 300–500 keV at a beam current in the range 500–2000 A. This current range was somewhat below the limiting current. The beam was confined and guided by an axial magnetic field of 10 kG. Damage patterns of the beam taken downstream of the structure showed no gross breakup or filamentation at these fields.

The microwave emission was monitored in the *X*, *Ku*, *K*, *Ka*, and *V* bands. With both structures, significant radiation was only monitored in the *K*, *Ka*, and *V* bands. Based on the detector characteristics, we conclude that the deeper tooth structure oscillated at a frequency very close to the cutoff of the *Ka*-band detector and the shallow tooth structure oscillated in the *Ka* band. These results are consistent with calculations of the dispersion relations for the system which predict oscillation at 20–22 GHz and 26–28 GHz, respectively. The *V*-band detector was uncalibrated but recorded RF emission in the 50–75-GHz range. No absolute signal level statements can be made, but the emission was at least 25 dB above the noise level. The *V*-band radiation could arise from an interaction with the second harmonic of the two structures. There was little variation of the output power with the beam voltage or current in the range of conditions used. Varying the length of the structure also enabled us to find the minimum structure length for oscillation. This was about 15 cm for the beam currents used and is in reasonable agreement [16] with calculations of the starting conditions. The excess structure length also enhances the probability of exceeding the switch on conditions for the higher frequency radiation. The complete removal of the structure, or the covering of the ridges with a thin alu-

minum foil, reduced the signal level by at least 40 dB. Finally, we note that there was no dependence of the radiation, other than that noted above, on the magnetic field strength. The power in both ridged guide structures was estimated to be about 2.5 MW.

The BWO was also operated directly from the Marx and ran at slightly reduced power levels. It was, however, subject to switching on and off during the $\frac{1}{2}$-μs pulse. It seems possible that this results from the poor field geometry, where substantial enhancements of the local electric field can occur close to the sharp corners of the ridges and may result in breakdown. Even allowing operation at only the current power densities, a scaling of the system to a 50-cm width should lead to radiation powers of about 25 MW. This radiation level is comparable to that achieved in the transverse bunching devices. Present experiments are aimed at running with wider beams and at improving the electric field geometry within the slow wave structure. The scaling to greater widths will be accomplished in a coaxial geometry where the inner and outer conductor radii are approximately equal. This has the advantage of removing possible fringing field instabilities and also permits any off-axis waves to grow before decoupling from the system.

We conclude that it seems possible to use striplines as a means of enhancing the total power capability in the intermediate frequency range (say 10–100 GHz). Assessments of overall efficiency and ultimate widths obtainable require additional work. Modest devices appear capable of producing at least comparable power to that achieved using harmonic interactions of the cyclotron maser.

References

[1] M. Friedman, "Emission of intense microwave radiation from an automodulated relativistic electron beam," *Appl. Phys. Lett.*, vol. 26, pp. 366–368, 1975.

[2] Y. Carmel, J. Ivers, R. Kribel, and J. A. Nation, "Intense coherent Cherenkov radiation due to the interaction of a relativistic electron beam with a slow wave structure," *Phys. Rev. Lett.*, vol. 33, pp. 1278–1282, 1974.

[3] N. Kovalev, M. I. Petelin, M. D. Raiser, A. V Smorgonskii, and L. E. Topp, "Generation of powerful electromagnetic radiation pulses by a beam of relativistic electrons," *Zh. Eksp. Teor. Fiz. Pis'ma Red.*, ol. 18, pp. 232–235, 1973.

[4] V. L. Granat tein, M. Herndon, P. Sprangle, Y. Carmel, and J. A. Nation, "Gigawatt microwave emission from an intense relativistic electron beam," *Plasma Phys.*, vol. 17, pp. 23 28, 1975.

[5] V. L. Granatstein, M. Herndon, R. K. Parker, and S. P. Schlesinger, "Strong submillimeter radiation from intense relativistic electron beams," *IEEE Trans. Microwave Theory Tech.*, vol. MTT-22, pp. 1000 1004, 1974.

[6] M. Friedman and M. Herndon, "Emission of coherent microwave radiation from a relativistic electron beam propagating in a spatially modulated field," *Phys. Fluids*, vol. 16, pp. 1982–1995, 1973.

[7] V. L. Granatstein, P. Sprangle, M. Herndon, and R. K. Parker, "An electron synchrotron maser based on an intense relativistic electron beam," *J. Appl. Phys.*, vol. 46, pp. 2021–2028, 1975.

[8] V. L. Granatstein, R. K. Parker, and P. Sprangle, "Cyclotron resonance phenomena in microwave and submillimeter radiation from an intense relativistic electron beam," *Proc. Int. Topical Conf. Electron Beam Research and Technology*, Albuquerque, NM, pp. 401–423, Nov. 1975.

[9] V. L. Granatstein, S. P. Schlesinger, M. Herndon, R. Parker, and J. Pasour, "Production of megawatt submillimeter pulses by simulated magneto-resonant Raman scattering," *Conf. Digest-Second Int. Conf. Winter School on Submillimeter Waves and Their Applications*, pp. 122–123, 1976.

[10] P. Sprangle and A. Drobot, "Stimulated collective scattering from a magnetized relativistic electron beam," *Proc. Second Int. Conf. Winter School on Submillimeter Waves and Their Applications*, pp. 124–125, 1976.

[11] M. R. Mross, T. C. Marshall, P. Epthimion, and S. P. Schlesinger, "Submillimeter wave generation through stimulated scattering with an intense relativistic electron beam and zero frequency pump," *Conf. Digest-Second Int. Conf. Winter School on Submillimeter Waves and Their Applications*, pp. 128–129, 1976.

[12] L. S. Bogdankevitch and A. A. Rukhadze, "Stability of relativistic electron beams in a plasma and the problem of critical currents," *Sov. Phys. Uspekhi*, vol. 14, pp. 163–179, 1971.

[13] M. E. Read and J. A. Nation, "Space charge limits in unneutralized relativistic electron beams," *J. Plasma Phys.*, vol. 13, pp. 127–137, 1975.

[14] Y. Carmel and J. A. Nation, "Instability of an unneutralized relativistic electron beam," *Phys. Rev. Lett.*, vol. 31, pp. 286 289, 1973.

[15] A. W. Lines, G. R. Nicoll, and A. M. Woodward, "Some properties of waveguides with periodic structure," *Proc. IEE*, vol. 97 III, pp. 263–276, 1950.

[16] H. Heffner, "Analysis of the backward-wave traveling-wave tube," *Proc. IRE*, vol. 42, pp. 930–937, 1954.

LABORATORY OF PLASMA STUDIES

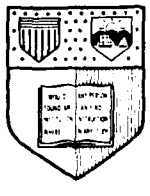

CORNELL UNIVERSITY

ITHACA, NEW YORK

Observations on Microwave Radiation Generation in the Fundamental Circular Waveguide Mode by a Relativistic Electron Beam

A. J. Dudas, J. A. Nation, and M. E. Read

Laboratory of Plasma Studies
School of Electrical Engineering
Cornell University
Ithaca, NY 14853

LPS 215 January 1977

Abstract

Observations of microwave radiation generated in the fundamental (TE_{11}) circular waveguide mode by an intense relativistic electron beam are reported . Radiation is in the X band at power levels to 10 MW. The radiation is generated in a smooth guide, and is attributed a fast cyclotron wave. Radiation at reduced power levels in the Ku, K, Ka, and V bands is also reported.

The production of microwaves using intense relativistic electron beams has been a topic of continuing research for some time. Of most interest has been the interaction of the fast cyclotron mode of an IREB with smooth circular waveguide modes. Very high powers in the cm and mm bands have been achieved with this interaction, the largest being 1.0 GW in the 3 cm band[1] and 3 GW in the 10 cm band.[2] The power from the 3 cm band experiment was attributed to an instability arising from a population inversion.[3] This type of device, generally termed a "cyclotron maser" has been successful in producing high power in the cm and mm bands and, with 25 - 100 KV electron energies, at high efficiency.[4] Thus it appears promising as a useful source for fusion research and high power communications.

We report here on work examining the production of microwave in the cm and mm bands where diode conditions have been used to impart perpendicular energy to the beam. Emphasis is placed on the radiation from the fundamental (TE_{11}) mode of a 2.8 cm diameter waveguide. Powers of up to 10 Mwatts were observed in this mode with lesser powers at frequencies up to 70 GHz. The radiation peaks at low magnetic fields where the perpendicular energy of the beam is expected to be greatest.

The experiment is shown in Figure 1. An IREB was produced by a cold cathode diode fed by a 7 Ω Marx-Blumlein pulse forming system. Diode voltages up to 600 kV with a pulse width of 90 ns were used. Beam currents were on the order of 1 KA. For most of the experiments the beam was annular with an outer diameter of 1 cm. The beam was propagated in vacuum in 2.8 to 7.5 cm diameter

smooth wall drift tubes. The 2.8 cm tube would propagate only the fundamental guide mode for frequencies under 10.1 GHz. The radiation was coupled out with a 10° half angle horn. Detection of the radiation was by broad band crystal detectors, coupled by standard gain microwave horns and guide. The frequency in the X band was determined by a dispersive guide. The frequencies of higher modes were estimated using Ku, K, Ka, and V band waveguides as high pass filters. The diode voltage and current, and beam current were measured conventionally.

Radiation was observed in the X, Ku, K, Ka and V bands, but extensive measurement was undertaken only in the X band. We discuss observations in the higher bands near the end of this note.

With the 2.8 cm diameter drift tube, the X band radiation appeared at two separate frequencies. The lower frequency (< 9 GHz) radiation peaked at approximately 4 kGauss, dropping rapidly as the magnetic field increased. See Figure 2. The frequency of the radiation increased monotonically with magnetic field, as shown in Figure 3. Higher frequency radiation was observed simultaneously, having a much slower fall-off with magnetic field and was similar to that reported by Friedman et al.[5]

The power of this radiation was strongly dependent upon the contour of the magnetic field, requiring a mirror at the diode to maximize the microwave emission. The optimum mirror ratio was 1.4/1.

The radiation produced below 10.1 GHz must be in the TE_{11} mode since all other modes are cut off. Since the radiation is

strongly magnetic field dependent and produced in a smooth waveguide, where the waveguide modes have phase velocities greater than the spped of light, we attribute it to the fast cyclotron mode of the beam. A comparison of the observed frequencies with those predicted by intersections of the fast cyclotron beam mode ($\omega = kv + \Omega_c/\gamma$) and the TE_{11} waveguide mode dispersion relations is shown in Figure 3. The disagreement of about 1 GHz may be due to space charge effects not included in the theoretical prediction. The higher frequency radiation may be due to the interaction of the TE_{21} waveguide mode and the first harmonic of the cyclotron mode.

Both the fast cyclotron and waveguide modes are positive energy waves, and therefore require a source of free energy in the form of a population version inversion or temperature annotropy for growth. In this experiment a population inversion is apparently provided in the diode by EXBdrifts producing large amounts of perpendicular energy on the beam for low magnetic fields. The mirror enhances this perpendicular energy and provides a large enough magnetic field to allow good beam propagation in the drift section. Analysis of the beam dynamics shows that it is not possible (although only marginally), with the magnetic fields utilized, for single electron orbits to encircle the axis. With the single electron orbits not encircling the axis the interaction cannot be attributed to the "rigid rotor" interaction described by Sprangle.[6] Rather, this interaction seems to be best described in the cyclotron maser mechanism discussed by Ott and Manheimer,[3] and, in the nonlinear regime, by Sprangle and Manheimer[7]. Growth lengths on the

order of 2-3 cm (e folding) are in agreement with those predicted and with other experiments where this mechanism was assumed.

Maximum powers observed were about 10 Mwatts, indicating a relatively low ($\sim$ 2%) efficiency. This is in line with experiments where a ripple in the magnetic field was employed to introduce beam perpendicular energy. It is, however, much less than the 30% that was reported for a similar experiment in the 10 cm band by Didenko et al.[2] Didenko found, however, that somewhat higher beam energies (900-1200 KeV) were necessary for efficient microwave production.

Power was also observed in Ku, K, Ka, and V bands. The dependence of the radiated power with the magnetic field strength is given in Figure 4 for the Ku, K, and Ka bands. No calibrations were available for the V band detector. The presence of substantial power at high frequencies is a characteristic of the harmonics with the fast cyclotron interaction, and has been observed elsewhere.[8]

In conclusion, it has been observed that it is possible to excite radiation in the TE_{11} mode with a fast cyclotron wave. Efficiencies achieved were similar to those seen with the TE_{01} mode. The interaction seems best attributed to a cyclotron maser mechanism, although the "rigid rotor" type mechanism cannot positively be ruled out. Experiments at higher electron energy may better define the interaction.

References

1. V. L. Granatstein, M. Herndon, P. Sprangle, Y. Carmel, and J. A. Nation, Plasma Physics 17, 23 (1975).
2. A. N. Didenko, A. G. Zherlitsyn, V. I. Zelentsov, A. S. Sulakshin, G. P. Fomenko, Yu. G. Shtein, and Yu. G. Yushkov, Fiz. Plasmy 2, 514 (1976).
3. E. Ott and W. M. Manheimer, IEEE Trans. on Plasma Science PS-3, 1 (1975).
4. N. I. Zaytsev, T. B. Pankratova, M. I. Petelin, and V. A. Flyagin, Radio Engineering and Electronic Phys. 19, 103 (1974).
5. M. Friedman, D. A. Hammer, W. M. Manheimer, and P. Sprangle, Phys. Rev. Letters 31, 752 (1973).
6. P. Sprangle, J. of Appl. Phys. 47, 2935 (1976).
7. P. Sprangle and W. M. Manheimer, Phys. Fluids 18, 224 (1975).
8. M. Friedman and M. Herndon, Phys. Fluids 16, 1982 (1973).

Work supported by AFOSR contract # F44620-75-C-0054.

Figure Captions

Figure 1: Diagram of the experiment.

Figure 2: Power received in the X-band as a function of magnetic field strength. Circles and squares represent radiation of frequency less than and greater than 9 GHz, respectively.

Figure 3: Observed and calculated frequencies of radiation in the TE_{11} mode as a function of magnetic field strength.

Figure 4: Power of radiation in the Ku, K, and Ka bands as a function of magnetic field strength. The ordinate scale is approximately equal to that of Figure 1.

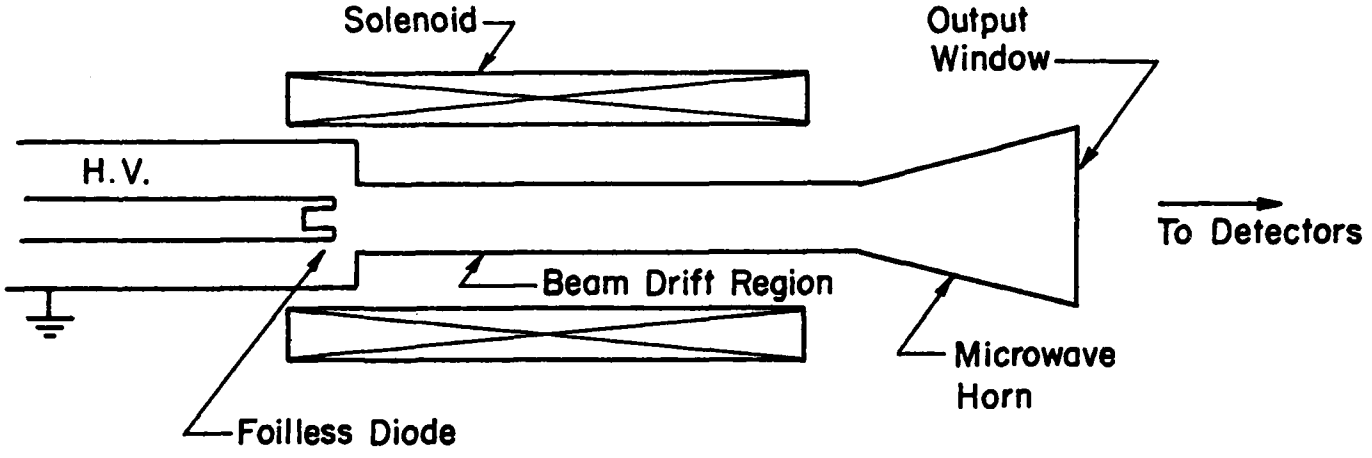
Solenoid
Output
Window
H.V.
To Detectors
Beam Drift Region
Microwave
Horn
Foilless Diode

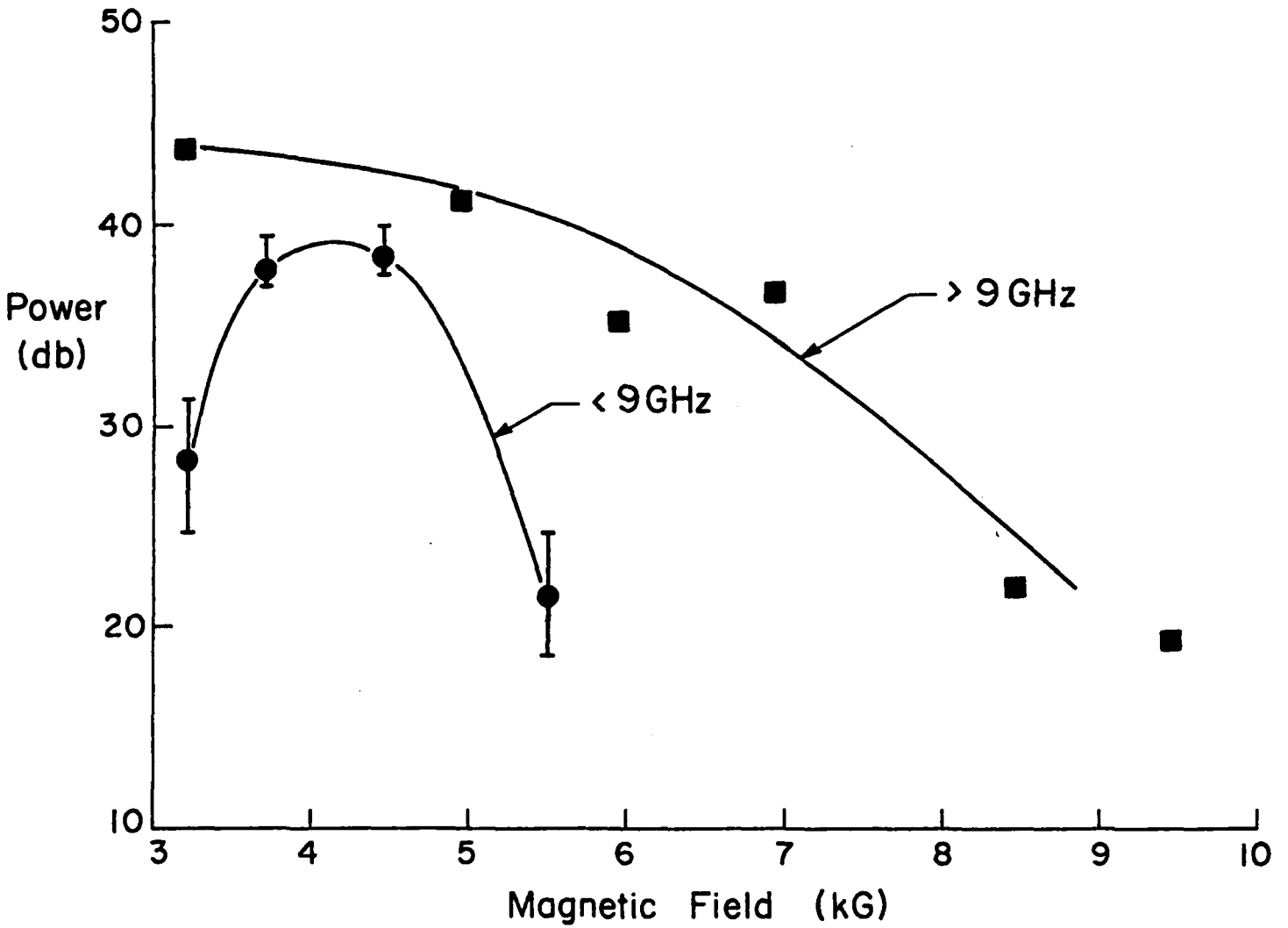
50
40
30
20
10
Power
(db)
> 9 GHz
< 9 GHz
3
4
5
6
7
8
9
10
Magnetic Field (kG)

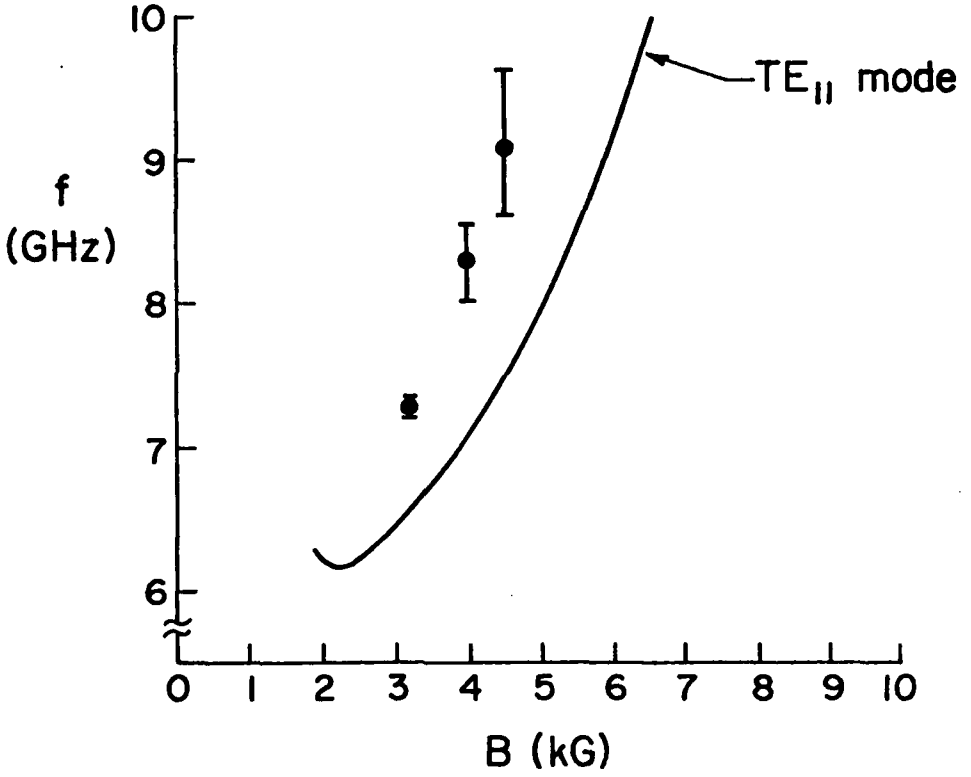
10
9
8
7
6
f
(GHz)
TE11 mode
0 1 2 3 4 5 6 7 8 9 10
B (kG)

A WAVE ACCELERATOR FOR COLLECTIVE ION ACCELERATION

R. Adler, G. Gammel, J. A. Nation, M. E. Read* and R. Williams

Cornell University, Ithaca, New York 14853

and

P. Sprangle and A. Drobot

Naval Research Laboratory, Washington, D.C. 20375

Abstract

Aspects of the experimental program at Cornell for the generation of a large amplitude space charge wave, suitable for the demonstration of a wave particle accelerator, are presented.

An account is given of the wave growth in a slow wave structure, and of the measured values of the electric field and phase velocities of the wave, after extraction into a uniform tube. The electric field measured is in excess of 30 kV/cm and the phase velocities consistent or slightly lower than the expected values.

Progress towards the development of a suitable ion source for use as an injector is also summarized and experiments designed to elucidate the collective processes involved are described.

Introduction

The application of relativistic electron beams to collective ion acceleration has been studied in many laboratories. Most of these schemes use the acceleration occurring in the potential well at the head of the electron beam. Sloan and Drummond [1] first proposed the use of negative energy waves on a relativistic electron beam as a technique for

* Present address: Naval Research Laboratory, Washington, D.C. 20375.

coupling from electron beams to protons in an accelerator. Since that time, Nation [2], Sprangle [3], and other workers [4] have proposed configurations in which the slow space charge wave may be used for the proton acceleration.

As shown in this paper, techniques exist for the growth of large amplitude space charge waves and diagnostics have been developed to measure both the wave amplitude and phase velocity. The limits achievable on these parameters remain to be determined.

Theoretical analysis shows that the space charge wave will only have a zero phase velocity at the space charge limiting current. Present experimental studies and computer simulations are attempting to resolve how low a phase velocity is realizable in practice in the presence of a large amplitude wave.

Concurrent with the presently reported studies on wave growth and extraction we are also studying approaches to providing a suitable ion injector for the wave accelerator. In the first of these we plan to use a Luce diode configuration to provide a proton beam with a sufficiently high energy to inject into the wave. The aspects of that activity reported in the present work indicate briefly recent diagnostic developments which help elucidate the collective acceleration mechanism involved. In an alternate approach, the initial low energy acceleration is accomplished in a modified wave growth section where the first spatial harmonic is used to couple to the protons. Numerical solutions to the linear dispersion relation in this type of structure have also been obtained.

Experimental Observations of Space Charge Waves

The experimental configuration used in the wave generation is shown in Fig. 1. The electron beam is provided from a pulse line which has been typically operated in the range 250 kV to 950 kV with extracted beam currents of up to 1 kA. The pulse duration is 100 nsec. The beam is generated in and propagated along a strong axial magnetic field ($B_z \geq 10$ kGauss).

The slow wave structure is a disk loaded waveguide with cavities having a period of 5.0 cm and a diameter of 12.7 cm. It supports TM modes in the central section and standing TEM modes in the radial cavities. The electrical length of the radial cavities is increased through the use of the lucite filler. This permits lower frequency operation of the system, which, with the parameters used, behaves as a series of weakly coupled TM 010 mode cavities. Higher frequency oscillation is also present corresponding to an interaction between the beam and the TM 020 cavity mode. In comparison with the slow wave structure described later in this paper, the ratio of the amplitudes of the first space harmonic to the amplitude of the fundamental is small. The experimental device also does not support a TEM mode contribution to the dispersion relation.

The measured output wavetrain is always close to 1.25 GHz, a frequency about 10% higher than that obtained in the unloaded transmission structure. At the lower voltage range used, the wave energy propagation is against the electron beam motion and signal delays in the envelope corresponding to group velocities as low as -0.05 c have been observed. In the higher voltage mode of operation the instability appears to be convective and growth exponential throughout the full 115 cm of the slow wave system. The measured growth rate, observed from magnetic probes located close to the ends of the radial arms, was as high as 0.3 db/cm. Instability corresponding to an interaction between the beam and the TM 020 mode of the cavity at a frequency of 3.0 GHz has also been observed.

e signal level in this mode is not yet well established, but is a sig-
ificant fraction of that found for the fundamental mode. It seems possi-
e to suppress the higher frequency mode through the use of appropriate-
designed coupling between the adjacent cavities. Figure 2 shows a
ot of the signal strength versus position in the slow wave structure.
e beam had an energy of about 700 keV.

At present we have only grown waves on beams with ratios of current
limiting current of less than about 0.5. The electric field of the
e, in these cases, varies between 20 and 30 kV/cm. The wave field
dition determining the onset of self trapping of the electrons is
en by

$$E_z \approx \frac{k}{\gamma_{ph}} (\gamma_{ew} - 1) \frac{m_o c^2}{e}$$

re

$$\gamma_{ew} = \gamma_e \gamma_{ph} [1 - \beta_o \beta_{ph}]$$

the value of the relativistic factor measuring the difference in the
ctron velocity and the wave phase velocity. γ_{ph} is the relativistic
tor for the wave phase velocity measured in the laboratory frame.
s field has a value estimated in the range E ~ 10 - 60 kV/cm. This
ld is in the range of the fields measured experimentally. It should
noted that at higher values of the ratio I/I_L the trapping field
reases to a value an order of magnitude greater than that quoted above
that fields of a few hundred kilovolts/cm should be attainable with a
rate energy beam before self trapping develops.

Following the wave growth section the beam is extracted into a
form pipe with a diameter of 2.9 cm. Extensive development of diag-
tic techniques to measure the wave electric field and phase velocity
this section, where the slow electromagnetic wave is cut off, has been

completed and first measurements of these parameters have been obtained. The measurement technique, which is described elsewhere [5], uses a double loop mounted in a side tube, just outside the waveguide wall, oriented to pick up the wave magnetic field. The loop feeds a subtractor to reduce common mode pick-up of the electrostatic field. The loop is calibrated at the wave frequency in a coaxial system using the pipe as the outer conductor of the coaxial cable. The calibration permits measurement of the wave magnetic field as a function of time and with the aid of the known dispersion relation for the wave, permits calculation of the electric field on axis. To complete this evaluation it is necessary to know the wave phase velocity. This has been determined using two similar calibrated probes separated from each other by a known distance, in an interferometer arrangement. The interference signal from the two detectors gives a direct measurement of the wavelength of the space charge wave and hence the phase velocity.

The results obtained in the experiments performed so far are summarized in Table 1.

V_D(kV)	I (A)	I/I_L	β_{ph}(calc.)	β_{ph}(expt.)	E_z(r=0)kV/cm
700	700	0.2	0.75	0.70±0.07	20
270	800	0.50	0.50	0.30±0.10	32

Table 1.

The experimental results are consistent with or less than those expected based on calculations of the wave phase velocity as a function of the ratio of the beam to limiting current. The low voltage result may indicate that non-linear effects result in a reduction of the slow wave phase

velocity. Further experiments are in progress to confirm this result. The modulation of the beam is substantial with potential well depth to beam injection voltage ratios of 0.13 and 0.34, respectively. The corresponding ratios for the ratio of the r.f. current to the beam current are 0.25 and 0.33 , respectively. With lower phase velocities the wave potential well is smaller for comparable electric fields. The permissible electric field to remain in the linear regime also increases rapidly with decreasing phase velocity.

Particle Injector Studies

In view of the problems associated with the generation of very low phase velocity waves, we plan to develop an injector which will produce protons with energies of order 20 - 30 MeV. A device suitable for this ion generation in a wave acceleration test concept experiment is the Luce [6] diode. This device has been shown to generate protons with energies of up to 22 times the diode injection energy. It relies on a three stage acceleration process which is not well understood. In our present experiments we have concentrated on developing a single stage device and on devising new diagnostics techniques to elucidate the acceleration mechanism involved. Previous experiments [7] have strongly suggested that the acceleration is associated with ions being trapped in the moving space charge well at the head of the electron beam. The virtual cathode formed propagates in this case as a result of the neutralization of the beam by the fast protons. A new probe system has been devised which may be mounted in either the side wall of the tube or in the end of the tube. The probe consists of a Faraday cup covered with multiple layers of absorber and measures the relative electron current to each layer of the absorber. The probe therefore gives a measurement of the relative distribution of electron energies and is capable of resolving electrons

with energies greater than the injection energy. Such electrons have been predicted in beam head acceleration analysis where well depths of up to three times the beam energy are expected. The side wall cups also record the motion of the well. Preliminary experiments suggest the presence of some electrons with energies greater than the beam injection energy. The single stage device used produces [7] protons with energies up to eight times the diode voltage.

An alternate acceleration mechanism capable of accelerating low energy ions in a space charge wave uses the space harmonic properties of a periodic structure. This mechanism, which was originally proposed by Sprangle, is described with reference to Fig. 3. An annular beam is propagated close to the boundary of a ridged waveguide. The gap length is one-half of the period of the structure. To satisfy the boundary conditions at the ridged surface requires that the wave be composed of a number of space harmonics, with appropriate ratios of amplitudes to satisfy the requirement that the electric field drop to zero on the conducting surfaces and be finite in the gaps. At any operating frequency having any frequency ω and wave number k there will also exist a spectrum of space harmonics with wavenumbers

$$k_n = k_o + \frac{2\pi n}{L}$$

where L is the period of the structure and n an integer. For the structure shown, the amplitude of the first space harmonic varies from $2/\pi$ of the amplitude of the fundamental at the ridged surface to zero at the smooth wall. In this form of accelerator, we propose to grow a large amplitude wave by means of the unstable interaction between the slow space charge wave and the fundamental (ω, $k = k_o$) of the structure and to trap the ions in the first space harmonic. The ion energy may be

increased by adiabatically increasing the period of the structure. The lowest unstable portions of the dispersion relation for a uniform structure of the type illustrated in Fig. 3 is shown in Fig. 4. In this figure we show the real and imaginary parts of the frequency as a function of the wavenumber k. Only that portion of the curve appropriate to the interaction in the fundamental mode is shown. The wave is unstable over a broad range of values of k_o and has a peak corresponding to a phase velocity of about 0.6 c. The ratio of the beam to limiting current in this case was about 0.2 and corresponds to conditions easily achievable. The growth rate of the instability is very large and is comparable to the wave frequency, as was observed in the experiments reported earlier, albeit in a somewhat different configuration. The second peak in the growth rate of the instability corresponds to the interaction between the space charge wave and a higher frequency mode of the structure. The growth rate of this instability is comparable to that found for the fundamental interaction. This result is consistent with observations in the experiment.

In addition to this interaction between the beam and the waveguide mode we must also examine the interactions occurring with the space harmonics. These interactions must exist simultaneously with the wave number $k = k_o$ interaction and also must have appropriate ratios of amplitudes to satisfy the boundary conditions. The amplitude of the first space harmonic has a peak value for the configuration used and its amplitude is greater than 60% of the fundamental. In this example, which has not been optimized, the wave has a phase velocity of about 0.6 c. The first space harmonic has a phase velocity of about 0.15 c. This corresponds to a proton energy of less than 10 MeV. This proton energy is much more readily achieved than the higher energy ions needed for acceleration in a

uniform tube, and it seems likely that even this energy requirement can be relaxed if necessary.

Conclusions

Present experiments have shown that it is possible to generate slow space charge waves on pencil beams in slow wave structures and to extract the beams into a uniform tube. Wave phase velocities have been measured, with modest ratios of beam to limiting current, of order 0.3 c and are expected to become lower as the beam current is enhanced. The wave electric field is about 30 kV/cm in these experiments and is also expected to scale with increased beam current. Numerical calculations of the growth rate in a similar class of structure, but with an external annular beam, have shown that high instability growth rates are readily achievable. The results bear a strong similarity to those found in the experiment.

Future work will concentrate on the development of simulation codes, and experimentally on the control of the instability growth. Future experiments will also use structures with high space harmonic content so as to be able to exploit the acceleration capability of the first space harmonic of the wave electric field.

Acknowledgment

The Cornell work was supported by the National Science Foundation. The collective acceleration studies in the Luce diode configuration were also supported, in part, by B.M.D.A.T.C.

References

1. M. Sloan and W. Drummond, Phys. Rev. Lett. 31, 1234 (1973).
2. G. Gammel, J. A. Nation, and M. E. Read, Bull. Am. Phys. Soc. 21, 1184 (1976). Also based on a research proposal submitted in 1974.

P. Sprangle, A. Drobot, and W. Mannheimer, Phys. Rev. Lett. 36, 1180 (1976).

S. Yadavalli, Appl. Phys. Lett. 29, 272 (1976).

G. Gammel, J. A. Nation, and M. E. Read, to be published in Rev. Sci. Instruments.

J. S. Luce, Ann. N.Y. Acad. Sci. 217 (1975).

R. Williams, J. A. Nation, and M. E. Read, Bull. Am. Phys. Soc. 21, 1059 (1976).

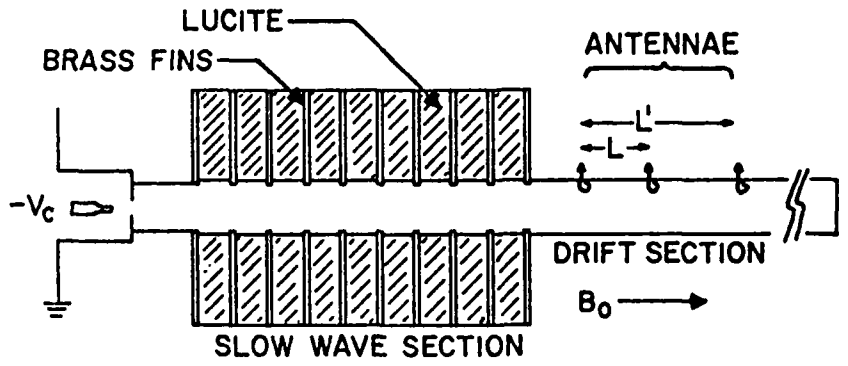

Fig. 1. Experimental configuration showing wave-growth section. Beam phase velocity and electric field measurements are made in the uniform section.

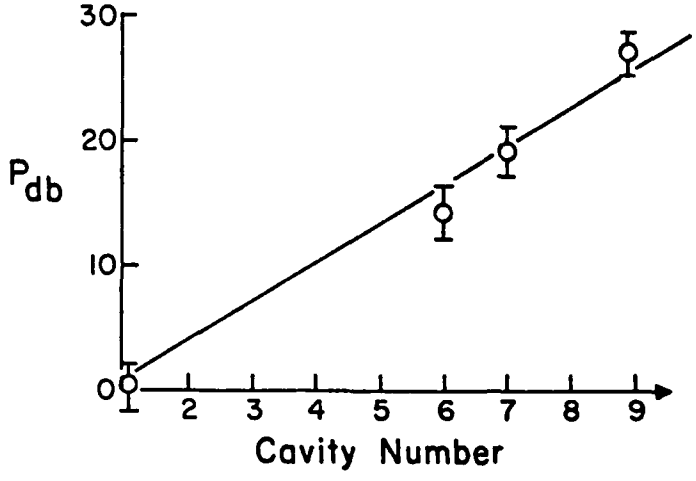

Fig. 2. Relative signal strength versus cavity number, for a 700 keV beam.

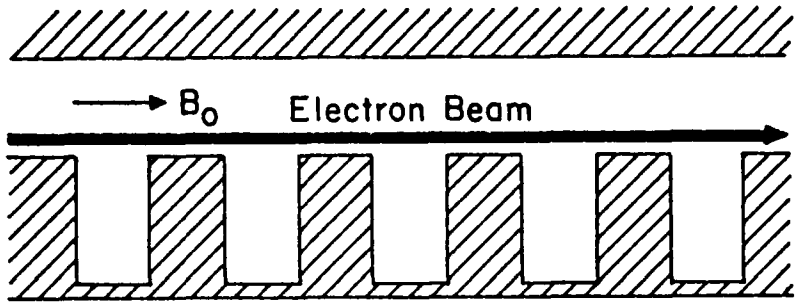

Fig. 3. Slow wave structure, and beam geometry used in determining the dispersion relation in Fig. 4. The beam is located about 2 mm from the wall and carries a current of about 2 kA/cm.

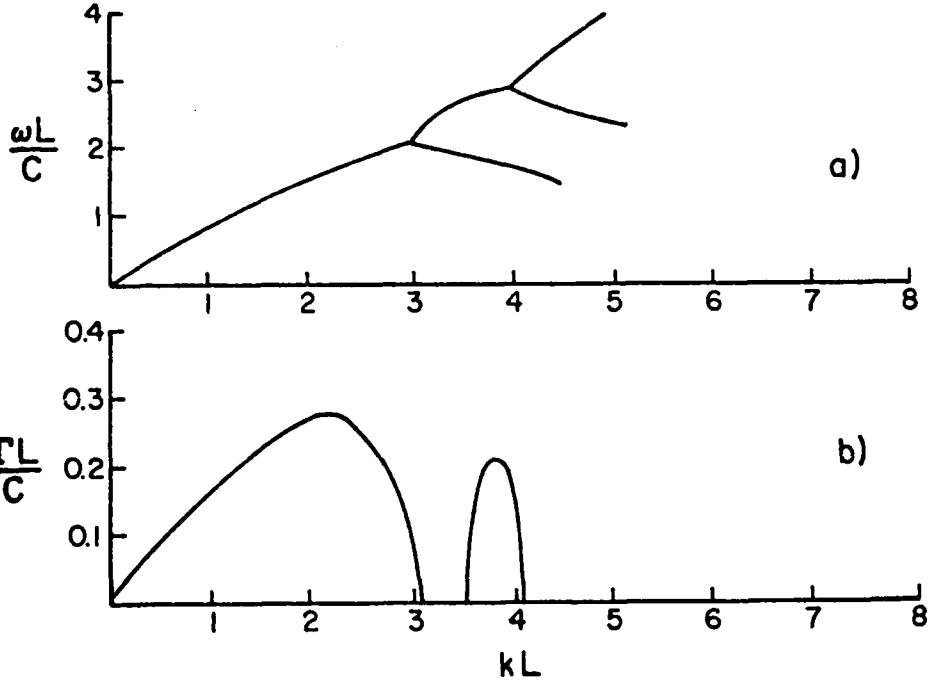

Fig. 4. The real (ω) and imaginary (Γ) parts of the wave frequency. The periodic structure length is of order 2 cm and the beam energy 650 keV.

Slow space-charge wave propagation on a relativistic electron beam

G. Gammel,[a] J. A. Nation, and M. E. Read[b]
Laboratory of Plasma Studies and School of Electrical Engineering, Cornell University, Ithaca, New York 14853

(Received 18 January 1979; accepted for publication 8 May 1979)

A description is presented of an experimental study of the growth and propagation of a large-amplitude slow space-charge wave on a weakly relativistic electron beam. The wave is grown as a result of an unstable interaction between a slow space-charge wave on the electron beam, and the TM modes of a periodic waveguide. Following wave growth the modulated beam is propagated through a cylindrical waveguide. Experimental results show that we have grown, and can propagate, a coherent wave, having a peak electric field of 60 kV/cm, with a phase velocity of $0.29c$. The results presented have application to the collective acceleration of ions in intense relativistic electron beams.

PACS numbers: 41.80.Dd, 52.35.Fp

INTRODUCTION

A number of experiments have been reported [1-11] in which high-power relativistic electron beams are used for collective ion acceleration. Many of these accelerators rely on the acceleration which occurs at the head of an electron beam, as it propagates into a low-pressure gas, or into a vacuum through a dielectric anode. We describe in this paper experiments carried out to investigate the applicability of a train of large-amplitude slow space-charge waves to collective acceleration. This scheme, [12-14] and related wave accelerator [15-17] devices proposed elsewhere, provides acceleration of the ions by the control of the phase velocity of the wave. This approach is scalable to yield high-energy ion pulses.

In the following sections we describe the results of an experimental investigation of the growth, propagation, and control of large-amplitude space-charge waves on a weakly relativistic electron beam. The experiments demonstrate that we have succeeded in growing a coherent space-charge wave train on an electron beam. The wave has a measured electric field of up to about 60 kV/cm, and the phase velocity of the wave has been shown to vary experimentally as predicted with the experimental conditions employed. In the configuration described a wave velocity of less than 0.3c has been achieved. This is consistent with expected values for the experimental configuration used. Methods for reduction of the phase velocity to about 0.2c will be indicated and possible injection devices for preaccelerating protons to this velocity will be described.

REVIEW OF ACCELERATOR CONCEPT

A space-charge wave accelerator is shown schematically in Fig. 1. It consists of three essentially independent sections: (i) an ion preaccelerator; (ii) a wave-growth section; and (iii) an acceleration section.

The preacceleration section is required to generate an adequate supply of about 20 MeV ($\beta \sim 0.2$) protons for injection into the collective accelerator. It has been proposed that the wave will be grown around the ions and that the accelerator phase will follow. In this report we shall describe the wave-growth section, and provide data on the propagation characteristics of the unloaded wave in a uniform waveguide.

The wave-growth section consists of a disk-loaded waveguide in which a series of up to nine weakly coupled cavities are excited in the TM010 cavity mode. The coupling between the cavities is essentially provided by the electron beam as it propagates through a central iris in the slow wave structure. Wave growth, which is extremely rapid (the distance for the signal to e-fold is approximately equal to the length of a single cavity), occurs as a result of the unstable interaction between a slow space-charge wave on the electron beam and the electromagnetic modes of the structure. Coupling occurs betwen the axial electric field of the space-charge wave and the axial fields of the TM modes in the system. Structures of this type have been extensively investigated in the context of microwave tubes and have been widely reported in the literature. [18]

Following growth of the wave to its desired amplitude it is extracted into a uniform cylindrical pipe. In this section the electromagnetic modes are beyond cutoff and coupling of the wave to the protons occurs, provided that the ion velocity is sufficiently close to the wave phase velocity. In the absence of ion loading the phase velocity of the wave is given by

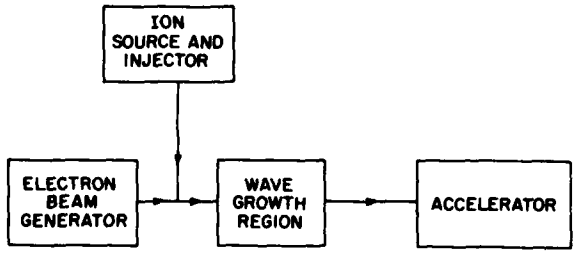

FIG. 1. Block diagram illustrating the principal components of a space-charge wave accelerator.

[a] Present address: Brookhaven National Laboratory, Upton, Long Island, N.Y. 11973.
[b] Present address: Naval Research Laboratory, Washington, D.C. 20375

 0021-8979/79/095603-06$01.10

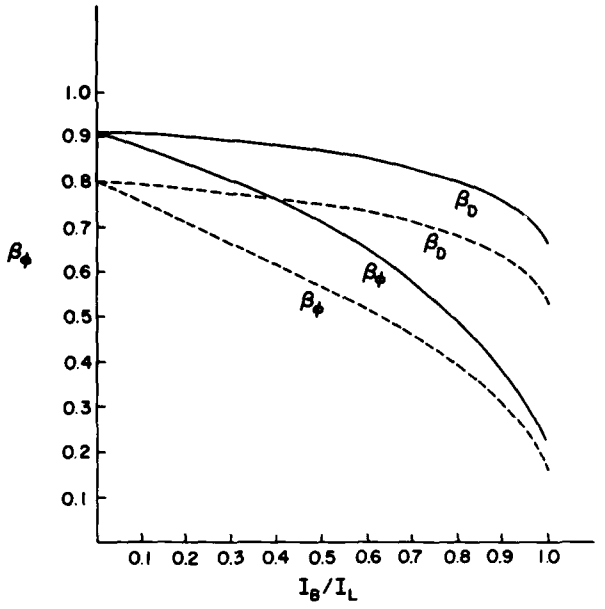

FIG. 2. Electron and wave phase velocities, normalized to the speed of light, versus the ratio of the electron beam to space-charge-limiting current. The solid curves apply to a 700-kV beam and the dashed curves to a 350-kV beam. The electron velocity curves are characterized by the subscript D and the wave phase velocity by the subscript ϕ.

$$\frac{p J_0(k_\perp a)}{k_\perp J_1(k_\perp a)} = \frac{I_0(pb)K_0(pa) - I_0(pa)K_0(pb)}{I_0(pb)K_1(pa) + I_1(pa)K_0(pb)},$$

where $p^2 = k_Z^2 - \omega^2/c^2$ and J, K, and I are Bessel functions. In these expressions we assume a uniform beam of radius a, which is guided by a strong axial magnetic field, propagates through a tube of radius b. The transverse wave number $k_\perp$ is related to the axial wave number k_Z and the beam parameters through the relation

$$\omega \simeq k_Z v - \omega_p \left(\frac{k_Z^2 c^2 - \omega^2}{(k_\perp^2 + k_Z^2)c^2 - \omega^2} \right)^{1/2},$$

where $\omega_p = (ne^2/\gamma^3 \epsilon_0 m)^{1/2}$, and v are the plasma frequency and beam velocity, respectively. One may approximate the full relation, at least at low phase velocities, by

$$\omega = k_z v - \omega_p \frac{k_z}{k}$$

where $k^2 = k_\perp^2 + k_Z^2$ and

$k_\perp a \simeq 2.4$.

Figure 2 shows a plot of phase velocity of the wave, as a function of the beam to limiting current, in the structure used in these experiments. The plots given are appropriate to the wave frequency excited by the structure. The upper curves show the electron drift velocity in the beam. The two curves are appropriate to injection energies of 700 and 350 keV, respectively.

To utilize the slow wave for ion acceleration requires that the ions be injected into the wave train nonadiabatically, and at an energy such that they can be trapped in the wave space-charge wells. These wells are typically about 200 kV deep and travel, at beam currents close to the space-charge limit, at a velocity of about 0.2c. For protons this will require a 20-MeV injection energy. Subsequent acceleration may be achieved by increasing the wave phase velocity at a rate matching the acceleration achieved due to the wave electric field. The phase velocity may be controlled by varying the effective plasma frequency of the beam electrons. Several techniques have been proposed to achieve this including expanding the beam in a diverging field, [19] and also by converging the waveguide walls. [16] This latter scheme is probably the most attractive one since it retains the well-collimated small-diameter beam. The attractiveness of such an accelerator lies in its capability of accelerating at very high electric fields ($\sim$ 1 MV/cm) while providing focusing of the ions in the electrostatic well of the electron beam. In addition the high pulse power technology which has been developed in recent years allows acceleration of high flux densities of ions.

Figure 2 also illustrates one of the problems associated with the use of the slow-charge wave for ion acceleration. The low phase velocities required to pick up the injected ions are only available at beam currents close to the limiting current. [20-22] The lowest phase velocity attainable in the experimental configuration reported here is about 0.2c; this does not reflect the lowest velocity attainable in any practical device. It has been shown that the wave phase velocity tends to zero at low frequencies when the current approaches the limiting current. In fact Godfrey has shown that for arbitrary beam profiles the wave phase velocity v_ϕ varies as

$$v_\phi \propto (I_L - I_B)^{1/2}$$

at currents close to the limiting current. [Godfrey [23] has also shown that the lowest attainable phase velocity is magnetic field dependent and approximately given by $v_\phi|_{\min} \simeq \frac{1}{2} \gamma v_z (\omega_p/\omega_c)^2$.] The limitation imposed by the beam dependence of the wave phase velocity on the beam current is not present if one excites the cyclotron wave. This wave has been studied extensively theoretically and by computer simulation. [15,24] Previous efforts to excite this wave, albeit at high frequency, have however only met with limited success.

In the following we shall describe the results of experiments investigating (a) wave growth and extraction and (b) wave propagation. A brief discussion of a possible injection system, suitable for the space charge accelerator is also given.

EXPERIMENTAL ARRANGEMENT AND RESULTS

In the experiments reported the electron beam was generated using either a Marx-Blumlein arrangement or by directly connecting the Marx generator to a vacuum diode. These facilities yielded electron beams with durations of order of or greater than 100 nsec at diode voltages of 700 and 300 kV, respectively. Diode currents in excess of the space-charge-limiting current were readily available. The electron beam was generated using a foiless diode and a pencil beam carrying a current of order 1 kA propagated through the experimental device. The beam was guided and confined radially by an axial magnetic field. In most experiments the magnetic field strength was maintained about 12 kG, although in some later experiments it was decreased to 6 kg in

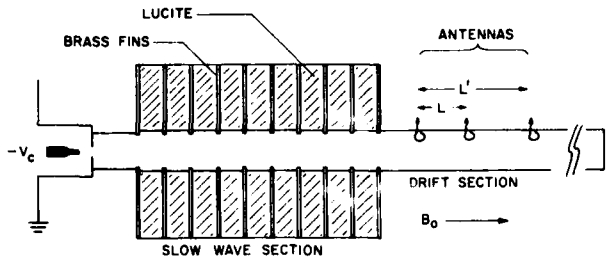

FIG 3. Schematic illustration showing wave growth and drift regions. The antenna loops are, in fact, recessed behind the drift-tube walls.

order to provide a confinement over a total experimental length of about 2.5 m. The beam current was measured at axial locations using Rogowski coils, and the beam location and size (as required for estimating the space-charge-limiting current) determined by witness plates. A schematic of the experimental section is given in Fig. 3.

Measurements were made of the wave characteristics using magnetic pick-up loops. In the wave-growth region these probes were single loops located at the end of the cavities. Electrostatic pick-up was unimportant since the probes were well shielded by the cavity walls. In the transport region, following the wave growth, the probes were recessed behind the wall of the guide and consisted of two oppositely wound turns feeding a hybrid coupler operated in the 180° mode. As evidenced by the rotation of the probes through 90° the common mode electrostatic pick-up was more that 13 dB below the detected magnetic pick-up signal. The output of the pick-up loops was either fed directly to a fast oscilloscope or to a calibrated crystal detector. The probes were calibrated using a sweep oscillator feeding a transmission line consisting of the experimental guide and a center conductor. With this arrangement the probe signal was directly calibrated in terms of the azimuthal magnetic field immediately inside the waveguide wall.

The pick-up loops were used for two measurements, first to determine the axial electric field of the wave and secondly to measure the phase velocity of the wave. The former quantity was determined by measuring the magnetic field of the wave (using the pick-up loop and calibrated crystal detector) and from it and a knowledge of the wave-field relations, the electric field on axis was evaluated. The phase velocity measurements were made by determining the phase shift between a pair of magnetic pick-up loops separated by a known distance. This interferometric measurement technique and the electric field determination technique are described in detail elsewhere. [12]

WAVE-GROWTH MEASUREMENTS

Wave growth was monitored as a function of position in the nine cavity system shown schematically in Fig. 3. Each cavity was 6.3 cm in radius and 5.0 cm long. The radial fins were approximately 3 mm thick and were coupled through central 2.6-cm-diam irises. The effective electrical length of the radial stubs was increased by filling them with Lucite. With a beam current of about 1 kA the wave growth rate was measured and found to be about 4 dB per cavity at 700 kV and 2 dB per cavity at 330 kV. In some experiments a shorter wave-growth section was used. In this system the radial fins were terminated (see inset in Fig. 4) in annular disks of 1.1 cm radius and 2.5 cm long. The cavity Q was somewhat higher in this configuration and the growth rate correspondingly larger having a value of 5 dB/cavity at 330 kV. The operating frequency was slightly lower for this latter structure with wave growth at 1.05 GHz instead of 1.25 GHz observed with the simple fin structure. In both cases the bandwidth of the structure was small and was measured as less than 40 MHz. High-sweep-speed oscillographs show coherent single-frequency wave trains extending over at least 30 nsec.

Wave growth also occurs at a frequency of about 3.0 GHz in the structure shown. The growth occurs as a result of the unstable interaction between the slow space-charge wave and a higher-order mode (TM02) of the slow wave system. The growth occurs later in the pulse than the fundamental and requires a higher beam current. Detailed measurements were made of this effect at lower frequency. With an artificial dielectric, having a relative permittivity of 12, the fundamental was observed at 0.57 GHz and the next passband was centered on 1.4 GHz. The 570-MHz signal grew to a maximum and decayed being replaced, about 40 nsec into the pulse, by the higher-frequency mode. The electric field associated with the higher-frequency wave was estimated to be about 25% of that found for the fundamental.

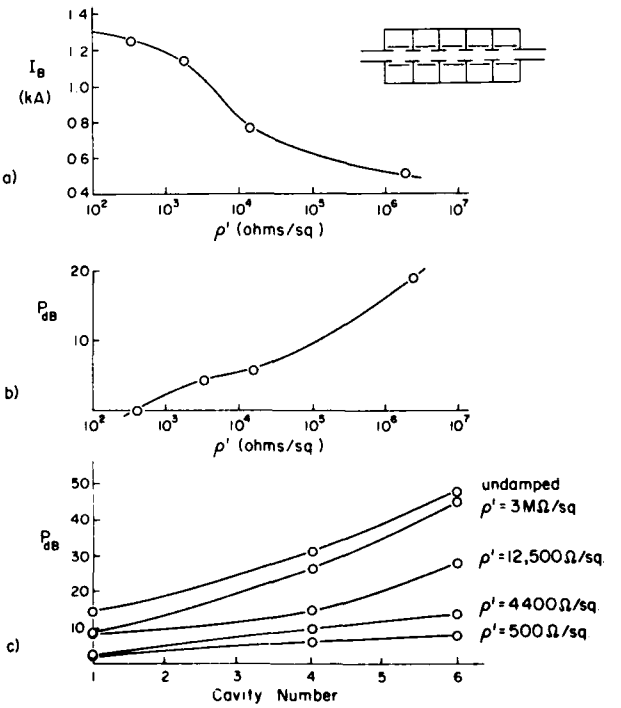

FIG. 4. Wavegrowth results. (a) Current threshold for wavegrowth as a function of the resistivity (in $\Omega/\square$) of the resistive sheet in each cavity. (b) Output power, in the homogeneous drift region, as a function of the resistive damping. (c) Relative signal strength in the wave-growth cavities as a function of the cavity number, measured from the diode end of the structure. The different curves are appropriate to the resistivity of the resistive sheets in each cavity.

The high growth rate of the waves is not entirely desirable and experiments were carried out to investigate a technique for the control of the wave growth rate. Figure 4 shows the result of inserting resistive sheets in the cavities at the location of the inside edge of the dielectric filler. The insert in the upper part of Fig. 4 shows schematically the wave-growth structure used in this experiment. The upper curve indicates the onset current for the instability as a function of the resistivity (in $\Omega/\square$) of the resistive sheet. The middle curve shows the relative signal detected on a probe in a uniform pipe, following the growth of the signal through the structure. The growth rate was reduced from approximately 5 dB per cavity to less than 1 dB per cavity as the resistivity was reduced to 500 $\Omega/\square$. Even in the undamped nine cavity case the signal had not saturated and hence the extracted wave amplitude was not maximized. Simple arguments confirm that resistive films having resistivities of order of 2 k$\Omega/\square$ wil lead to dissipation rates in the cavities sufficient to cause a significant reduction in the stored energy. Note that the additional dissipation in the cavities does not lead to enhanced instability with the negative energy wave as would occur with resistive walls in the uniform section.

WAVE AMPLITUDE AND PHASE VELOCITY MEASUREMENTS

Following the wave-growth region the modulated beam is extracted into a uniform cylindrical pipe. In this region the electromagnetic modes are cut off and only the modulated beam propagates. In the finite-size tube the space-charge wave propagates and is described by the dispersion relationships given in Eqs. (1) and (2). Due to the proximity of the walls, there is a finite electromagnetic field component associated with the wave. The magnetic field of the slow wave is measured by the double probe described earlier and in more detail elsewhere. [12] Two double-probe assemblies, separated from each other by a known distance, were used to determine the phase shift between the probes and hence the wave phase velocity. Figure 5 give a reproduction of oscilloscope

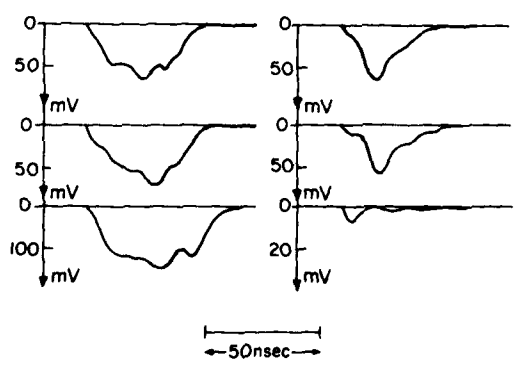

FIG. 5. Oscilloscope traces showing the detector outputs from the interferometer. The left-hand data corresponds to constructive interference and the right-hand data to destructive interference. The top four traces represent the reference signals from the probes (on a 50 mV/div sensitivity) and the lower traces the interference signals (on 100 mV/div constructive interference, and on 20 mV/div for the destructive interference). The bottom scale mark shows a 50-nsec time interval.

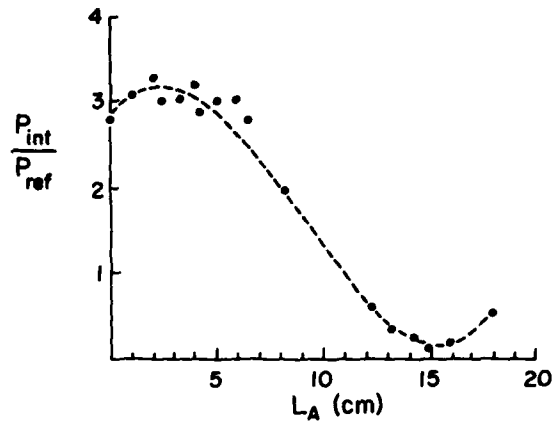

FIG. 6. Interference pattern obtained by charging the length of an air section in one of the interferometer arms.

traces showing the reference signals, and the combined signal at locations close to a maximum and close to a minimum in the interference pattern. An interference pattern, obtained by varying the length of one of the arms of the interferometer, is shown in Fig. 6. The points were obtained on a shot-to-shot basis and were accepted if the reference signals (taken from each probe before superimposing the waves) were equal to within $\pm$ 10%. The abscissa gives the length of the telescoping air section in one of the interferometer arms. The phase velocity is determined directly from this measurement and is correct to $\pm$ 10%. The experimental error results from two contributions; the error in the determination of the location of a minimum in the standing-wave pattern and second from the error in the determination of the difference in the rather long cable lengths ($\sim$ 50 m) from the experiment to the screen room. The latter determinations was accomplished using an interferometer and a time-domain reflectometer. The results agree with each other. In some experiments it was possible to interpret the observations with two possible values of the phase velocity. This ambiguity could be resolved using three pairs of probes. With the three-probe measurement the difference in cable lengths can also be eliminated from the phase velocity determination.

The results of this investigation are shown in Fig. 7. The ordinate on these curves represents the space-charge wave velocity normalized to the calculated drift velocity. The drift velocity, computed as a function of the current to the limiting current, has been shown in Fig. 2. The ratio of the beam current to limiting current was determined by the amplitude of a Rogowski coil output, measured close to the phase velocity measurement ports, and compared to the limiting current determined from the relation

$$I_L = \frac{17000(\gamma^{2/3} - 1)^{3/2}}{1 + 2\ln(b/a)}.$$

The beam radius a was estimated from damage patterns.

The wave electric field was determined from measurement of the magnetic probe output. The system was calibrated to determine the detected signal, in terms of the magnetic field, at a radius just inside the drift-tube wall. Cable losses

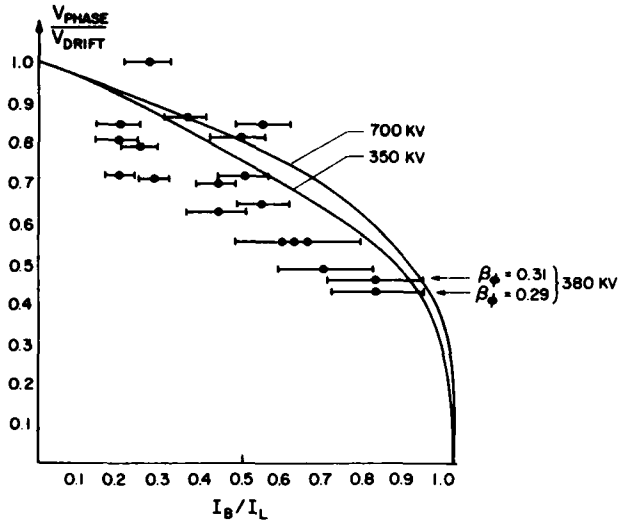

FIG. 7. Summary of wave phase velocity data obtained as a function of the beam to space-charge-limiting current.

and insertion losses of all components were carefully measured. The electric field at the beam location was then calculated from the magnetic field using Eq. (1) where a previous experimental result, for the determination of the wave velocity, was used to determine k_z and k at the operating frequency.

The experimental results obtained indicated electric fields of up to 60 kV/cm at the beam location. At these fields this corresponded to rf peak-to-peak voltages of up to 60% of the diode accelerating voltage. The rf current amplitude reached 90% of the net dc beam current. The spread in data at a given set of operating conditions corresponded to about a 20% scatter in the calculated field strengths.

Measurements of the wave amplitude along the length of the uniform section showed that the wave amplitude decayed at a rate of about 8 dB/m.

An additional measurement was made to establish control of the wave phase velocity by changing the waveguide wall size. In this experiment the drift-tube size was increased from a 2.9-cm to a 7.2-cm diameter in a length of 130 cm. Due to the increased length of the experiment we could only provide a 6-kG magnetic field. The experiments indicated that the wave phase velocity initially decreased and subsequently increased again. This unexpected result was found to be independent of the wave and purely a function of the weaker magnetic guide field. Damage patterns taken along the length of the expansion cone showed that the beam expanded in transit through the section. The observed reduction in phase velocity and the subsequent increase is adequately described by the dispersion relations, provided the beam expansion across the magnetic field lines is included in determining the ratio of beam to limiting current. This effect, which was strongest at higher beam currents and weak magnetic fields, is most likely due to the presence of Diocotron instability. Diocotron instability can develop at higher beam currents, even with a solid pencil beam injected, due to the tendency of the beam to become hollow as the current approaches the space-charge limit.

Present work includes experiments, using annular beams at current approaching the space-charge-limiting value, to obtain low-phase-velocity high-electric-field amplitude wave propagation. Magnetic shear will be introduced at the beam location in an attempt to control the anticipated Diocotron instability.

DISCUSSION OF RESULTS

The previously described results may be summarized as follows:

(1) Slow wave structures have been successfully used to grow large-amplitude space-charge waves on a relativistic electron beam. Dissipative elements, within the structure cavities, have been successfully used to control the instability growth rate.

(2) Measurements have been made of the wave phase velocity following extraction of the modulated beam into a uniform tube. The phase velocity variation with the ratio of beam to limiting current compares well with theoretical estimates. The lowest value of phase velocity obtained was 0.29c. With a modified structure, designed to support a lower phase velocity wave, it seems probable that velocities down to 0.2c will be achieved. An experiment using an annular beam is currently in progress to identify the useful lowest phase velocity achievable.

(3) Wave electric fields of up to 60 kV/cm have been obtained. These values are comparable to those achieved in conventional accelerator systems. The systems used showed no signs of saturation at the operating levels. With the current annular beam system we anticipate that we shall be able to investigate wave growth to levels approaching 300 kV/cm.

(4) The observed variation of the phase velocity of the wave with the beam current (Fig. 7) coupled with the diverging guide experiment show that it is possible to control the wave phase velocity. A method to control Diocotron instability has been analyzed by Ott and Wersinger [25] and is currently being tested experimentally.

At this stage it appears resonable to achieve a collecteive accelerator system which will accelerate ions from 0.2c or slightly lower velocity, with fields competitive to or greater than those presently used in accelerators. The experiments carried out to date have established wave coherence over the pulse duration and throughout the maximum drift region (~ 1.5 m) used. The major practical impediment in the way of utilizing a space-charge wave collective accelerator is the high injection energy required. Assuming an injection velocity of $0.2c$ means that we require a preacceleration of protons to about 20 MeV. Perhaps the most suitable injector for a high flux wave accelerator would be the linear induction accelerator. To data no experiments have been carried out in which high current ion pulses have been accelerated in an induction accelerator, although work is currently under way at Berkeley in which it is planned to accelerate caesuium ions in such a device.

For the purposes of demonstrating the wave accelerator

in a test device we plan to utilize another collective accelerator, namely, a Luce diode, to produce the 20-MeV protons. The configuration planned to generate the ion beam and a second generator for the wave growth have been described elsewhere. [14]

ACKNOWLEDGMENTS

We are grateful to E. Ott and P. Sprangle for helpful discussions. This work was supported by A.F.O.S.R. and N.S.F.

[1]S. Graybill and J. Uglum, J. Appl. Phys. **41**, 236 (1970).
[2]J. Rander, B. Ecker, G. Yonas, and D. Drickey, Phys. Rev. Lett. **24**, 283 (1970).
[3]S. Putnam, Phys. Rev. Lett. **25**, 1129 (1970); B. Ecker and S. Putnam, IEEE Trans. Nucl. Sci. **NS-24**, 165 (1977).
[4]D. Straw and R. Miller, IEEE Trans. Nucl. Sci. **NS-24**, 1645 (1977); R. Miller and D. Straw, J. Appl. Phys, **48**, (1977); D. Straw and R. Miller, Appl. Phys. Lett **25**, 379 (1977).
[5]G. Kuswa, Ann. N.Y. Acad. Sci. **251**, 514 (1975).
[6]A.A. Plyutto and A.T. Kapin, Sov. Phys. Tech. Phys. **20**, 1578 (1976) [Zh. Tekh. Fiz. **45**, 2533 (1975)].
[7]A.A. Kolomensky and V. Likhachyov, IEEE Trans. Nucl. Sci. **NS-22** 1983 (1975); A.A. Kolomensky and B. Yabloklov, Sov. Phys. JETP **41**, 26 (1975).
[8]C. Olsen, Phys. Fluid **18**, 585 (1975).
[9]J.C. Luce, W. Bostick, and V. Nardi, Lawrence Livermore Laboratory Report UCID 17232, 1976; Ann. N.Y. Acad. Sci. **25**, 2171 (1975).
[10]G. Zorn, H. Kim, and C. Boyer, IEEE Trans. Nucl. Sci. **NS-22**, 1006 (1975).
[11]R. Hoeberling, R. Miller, D. Straw, and D. Payton III, IEEE Trans. Nucl. Sci. **NS-24**, 1662 (1977); R. Miller and D. Straw, J. Appl. Phys. **47**, 1897 (1976); D. Straw and R. Miller, J. Appl. Phys. **47**, 4681 (1976).
[12]G. Gammel, J.A. Nation, and M.E. Read, Rev. Sci. Instrum. **49**, 507 (1978).
[13]R. Adler, G. Gammel, J.A. Nation, M.E. Read, R. Williams, P. Sprangle, and A. Drobot, Proc. 2nd Int. Conf. on High Power Electron and Ion Beam Research and Technology, Ithaca, 1977, Vol. II, p. 509.
[14]R. Adler, G. Gammel, J.A. Nation, G. Providakes, and R. Williams, *Proc. 3rd Int. Conf. on Collective Methods of Acceleration, Laguna Beach*, 1978 Harwood Academic Publishers, 1979).
[15]M. Sloan and W. Drummond, Phys. Rev. Lett. **31**, 1234 (1973).
[16]P. Sprangle, A. Drobot, and W. Manheimer, Phys. Rev. Lett. **36**, 1180 (1976).
[17]S. Yadavelli, Appl. Phys. Lett. **29**, 272 (1976).
[18]See for example R. Hutter, *Beam and Wave Electronics in Microwave Tubes* (van Nostrand, New York, 1960).
[19]J. Nation (unpublished); see also, G. Gammel, M. Read, and J. Nation, Bull. Am. Phys. Soc. **21**, 1186 (1976).
[20]R. J. Briggs, Phys. Fluids **19**, 1257 (1976).
[21]B.B. Godfrey, LASL report LA-UR-76-2646, 1976.
[22]J.R. Thompson, Austin Research Associates Technical Memorandum Report, 1976.
[23]B. Godfrey (private communication).
[24]See, for example, B. Godfrey, LASL Report LA-UR-76-1610, 1976.
[25]E. Ott, J.M. Wersinger, J. Nation, and V. Serlin, Bull. Am. Phys. Soc. **23**, 853 (1978).

Space Charge Waves and Collective Ion Acceleration

R. Adler, G. Gammel, J. A. Nation,
G. Providakes, and R. Williams

Laboratory of Plasma Studies
Cornell University
Ithaca, New York 14853

LPS 248 July 1978

SPACE CHARGE WAVES AND COLLECTIVE ION ACCELERATION

R. ADLER, G. GAMMEL, J. A. NATION, G. PROVIDAKES AND R. WILLIAMS
Laboratory of Plasma Studies and School of Electrical Engineering
Cornell University
Ithaca, N.Y. 14853

The Cornell University program, to investigate the use of large amplitude space charge waves on electron beams for collective ion acceleration, has been outlined at the 2nd International Topical Conference on High Power Electron and Ion Beam Research and Technology[1]. In this paper we report on progress made towards achieving a coherent wave train with a low phase velocity, and a large amplitude electric field.

Experiments will be reported which describe the variation of the wave phase velocity with the ratio of the beam to limiting current. Experimental measurements show that we have achieved slow waves with large electric field amplitudes, and that we can control the phase velocity of the wave by adjusting the ratio of the beam current to the limiting current.

The wave accelerator requires an ion injector having an output proton energy of up to about 20 MeV. For the demonstration accelerator project, we plan to use a Luce diode to collectively accelerate the protons to the required injection energy. A progress report is presented describing the performance of our injector system and the outcome of experiments designed to help elucidate the

physics involved in the ion acceleration.

INTRODUCTION

We describe in this paper results of a study of the generation and propagation of a large amplitude space charge wave along a magnetically confined weakly relativistic electron beam. The experimental results obtained illustrate the dependence of the phase velocity of the wave on the ratio of the current to the space charge limiting current[2]. As expected, the phase velocity of the wave is a rapidly varying function of the ratio of the beam to limiting current. In addition we observe that the beam exhibits an instability at higher currents and that this limits the coherence of the wave train in the parameter range where we expect low phase velocities.

The experimentally observed growth rate of the instability forming the slow space charge wave is extremely high, with growth rates of several dB per wavelength. We report, in this paper, on a method of controlling the growth rate through the use of resistive damping in the growth section.

Finally we summarize some observations on the injector development, stressing the physical mechanisms determining the acceleration. A conceptual realization of a configuration to inject the ions into the wave growth and propagation region is also presented.

We now describe these aspects of the program in more detail.

EXPERIMENTAL EQUIPMENT AND RESULTS.

The experimental configuration used in these experiments is shown schematically in Figure 1. The electron

beam is injected, using a foilless diode, into a series

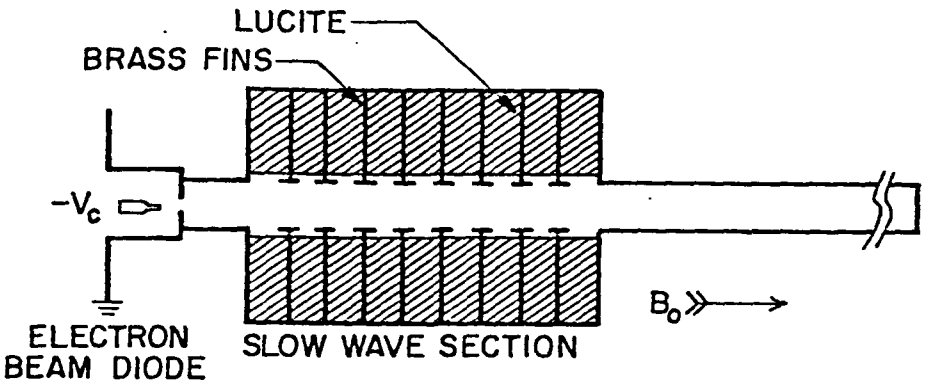

Figure 1. Experimental configuration used in slow wave experiments.

of weakly coupled cavities operated in the TM 010 mode. The negative energy slow space charge wave couples to the axial electric field of the cavity modes, and instability growth occurs. The instability growth rate is dependent on the beam current and on the detailed cavity design. Two configurations have been used; one a disk loaded waveguide, and the second a disk loaded waveguide with the disks terminated in annular rings. The second configuration is shown in Figure 1. Measurements of the growth of the signal, as measured by magnetic pick up loops located in the cavities, showed that the signal strength increased exponentially throughout the length of the growth section. Growth rates ranging from two to more than 5 dB per cavity were recorded, with the highest growth rates occurring in the configuration shown and with the highest beam currents.

In the configuration described above, the cavities were loaded with lucite to increase their effective electrical length.

We have established that it is possible to control the instability growth in the slow wave structure by coating the front surface of the lucite dielectric, in the radial stubs, with a dissipative material. This loading is situated close to the region where the electric field strength is a maximum, and hence the damping most effective. The results of this are shown in Figure 2 in which a plot is presented of the signal strength in the six cavity system as a function of the cavity numbers. As may be seen from the figure the growth rate is reduced from slightly greater than five dB per cavity, in the absence of dissipative material, to about one dB per cavity with a 500 Ohm per square coating.

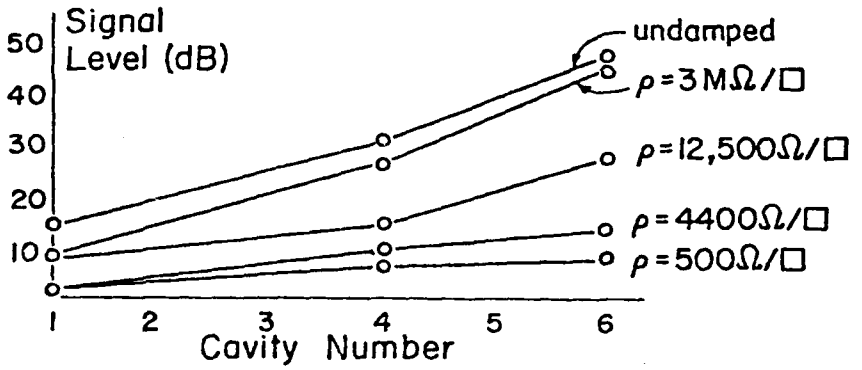

Figure 2. Signal growth as a function of the surface resistivity of the lucite insert in the radial cavities.

SPACE CHARGE WAVE ACCELERATION

Accompanying the reduction in the growth of the signal, as the surface damping is increased, we find that the onset of the instability is delayed. In the absence of dissipation the signal growth usually occurs for beam currents in excess of 500 Amperes. This onset current increases monotonically as the surface resistivity is decreased. The instability growth is only significant with the 500 Ohm per square damping for beam currents in excess of 1.2 kA. We therefore conclude that it is possible to control the wave growth independently of the beam current. This is important if one is to be able to avoid saturation of the instability, due for instance to self trapping of the electrons in the wave, at high beam currents where the low phase velocities are expected.

We conclude this discussion of wave growth by observing that we have monitored a second instability growth in the structure at a frequency of about 3 GHz (as opposed to the usual 1.1 GHz found for the wave growth previously described). This corresponds to the unstable interaction of the space charge wave with a higher order axisymmetric mode of the slow wave system. The electric field in the wave is estimated, for the high frequency case, to be about 25% of that found for the 1.1 GHz wave. It is also found that the higher frequency instability growth only becomes significant late in the current pulse, when the beam current is high. The effects of damping on this mode have not yet been determined. If necessary, we plan to carry out experiments to eliminate the higher frequency growth, either by the use of the dissipative technique described earlier or through the use of inductive coupling between adjacent cavities. The temporal difference in the two

signals may indicate that this suppression is not required for an ion accelerator system.

Following the wave growth section, the beam has been extracted into a homogeneous waveguide of 2.9 cm diameter. Experiments have also been carried out in which the beam is propagated through a diverging tube. Measurements have been made of the phase velocity of the wave in this section using the technique described elsewhere[3]. Basically we use an interferographic method in which the phase change in a given length of the tube is determined by comparison with the phase shift found for the same wave propagating in a vacuum section of coaxial line. The results of this set of observations are given in Figure 3. in which we plot the wave phase velocity as a function of the ratio

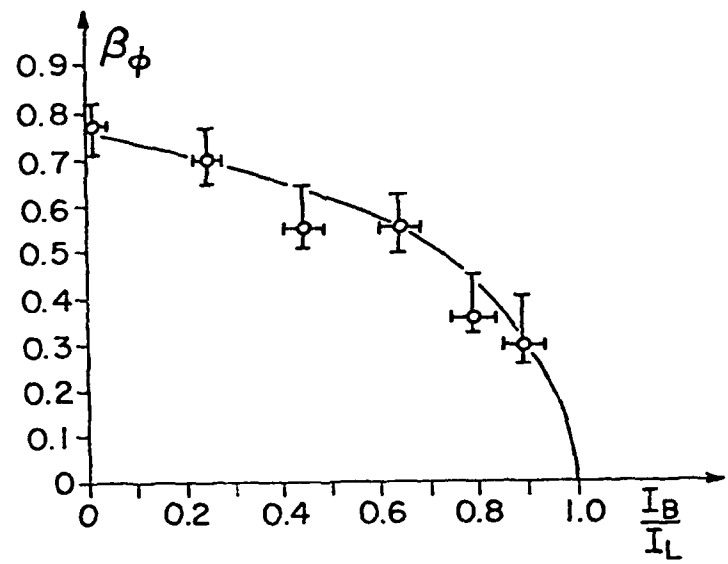

Figure 3. Variation of the phase velocity of the space charge wave with the beam to limiting current ratio.

of the beam current to the space charge limiting current. In obtaining this graph the following procedure was followed. Reference signals were obtained from two adjacent magnetic probes and the signals made approximately equal through the use of variable attenuators in the two lines. The interference pattern, and hence the phase velocity data, were then obtained on a shot to shot basis, taking only those shots in which the reference arm signals were equal within about 10% of each other. This method of selecting data had little effect at the lower beam currents, but restricted the data at the higher beam currents to about one shot in three or four. The point corresponding to the lowest phase velocity shown in Figure 3 was obtained at the mid point of a one meter long diverging pipe. The pipe diameter was increased from a diameter of 2.9 cm at the injection end to approximately 7.5 cm at the far end. The phase velocity was monitored as 0.55 c at the 2.9 cm. end and had decreased[4] to about 0.35 c at the mid plane. Beyond the mid plane the beam behavior was erratic and no results are quoted. Our present observations indicate that the wave train behaviour is irreproducible when the beam current exceeds about 1200 Amperes in the 2.9 cm. pipe. The origin of this is not yet determined; its effects are however quite evident in the Rogowski traces reproduced in Figure 4. These beam current measurements were taken at the 7.5 cm location in the diverging tube experiment. The periods of uniform r.f. emmission are marked on the figure. The r.f. emission is uniform throughout the duration of the lower current pulse, while the emission becomes incoherent during those intervals where the current is large. Large fluctuations are

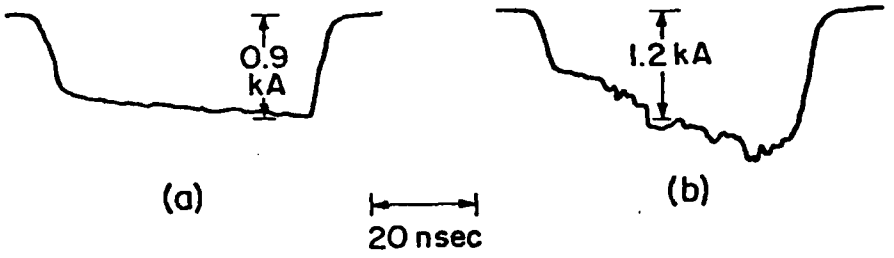

Figure 4. Rogowski traces of the beam current illustrating conditions for stable and unstable r.f. generation. The beam and emission are stable over the complete pulse duration in 4a, and for the first 20 nsec of 4b. The Rogowski trace irregularities in Figure 4b are typical of those found when the beam is unstable and the emission non-uniform.

also observed in the beam current during this time interval. The erratic r.f. and the beam current fluctuations are accompanied by a loss of confinement of the electron beam by the eight kilogauss axial magnetic field. Based on damage pattern observations, the beam appears to have expanded to about three times its original diameter. At present we can only speculate about the origin of the instability. Two mechanisms seem possible sources of the instability. Firstly, at high beam currents, we expect the beam to hollow out and the shear to increase; secondly, at the higher wave fields associated with the high beam currents, electron trapping may become important. In either case it is possible to stabilize the instability, and work

is proceding on this problem.

The electric field of the wave has been calculated using the measured magnetic field of the wave at the wall probe used in the interferometer. From this field, and the measured phase velocity of the wave, it is possible to determine the electric field of the wave from a knowledge of the field distribution in the pipe. This was described in detail in reference 3. The measurement yielded values of the wave electric field of up to 50kV/cm at the lower phase velocities. This field strength is comparable with that obtainable in many conventional particle accelerators, but still significantly below that obtained in some other forms of collective accelerator. A new wave growth and propagation section which will operate at a fundamental frequency of about three gigaHertz with an annular beam is presently under construction. This system should allow for large electric fields in the wave, without wave trapping limitations.

In addition to the wave growth experiments we have carried out an independent study of collective acceleration of protons in a Luce diode geometry.[5] The object of this part of our investigation is to provide a proton source for injection into the wave accelerator. Since the wave phase velocity is a sharplyvarying function of the current to limiting current, it is desireable to have the proton injection energy as a large as possible. For the demonstration experiment we have elected to attempt to produce about 18 MeV protons from the injector. At present the most effective source of high energy protons is the Luce diode configuration. This is itself a collective accelerator and only yields a short pulse of high energy ions; hence it is

not suitable for a final injection source into a useful accelerator. It does however serve a useful purpose for the acceleration demonstration device. The Luce diode configuration used is shown in Figure 5. It has a polyethylene anode connected to the ground plane of the accelerator. A plasma is formed at the surface of the polyethylene due to bombardment by the beam electrons and surface breakdown to the ground plane. In our current experiments the generator has been operated at a diode voltage of 750 keV and beam current of 35 kA. Proton pulses accelerated from the anode plasma having more than 10^{13} protons with energies in excess of the electron injection energy have been recorded. The energy distribution function for the ions is found from stacked copper foil activations and is a monotonically decreasing function of the proton energy. The distribution function may typically be fitted to an exponential, in the proton energy, of the form $N = N_0 \exp(-E/1.5)$, for $E > 4$ MeV and where E is the proton energy in MeV.

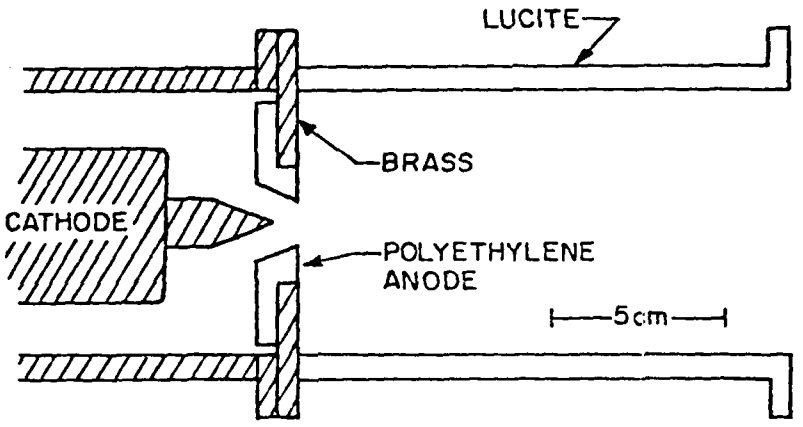

Figure 5. Luce diode configuration used for proton generation.

SPACE CHARGE WAVE ACCELERATION

Peak energies of about 8.5 MeV have been observed corresponding to ion energies in excess of ten times the electron beam energy. Much of the current experimental investigation of the injector system has been directed to obtaining an understanding of the physics of the acceleration. Our observations[6], based mainly on activation analysis and fast absorber covered Faraday cup response, for both ions and electrons, show that the potential well formed at the head of the beam has average depth approxiamtely equal to the beam injection energy. The average well depth is the important parameter for the ion acceleration as it is the electric field corresponding to the average well depth (averaged on a time scale corresponding to a few plasma periods) that is felt by the ions during the acceleration. We found no evidence with the Faraday cups for the presence of electrons with energies significantly in excess of the injection energy for the electrons.

Additional support for the moving well model of the acceleration was provided by the activation of stacked mylar foils. In some cases the activation yield was anomalously high compared to the results typically obtained from the stacked Faraday cups and to the copper activations. The results obtained can be accounted for by assuming that there are also deuterons being accelerated to about twice the energy of the protons. The number of deuterons required was taken to correspond to the natural abundance of the deuterium in the polyethylene. A deuteron flux with the abundance just quoted, but with the same energy as the protons could not account for the observed yield. Deuterons with twice the energy of the proton beam are consistent with a moving potential well picture rather than with a deep static well model.

Current experimentation is aimed at resolving this issue and at enhancing the injection velocity of the ions to about 0.2 c from the presently observed value of 0.13 c.

A WAVE ACCELERATOR CONFIGURATION.

The work performed to date has concentrated on the development of a slow wave system and on generating a suitable ion source for injection into the wave. It is relevant now to question methods of combing these two configurations so as to produce a test accelerator. Since the electron beam used in the ion injector will be badly degraded in the Luce diode system, it is clearly desireable to dump these electrons and extract only the protons. Subsequent to this we require a wave growth section with a second electron beam. Our present observations indicate that this beam should operate at about 300 keV and at rather low (1-2 kA) beam currents. A conceptual design for such a combined accelerator is shown in Figure 6. In this figure we show that the output of a pulse line feeding a copper sulfate termination. The termination has an impedance somewhat greater than the characteristic impedance of the line. The central cathode feeds a Luce diode, which has its anode plane introduced through a second cathode coupled to the device through the load. A similar technique[7] has previously been used to introduce a grounded plane through a high voltage conductor. The majority of the electrons in the primary beam are deposited in the walls of the diode. The flux of ions removed, for injection into the second beam region is controlled by the size and location of the aperture in the grounded cavity of the Luce diode accelerator. A transverse magnetic field may be used, if required, to remove surplus electrons. The

SPACE CHARGE WAVE ACCELERATION

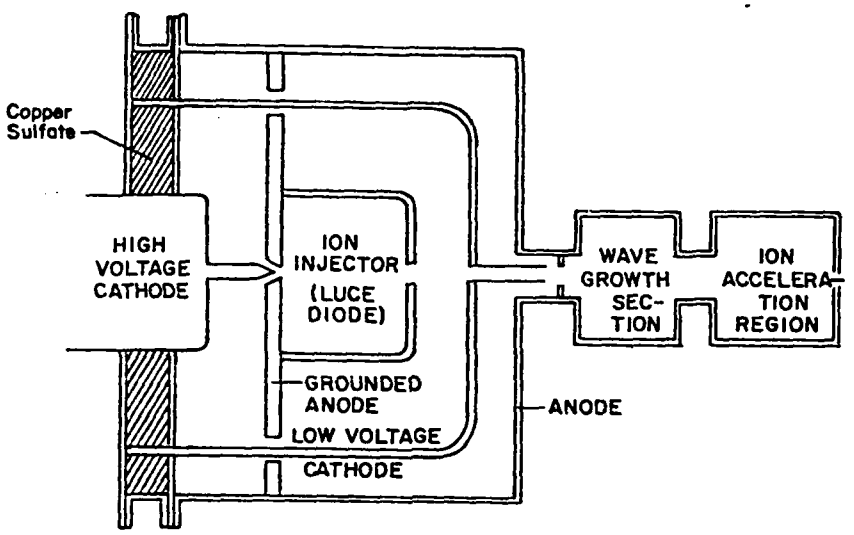

Figure 6. A conceptual design for extracting two electron beams from a single generator.

second high impedance beam used in the wave growth region is generated from the cathode, coupled to the generator through the copper sulfate load. The RC time of this device is about 4 nsec in a practical configuration. The second beam impedance is large compared to the copper sulfate load and hence does not load the device. This technique when applied in a practical configuration should allow us to produce the preaccelerated protons for injection into the wave generated from a second cathode. The coupling suggested between the preinjector and the wave growth section is also relevant to a practical device in which several stages of acceleration may be required.

This work was supported by the N.S.F., A.F.O.S.R., and B.M.D.A.T.C.

REFERENCES.

1. R. Adler, G. Gammel, J.A. Nation, M.E. Read, R. Williams, P. Sprangle, and A. Drobot. Proc. 2nd International Conference Topical Conference on High Power Electron and Ion Beam Research and Technology, 2, 509, (1977) (Cornell University)

2. B. B. Godfrey, To be published in I.E.E.E. Trans on Plasma Science.

3. G. Gammel, J. A. Nation, and M.E. Read, Rev. Sci. Instrum. 49, 507, (1978).

4. P. Sprangle, A. Drobot, and W. Manheimer, Phys. Rev. Letts. 36, 1180, (1976).

5. J. S. Luce, Annals N.Y. Acad. of Science. 251, 217, (1975).

6. R. Adler and J. A. Nation, To be published.

7. M. E. Read and J.A. Nation, J. Appl. Phys. 47, 5236, (1976).

Plasma Preprint PL #80-031

#7

Submitted for Publication

NONLINEAR SPACE CHARGE WAVES ON CYLINDRICAL ELECTRON BEAMS AND PLASMAS

by

Thomas P. Hughes
Cornell University, Ithaca, New York 14853

and

Edward Ott
University of Maryland, College Park, Maryland 20742

Physics Publication Number
Technical Report Number

February 1980

NONLINEAR SPACE CHARGE WAVES

ON CYLINDRICAL ELECTRON BEAMS AND PLASMAS

Thomas P. Hughes
Department of Electrical Engineering,
Cornell University,
Ithaca, New York 14853

and

Edward Ott
Departments of Physics and Astronomy and of Electrical Engineering,
University of Maryland,
College Park, Maryland 20742

ABSTRACT

Nonlinear space-charge waves in a strongly magnetized cylindrical plasma are investigated. Soliton and periodic wave solutions are obtained. For the case of an intense unneutralized electron beam, a significant decrease in the phase velocity of the slow space-charge wave is found at large amplitudes. The importance of this result for some collective ion acceleration schemes is discussed.

I. INTRODUCTION

In this paper we present a study of nonlinear space-charge waves on a strongly magnetized plasma column (Fig. 1). We study both a charge neutralized situation, in which region I of Fig. 1 is a stationary plasma, and a situation in which region I is an unneutralized electron beam propagating in a vacuum. Our results for the unneutralized case will be shown to have important implications for some collective ion acceleration schemes[1,2]. Since only axisymmetric field configurations are studied, the problem to be treated is a two-dimensional one. Two-dimensional nonlinear problems are notorious for their analytical intractability, and, indeed, only weakly nonlinear theories for the problem considered here are presently available.[3,4] Furthermore, existing analytical results apply only to waves in a neutral plasma. In order to obtain strongly nonlinear solutions relevant to intense, unneutralized electron beams, we shall employ a numerical technique (see Appendix for details). Section II formulates the problem. An outline of the weakly nonlinear theory of space-charge solitons for the geometry of Fig. 1 is presented in Sec. III. Section IV presents results and discussion. Conclusions are given in Sec. V.

II. FORMULATION

We take the magnetic field in the plasma column to be $\underset{\sim}{B}_o = B_o\hat{z}$, with $B_o \to \infty$. For an infinite, stationary, homogeneous plasma immersed in this field, the linear dispersion relation for space-charge waves with space-time dependence $\exp(-i\omega t + ik_z z + i\underset{\sim}{k}_\perp \cdot \underset{\sim}{x}_\perp)$ is

$$1 - (\omega_e/\omega)^2(k_z/k)^2 = 0 \quad , \tag{1}$$

where $k^2 = k_z^2 + k_\perp^2$, and ω_e is the electron plasma frequency. It is assumed that the electron temperature is negligible and that the ions are immobile. For the geometry of Fig. 1, Eq. (1) still applies, but permissible, discrete, values of $k_\perp$ are determined by the solution of a radial eigenvalue problem. In the case $k_z^2 \ll k_\perp^2$, Eq. (1) gives

$$\omega/k_z \cong (\omega_e/k_\perp)[1 - \tfrac{1}{2}(k_z/k_\perp)^2] \ , \tag{2}$$

i.e., the plasma-wave modes are weakly dispersive. In such a case one expects that the nonlinearity of the fluid equations will lead to the possible existence of solitons.

An unneutralized beam will in general have nonuniform equilibrium velocity and density profiles, so that the above equations only indicate the qualitative behavior of the beam space-charge modes.

Now we shall derive the exact nonlinear equation for space-charge waves in the plasmas we are studying. The continuity and momentum equations, together with Maxwell's equations, describe the cold electron fluid:

$$\frac{\partial n}{\partial t} + \frac{\partial}{\partial z} nv = 0 \ , \tag{3a}$$

$$(\frac{\partial}{\partial t} + v \frac{\partial}{\partial z})\gamma mv = -eE_z \ , \tag{3b}$$

$$c\nabla x\underset{\sim}{B} = -4\pi ne\underset{\sim}{v} + \frac{\partial \underset{\sim}{E}}{\partial t} \ , \tag{3c}$$

$$c\nabla x\underset{\sim}{E} = -\frac{\partial \underset{\sim}{B}}{\partial t} \ , \tag{3d}$$

where n is the total electron density, $\underset{\sim}{v} = v\hat{z}$ is the z-velocity of the electrons, $\gamma = (1 - v^2/c^2)^{-1/2}$, $\underset{\sim}{B} + B_o\hat{z}$ is the magnetic field, and $\underset{\sim}{E}$ is the total electric field. We wish to consider solutions which depend only on r (the radial variable in cylindrical coordinates) and z - Ut, where U is the velocity of the wave-form measured in the laboratory frame. If we go to the frame traveling with the wave, then in the new coordinate system (r,z',t'), we have $\partial/\partial t' = 0$, so Eq. (3a) and Eq. (3b) become

$$\frac{\partial}{\partial z'}(n'v') = 0 \ , \tag{4a}$$

$$v'\frac{\partial}{\partial z'}(m\gamma'v') = -eE'_z, \tag{4b}$$

where primes on n, v, E_z, γ mean that these are measured in the new frame. Equations (3c) and (3d) can be replaced by Poisson's equation,

$$\nabla'^2\phi = 4\pi n'e \ , \tag{4c}$$

and,

$$E'_z = -\frac{\partial \phi}{\partial z'} \ . \tag{4d}$$

The primes will be dropped from here on.

For the case of a solitary wave, the following boundary conditions are used:

$$n(r,z) \to N_U(r) \text{ as } z \to \pm \infty \quad , \tag{5a}$$

$$\phi(r,z) \to \phi_U(r) \text{ as } z \to \pm \infty \quad , \tag{5b}$$

$$\phi(b,z) = 0 \quad . \tag{5c}$$

N_U is related to the density measured in the laboratory frame, N_o, by

$$N_U = \frac{N_o \gamma_u}{\Gamma} \quad , \tag{6}$$

where $\gamma_u = (1-u^2(r)/c^2)^{-1/2}$, $\Gamma = (1 - \frac{v_o^2(r)}{c^2})^{-1/2}$, and $u(r)$, $v_o(r)$ are the velocity profiles in the wave and laboratory frames, respectively, as $z \to \pm \infty$. For the charge-neutralized case, in which the plasma column is stationary in the laboratory frame, $u(r) = -U$. Also for this case, we shall choose N_o to be constant, $N_o(r) = N_o$ for $0 < r < a$, and ϕ_U, the equilibrium potential, is obviously zero.

For the case of a solitary wave on an unneutralized beam we shall assume that all the electrons are injected into the drift tube with the same energy $\gamma_o mc^2$, measured in the laboratory frame. Then $u(r)$ is obtained from the conservation of energy and the relativistic addition of velocities:

$$(1 - \frac{v_o^2(r)}{c^2})^{-1/2} - \frac{e\phi_o(r)}{mc^2} = \gamma_o \quad , \tag{7a}$$

$$u(r) = \frac{v_o(r) - U}{1 - v_o(r)\frac{U}{c^2}} \quad . \tag{7b}$$

$\phi_o(r)$, the equilibrium potential in the laboratory frame, is obtained from the beam density profile. If we choose a constant profile $N_o(r) = N_o$, $0 < r < a$, in the laboratory frame, then $\phi_o(r)$ is given by

$$\phi_o(r) = \pi N_o e[r^2 - a^2 + 2a^2 \log \frac{a}{b}] \ , \tag{8}$$

for $0 < r < a$.

Proceeding with the derivation, we integrate Eqs. (4a) and (4b) to get

$$nv = N_U u \ , \tag{9a}$$

$$\gamma mc^2 - e\phi = \gamma_u mc^2 - e\phi_U \ . \tag{9b}$$

Solving Eq. (9b) for v and substituting into Eq. (9a) we get

$$n = N_U \frac{u}{c} \left[1 - \left(\gamma_u + \frac{e(\phi - \phi_U)}{mc^2} \right)^{-2} \right]^{-1/2} \ . \tag{10}$$

Poisson's equation then gives the following nonlinear equation for the perturbed potential $\tilde{\phi} = \phi - \phi_U$:

$$\nabla^2 \tilde{\phi} = 4\pi e N_U \left[\left(1 - \left(\gamma_u + \frac{e\tilde{\phi}}{mc^2} \right)^{-2} \right)^{-1/2} \frac{u}{c} - 1 \right] \ . \tag{11}$$

For periodic waves, one cannot in general refer to an unperturbed region of the beam, as in Eqs. (5a) and (5b), to specify the boundary conditions, because of the presence of an excitation region with unknown time-varying fields. This will be discussed further in Sec. IV C.

III. WEAKLY NONLINEAR ANALYSIS

For future reference, we present here the weakly nonlinear analysis of space charge waves on a neutralized plasma column[4] ($\phi_o \equiv 0$). We shall consider only the nonrelativistic version of Eq. (11), and apply it to the stationary plasma column (Fig. 1) with a = b. Thus,

$$\nabla^2\tilde{\phi} = 4\pi e N_o\left[\left(1 + \frac{2e\tilde{\phi}}{mU^2}\right)^{-1/2} - 1\right] \equiv R[\tilde{\phi}] \ . \tag{12}$$

If we consider only axi-symmetric solutions, the radial dependence of $\tilde{\phi}$ can be expanded in the complete set of functions $J_o(k_{\perp_p} r)$, where $k_{\perp_p} a = \lambda_p$ are the zeroes of J_o:

$$\tilde{\phi} = \sum_{p=1}^{\infty} f_p(z)\, J_o(k_{\perp_p} r) \ , \tag{13}$$

where the $f_p(z)$ are determined by the coupled, nonlinear differential equations,

$$\left(\frac{d^2}{dz^2} - k_{\perp_p}^2\right) f_p = \frac{\int_0^a r dr\, J_o(k_{\perp_p} r) R\left[\sum_{i=1}^{\infty} f_i\, J_o(k_{\perp_i} r)\right]}{\int_0^a r dr\, J_o^2(k_{\perp_p} r)} \ . \tag{14}$$

$R[\tilde{\phi}]$ represents the right-hand side of Eq. (12). If the wave amplitude is not large and dispersion is small, the wave velocity is close to the linear, dispersionless value $\omega_e/k_{\perp_p}$ [cf. Eq. (2)]. Thus the strongly coupled modes are those with the same value of $k_{\perp_p}$. Different radial modes have appreciably different linear velocities, especially the lowest order ones. Thus, for small amplitude solutions with few radial zeros, one of the f_p will dominate, and the solutions will be either periodic or soliton-like, as in the one-dimensional case.

Expanding $R[\tilde{\phi}]$ to second order in $e\tilde{\phi}/mU^2$ gives

$$R[\tilde{\phi}] \simeq \omega_e^2[-\frac{\tilde{\phi}}{U^2} + \frac{3}{2}\frac{e\tilde{\phi}^2}{mU^4}] \ , \tag{15}$$

where ω_e is the electron plasma frequency. Using the weak radial-mode coupling to write $\tilde{\phi} \simeq f_1 J_o(k_{\perp 1} r)$ for the p=1 solution, Eq. (14) gives

$$\frac{d^2 f_1}{dz^2} = (k_{\perp 1}^2 - \frac{\omega_e^2}{U^2}) f_1 + \frac{3}{2}\frac{e\omega_e^2}{mU^4}\alpha f_1^2 \ , \tag{16}$$

where $\alpha = \int_0^a J_o^3(k_{\perp 1} r) r dr [\int_0^a J_o^2(k_{\perp 1} r) r dr]^{-1} \simeq 0.72$. We normalize Eq. (16) as follows: $\hat{z} = k_{\perp 1} z$; $f_1 = \frac{m}{e}\frac{\omega_e^2}{k_{\perp 1}^2}\hat{f}_1$; $U = M\frac{\omega_e}{k_{\perp 1}}$; where M is the "Mach number". Equation (16) then yields,

$$\frac{d^2 \hat{f}_1}{d\hat{z}^2} = (1 - \frac{1}{M^2})\hat{f}_1 + \frac{3}{2}\frac{\alpha}{M^4}\hat{f}_1^2 \ . \tag{17}$$

This has a soliton-like solution,

$$\hat{f}_1 = -2\delta M \alpha^{-1} \mathrm{sech}^2[\hat{z}(\delta M/2)^{1/2}] \ , \tag{18}$$

where we have set $M = 1 + \delta M$ and assumed $\delta M \ll 1$. Thus, for small amplitudes, the nonlinear velocity increase is proportional to the amplitude. Periodic traveling wave solutions of Eq. (17) can also be obtained in terms of elliptic functions, but will not be given here.

IV. RESULTS AND DISCUSSION

A. Plasma Cylinder - Solitary Waves

Equation (12) was solved for neutralized electrons with a=b (cf. Fig. 1). Figure 2 is a plot of Mach number (M) versus the amplitude of the potential at r=z=0. Interestingly, this plot turns out to be almost exactly linear except near the breaking amplitude. The weakly nonlinear analysis predicts this linearity only for very small amplitudes, $k_{\perp 1}^2 e/(m\omega_e^2)\tilde{\phi} \lesssim 0.1$ [in general it predicts that the amplitude is proportional to $M^2(M^2 - 1)$]. The numerical results are seen to agree with theory in this regime.

A breaking amplitude ϕ_b can be defined by $e\phi_b = \frac{m}{2}(\omega_e/k_{\parallel 1})^2 M^2$, the kinetic energy of an electron in the soliton frame. The largest amplitude solution obtained was 0.95 ϕ_b at M = 1.23. Figures 3 and 4 compare the analytical, weakly nonlinear solution to the numerical one at this amplitude. At the wave-breaking amplitude, electrons traveling along r=0 (center of the cylinder) come to a stop at z = 0, i.e. at the center of the soliton, and the density goes to infinity at this point. The analytical result does not show this singularity due to the approximation made in Eq. (15). Figure 4 shows that the density profile is very spiked at M = 1.23, and the numerical method begins to fail. Up to an amplitude of at least 0.9 ϕ_b, however, the amplitude changes by less than 1% on doubling the number of grid-points.

Figure 5 compares the radial dependence of the potential at M = 1.23, normalized to unity, to the Bessel function J_o. The close agreement between the two curves shows that radial mode-coupling is a small effect even near the breaking amplitude.

B. Unneutralized Electron Beam - Solitary Waves

We shall now discuss solitary wave solutions to Eq. (11) for a unneutralized beam. The total current of such a beam is commonly specified as a fraction of

the maximum or limiting current I_L. This maximum is due to the self-field of the beam [cf. Eq. (8)]. Assuming, as before, that the electrons all have the same total energy $\gamma_o mc^2$, Eq. (7a) gives the electron velocity profile $v_o(r)$. With $\phi_o(r)$ given by Eq. (8), we find

$$I(N_o) = \int_0^a N_o e v_o(r) 2\pi r dr$$

$$= I_o \left\{ \sqrt{y_1^2 - 1} - \cos^{-1} \frac{1}{y_1} - \sqrt{y_2^2 - 1} + \cos^{-1} \frac{1}{y_2} \right\} , \tag{19}$$

where

$$y_1 = \gamma_o + \frac{\pi N_o e^2 a^2}{mc^2} \left(1 - \frac{g^2}{a^2}\right) ,$$

$$y_2 = \gamma_o - \frac{\pi N_o e^2 g^2}{mc^2} ,$$

$$g^2 = a^2 \left(1 - 2 \log \frac{a}{b}\right) ,$$

and

$$I_o = mc^3/e .$$

Equation (19) is plotted against $e|\phi_o(0)|/mc^2$ for $\gamma_o = 1.49$ (250 keV electrons), and $a/b = 0.44$ in Fig. 6. The limiting current I_L occurs in this case at $e|\phi_o(0)|/mc^2 = .417$, i.e., $\phi_o(0) = -213$ kV.

For collective ion acceleration, one is interested in the slow space-charge wave on the beam.[1,2] A general proof due to Godfrey[5] shows that the linear phase velocity of long-wavelength waves (the slowest ones at a given frequency) goes to zero only at the limiting current. Furthermore, the dependence of the phase velocity on the current is $(I - I_L)^{1/2}$. This makes it difficult to reduce the phase velocity enough to load ions easily.[6] The results presented below show that nonlinearity can cause a significant reduction in the phase velocity of slow space-charge solitons.

Equation (11) was solved for $\frac{a}{b} = .44$ with currents in the range $.5I_L$ to $.97\ I_L$, and electrons injected at 250 keV. The results are shown in Figs. 7 and 8. Two things are striking. First, it is possible to have solitons with $U \leq 0$ (i.e., traveling backwards in the laboratory frame) without exceeding I_L. Second, there is a sizeable change in velocity as the amplitude increases: at $I = .9I_L$, a value which is readily attained in experiments, the velocity decreases to almost half the small amplitude value before the wave breaks. At $.5I_L$, the change is much less. In Fig. 8, the amplitude at which wave-breaking occurs is marked by an x. Figure 9 shows how the half-width of the potential solution narrows as the amplitude grows. This curve is not very sensitive to the current.

C. Unneutralized Electron Beam - Periodic Waves

We now consider periodic traveling wave solutions to Eq. (11). In the case of solitons, the quantity u(r) in Eq. (11) is specified by the unperturbed equilibrium. In the case of an infinite periodic wave train however, there is a fundamental difficulty in specifying this quantity. In particular, u(r) will depend on the exact process of excitation of the wave. For example, in collective ion acceleration schemes, the wave is initiated by passing the beam through a region adjacent to a periodic array of resonant structures. The interaction of the negative energy slow space-charge wave on the beam with these structures then leads to wave-growth. The total particle energy flux decreases by the amount required to set up the energy flux of the wave, so the electron energy is no longer $\gamma_b mc^2$ along each field-line. On the other hand, in the case where the wave is stationary in the laboratory frame, energy conservation holds through the growth region. Stationary waves are particularly interesting because they could be excited without any growth section, in the process of beam injection at the diode and cause a nonuniform equilibrium in the drift tube. Figure 10 shows two stationary wave solutions at $I = .97\ I_L$. As the wavelength decreases, the peaks become more and more

isolated from each other, and one approaches the soliton limit.

To treat nonlinear periodic waves with a nonzero velocity, we shall continue to use the u(r) obtained from Eqs. (7a) and (7b). This is not self-consistent, but we expect the results to yield a good qualitative indication of what happens for the following reasons. As the wave amplitude decreases, the error made in assuming energy conservation along field-lines through the growth region gets smaller. Also, if the wave phase velocity U becomes zero at a large amplitude, then the assumed u(r) is again correct at this amplitude. Thus, the result is justified for both small amplitude and for one particular large amplitude. Figure 11 shows results at $I = 0.95\ I_L$ and $0.97\ I_L$, with $\gamma_0 = 1.49$, $\frac{a}{b} = 0.421$, and $\frac{\lambda}{b} = 0.3$ and 0.55 (λ is the wavelength in the z-direction). The behavior is very similar to that of solitons at these currents. Currents near $0.95\ I_L$ should be attainable experimentally, so that these results are encouraging for collective ion acceleration schemes.

V. CONCLUSIONS

We have obtained numerical solutions for slow space-charge solitons and periodic waves on neutralized and unneutralized, strongly magnetized electron beams. We have also compared numerical results for solitons in a neutral plasma with the predictions of weakly nonlinear theory. With reference to the possibility of collective ion acceleration by space waves[1,2], our electron beam results show that it may be possible to have space-charge waves with phase velocities slow enough to allow ion loading with significantly reduced ion preacceleration requirements.

VI. ACKNOWLEDGEMENTS

We thank Professor J. A. Nation for helpful discussion. This work was supported by the U.S. Air Force and by the National Science Foundation.

VII. APPENDIX

Numerical Technique.

Equation (11) is not straightforward to solve numerically. Iterative methods[7] based on the receipe $\nabla^2\tilde{\phi}_{n+1} = R(\tilde{\phi}_n)$ yield only $\tilde{\phi} = 0$ as a solution even for "good" trial functions. Writing Eq. (11) in the form for Newton iteration[8] gives,

$$\nabla^2\tilde{\phi}_{n+1} - R'(\tilde{\phi}_n)\tilde{\phi}_{n+1} = R(\tilde{\phi}_n) - R'(\tilde{\phi}_n)\tilde{\phi}_n \ , \qquad (20)$$

where the prime denotes the derivative of the function. The operator on the left-hand side of Eq. (20) is neither positive nor negative definite, so that standard iterative methods[7] are not guaranteed to work (and did not work) on this linear equation. We have found that Gaussian elimination[9] can be used to provide solutions to Eq. (20) provided special programming is done to take advantage of the small bandwidth of the matrix. No pivoting was necessary, and up to 2060 grid-points were used. Equation (20) was solved successively until the error in the solution of the original nonlinear equation was acceptably small. The error measure used was

$$\varepsilon^2 = \frac{\sum_{i,j} \left\{ \nabla^2_{ij}\phi_{ij} - R(\phi_{ij}) \right\}^2}{\sum_{i,j} \left\{ |\nabla^2_{ij}\phi_{ij}| + |R(\phi_{ij})| \right\}^2} \ , \qquad (21)$$

where ∇^2_{ij} denotes the five-point discretization of the Laplacian. $\varepsilon < 10^{-7}$ was required for an acceptable solution. On average, about seven iterations were required to satisfy this criterion.

VIII. REFERENCES

1. P. Sprangle, A. T. Drobot, and W. M. Manheimer, Phys. Rev. Lett. 38, 1180 (1976).

2. G. Gammel, J. A. Nation and M. E. Read, Bull. Am. Phys. Soc. 21, 1184 (1976); G. Gammel, J. A. Nation and M. E. Read, J. Appl. Phys. 50, (9) (1979).

3. V. I. Kurilko and A. P. Tolstoluzhskii, Zh. Tekh. Fiz. 44, 1418 (1974) [Sov. Phys. Tech. Phys. 19, 887 (1975)].

4. H. Ikezi, P. J. Barrett, R. B. White and A. Y. Wong, Phys. Fluids 14, 1997 (1971).

5. B. B. Godfrey, IEEE Trans. Plas. Sci. PS-6, 380 (1978).

6. R. J. Briggs, Phys. Fluids 19, 1257 (1976).

7. R. S. Varga, Matrix Iterative Analysis (Prentice-Hall, New Jersey, 1962).

8. J. M. Ortega and W. C. Rheinbolt Iterative Solution of Nonlinear Equations in Several Variables (Academic Press, New York, 1970).

9. G. W. Stewart, Introduction to Matrix Computations (Academic Press, New York, 1973).

IX. FIGURE CAPTIONS

Fig. 1. Region I: plasma or beam, and region II: vacuum.

Fig. 2. (a) numerical, and (b) analytic results for the Mach number M versus normalized amplitude of the potential at r = 0, z = 0 [$\tilde{\phi}_{max} \equiv \tilde{\phi}(0,0)$]. The x marks the breaking amplitude.

Fig. 3. Profiles at (a) r = 0, and (b) z = 0 of the (1) analytic, and (2) numerical solution for the perturbed potential at M = 1.23. $k_{\perp 1} = \lambda_1/a$, where $\lambda_1 \tilde{=} 2.4$ is the first zero of the Bessel function J_o.

Fig. 4. Profiles at (a) r = 0, and (b) z = 0 of the (1) analytic, and (2) numerical solution for the density at M = 1.23.

Fig. 5. (a) $J_o(r)$. (b) Radial dependence of numerical solution for perturbed potential at z = 0, normalized to unity, for M = 1.23.

Fig. 6. Current versus the radial well-depth $|\phi_o(r = 0)|$. The limiting current is indicated. $I_o \equiv mc^3/e$.

Fig. 7. Soliton velocity versus perturbed potential amplitude at r = 0, z = 0 (center of soliton). The amplitude is normalized to the radial well-depth, $\phi_o(0)$. The x's mark the breaking amplitudes.

Fig. 8. Longitudinal and radial profiles of perturbed potential and perturbed density, normalized to unity, for $\tilde{\phi}_{max}/\phi_o = 0.16$ [curves (a) and (b)] and $\tilde{\phi}_{max}/\phi_o = 0.35$ [curves (c) and (d)]. $I/I_L = 0.95$ for both cases.

Fig. 9. Axial half-width of the perturbed soliton potential, Δ, normalized to the tube radius b, versus $|\tilde{\phi}_{max}|$. Δ is defined by $2\tilde{\phi}(0,\Delta) = \tilde{\phi}(0,0)$.

The curve is very nearly the same for the three currents considered, $I/I_L = 0.9, 0.95, 0.97$.

Fig. 10. Perturbed potential at r = 0, normalized to unity, for periodic waves with U = 0. λ is the wavelength in the z-direction and $I/I_L = 0.97$.

Fig. 11. Phase velocity versus amplitude for periodic waves with $\lambda/b = .3$ (solid curves) and $\lambda/b = .55$ (dashed curves).

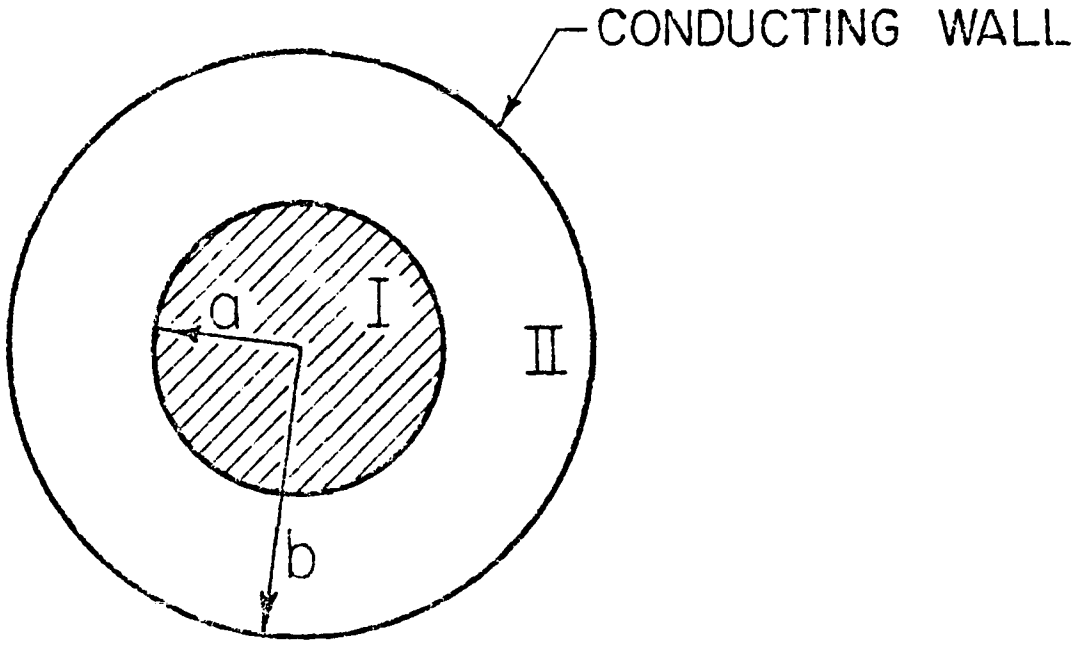

FIG. 1

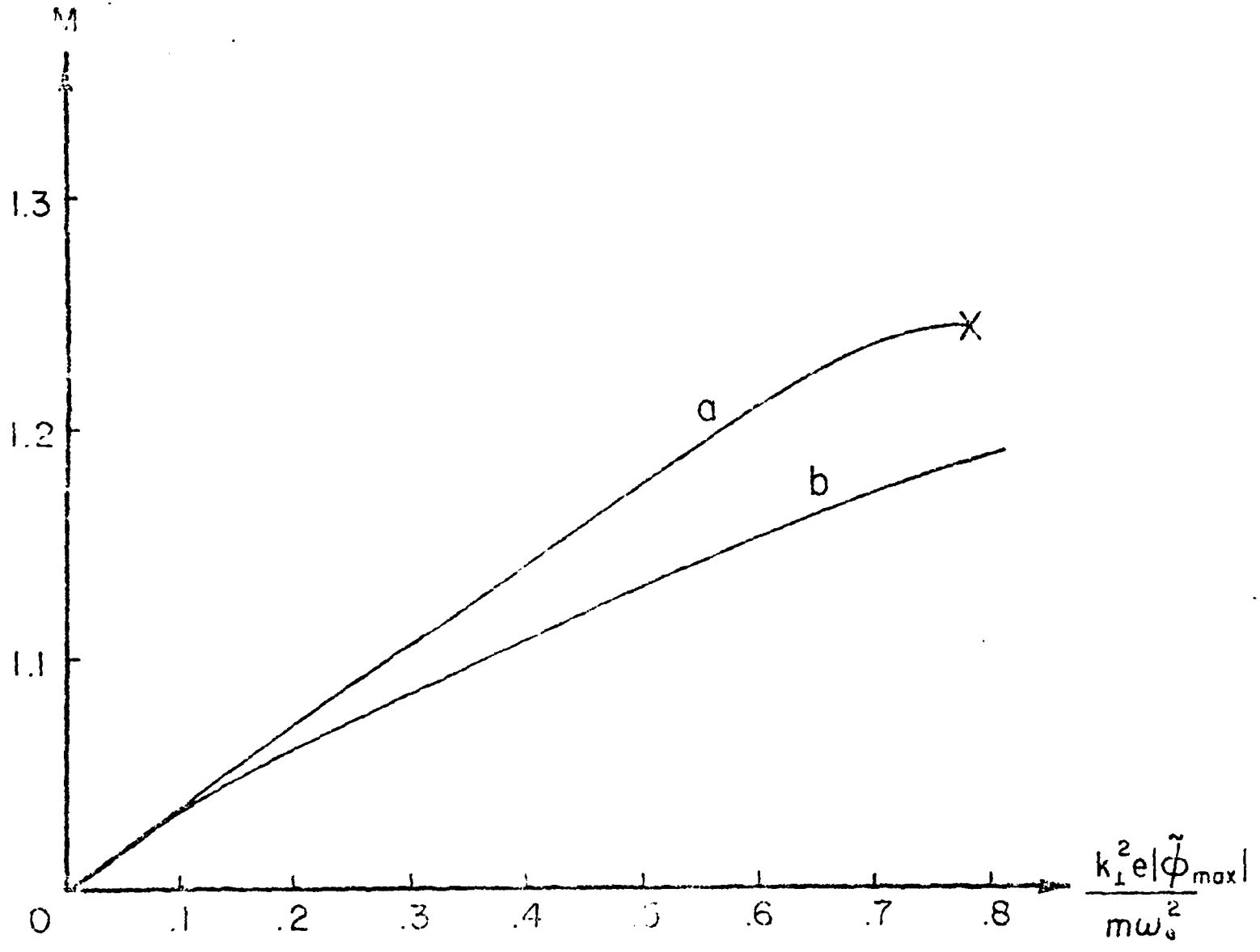

FIG. 2

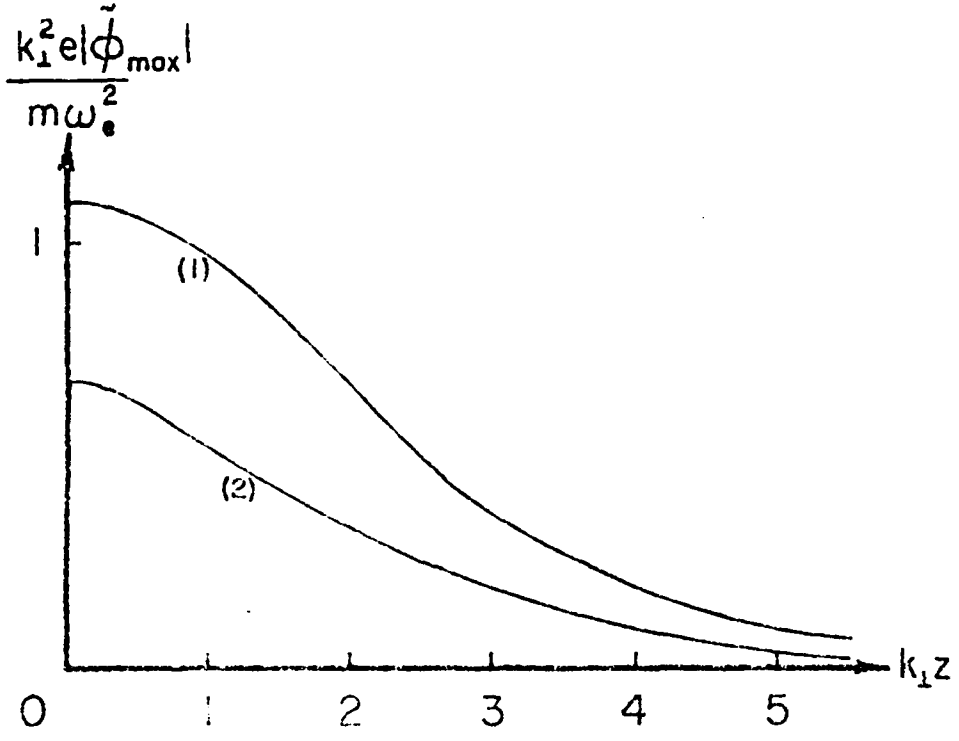
$\frac{k_\perp^2 e|\tilde{\phi}_{max}|}{m\omega_e^2}$
1
(1)
(2)
$k_\perp z$
0
1
2
3
4
5

(a)

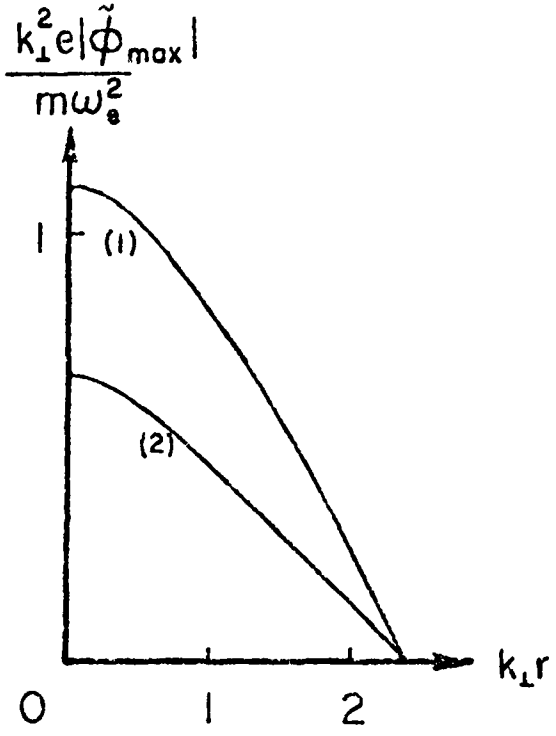
$\frac{k_\perp^2 e|\tilde{\phi}_{max}|}{m\omega_e^2}$
1
(1)
(2)
$k_\perp r$
0
1
2

(b)

FIG. 3

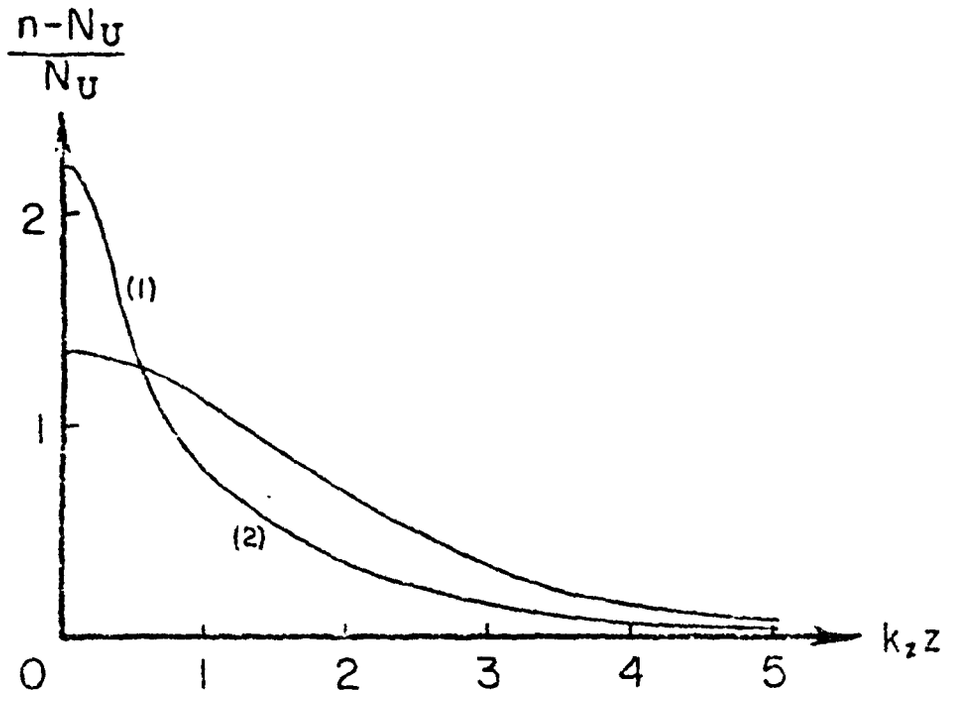

(a)

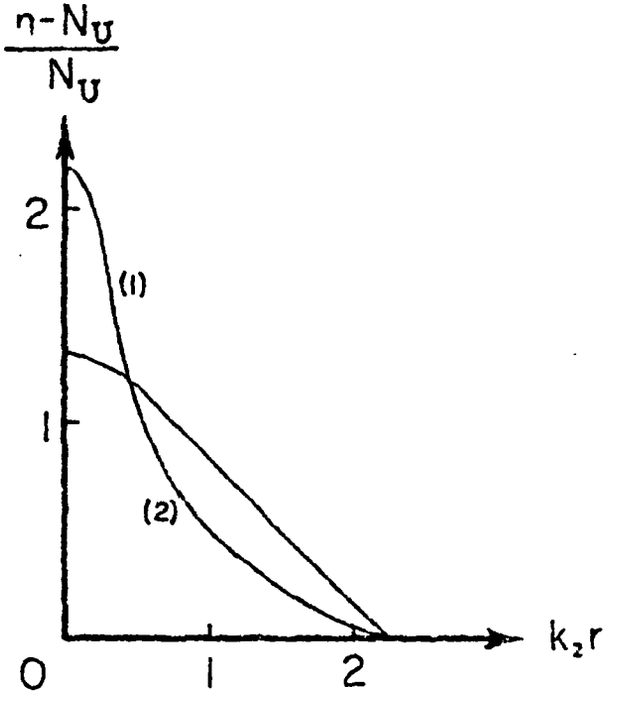

(b)

FIG. 4

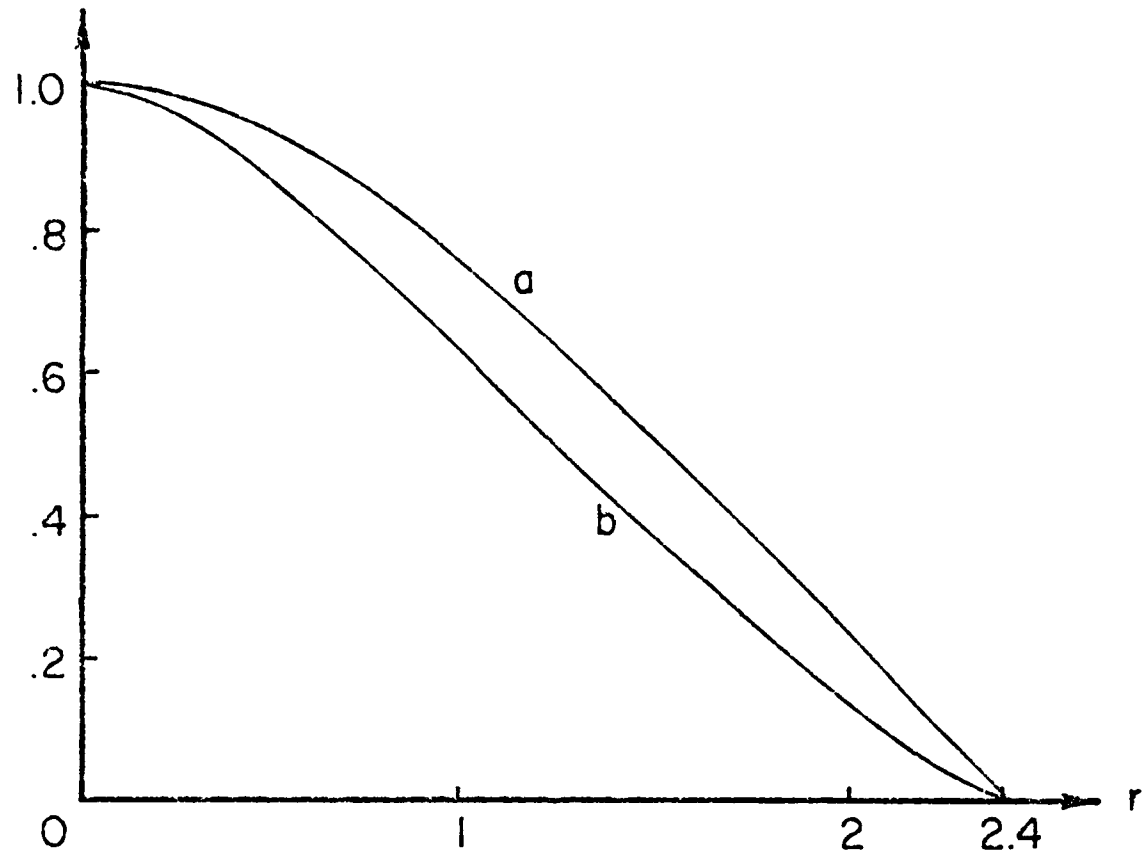

FIG. 5

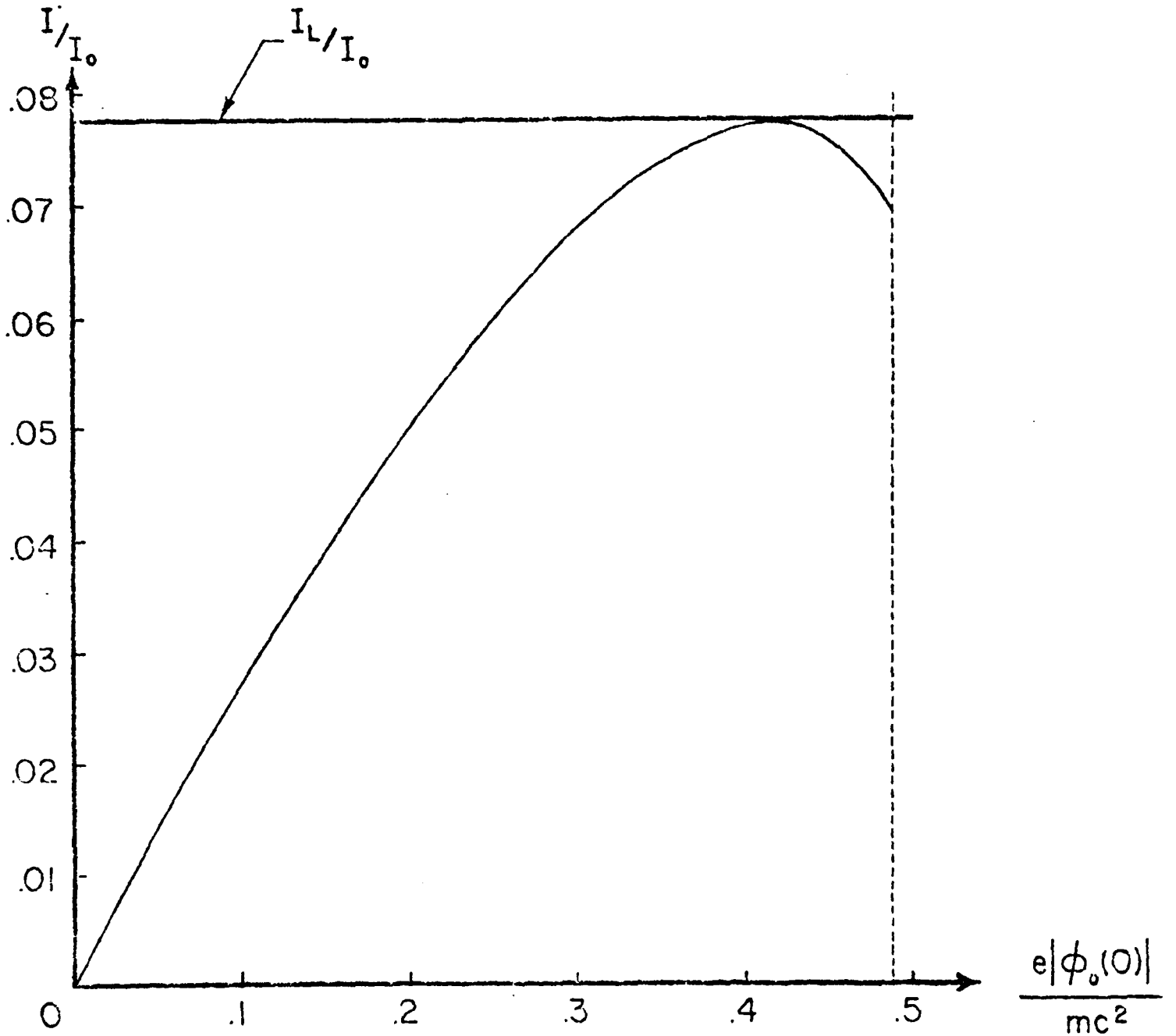

FIG 6

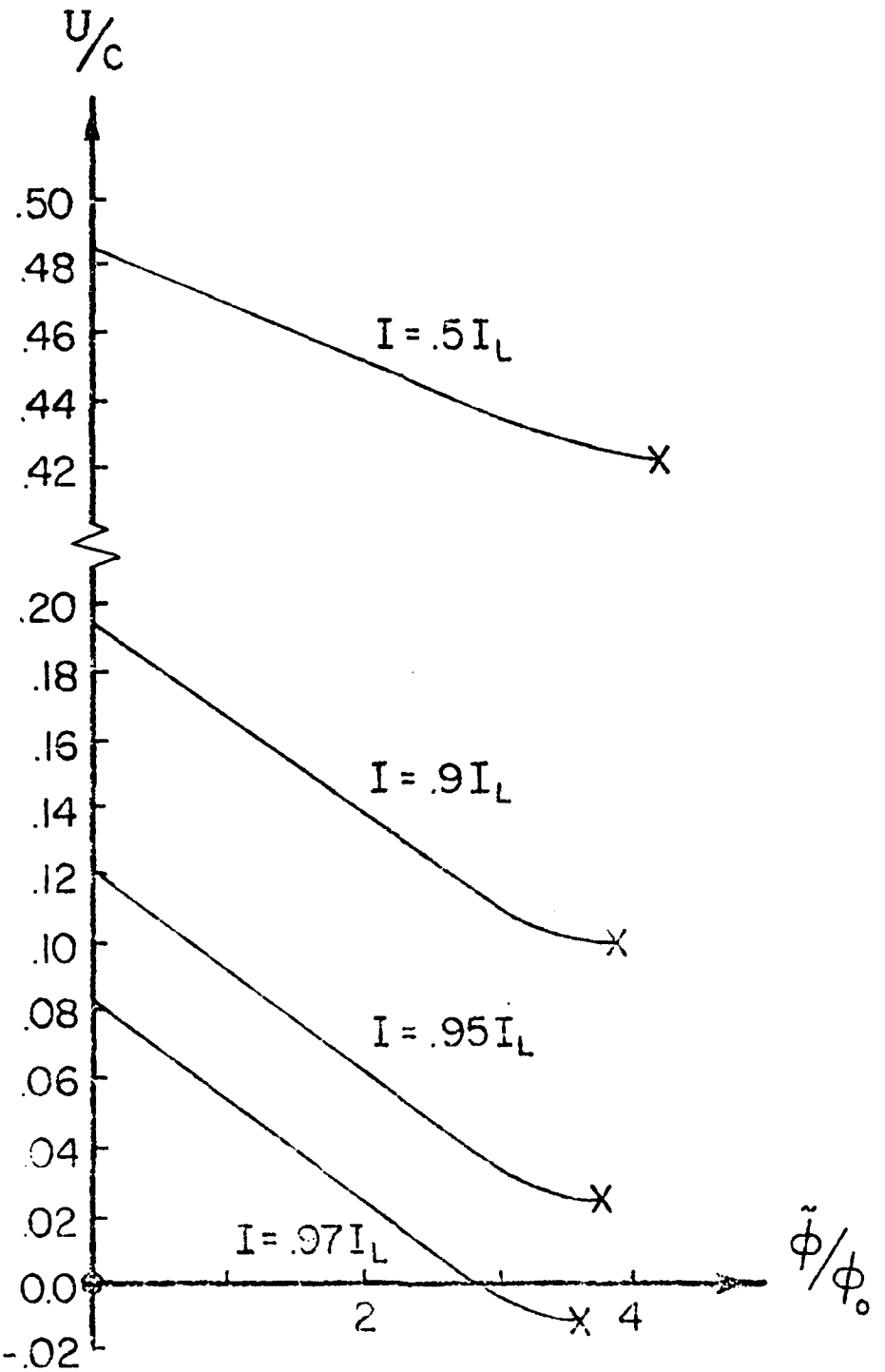
U/c
.50
.48
.46
.44
.42
.20
.18
.16
.14
.12
.10
.08
.06
.04
.02
0.0
-.02
I = .5 I_L
I = .9 I_L
I = .95 I_L
I = .97 I_L
2
4
φ̃/φ_o

FIG. 7

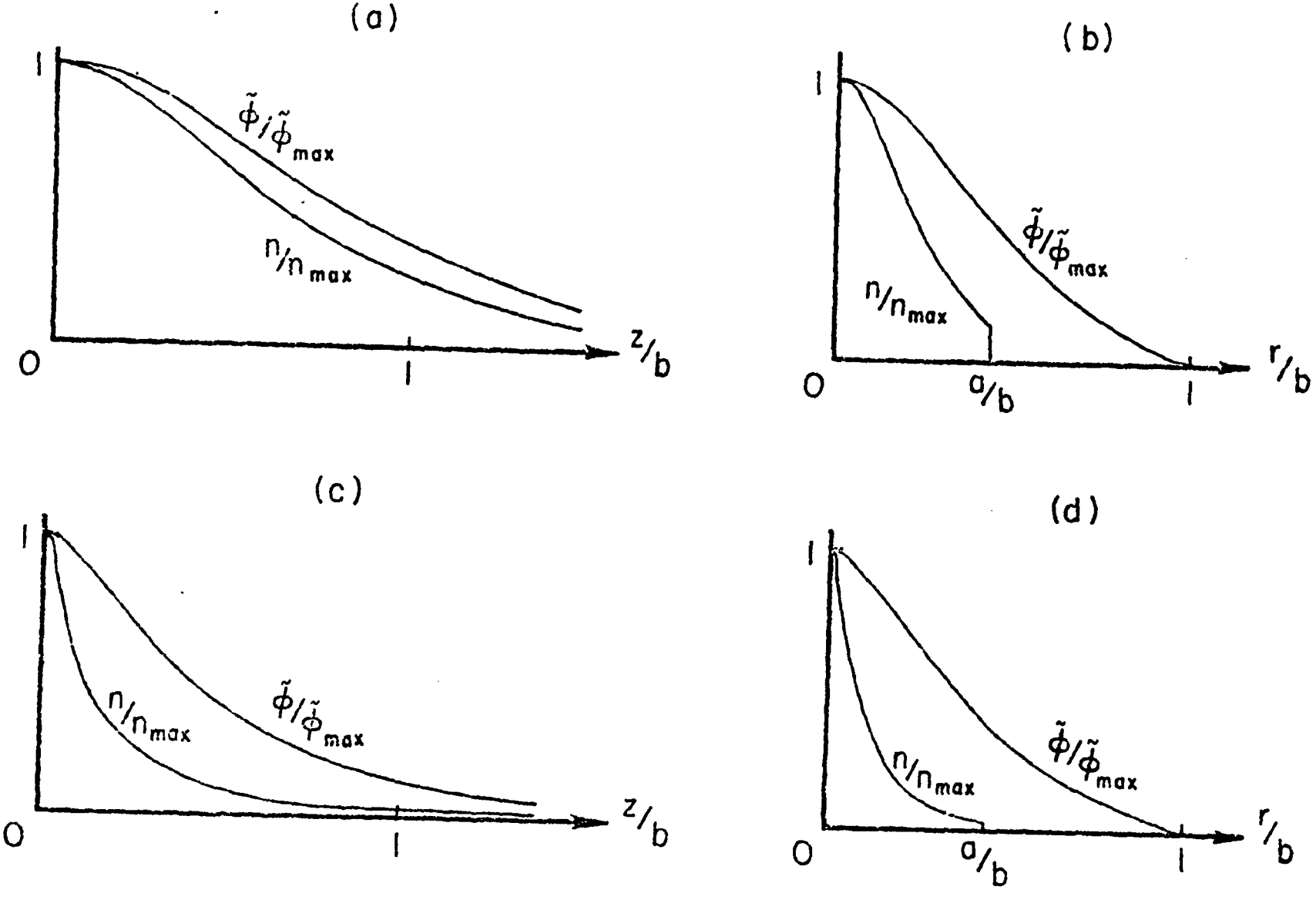
(a)
1
$\tilde{\phi}/\tilde{\phi}_{max}$
n/n_{max}
0
1
z/b
(b)
1
$\tilde{\phi}/\tilde{\phi}_{max}$
n/n_{max}
0
a/b
1
r/b
(c)
1
n/n_{max}
$\tilde{\phi}/\tilde{\phi}_{max}$
0
1
z/b
(d)
1
n/n_{max}
$\tilde{\phi}/\tilde{\phi}_{max}$
0
a/b
1
r/b

FIG. 8

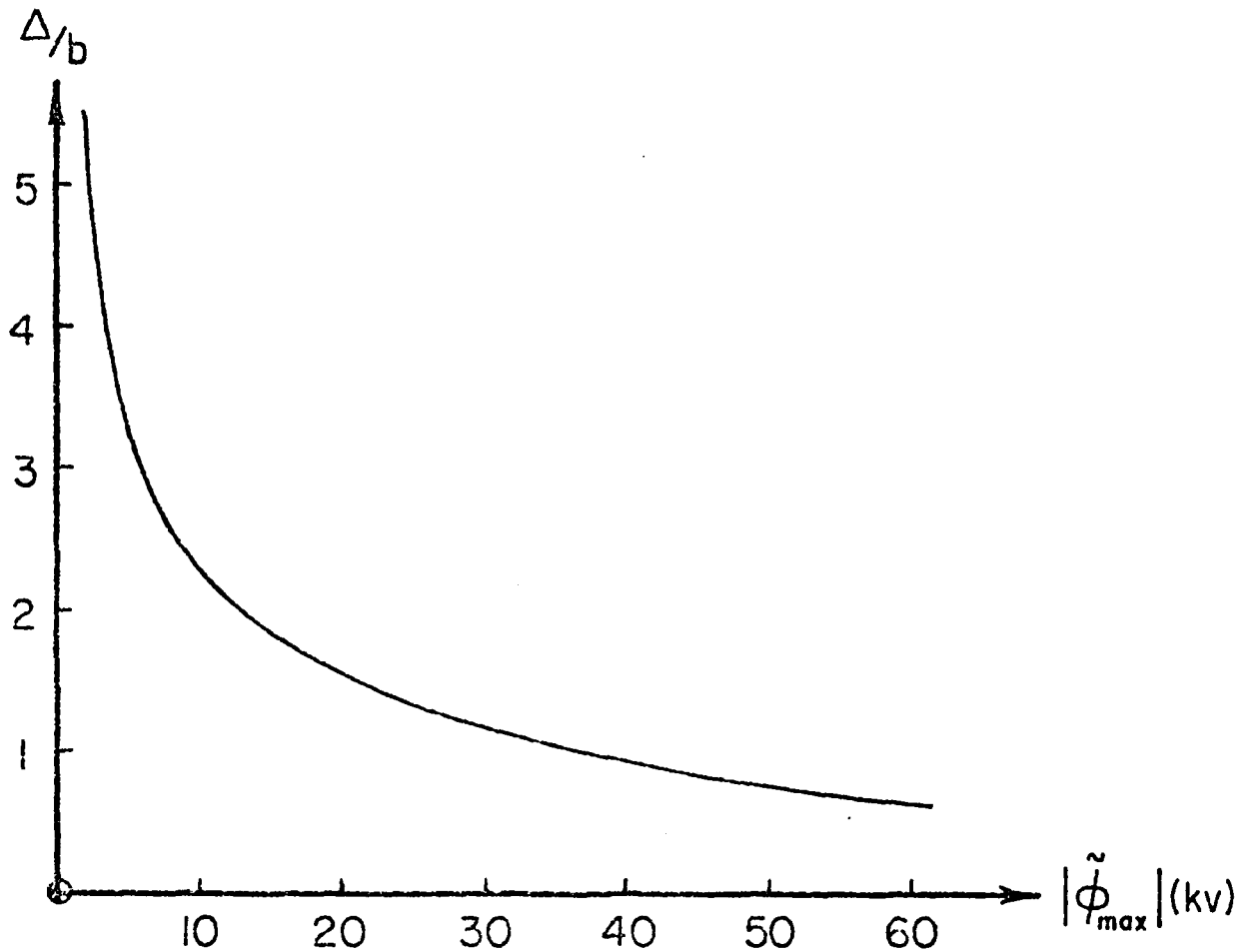

FIG. 9

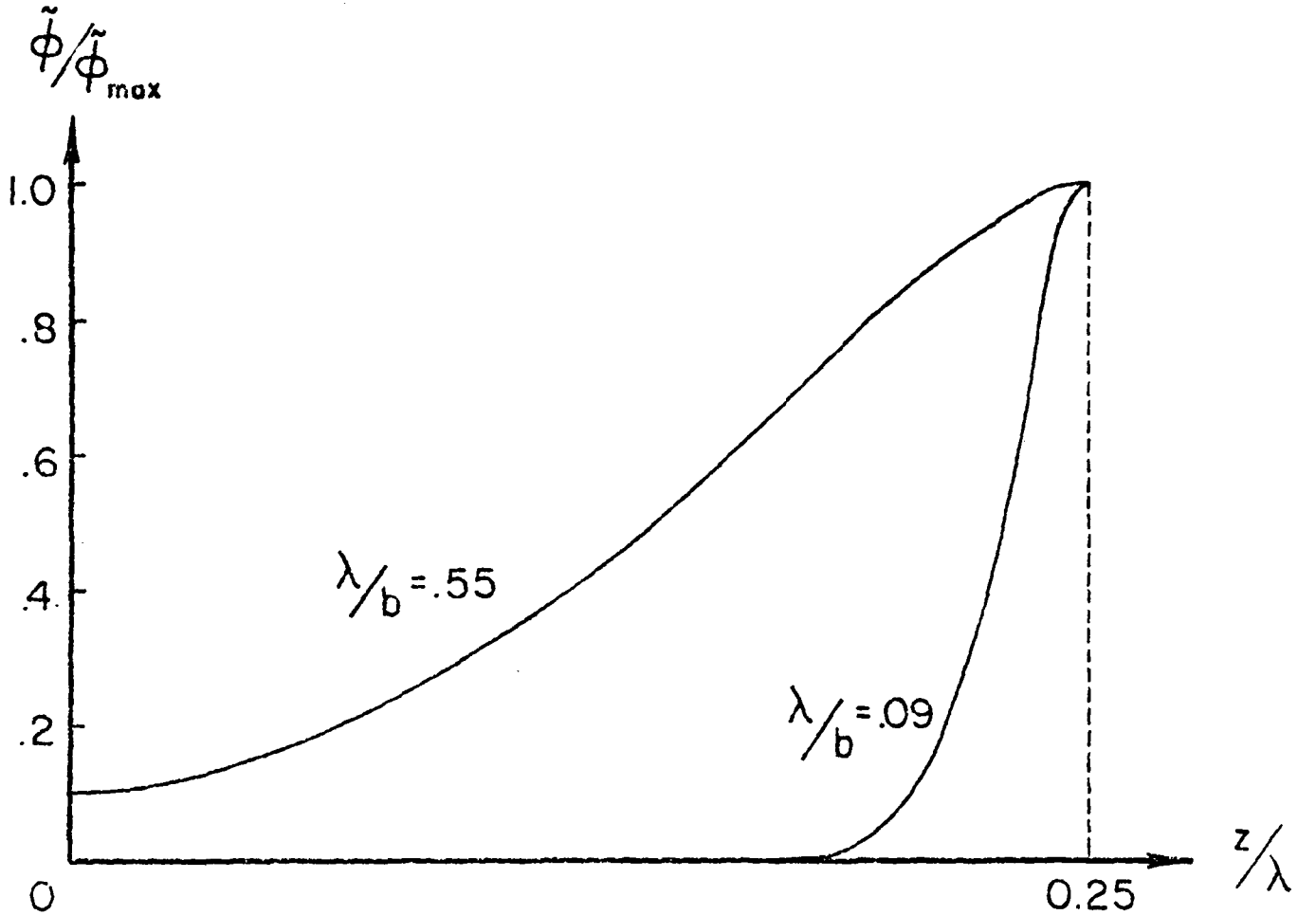
$\tilde{\phi}/\tilde{\phi}_{max}$
1.0
.8
.6
.4
.2
0
$\lambda/b = .55$
$\lambda/b = .09$
0.25
z/λ

FIG. 10

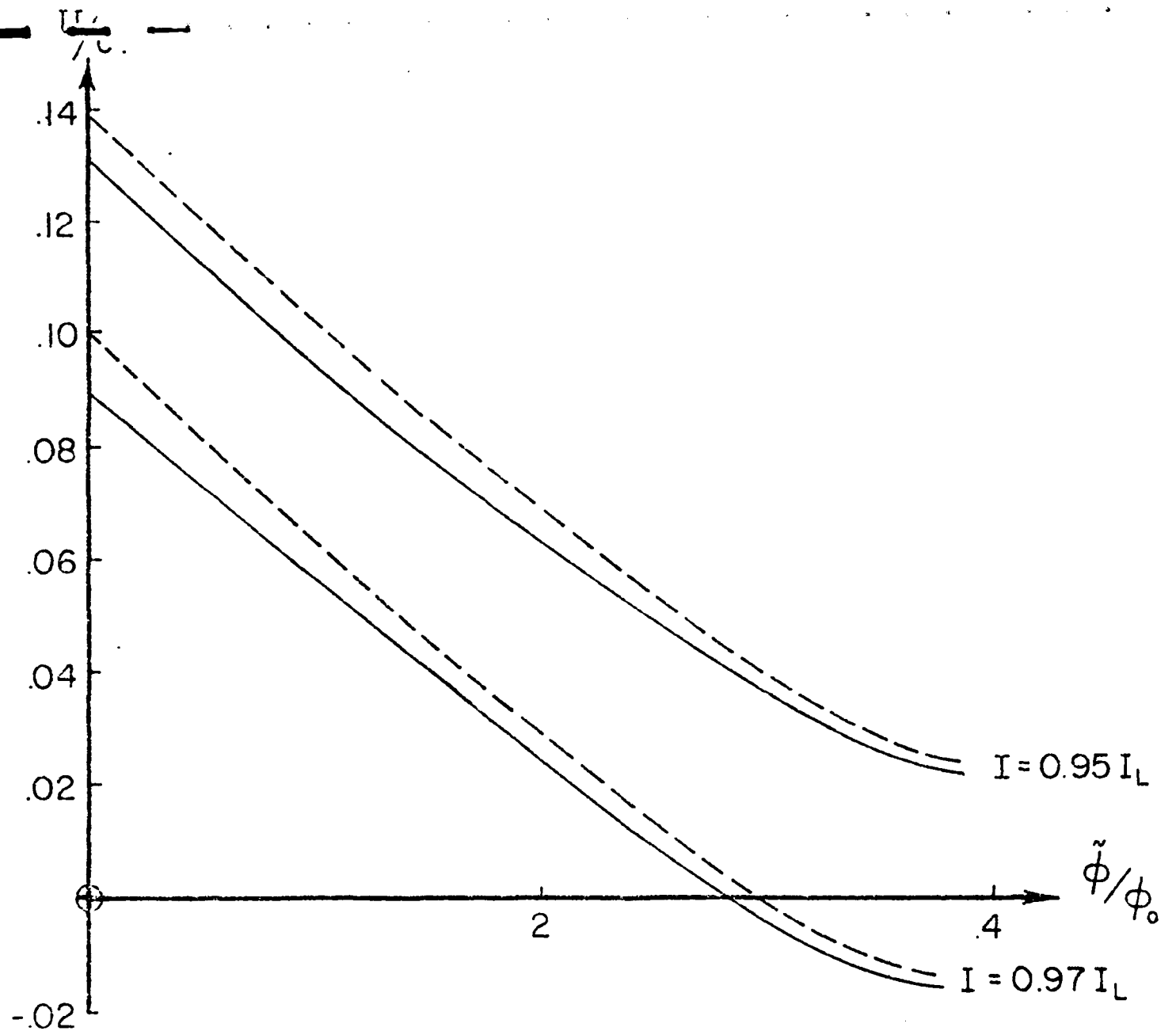

FIG. 11

Physics of Fluids 23, 324, (1980)

#8

Magnetic Shear Stabilization of the Diocotron Modes of a Relativistic Electron Beam

E. Ott and J.-M. Wersinger

Laboratory of Plasma Studies

Cornell University

Ithaca, New York 14853

Abstract

The stability of the diocotron modes of an annular, relativistic, unneutralized, electron beam is examined when the guide magnetic field is sheared. Stabilization results from the reduction in the electron velocity shear. The "low density limit" is found to be a surprisingly good approximation in the case of a slab, nonrelativistic model. The case of an annular relativistic beam propagating in a cylinder is analyzed in this limit. Magnetic shear stabilization is found to be a promising means of obtaining stable beam propagation.

I. Introduction

A basic instability of an unneutralized plasma in propagation along a guide magnetic field $\underset{\sim}{B}$, is the diocotron instability.[1-4] The mechanism driving this instability is the shear in the equilibrium $\underset{\sim}{E} \times \underset{\sim}{B}$ velocity resulting from the spatial dependence of the self-electric field, $\underset{\sim}{E}$, created by the equilibrium charge density. Recently, this instability has been observed[3] on annular relativistic electron beams, leading to beam break-up. For applications (such as collective ion acceleration[5]) in which it is desired to propagate such a beam over relatively long distances, the diocotron instability may be harmful. It is the purpose of the present paper to propose a method for stabilizing this mode. In particular, it is shown that the introduction of shear in the magnetic field lines can stabilize the diocotron instability. For the case of an annular electron beam in an axial guide magnetic field, this can be accomplished by passing a thin current carrying wire down the axis. The combined axial magnetic field and the small azimuthal magnetic field due to the wire current are sheared. Experiments motivated by the analysis to be presented are in progress.[6]

Sections II - IV examine the case of slab geometry with $(V_0/c)^2$ neglected compared to unity (V_0 is the beam injection velocity and c is the speed of light). Section V includes cylindrical and finite $(V_0/c)^2$ effects. Section II presents the basic equations in slab geometry and shows that magnetic shear in conjunction with the finite beam injection velocity leads to a velocity shear component which

AD-A085 312 CORNELL UNIV ITHACA NY LAB OF PLASMA STUDIES F/G 20/7
COLLECTIVE ION ACCELERATION.(U)
1980 J A NATION F44620-75-C-0054
UNCLASSIFIED AFOSR-TR-80-0440 NL

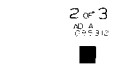

can oppose the destabilizing $\underset{\sim}{E} \times \underset{\sim}{B}$ velocity shear. Section III analyzes the effect of magnetic shear in the "low density limit", obtaining complete results for the case of a constant density beam and a general stabilization condition for arbitrary density profiles. The latter result is based on a quadratic form obtained from the second order ordinary differential eigenvalue equation. In Sec. IV, we examine the conditions for marginal stability of a constant density beam without making the low density approximation. Comparing these arbitrary density results with results obtained from the low density approximation, we find that the low density approximation is good, even when the density is not very low. This provides added confidence in the results of Sec. V which utilizes this approximation to study the effects of cylindrical geometry and finite $(V_0/c)^2$. Section VI summarizes results and presents conclusions.

II. Basic Equation in Slab Geometry

As a model, we consider a planar cold, unneutralized electron beam immersed in a sheared magnetic field with shear length L_s

$$\underset{\sim}{B} = B_0(\underset{\sim}{x}_0 \frac{y}{L_s} + \underset{\sim}{z}_0). \tag{1}$$

The beam is of infinite extent in the x and z directions but is finite in the y direction with thickness 2Δ. These features are illustrated in Fig. 1. The confining magnetic field is strong, i.e., $\omega_p^2 << \omega_c^2$, where $\omega_p^2(y) = e^2 n_0(y)/(\varepsilon_0 m_e)$ is the plasma frequency and $\omega_c = eB_0/m_e > 0$, is the electron-cyclotron frequency.

The equilibrium electric potential ϕ_0, associated with the unneutralized beam is a function of y only and obeys Poisson's equation

$$\frac{d^2\phi_0}{dy^2} = \frac{en_0(y)}{\varepsilon_0} \quad . \tag{2}$$

The y dependent equilibrium electric field $E_y = -d\,\phi_0/dy$ produces an $\underset{\sim}{E} \times \underset{\sim}{B}$ velocity shear, which in turn drives the diocotron instability. In the presence of magnetic shear, as defined in Eq. (1), the equilibrium electron drift velocities are

$$v_{0x} \cong -\frac{1}{B_0}\frac{d\,\phi_0}{dy} + V_0\frac{y}{L_s} \quad ,$$

$$v_{0y} = 0,$$

$$v_{0z} \cong \frac{1}{B_0} \frac{d\phi_0}{dy} \frac{y}{L_s} + V_0, \tag{3}$$

where the beam injection velocity along the magnetic field lines $V_0 \equiv (\underset{\sim}{v}_0 \cdot \underset{\sim}{B})/|\underset{\sim}{B}|$, is taken to be constant, and we have assumed $\Delta << L_s$. We find that, if the shear in v_{0x} created by the magnetic shear opposes the shear in v_{0x} created by the $\underset{\sim}{E} \times \underset{\sim}{B}$ drift, then stability is enhanced.

To obtain the governing wave equation, the cold fluid equations are linearized for density and velocity perturbations around the equilibrium. All velocities are assumed sufficiently nonrelativistic so that the electric field perturbations derive from a potential ϕ. (Relativistic effects are considered in Sec. V.) In order to describe the most unstable case, no z dependence is allowed for the perturbed quantities.[4] A Laplace transform in time and a Fourier transform in x are applied to the linearized equations (i.e., we substitute $\partial/\partial t \equiv s$, $\partial/\partial x \equiv ik$, $\partial/\partial z \equiv 0$), and we define $s_k(y) \equiv s + ik\, v_{0x}(y)$. The components of the linearized momentum equation,

$$s_k \underset{\sim}{v} + v_y \frac{d\underset{\sim}{v}_0}{dy} = \frac{e}{m_e} (\nabla\phi - \underset{\sim}{v} \times \underset{\sim}{B}), \tag{4}$$

are taken along and across the magnetic field lines in the low frequency limit (polarization drifts neglected). It is also assumed that at most $V_0/L_s \sim 0\ (\omega_p^2/\omega_c)$, and terms proportional to ω_p^2/ω_c^2 are neglected when compared to terms of order unity. Furthermore, the weak shear

assumption is made, i.e., $\Delta << L_s$, so that we neglect $(y/L_s)^2$ compared to unity. We then obtain

$$v_y \simeq ik\phi/B_0,$$

$$\nabla\cdot\underset{\sim}{v} \simeq - \frac{e}{m_e} \left(\frac{ky}{L_s}\right)^2 \frac{\phi}{s_k(y)} , \tag{5}$$

which are used in the linearized continuity equation

$$s_k n + v_y \frac{dn_0}{dy} + n_0(\nabla\cdot\underset{\sim}{v}) = 0. \tag{6}$$

Poisson's equation closes the set and yields the following wave equation

$$\frac{d^2\phi}{dy^2} - k^2 \left[1 + \frac{\omega_p^2(y)\,(y/L_s)^2}{s_k^2(y)}\right]\phi = - i \frac{\omega_p^2}{\omega_c} \frac{k\phi}{s_k(y)} \frac{1}{n_0} \frac{dn_0}{dy} . \tag{7}$$

III. Low Density Limit

In this section we analyze the low density case, i.e., we assume that over the entire extent of the beam, $\omega_p^2(y)(y/L_s)^2 s_k^{-2}(y)$ can be neglected in (7). (This assumption will be checked in Sec. IV.) Much of the work on the diocotron instability was done for a sharp boundary, constant density beam. We analyze the stabilization of the diocotron instability by magnetic shear in this case first. We shall then present a more general result valid for smoothly varying density profiles.

A. Sharp Boundary Case

The equilibrium density is

$$n_0(y) = \begin{cases} N \text{ for } -\Delta \leqslant y \leqslant \Delta, \\ 0 \text{ for } |y| > \Delta. \end{cases}$$

In the low density case, the wave equation, Eq. (7), now becomes

$$\frac{d^2\phi}{dy^2} - k^2\phi = -\frac{\omega_p^2}{\omega_c}\frac{ik\,\phi}{s_k(y)}\,[\delta(y+\Delta) - \delta(y-\Delta)], \tag{8}$$

and magnetic shear appears only in $s_k(y)$ through the expression of $v_{0x}(y)$. From (2) and (3) with $n(y)$ constant,

$$v_{0x} = \frac{\omega_p^2}{\omega_c}(\alpha - 1)y, \quad |y| \leqslant \Delta,$$

$$\alpha \equiv \frac{V_0\,\omega_c}{L_s\,\omega_p^2}. \tag{9}$$

Note that the velocity shear can be reversed by magnetic shear provided $\alpha > 1$. We now show that this effect stabilizes the diocotron instability (within the framework of the low density approximation). Equation (8) is solved subject to the boundary conditions: $\phi(\pm\infty) = 0$, continuity of ϕ at $y = \pm\Delta$ and jump conditions on $d\phi/dy$ at $y = \pm\Delta$. The jump conditions are obtained by integration of Eq. (8) across the beam-vacuum interface

$$\phi'(\pm\Delta\mp\varepsilon) - \phi'(\pm\Delta\pm\varepsilon) = -i \frac{\omega_p^2}{\omega_c} \frac{k\phi(\pm\Delta)}{s_k(\pm\Delta)}, \tag{10}$$

where $\phi'(y)$ is the derivative $d\phi/dy$ and ε is an arbitrarily small positive number. The resulting dispersion relation is

$$s = \pm \frac{\omega_p^2}{2\omega_c} \{\exp(-4k\Delta) - [1 + 2k\Delta(\alpha - 1)]^2\}^{1/2}, \tag{11}$$

where k is positive. The diocotron mode is unstable (purely growing) for values of $k\Delta$ such that the square root in Eq. (11) is positive. The unstable domain in $k\Delta$ shrinks and occurs for larger values of $k\Delta$ as α increases from zero to one. When $\alpha > 1$ the mode is stabilized. This is illustrated in Fig. 2.

For practical purposes, it might not be necessary to completely stabilize the diocotron instability, i.e., obtain values of $\alpha > 1$. Indeed, due to the finite length of devices, one can accomodate small growth rates without causing the beam to break up. On the other hand, there are several other stabilizing factors that were not considered

in this section. Amongst them are the presence of conducting walls at finite distances and finite Larmor radius effects which may stabilize short wavelengths which are the only unstable modes when α becomes of order unity. Also, relativistic effects turn out to be stabilizing (see Sec. VI).

A plot of the maximum growth rate as a function of α is presented in Fig. 3. The growth rate s is normalized: $\Omega \equiv 2s\omega_c/\omega_p^2$. From Fig. 3 it is seen that maximum growth rates are reduced by a factor of two for $\alpha = 0.4$ and by a factor of ten for $\alpha = 0.7$. Thus, depending on the experimental conditions, a value of α somewhat less than unity may be sufficient for effective stabilization of the mode.

B. Generalization to an Arbitrary Density Profile

Taking the low density limit of Eq. (7), multiplying it by ϕ^* (complex conjugate of ϕ), and integrating over all y, we obtain

$$\int_{-\infty}^{+\infty} dy\left(\left|\frac{d\phi}{dy}\right|^2 + k^2|\phi|^2\right) = \frac{ike}{\varepsilon_o B_o}\int_{-\infty}^{+\infty} dy|\phi|^2 \frac{[s_r - i(s_i + kv_{0x})]}{|s_k|^2}\frac{dn_0}{dy}, \quad (12)$$

where s_r and s_i are the real and imaginary parts of s, respectively. The imaginary part of (12) is

$$s_r \int_{-\infty}^{+\infty} dy \frac{|\phi|^2}{|s_k|^2}\frac{dn_0}{dy} = 0. \quad (13)$$

Using the assumption $s_r \neq 0$ in (13), the real part of (12) yields

$$\left(\frac{ek^2}{\varepsilon_o B_o}\right)\int_{-\infty}^{+\infty} dy \left(\frac{|\phi|^2}{|s_k|^2}\frac{dn}{dy} v_{0x}\right) = \int_{-\infty}^{+\infty} |d\phi/dy|^2 + k^2|\phi|^2)dy. \quad (14)$$

Consider the case where $n_0(y)$ monotonically increases with y in $y < 0$, reaches a peak at $y = 0$, and monotonically decreases for $y > 0$; then $v_{0x}\, dn_0/dy \lessgtr 0$, if $v_{0x}(y) \gtrless 0$ for $y \gtrless 0$ ($v_{0x}(0) \equiv 0$). In this case, the righthand side of (14) will be negative. The lefthand side of (14), however, is manifestly positive. Thus, in this case, the original assumption $s_r \neq 0$ cannot hold. Hence, for $v_{0x}' > 0$, there can only be stable, purely oscillatory modes, $s_r = 0$.

IV. Arbitrary Density: Analysis of Marginal Stability

A. Marginal Stability Condition

In order to assess the validity of the low density results, we analyze the case of a sharp boundary, constant density beam. In the beam region, the wave equation, Eq. (7), is a Whittaker equation. The eigenvalue problem turns out to be complicated, except at $s = 0$. In the low density case, it is seen from Eq. (11), that $s = 0$ corresponds to the boundary between stability and instability. We shall show subsequently that $s = 0$ also corresponds to marginal stability in the general case. For $s = 0$, Eq. (7) is simply

$$\frac{d^2\phi}{dy^2} - [k^2 - \frac{\omega_p^2}{L_s^2(v'_{0x})^2}]\phi = - \frac{\omega_p^2 \phi}{\omega_c v'_{0x} y} [\delta(y + \Delta) - \delta(y - \Delta)]. \qquad (15)$$

Here, $v_{0x} \equiv v'_{0x} \cdot y$, and from (9), $v'_{0x} \equiv \omega_p^2(\alpha-1)/\omega_c$. Applying the same boundary conditions as in the previous section, it turns out that the eigenfunctions are either odd or even functions of y. The odd mode obeys the eigenvalue equation

$$k\Delta + \kappa\Delta \coth(\kappa\Delta) = - \frac{\omega_p^2}{\omega_c v'_{0x}}, \qquad (16a)$$

and the even mode obeys

$$k\Delta + \kappa\Delta \tanh(\kappa\Delta) = - \frac{\omega_p^2}{\omega_c v'_{0x}}, \qquad (16b)$$

where $\kappa^2 \equiv k^2 - \omega_p^2/(v'_{0x}L_s)^2$. To analyze Eqs. (16a) and (16b), we define

the following normalized quantities: $X \equiv k\Delta$, $\Gamma \equiv V_0/(\omega_p\Delta)$, $\varepsilon \equiv \omega_c\Delta/(\omega_p L_s)$. Using Eq. (9), the $s = 0$ eigenvalue equations become

$$(1 - \varepsilon\Gamma)\{X + [X^2 - (\frac{\varepsilon}{1-\varepsilon\Gamma})^2]^{1/2} \coth[X^2 - (\frac{\varepsilon}{1-\varepsilon\Gamma})^2]^{1/2}\} = 1, \quad (17a)$$

and

$$(1 - \varepsilon\Gamma)\{X + [X^2 - (\frac{\varepsilon}{1-\varepsilon\Gamma})^2]^{1/2} \tanh[X^2 - (\frac{\varepsilon}{1-\varepsilon\Gamma})^2]^{1/2}\} = 1. \quad (17b)$$

Clearly, the low density results must be recovered in the limit $\varepsilon << 1$. To describe velocity shear reversal ($\Gamma\varepsilon > 1$) for $\varepsilon << 1$, we require $\Gamma >> 1$. In order to estimate the validity of the low density results, several values of Γ were tried. Surprisingly, the discrepancy between the exact results and the results in the low density approximation is small for values of Γ as low as 2. This is illustrated in Fig. 4. Consequently, the low density results ought to yield a fairly good assessment of the situation for $\Gamma \gtrsim 2$.

B. Perturbation About $s = 0$

We now proceed to an exapnsion about $s = 0$. This expansion will confirm our claim that $s = 0$ corresponds to marginal stability. We set

$$k = k_0 + \varepsilon k_1 + \varepsilon^2 k_2 + \ldots ,$$

$$s = \varepsilon s_1 + \varepsilon^2 s_2 + \ldots ,$$

$$\phi = \phi_0 + \varepsilon\phi_1 + \varepsilon^2\phi_2 + \ldots , \tag{18}$$

in Eq. (7). Here, the subscript zero denotes quantities evaluated for $s = 0$. In order to define the singular terms of Eq. (7) in the complex y plane for $s \to 0$, we use causality and replace y by $y - i\eta$, where η is a small positive (negative) number if $kv'_{0x} > 0$ ($kv'_{0x} < 0$). Thus,

$$\frac{\omega_p^2 (y/L_s)^2}{(s + ikv'_{0x}y)^2} \to - \frac{\omega_p^2}{(kL_s v'_{0x})^2} \sum_{n=0}^{\infty} \left(\frac{i\,s}{kv'_{0x}}\right)^n \left(\frac{1}{y - i\eta}\right)^{(n+1)}. \tag{19}$$

For example, the denominator for $n = 1$ is

$$\lim_{\varepsilon \to 0} \frac{1}{y - i\eta} \equiv P\,\frac{1}{y} + i\pi\delta(y). \tag{20}$$

Let us write Eq. (7) as

$$L\phi = 0,$$

with

$$L = L_0 + \varepsilon L_1 + 0(\varepsilon^2),$$

$$L_0 \equiv \frac{d^2}{dy^2} - k_0^2\left[1 - \left(\frac{\omega_p}{k_0 L_s v'_{0x}}\right)^2\right] - \frac{\omega_p^2}{\omega_c}\,\frac{[\delta(y+\Delta) - \delta(y-\Delta)]}{\Delta\, v'_{0x}}\,, \tag{21}$$

$$L_1 \equiv -2\, k_0 k_1 + \left(\frac{\omega_p}{v'_{0x} L_s}\right)^2 \frac{2is_1}{k_0\, v'_{0x}} \left[P\,\frac{1}{y} + i\pi\delta(y)\right]$$

$$+ i\,\frac{\omega_p^2}{\omega_c}\,\frac{s_1}{k_0(\Delta v'_{0x})^2}\,[\delta(y+\Delta) - \delta(y-\Delta)].$$

The solvability condition for ϕ_1 yields

$$\int_{-\infty}^{+\infty} dy\ \phi_0^* L_1 \phi_0 = 0. \tag{22}$$

The marginal stability eigenfunction ϕ_o is either even or odd and may be assumed real. Equation (22) yields

$$\left[\left(\frac{\omega_p}{L_s v'_{0x}}\right)^2 \frac{\pi\,\phi_0^2(0)}{|k_0\, v'_{0x}|}\right] s_1 = -\,k_0 k_1 \int_{-\infty}^{+\infty} dy\ \phi_0^2. \tag{23}$$

We now examine separately even and odd marginal stability eigenmodes.

Even modes. For even modes $\phi_0(0) \neq 0$ and Eq. (23) yields a relation between k_1 and s_1

$$s_1 = -\,\frac{k_1}{|k_0|}\left|\frac{v'_{0x}}{\omega_p}\right|^3 (k_0 L_s)^2 f, \tag{24}$$

where $f > 0$,

$$f = \frac{k_0}{\kappa_0}\sinh(2\kappa_0\Delta) + 2k_0\Delta + 1 + \cosh(\kappa_0\Delta).$$

Thus, there is instability (stability) for $k_1 < 0$ ($k_1 > 0$). This is in agreement with the result from the low density case, but now the character of the instability has changed. In particular, in the low density limit, the onset of instability occurs when s^2 changes sign, while here s itself changes sign (and s is real). Also, in the present case the instability is due to the $i\pi\delta(y)$ term, i.e., it results from resonant particles near $y = 0$.

Odd modes. For odd modes $\phi_0(0) = 0$ so that (23) yields $k_1 = 0$, but leaves s_1 undetermined. To determine s_1, we proceed to second order in ε. Equation (7) then becomes

$$L_0\phi_2 + L_1\phi_1 + L_2\phi_0 = 0, \tag{25}$$

and the solvability condition for ϕ_2 is

$$\int_{-\infty}^{+\infty} dy\ \phi_0 L_2 \phi_0 + \int_{-\infty}^{+\infty} dy\ \phi_0 L_1 \phi_1 = 0. \tag{26}$$

In (26) we need only include that part of L_2 which is even in y since the odd part makes no contribution to the integral. The even part of L_2 is

$$s_1^2 \left\{ \frac{\omega_p^2}{\omega_c k_0^2 (\Delta v'_{0x})^3} \left[\delta(y+\Delta) - \delta(y-\Delta)\right] - 3 \left(\frac{\omega_p}{k_0 L_s y}\right)^2 \left(\frac{1}{v'_{0x}}\right)^4 \right\} - 2k_0 k_2.$$

The function ϕ_1 satisfies the order-ε wave equation

$$L_0 \phi_1 + L_1 \phi_0 = 0, \tag{27}$$

which we solve for ϕ_1 by variation of parameters. Since $k_1 = 0$ and $\phi_0(0) = 0$, only the odd part of L_1 contributes to Eq. (26) [cf. Eq. (21)]. Also, note that the inhomogeneous term in (27), $L_1\phi_0$, is even. Thus, the solution of (27) for ϕ_1 can be expressed as the sum of a homogeneous solution and a particular solution which is even. Since only the even part of ϕ_1 contributes to (26) we may drop the odd homogeneous part of ϕ_1 and represent ϕ_1 as

$$\phi_1 = C\, \phi_0^{(e)}(y) + u(y)\phi_0^{(o)}(y), \tag{28}$$

where C is a constant, the superscripts o and e refer to the odd and even homogeneous solutions of $L_0\phi_0 = 0$, and u(y) is an odd function of y. The term $u(y)\phi_0^{(o)}(y)$ is the particular solution of (27). From Eq. (27) we obtain

$$u(y) = -\int_a^y dy' \left[\frac{1}{\phi_0^{(o)}(y')}\right]^2 \int_b^{y'} dy''\, L_1(y'') \left[\phi_0^{(o)}(y'')\right]^2,$$

and the lower limits of integration are a = 0, in order for u(y) to be odd, and b = 0, so that the y' integral does not blow-up. The constant C in Eq. (28) is determined by the condition $\phi_1(\infty) \to 0$. This is accomplished in the following way. The odd part of the operator L_1 is a sum of two terms. The first term gives a contribution to u(y) of the form

$$I(y) \equiv \int_0^y dy' \left[\frac{1}{\phi_0^{(o)}(y')}\right]^2 \int_0^{y'} dy'' \frac{[\phi_0^{(o)}(y'')]^2}{y''} \quad . \tag{30}$$

Using the expression for $\phi_0^{(o)}(y)$ for $y \to \infty$ it is readily shown that $I(\infty)\cdot\phi_0^{(o)}(\infty) \to 0$. The other term in the expression of $u(y)$ is proportional to $\{1-\exp[2k_0(|y|-\Delta)]\}$ and causes $u(y)\phi_0^{(o)}(y)$ to blow-up at $y \to \infty$ as $\exp(k_0|y|)$. The next step is to obtain the expression of $\phi_0^{(e)}(y)$. For $y \gtrless \Delta$, $\phi_0^{(e)}(y) = A_1 \exp(-k_0 y) + B_1 \exp(k_0 y)$. The constants A_1 and B_1 are determined by the continuity of $\phi_0^{(e)}(y)$ at the beam boundaries [for $|y| \lessgtr \Delta$, $\phi_0^{(e)}(y) = \cosh(\kappa_0 y)$], and by the jump condition of the derivatives $d\phi_0^{(e)}/dy$ across the beam-vacuum interface

$$\left.\frac{d\phi_0^{(e)}}{dy}\right|_{y=\Delta^+} - \left.\frac{d\phi_0^{(e)}}{dy}\right|_{y=\Delta^-} = \frac{\omega_p^2}{\omega_c v_{0x}'} \frac{\phi_0^{(e)}(\Delta)}{\Delta} \quad .$$

Using the eigenvalue equation for odd modes, Eq. (16a), we finally obtain

$$A_1 = \frac{\exp(k_0\Delta)}{2}\left[2\cosh(\kappa_0\Delta) + \frac{\kappa_0}{k_0}\frac{1}{\sinh(\kappa\Delta)}\right],$$

$$B_1 = -\frac{\exp(-k_0\Delta)}{2}\frac{\kappa_0}{k_0}\frac{1}{\sinh(\kappa_0\Delta)} \quad .$$

The constant C is then chosen so that the exponentially diverging terms in $C\phi_0^{(e)}(y)$ and $u(y)\phi_0^{(o)}(y)$ cancel (and $\phi_1(\infty) \to 0$):

$$C = \frac{is_1 \omega_p^2 \sinh^2(\kappa_0 \Delta)}{\omega_c (k_0 v'_{0x} \Delta)^2} \left(\frac{k_0}{\kappa_0}\right). \tag{31}$$

It is now possible to calculate s_1 from Eq. (26). We obtain

$$Q s_1^2 = 2k_0 k_2 \int_{-\infty}^{+\infty} dy \, [\phi_0^{(o)}(y)]^2, \tag{32}$$

where Q is given in the Appendix. The sign of Q determines the wave stability properties near the odd mode marginal stability boundary. We have verified that $Q > 0$ for $\omega_p^2 = \omega_c |v'_{0x}|$ (no magnetic shear) and also for $\omega_p^2 \gtrsim 1.5 \omega_c |v'_{0x}|$ (cf. Appendix), and we believe that $Q > 0$ generally (although we have been unable to prove this). At any rate, for cases of interest the magnetic shear is usually strong enough so that $\omega_p^2 \gtrsim 1.5 \, \omega_c |v'_{0x}|$. With $Q > 0$, Eq. (32) shows that s^2 changes sign at the odd mode marginal stability boundary, and the system is unstable (stable) for $k_2 > 0$ ($k_2 < 0$).

V. Cylindrical and Finite $(V_0/c)^2$ Effects in the Low Density Limit

In the preceding sections we have shown, in slab geometry, that the low density results concerning marginal stability were good approximations to the arbitrary density results for $\Gamma \gtrsim 2$. We now examine the effect of magnetic shear on the diocotron instability in cylindrical geometry. Motivated by the confidence we have gained in the low density approximation, we shall apply this approximation to the cylindrical problem. We consider the geometry depicted in Fig. 5. A central rod of radius r_c has an electric charge Q per unit length and supports a current I. The annular electron beam of constant density n_o is located between the radii r_1 and r_2, and a metal cylinder surrounds the system at $r = r_a$. There is a constant applied magnetic field B_z. In an earlier paper, Levy[2] examined the case with I = 0 (i.e., no magnetic shear) and he neglected electromagnetic effects due to finite values of V_0/c, where $V_0 \equiv (\underset{\sim}{v}\cdot\underset{\sim}{B})/(\underset{\sim}{B})$ is the velocity of the beam along the magnetic field, and c is the speed of light. He studied, among other things, the stabilizing effect of the charge Q on the central rod. In this section, we show that the current I has an effect similar to Q and that electromagnetic effects enhance the stabilization properties of both Q and I.

We assume the total azimuthal magnetic field, $B_\theta^s + B_\theta^r \equiv B_\theta << B_z$, where B_θ^s is the self magnetic field of the beam, and B_θ^r is the field produced by the current I in the central rod. Consequently, we assume that $v_{0z} \simeq V_0$ and the beam current density $J_{0z} \cong -en_0V_0$ are constant. From Ampere's law

$$B_\theta^r = \frac{\mu_0 I}{2\pi r}, \text{ for } r \geq r_c,$$

$$B_\theta^s = 0, \text{ for } r \leq r_1,$$

$$B_\theta^s = \frac{\mu_0 J_{0z}}{2r} (r^2 - r_1^2), \text{ for } r_1 \leq r \leq r_2,$$

$$B_\theta^s = \frac{\mu_0 J_{0z}}{2r} (r_2^2 - r_1^2), \text{ for } r \geq r_2. \tag{33}$$

The equilibrium electric field $\underset{\sim}{E}_0$ is radial and induces an azimuthal equilibrium electron drift velocity

$$v_{\theta 0} = \frac{v_{0z} B_\theta(r)}{B_z} - \frac{E_{0r}(r)}{B_z}. \tag{34}$$

From Gauss' law, for $r_2 \geq r \geq r_1$

$$E_{0r}(r) = -\frac{1}{2} \frac{r^2 - r_1^2}{r} \frac{\omega_p^2}{\omega_c} B_z + \frac{Q}{2\pi r \varepsilon_0}, \tag{35}$$

so that we can express $v_{\theta 0}(r)$ as

$$v_{\theta 0}(r) = \frac{r}{2} \frac{\omega_p^2}{\omega_c} \frac{1}{\gamma_0^2} [1 - (1-\hat{\alpha})(\frac{r_1}{r})^2], \tag{36}$$

where

$$\hat{\alpha} \equiv \frac{\gamma_0^2}{e n_0 \pi r_1^2} (\frac{V_0 I}{c^2} - Q), \tag{37}$$

which is analogous to α in the slab case [cf. Eq. (9)]. We now define an equivalent charge by unit length

$$Q' \equiv \gamma_0^2 \left(Q - \frac{IV_0}{c^2}\right), \tag{38}$$

where $\gamma_0^{-2} \equiv 1 - V_0^2/c^2$. Evidently, Q and I have a similar effect on $v_{\theta 0}(r)$. We also notice that for a given set of values of Q and I, $|Q'|$ is increased when V_0 approaches the speed of light, c. Clearly, the self magnetic field enhances the effect of Q and I. The perturbed quantities are assumed to be of the form

$$f = f(r) \exp(st + im\theta). \tag{39}$$

We are looking for waves which have a phase velocity much smaller than the speed of light. Consequently, the density perturbation n is related to the perturbed potential through Poisson's equation

$$\nabla^2\phi \equiv \frac{1}{r}\frac{d}{dr}(r\phi) - \left(\frac{m}{r}\right)^2\phi = \frac{en}{\varepsilon_0}, \tag{40}$$

and produces, due to the velocity V_0 of the beam, a perturbed magnetic field given by Ampere's law

$$\nabla \times \underset{\sim}{B} = \mu_0 \underset{\sim}{J} = -\mu_0 e V_0 n \underset{\sim}{z}_0. \tag{41}$$

In the expression for $\underset{\sim}{J}$ we neglected the perturbed electron velocity, since we assume V_0 to be a finite fraction of c, so that $|\underset{\sim}{v}|/V_0 \ll n/n_0$,

as can be shown from the continuity equation. We write $\underset{\sim}{B}$ in terms of a vector-potential $\underset{\sim}{A} \equiv A\underset{\sim}{z}_0$

$$\underset{\sim}{B} = \underset{\sim}{\nabla}x(A\underset{\sim}{z}_0) = \underset{\sim}{\nabla}A \times \underset{\sim}{z}_0, \tag{42}$$

and from Eqs. (40) and (41) we see that $c^2A = V_0\phi$, so that Eq. (42) yields

$$\underset{\sim}{B} = \frac{V_0}{c^2}\ \underset{\sim}{\nabla}\phi \times \underset{\sim}{z}_0. \tag{43}$$

To obtain the wave equation we need to solve the electron continuity equation

$$s_m(r)n + v_r \frac{dn_0}{dr} = -n_0\underset{\sim}{\nabla}\cdot\underset{\sim}{v}, \tag{44}$$

where $s_m(r) \equiv s + i(m/r)v_{\theta 0}(r)$. Since the wavelength is infinite in the z direction, we need only the component of $\underset{\sim}{v}$ perpendicular to the magnetic field, say $\underset{\sim}{v}_\perp$. As in Sec. II, all frequencies are assumed to be small compared to ω_c. The equation of motion then yields

$$-\underset{\sim}{\nabla}\phi + \underset{\sim}{v}_\perp x \underset{\sim}{B}_0 + \underset{\sim}{v}_0 \times \underset{\sim}{B} = 0. \tag{45}$$

We replace $\underset{\sim}{B}$ by its expression in terms of ϕ_1 Eq. (43), and obtain $\underset{\sim}{v}_\perp$ from Eq. (45)

$$\underset{\sim}{v}_\perp = - \frac{\nabla\phi \times \underset{\sim}{z}_0}{\gamma_0^2 B_0} . \tag{46}$$

We now have all the elements to write down the wave equation, namely Eqs. (40), (44), and (46)

$$\frac{1}{r}\frac{d}{dr}\left(r \frac{d\phi}{dr}\right) - \left(\frac{m}{r}\right)^2 \phi = \frac{\omega_p^2}{\gamma_0^2 \omega_c} \frac{im/r\ \phi}{s_D(r)} \left(\frac{1}{n_0}\frac{dn_0}{dr}\right). \tag{47}$$

Our wave equation is identical to Levy's equation [Eq. (10) of Ref. 2], provided we replace ω by $+ i\gamma_0^2 s$ and Q by $\gamma_0^2(Q - IV_0/c^2)$. (Thus, with these transformations, Levy's numerical results[2] can be used directly.) The implications of this are the following. Compared to Levy's results, our results show that, provided the sign of IJ_{0z} is identical to Q, the current I has the same effect as Q (magnetic shear can reduce the velocity shear in the beam, thus enhance stability). Second, due to the selfmagnetic field of the beam, the actual Q and/or I necessary for stabilization are smaller by a factor γ_0^{-2}. Third, due to electromagnetic effects, the actual growth rate is smaller by a factor γ_0^{-2}. Finally, we note that for experiments currently planned at Cornell[6] velocity shear due to shear in $\underset{\sim}{B}$ dominates that due to charge on the wire; Q is typically a factor 10 smaller than IV_0/c^2.

VI. Conclusion

The motivation of this paper was to examine the influence of magnetic shear on the diocotron instability. The idea is that $\underset{\sim}{E}\times\underset{\sim}{B}$ velocity shear, which is the source of the diocotron instability, is reduced and can even be reversed by sufficient magnetic shear. As a first step, in order to assess the validity of the low density case, we examined, in Secs. II to IV, the stability of a planar unneutralized electron beam immersed in a strong magnetic field, i.e., $\omega_p^2 << \omega_c^2$. In Sec. II, the general wave equation for slow electrostatic waves is derived in the presence of magnetic shear. In Sec. III, we specialize to the low density case which turns out to be the most tractable case. It is found that as velocity shear is reduced, as a result of magnetic shear, the unstable domain in k-space shrinks and occurs for larger values of k. At the same time, the growth rate is reduced significantly. Overall, marginal stability is achieved when velocity shear is cancelled. In order to assess the results for marginal stability in k-space, we solved the arbitrary density case in Sec. IV, setting the frequency $s = 0$. It turns out that $s = 0$ is a limit in which the arbitrary density case is easily tractable. We conclude that the low density case results yield a fairly good assessment of the situation for values of $\omega_p \lesssim V_0/(2\Delta)$. We then check that $s = 0$ corresponds to marginal stability in the arbitrary density case by expanding the eigenvalues and eigenfunctions around $s = 0$. Finally, in Sec. V, we examine,

in the low density approximation, the cylindrical case, with a central rod supporting a current in order to produce magnetic shear. Including electromagnetic effects due to finite values of $(V_0/c)^2$, we obtain a wave equation similar to that obtained previously by Levy.[2] The comparison with Levy's wave equation and his consequent results leads us to the following conclusions. The current I in the central rod has the same effect as the charge Q on the rod for diocotron mode stabilization. Moreover, the values of Q and/or I needed for stabilization are reduced by a factor γ_0^2 due to the self magnetic field of the beam and similarly, the growth rates for a given value of $\gamma_0^2(Q - IV_0/c^2)$ are reduced by a factor γ_0^{-2} as compared to those obtained by Levy. This last effect is due to electromagnetic terms arising when finite $(V_0/c)^2$ is considered.

Acknowledgements

This work was supported by the U.S. Air Force Office of Scientific Research under Contract F44620-75-C-0054 and by the National Science Foundation under Grant #ENG77-19961.

Appendix

Here, we determine the quantity Q appearing in Eq. (33), and we show that $Q > 0$ both for $\omega_p^2 = \omega_c|v'_{0x}|$ (no magnetic shear) and for $\omega_p^2 > 1.5\ \omega_c|v'_{0x}|$. (We suspect Q to be always positive for $v'_{0x} < 0$.)

Using the results of Eqs. (27)-(33) we obtain

$$Q \equiv Q_1 + \frac{Q_2}{L_s^2} + \frac{Q_3}{L_s^4},$$

$$Q_1 \equiv \frac{2\ \omega_p^2 \sinh^2(\kappa_0\Delta)}{\omega_c k_0^2 (\Delta v'_{0x})^3} + \frac{2\ \omega_p^4}{\omega_c^2}\ \frac{\sinh^3(\kappa_0\Delta)\ \cosh(\kappa_0\Delta)}{\kappa_0 (\Delta v'_{0x})^4},$$

$$Q_2 \equiv \frac{-3\ \omega_p^2}{k_0^2 (v'_{0x})^4} \int_{-\Delta}^{+\Delta} dy\ \frac{\sinh^2(\kappa_0 y)}{y^2} - \frac{2\ \omega_p^4\ \sinh^2(\kappa_0\Delta)}{\kappa_0 k_0^2 \omega_c \Delta^2 (v'_{0x})^5}$$

$$\int_{-\Delta}^{+\Delta} dy\ \frac{\sinh(\kappa_0 y)\ \cosh(\kappa_0 y)}{y} - \frac{4\ \omega_p^4\ \sinh^2(\kappa_0\Delta)\ I(\Delta)}{\omega_c k_0^2 \Delta^2 (v'_{0x})^5},$$

$$Q_3 \equiv \frac{4\ \omega_p^4}{k_0^2 (v'_{0x})^6} \int_{-\Delta}^{+\Delta} dy\ \frac{\sinh^2(\kappa_0 y)\ I(y)}{y}.$$

It is clear that $Q_1 > 0$. From the definition of I(y), Eq. (31), it is immediately seen that I(y) is an odd function of y and that $yI(y) \geq 0$. Consequently, $Q_3 > 0$. Without magnetic shear ($L_s \to \infty$), Q reduces to Q_1 and $Q > 0$.

We now show that $Q_2 \geq 0$ for $v'_{0x} < 0$ when $\omega_p^2 > 1.5\ \omega_c|v'_{0x}|$. An integration by parts of Eq. (31) yields

$$\kappa_o I(\Delta) = \int_0^{+\Delta} dy\ \frac{\sinh(\kappa_0 y)\ \cosh(\kappa_0 y)}{y} - \coth(\kappa_0\Delta) \int_0^{+\Delta} dy\ \frac{\sinh^2(\kappa_0 y)}{y}\ .$$

Using the addition formula

$$\sinh(\kappa_0\Delta)\ \cosh(\kappa_0 y) - \cosh(\kappa_0\Delta)\ \sinh(\kappa_0 y) = \sinh[\kappa_0(\Delta-y)] \geq 0,$$

we replace $I(\Delta)$ by zero and obtain a sufficient condition for $Q_2 \geq 0$:

$$\frac{\omega_p^2}{\omega_c|v'_{0x}|}\ \frac{\sinh^2(\kappa_0\Delta)}{(\kappa_0\Delta)^2} \int_0^{+\Delta} dy\ \frac{\sinh(\kappa_0 y)\ \cosh(\kappa_0 y)}{y} \geq \frac{3}{2} \int_0^{+\Delta} dy\ \frac{\sinh^2(\kappa_0 y)}{\kappa_0 y^2}\ .$$

Furthermore, using the properties: $\cosh(x) > \sinh(x) \geq x$, we obtain the final sufficient condition for $Q_2 > 0$:

$$\frac{\omega_p^2}{\omega_c|v'_{0x}|} \geq 1.5.$$

References

1. W. Knauer, J. Appl. Phys. 37, 602 (1966); O. Buneman, R. H. Levy, and L. M. Linson, J. Appl. Phys. 37, 3203 (1966); O. Buneman, J. Electron Control 3, 507 (1957); R. L. Kyhl and H. F. Webster, IRE Trans. Electron Devices ED-3, 172 (1956); J. R. Pierce, IRE Trans. Electron Devices ED-3, 183 (1956).
2. R. H. Levy, Phys. Fluids 8, 1288 (1965).
3. Y. Carmel and J. Nation, Phys. Rev. Letters 31, 286 (1973); C. Kapetanakos, D. Hammer, C. Striffler, and R. Davidson, Phys. Rev. Letters 30, 1303 (1973).
4. T. M. Antonsen and E. Ott, Phys. Fluids 18, 1197 (1975).
5. M. Sloan and W. Drummond, Phys. Rev. Letters 31, 1234 (1973); R. Adler, G. Gammel, J. A. Nation, M. E. Read, and R. Williams, in Proceedings of the Second International Topical Conference on High Power Electron and Ion Beam Research and Technology, (Cornell University, Ithaca, New York, 1977), Vol. II, p. 509; P. Sprangle, A. Drobot, and W. Manheimer, Phys. Rev. Letters 36, 1180 (1976).
6. J. A. Nation and V. Serlin, private communication.

Figure Captions

Fig. 1 Planar beam with thickness 2Δ in the y-direction and infinite in the x and z directions. Magnetic shear in the y-direction.

Fig. 2 Stability boundary for diocotron modes as a function of $k\Delta$ and α for the low density case. Instability exists in the region between the two curves shown.

Fig. 3 Normalized maximum growth rates as a function of the velocity shear parameter α (low density case): $\Omega \equiv 2\omega_c s/\omega_{pe}^2$.

Fig. 4 Boundaries of unstable diocotron modes in k-space as a function of $\varepsilon \equiv \omega_c\Delta/(\omega_p L_s)$ for $\Gamma = 2$. The dashed lines are the low density case results, the full lines, the arbitrary density results.

Fig. 5 Annular electron beam in cylindrical geometry. The central rod of radius r_c supports a current I in the z-direction, producing a sheared magnetic field.

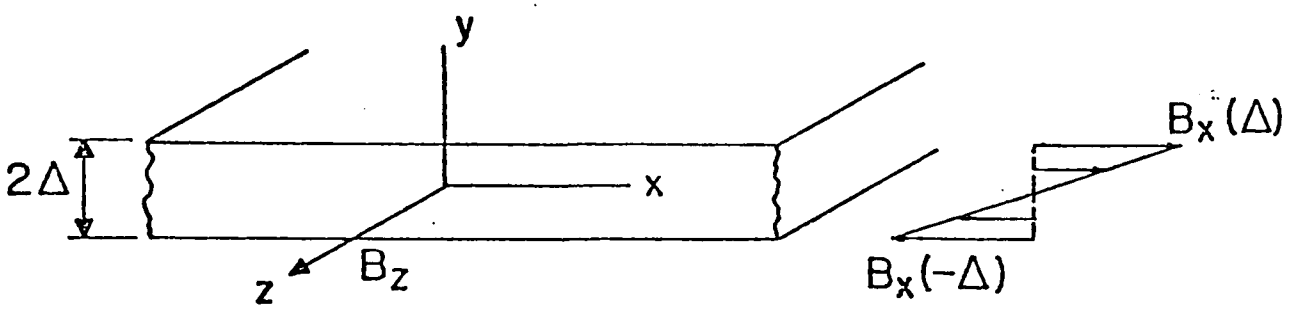
y
2Δ
x
z
B_z
$B_x(\Delta)$
$B_x(-\Delta)$

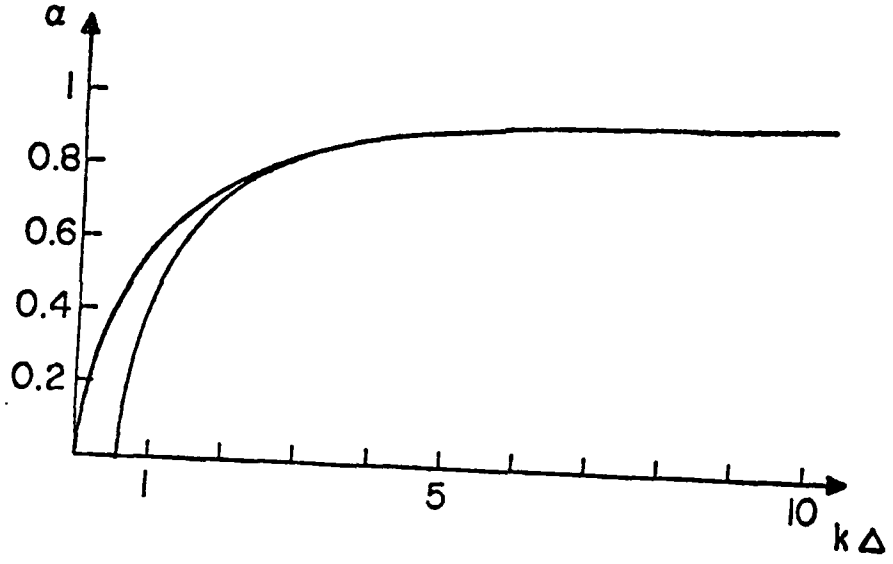
α
1
0.8
0.6
0.4
0.2
1
5
10
kΔ

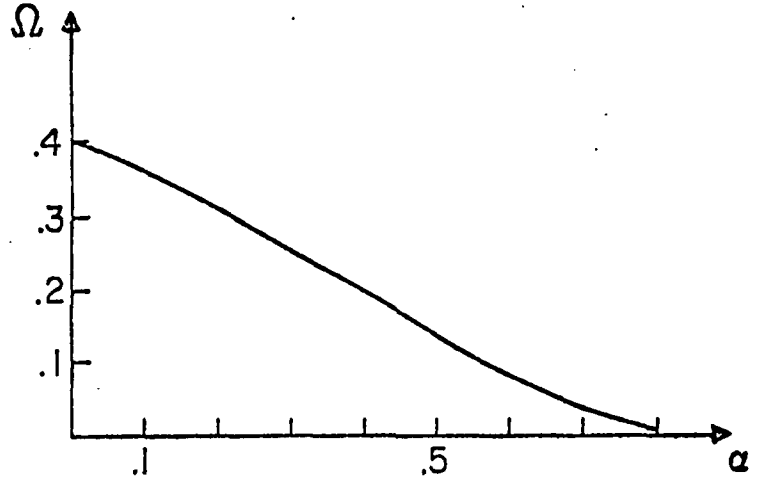
Ω
.4
.3
.2
.1
.1
.5
α

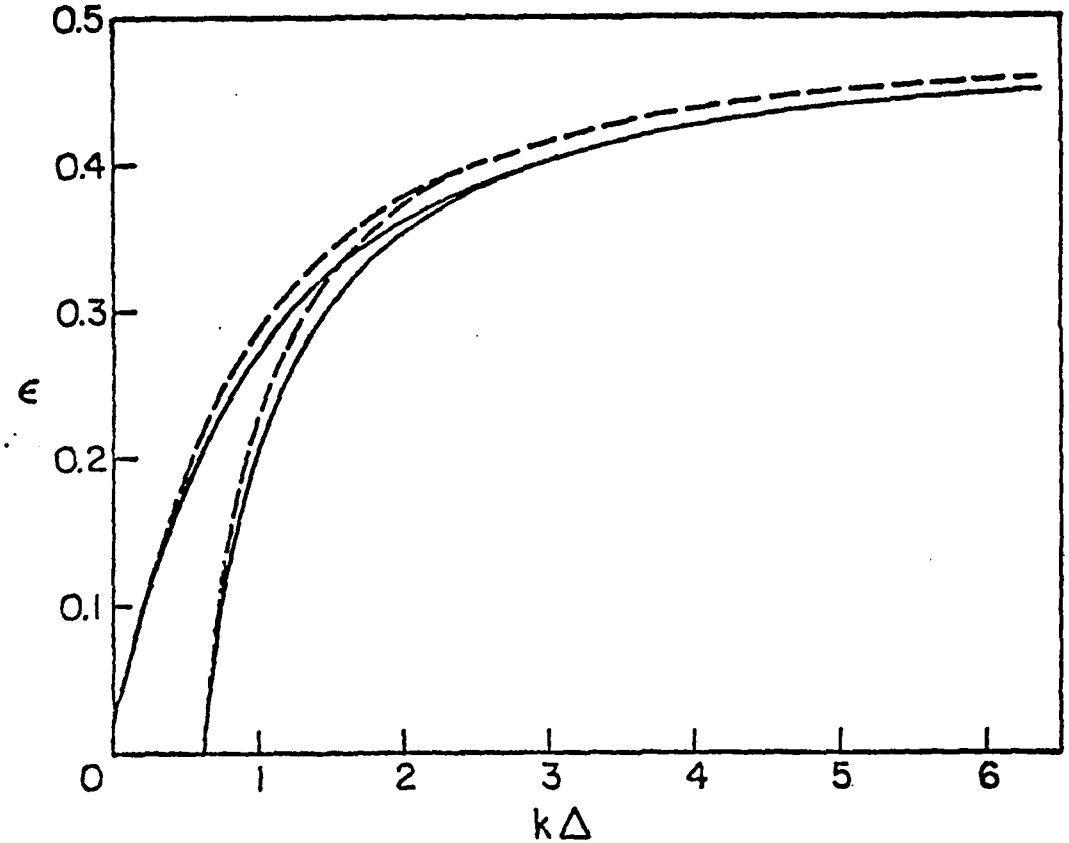
0.5
0.4
0.3
0.2
0.1
0
ϵ
1
2
3
4
5
6
kΔ

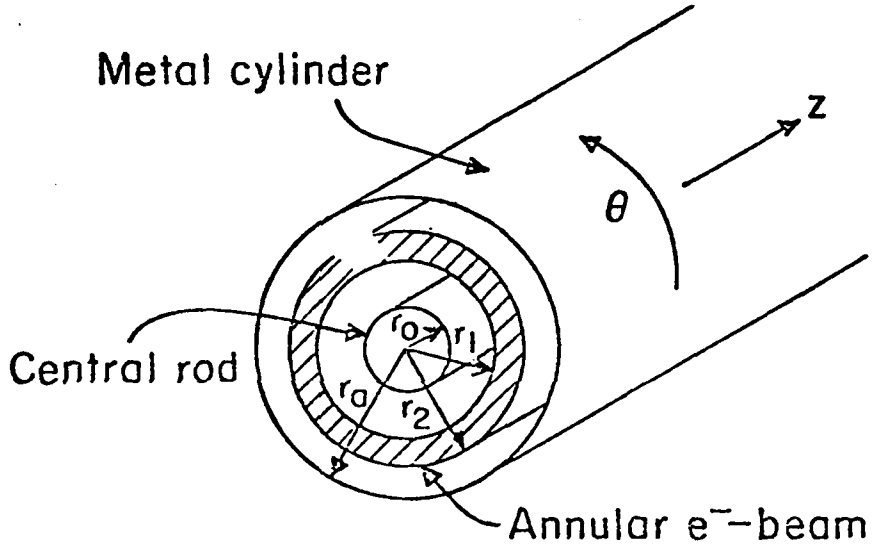
Metal cylinder
z
θ
Central rod
r0
r1
r2
Annular e⁻-beam

Ion-acceleration mechanisms in vacuum diodes

R. J. Adler and J. A. Nation
Laboratory of Plasma Studies and School of Electrical Engineering, Cornell University, Ithaca, New York 14853

(Received 11 September 1978; accepted for publication 29 March 1979)

A study of proton acceleration in a Luce diode has been carried out. Measurements of beam-neutralization times, electron and ion energy distributions, and induced radioactivity have been made. These measurements show that the effective potential-well depth at the beam head is less than the electron-accelerating voltage. Also, the relative activity of Mylar and copper foils indicates that ion energy increases with mass for $Z = 1$ particles. Both of these observations are consistent with ion acceleration resulting from a moving potential well.

PACS numbers: 41.80.Gg, 29.25.Cy

High-energy ions in intense relativistic electron beams were originally reported by Graybill and Uglum in beam-propagation experiments in a neutral gas. [1] More recently, Luce [2] observed high-energy ions from an evacuated tube when an electron beam was generated in a vacuum diode having a dielectric anode insert.

In the experiments described in this paper, protons of up to 10 times the electron injection energy eV_d have been produced. The experiments were designed to help improve the understanding of the acceleration process. Although a spectrum of ions with 0–10 times the beam energy is produced, interest is focused on the high-energy tail since efficient methods of producing the lower-energy ions already exist. [3]

Several models have been proposed to explain the acceleration [4–8]; however, at this time there is not enough evidence to prove any one of them correct. The acceleration mechanism is believed to be at least partially electrostatic, due to the apparent dependence of acceleration on the ratio of the beam current to the space-charge-limiting current. [7] The exact dynamics of the process appear to be extremely complicated although there are two main viewpoints which are used to qualitatively explain the acceleration.

The first view is that a deep (two or three times V_d) electrostatic potential well is formed downstream from the anode plane, and the bulk of the ion acceleration occurs in this quasistatic well.

The second view is that a potential well with a depth comparable to the cathode potential propagates at the head of the beam along with the bulk of the neutralizing ions.

A potential well having a depth of two to three times the cathode potential is intrinsically a nonequilibrium configuration and, as a result, must oscillate in time. Electrons will be present at the potential minimum and these electrons, together with the remaining electrons which form the well, will be continually repelled to the walls by the oscillating electric field. If the walls are far enough from the minimum so that a repelled electron takes more than one oscillation period to reach a detector mounted on the wall, then the highest energy electrons reaching the detector should have an energy equal to the time-averaged potential well depth. The time-averaged potential well determines the field which accelerates the ions since the ion-acceleration time scale is much longer than the electron time scale. In this experiment, electrons underwent approximately two oscillations before reaching the wall.

The preceding comments form the basis for the interpretation of the experiments to be described. The experimental setup is shown in Fig. 1. Typical electron-beam param-

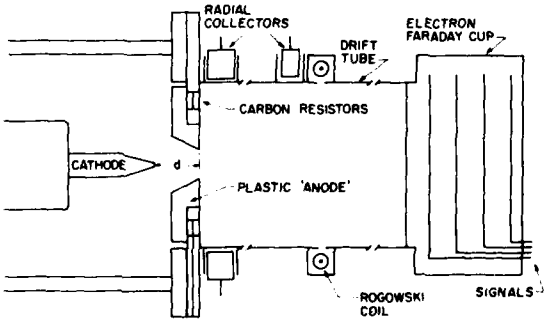

FIG. 1. Experimental schematic showing diagnostics used. The electron Faraday cup was replaced by the segmented ion Faraday cup or an activation sample for portions of the experiment.

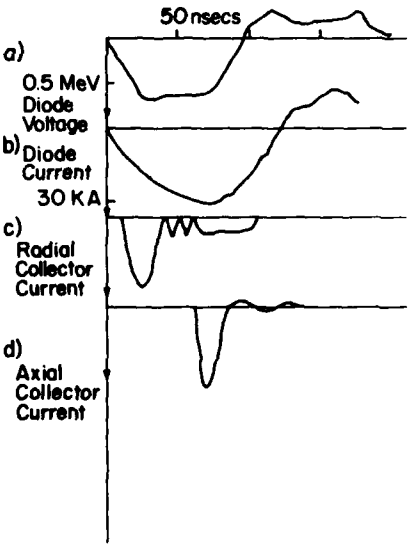

FIG. 2. (a) Diode voltage. (b) Diode current. (c) Radial-collector current (relative units) with a 0.48-mm-Al absorber. (d) Longitudinal-collector current (relative units) with a 1.04-mm-Al absorber.

 0021-8979/79/075025-03$01.10

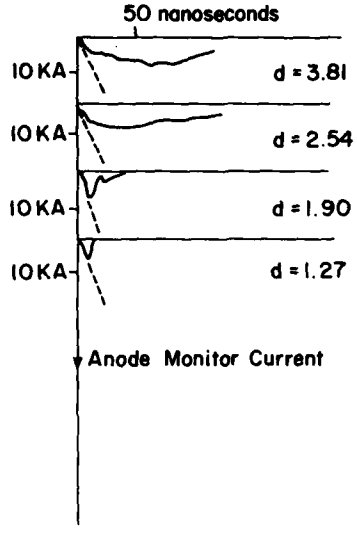

FIG. 3. Current-monitor signals with the values of diode gap d.

eters where $V_d = 0.4$–1.1 MeV and 15–50 kA in the diode. An aluminum cathode tapered down to 0.2 cm was positioned at a distance d from the downstream side of the 1.2-cm-thick polyethelene anode. The anode was tapered with a 22° half-angle, matching the cathode taper. It was held in position by an anode holder containing a resistive current monitor used to assess the time at which the neutralized electron beam detached from the anode surface. A variable-length 7.3-cm-diam drift-tube section followed the anode with vacuum fittings in the wall to house absorber-covered Faraday cups. A Rogowski current monitor was placed 25 cm downstream. The end of the drift tube had either a segmented Faraday cup to measure ion currents (the cup was preceded by a transverse magnetic field), a stacked-foil Faraday cup to measure electron currents and energies, or an activation sample. The base pressure in the system was always less than 8×10^{-4} Torr.

The absorber-covered Faraday cups on the sides of the drift tube used combinations of aluminum and Mylar foils of a thickness from 0.5 to 1.5 absolute electron ranges thick. Three cups including one at 45° to the drift tube were placed at 1.75, 17, and 38 cm from the anode. In the radial-collector measurements, electrons with energies $U \leq 0.8eV_d$ were measured. The radial collectors typically showed 15-nsec pulses occurring at times corresponding approximately to the time at which the beam front reached the cup as determined from the Rogowski current measurements. A typical radial absorber-covered–Faraday-cup trace is shown in Fig. 2.

A stacked-foil electron Faraday cup was also used in the search for high-energy electrons. When used as an electron detector, it consisted of a grounded aluminum foil separating the end of the drift tube from an isolated housing containing four foils spaced at 3-mm intervals, and each connected by a terminated 50-Ω cable to an oscilloscope. Typical signals are shown in Fig. 2. The electrons detected had $U \leq 1.2eV_d$ and reached the detector 20 nsec after the first ions were measured at the same monitoring position. Lower-energy ($U \leq 0.6eV_d$) electrons were detected ahead of both the high-energy electrons and ions.

The conclusion drawn from these measurements is that a deep potential well of two to three times the cathode potential is not associated in these experiments with the acceleration of ions to energies greater than the beam potential.

The time taken for the potential well to move a significant distance from the anode was inferred from the resistive current monitor in the anode holder. The monitor resistance was 0.13 Ω and was made up of six carbon slugs in parallel uniformly spaced in the azimuthal direction. The signals were attenuated and monitored on a Tektronix 454 oscilloscope.

Typical signals are shown for representative values of d in Fig. 3. The corresponding diode currents are indicated by the dashed line. A segmented foil-covered Faraday cup was used in this experiment to monitor ions with energies greater than 1.2 MeV. Two distinct classes of behavior can be discerned from these measurements. For $d \leq 2.54$ cm, ions of energy greater than 1.2 MeV were observed, signficiant beam currents ($I > 2$ kA) were detected 30 cm downstream, and the current-monitor signal consisted of a 6–10-nsec pulse at the beginning of the current rise. The monitor current is roughly equal to the diode current during this time. For $d > 2.54$ cm, little or no net beam current was propagated, no significant ion current was recorded, and the monitor current was proportional to the diode current for the duration of the pulse, although smaller in magnitude. The rise time of the monitor current as a function of d is shown in Fig. 4 with the ion-producing region delineated. Note that the rise time is less than the typical voltage rise time of 15 nsec for all ion-producing cases.

These results are consistent with a model in which the electron flow follows the radial field lines behind the diode to the anode holder until sufficient ion current is present to neutralize the electron beam. At this time the neutralized beam starts to propagate (possibly pinching behind the beam front), and the dominant radial electron flow occurs at the beam head as shown by the Faraday-cup measurements in

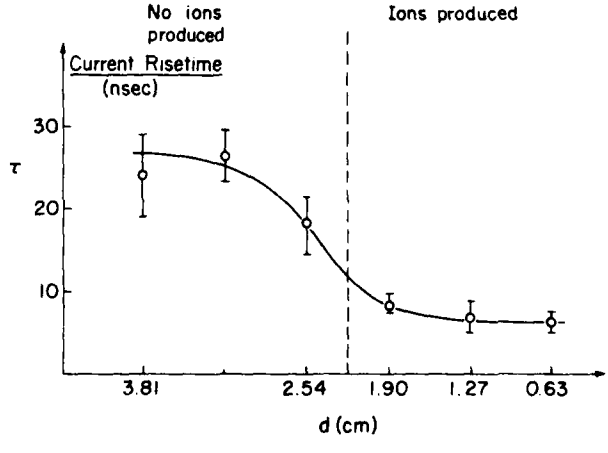

FIG. 4. Rise time of current-monitor signal as a function of d. The regions of ion production and no ion production are indicated.

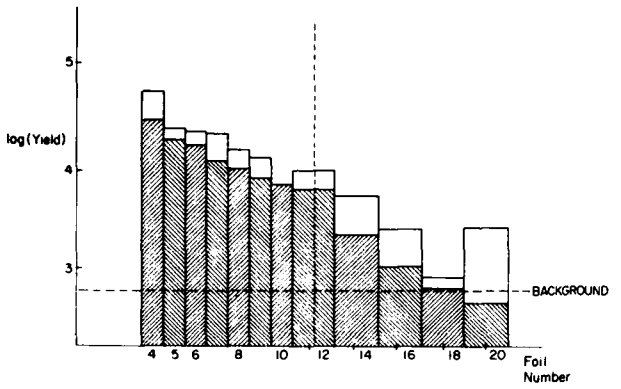

FIG. 5. The clear area indicates yield as a function of Mylar-foil number. The yield of the same foil inferred from copper-foil measurements is shown in the shaded area. The dashed line indicates the maximum depth at which a deuteron with an energy equal to the maximum proton energy would have a measurable probability of producing activations. The peak proton energy in this data is about 9.2 MeV.

Fig. 2(c). The relative time duration of the current-monitor and Faraday-cup signals are comparable and consistent with electron-beam loss at the beam head. These observations are all explained by the moving well view.

The natural isotopic abundance of deuterium present in all hydrogenous materials, coupled with the high cross sections of (d,n) reactions,[9,10] provides a single-shot method for assessing the effect of accelerated-ion mass independent of charge. In particular, the similarities between the reaction ^{63}Cu$(p,n)^{63}$Zn and ^{13}C$(p,n)^{13}$N[9] allow us to infer the yield of ^{13}N due to the reaction ^{12}C$(d,n)^{13}$N.

In our experiment, the ion beam was extracted into air through a 25-μm steel foil and struck an activation sample made up of half-circle Mylar and copper activation foil stacks. The ^{13}N yield (clear area) is compared with the yield due to protons only, inferred from the ^{63}Cu reaction (shaded area) in Fig. 5. The discrepancy can only be accounted for by a natural abundance of deuterons accelerated to an energy of 1.4 to 2.0 times the proton energy since other reaction yields are negligible, and the discrepancy persists beyond the range of a deuteron possessing the peak proton energy (9.2 MeV). The electron-energy and shunt-current measurements are each based on several hundred shots. Substantially less data (five shots) was analyzed for the deuteron measurements. However, in spite of varying conditions, the discrepancy between the ^{13}N yield and inferred yield was always very similar to that shown in Fig. 5 and consistent with the above interpretation. The presence of deuterons of energy greater than the proton energy in the same beam is strong evidence for the moving-well model.

The number of ions accelerated and the ion energies achieved are limited by the conservation of momentum. Application of the momentum conservation law yields a limit on the number of ions accelerated given by

$$N_i = 3.4\times 10^{10}\alpha I\gamma\tau/\bar{\beta}_i A,$$

where I is the diode current in kA, τ is the interaction time in nsec, A is the atomic mass in amu, and $\bar{\beta}_i$ is the average ion velocity acquired. The parameter α gives the fractional momentum of the electrons transferred to the ions and from our observations with Faraday cups is estimated as 0.5. For moving-well acceleration, the total ion acceleration scales inversely with the ion mass and the charge state only enters in determining the ion-trapping efficiency. In our experiment we estimate that the number of ions accelerated is very close to the value determined from the above equation. To achieve more efficient acceleration we require that only the most energetic ions are accelerated and that the low-energy ions are removed from the interaction process. Alternately, a more efficient ion acceleration might be achieved if one has reflexing electrons.

In conclusion, the experiments performed using the Luce diode support the moving-potential-well model of collective acceleration. The observations also suggest that conservation of total beam momentum, with the associated $(m_i)^{-1}$ scaling is the limit on total ion acceleration.

One of the authors (R.J.A.) would like to thank the National Research Council of Canada for providing a postgraduate scholarship for the period over which this research was performed. This research was supported by the U.S. AFOSR, BMDATC, and NSF.

[1] S. Graybill and J.R. Uglum, J. Appl. Phys. **41**, 236 (1970).
[2] J. Luce, Ann. N.Y. Acad. Sci. **251**, 217 (1975).
[3] See, for example, S. Humphries, J. Vac. Sci. Technol. **12**, 1204 (1975); S.C. Luckhardt and H.H. Fleischmann, Appl. Phys. Lett. **30**, 182 (1977).
[4] J.L. Adamski, P. Wei, J. Beymer, R.L. Gray, and R.L. Copeland, *Proc. 2nd Int. Conf. on High Power Electron and Ion Beam Research and Technology*, edited by J.A. Nation and R.N. Sudan (Cornell University, Ithaca, 1977), Vol. I, p. 497.
[5] G.T. Zorn, H. Kim, and C.N. Boyer, IEEE Trans. Nucl. Sci. **NS-22**, 1006 (1975).
[6] C.L. Olson, Phys. Fluids **18**, 585 (1975).
[7] R.F. Hoeberling, R.B. Miller, D.C. Straw, and D.N. Paynton III, IEEE Trans. Nucl. Sci. **NS-24**, 1662 (1977).
[8] J.W. Poukey and N. Rostoker, Plasma Phys. **13**, 897 (1971).
[9] A useful reference for nuclear activation diagnostics is F.C. Young, J. Golden, and C.A. Kapetanakos, Rev. Sci. Instrum. **48**, 432 (1977).
[10] R.J. Adler and J.A. Nation, Cornell University Report No. LPS 255, 1978.

Mechanisms for Collective Ion Acceleration in Vacuum

R. J. Adler, J. A. Nation, and V. Serlin
Laboratory of Plasma Studies
and
School of Electrical Engineering,
Cornell University,
Ithaca, New York 14853

Abstract

Ions, from a dielectric anode, have been accelerated to energies up to 22 times the injected electron energy by an electron beam in a vacuum drift tube. The beam front velocity has been measured with emphasis on the accelerating region. Measurements of the high energy ion production time demonstrate that the ions are produced far behind the beam front. Preliminary measurements indicate that there is a substantial high frequency (0.1-3 GHz) signal on the beam which is time correlated with the ion acceleration. This suggests wave acceleration may be the dominant mechanism for the high energy ions.

The large fields available in intense relativistic electron beams have been used to accelerate both electrons and ions. Accelerated ions have been observed during beam propagation in neutral gases[1], in experiments where a localized ion source is available at the anode[2-4], and when an ion source is available at the drift tube wall.[5] In the case of collective ion acceleration in neutral gases, the ion velocity has been shown to be equal to the beam front velocity[6], indicating that acceleration is due to space charge forces at the beam front.

A variety of beam front mechanisms have been proposed to explain collective acceleration in vacuum. These have included "deep potential well" models[7-9], which were subsequently demonstrated not to be important in the vacuum experiments,[10] and moving potential well models. One example of a moving well model is the "piston" model proposed by Destler et al.[11] In a moving well model, ion acceleration is due to space charge forces at the head of the electron-ion beam. The ions are accelerated by the space charge, resulting in an increased front velocity and further acceleration. One consequence of such a model is that some identifiable phase point defined as the beam front must accelerate and move with the fastest ions.

In this work measurements of the net beam current at various axial positions are reported. These measurements, which yield the beam front velocity, are compared to measurements giving the production time of high energy ions and hence provide a basis to determine the relevance of moving well theories. The results, which showed that the ion acceleration occurs well behind the beam front, prompted an investigation of beam current oscillations in the frequency range 0.1-3 GHz, and these results are also presented.

The experimental setup is typical of that used in Luce diode investigations.[2,4,9,10,12] During this study the electron beam parameters were .5-.6 MV diode voltage, and a 30-35 KA peak propagating current. The resulting peak ion energy was typically 8 ± 2 MeV. The diode used a tapered aluminum cathode which was positioned 6 mm from the downstream side of the 1.2 cm thick polyethylene anode. Both the anode aperture (which had a minimum diameter of approximately 1.4 cm) and the cathode had 25° half-angle tapers. The diameter of the polyethylene was 3.8 cm and the beam was propagated in a 7.3 cm diameter drift tube. If we define axial positions as the distance z from the downstream anode surface, then a Rogowski current monitor was fixed at position z = 2.3 cm. An axially movable Rogowski was positioned inside the drift tube. The perturbation introduced by this monitor did not affect ion acceleration in any measurable way. Magnetic field pickup loops for the rf measurements were positioned 4 mm inside the wall at z = 6.3 cm, and at z = 11.5 cm. The Faraday cup used for time resolved high energy ion measurements was positioned with the charge collecting surface at z = 50 cm. It was preceded by a transverse magnetic field region (3 KG average field) for 15 cm in order to deflect the beam electrons. A 75 μm steel foil preceded the Faraday cup so that only ions of energy $E_i > 4.7$ MeV were monitored. Other ion diagnostics used to assess ion production included stacked foil activation, total neutron yield measurements and neutron time of flight. Prompt γ signals from (p,γ) and (p,nγ) reactions were also measured on the neutron time of flight detector and compared to the Faraday cup signals.

All waveforms were recorded on a Tektronix R7912 Transient Digitizer (RF signals from 1.5-3 GHz were first detected with an HP 420A crystal so that only the signal envelope was measured). Relative timing information was obtained by using known cable lengths and delay lines and combining the two signals of interest using a passive summing network.

The beam front position as a function of time is shown by the circles in Fig. 1. The beam front transit time was defined as the delay between the starts of the two Rogowski signals. The best fit line shown in the figure corresponds to a velocity of .045 c. The 8-10 nanosecond delay in propagation is consistent with previous measurements which indicated that the beam does not propagate past the anode plane during the first 6-10 nanoseconds.[10]

The vertical bar in Fig. 1 indicates the timing of the high energy ion pulses measured by the Faraday cup. Because the foils limited the detected ions to those having velocities in the range 0.1 to 0.15 c we have estimated the time the ion acceleration was completed by translating the detection time at $z = 50$ cm to $z = 13$ cm, using a velocity of .1c. These measurements were also compared to the prompt γ pulse as measured by the time-of-flight neutron detector. Both signals indicated the same ion production time; at least 30 nsec after the beam front has passed.

The relative timing of various signals is demonstrated in Fig. 2 where the diode voltage, the net beam current at $z = 13$ cm, the Faraday cup current folded back to 13 cm, and the RF signals at $z = 11$ cm are shown. The Faraday cup currents on all shots stop when the flat-top

on the voltage pulse ends. The beginning of the high energy ion current varied from 50-80 nanoseconds after the start of the 90 nanosecond voltage flat-top. Since the ions are produced far behind the beam front, and the beam front velocity is lower than that required for the observed acceleration, we conclude that the high energy ions are not being produced by a beam front mechanism.

The late initiation of the ion acceleration in the beam pulse is difficult to explain by any mechanism other than those associated with wave-particle interactions. We assume a wavenumber such that the plasma approximation applies ($k < \omega p/c$) and a phase velocity such that ions can interact with the wave (~0.1c). This results in a frequency of a few GHz or less for our experimental parameters. Direct display of radiation in the .1 to 1.5 GHz range, using calibrated magnetic pick-up loops close to the tube wall, shows intense radiation bursts which have no correlation with the ion acceleration. In the range 1.5 to 3 GHz we generally detect two rf pulses, each lasting about 10-20 nsec. The second of the two pulses occurred at the start of the high energy ion acceleration time window, for all shots. Experiments using a variable frequency filter indicate that the signal is broadband (1 GHz bandwidth). Assuming a wave phase velocity of order .1c, a frequency of approximately 2 GHz, and using the measured beam diameter of 1.2 cm, the R.F. electric field in the beam can be estimated from the known R.F. magnetic field at the wall.[13] This results in axial electric fields of 1-10 MV/cm at the beam edge. The lower end of this range is comparable with the accelerating gradient inferred from the peak ion energy and acceleration length (1 MeV/cm).

A wave acceleration model is also consistent with previous measurements of high energy electrons. Electrons of more than 1.5 times the injection energy[10] were detected during the same time window in which high energy ions were accelerated.

The ion energy spectrum is exponential in character[12], as shown in Fig. 3 which displays the high energy tail as measured by neutron time of flight. The exponential nature of the energy spectrum is consistent with the quasi-linear stage of wave-particle interaction where the broadband spectrum increases the effective ion temperature.

A study of possible wave interactions which could lead to the measured acceleration shows that the electron-ion two stream instability is a strong possibility.[14-16] Once the beam current becomes uniform over the accelerating region (measured at 50 nanoseconds into the pulse) all of the conditions for instability growth are satisfied. The instability onset current is approximately 17 kA (half of the injected current in this case) for our parameters. The characteristic features of the instability, i.e. axial wave number k_z, and the real (ω_r) and imaginary (ω_i) parts of the wave angular frequency are given by:

$$k_z \sim \frac{2}{a\beta_e\gamma}\sqrt{\frac{I}{I_A}}$$

$$\frac{\omega_r}{k_z c} \sim \beta_i + \frac{1}{2}\left(\frac{m_e}{2m_i}\right)^{1/3}\beta_e\gamma_e$$

$$\omega_i \sim \sqrt{3}\left(\frac{m_e}{2m_i}\right)^{1/3}\frac{c}{a}\sqrt{\frac{I}{I_A}}$$

where a is the beam radius, and I_A is the Alfven-Lawson limiting current. Note that above we have assumed equal electron and ion densities since more than a 10% deviation from this condition would result in violation of the space charge limiting current condition. In our experiments, where $I/I_A \sim 1$, the above formulas give values of $k_z \sim 2\ cm^{-1}$, $\omega_r \sim 7 \times 10^9$, and $\omega_i \sim 5 \times 10^9\ sec^{-1}$. Here the average ion velocity $\beta_i c$ has been taken as equal to the beam front velocity of .045 c. The peak electric field dictated by single wave electron trapping is:[15]

$$E_{max} \sim k_z(\gamma_w - 1) \frac{mc^2}{e}$$

where γ_w is the electron γ measured in the wave frame. Numerically $E_{max} \sim 1$ MV/cm, consistent with the observed value inferred from the rf signal, and the average electric field given by the peak ion energy divided by the acceleration length.

We conclude that the high energy ions obtained in vacuum collective acceleration are not associated with travelling potential wells. Wave acceleration resulting from the electron-ion two-stream instability is probably the dominant acceleration mechanism.

The authors would like to thank George Providakes for advice on R.F. measurement techniques, and Jim Ivers and Frank Redder for technical assistance. This research was supported by AFOSR under contract no. 80-0087.

References

1. S. Graybill and J. Uglum, J. Appl. Phys. 41, 236 (1970).
2. J. S. Luce, Ann. N. Y. Acad. Sci. 251, 217 (1975).
3. R. J. Adler and J. A. Nation, submitted for publication; also Bull. A.P.S. 24, 1013 (1979).
4. W. W. Destler, L. E. Floyd and M. Reiser, Phys. Rev. Lett. 44, 70 (1980).
5. A. Greenwald and R. Little, Proc. 2nd Int. Conf. on High Power Electron and Ion Beam Res. and Tech., J. A. Nation and R. N. Sudan, eds. (Cornell University, Ithaca, New York, 1977), Vol. I, p. 553.
6. J. Rander, Phys. Rev. Lett. 24, 283 (1970).
7. J. Poukey and N. Rostoker, J. Plasma Phys. 13, 897 (1971).
8. J. L. Adamski et al., Proc. 2nd Int. Conf. on High Power Electron and Ion Beam Research and Technology, J. A. Nation and R. N. Sudan, eds. (Cornell University, Ithaca, New York, 1977), Vol. I, p. 497.
9. C. L. Olson, Phys. Fluids 18, 585 (1975).
10. R. J. Adler and J. A. Nation, J. Appl. Phys. 50, 5025 (1979).
11. W. W. Destler et al., J. Appl. Phys. 50, 3015 (1979).
12. V. Serlin, R. J. Adler, and J. A. Nation, to be published; also Bull. A.P.S. 24, 1013 (1979).
13. G. Gammel, J. A. Nation, and M. E. Read, Rev. Sci. Inst. 49, 507 (1978).
14. D. Johnson and J. Kerns, Appl. Phys. Lett. 25, 191 (1974).
15. B. B. Godfrey and L. E. Thode, Ann. N. Y. Acad. Sci. 251, 582 (1975).
16. R. C. Davidson, Theory of Nonneutral Plasmas (W. C. Benjamin, Inc., Reading, Mass., 1974).

Figure Captions

Fig. 1. Beam front position as a function of time. The start of the ion production is marked by the vertical bar.

Fig. 2. Relative timing of Faraday cup, diode voltage, current at 13 cm, and rf amplitude.

Fig. 3. The energy spectrum of ions above 2.5 MeV as measured by neutron time of flight at the end of the accelerating region.

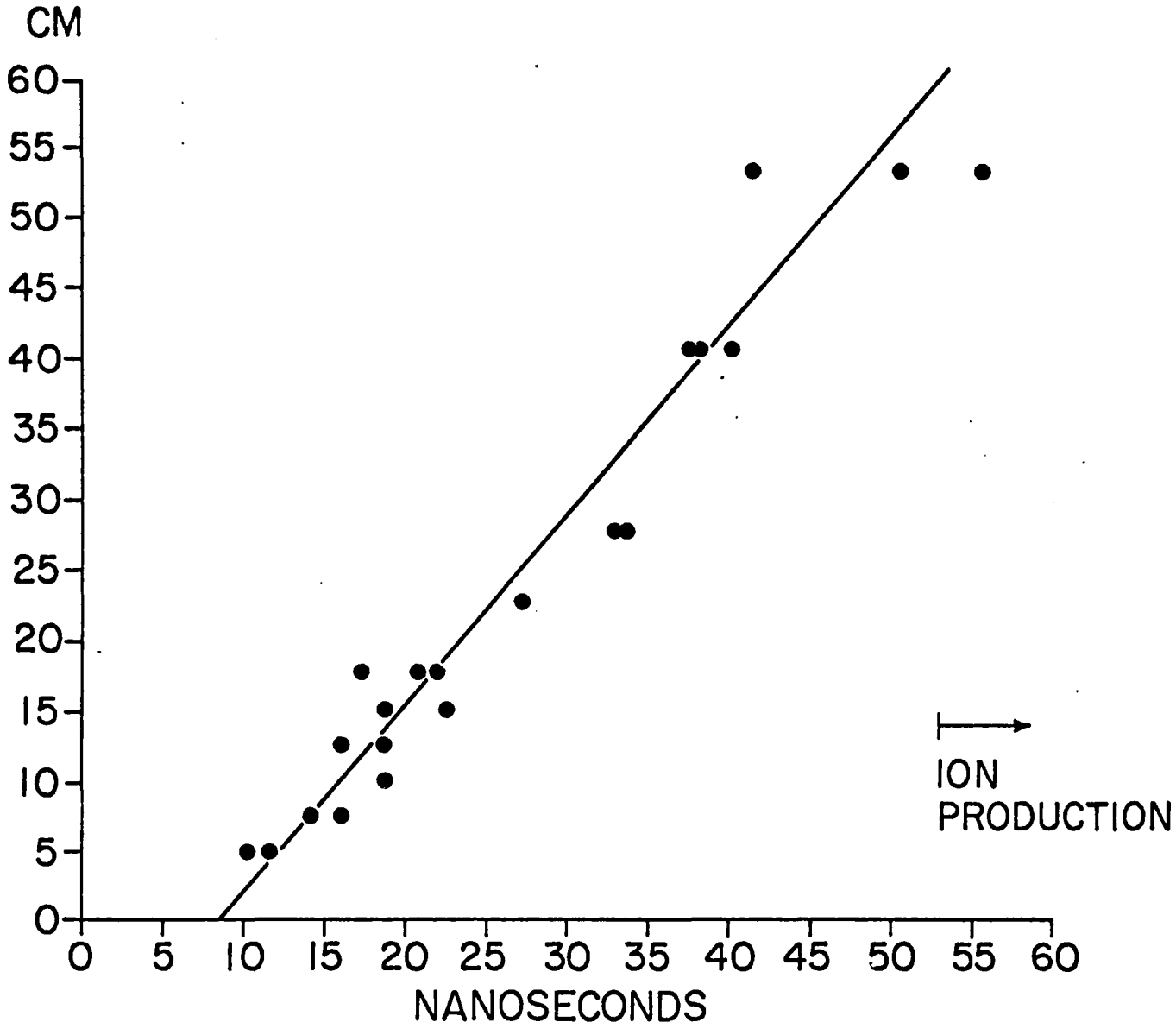
CM
60
55
50
45
40
35
30
25
20
15
10
5
0
0 5 10 15 20 25 30 35 40 45 50 55 60
NANOSECONDS
ION
PRODUCTION

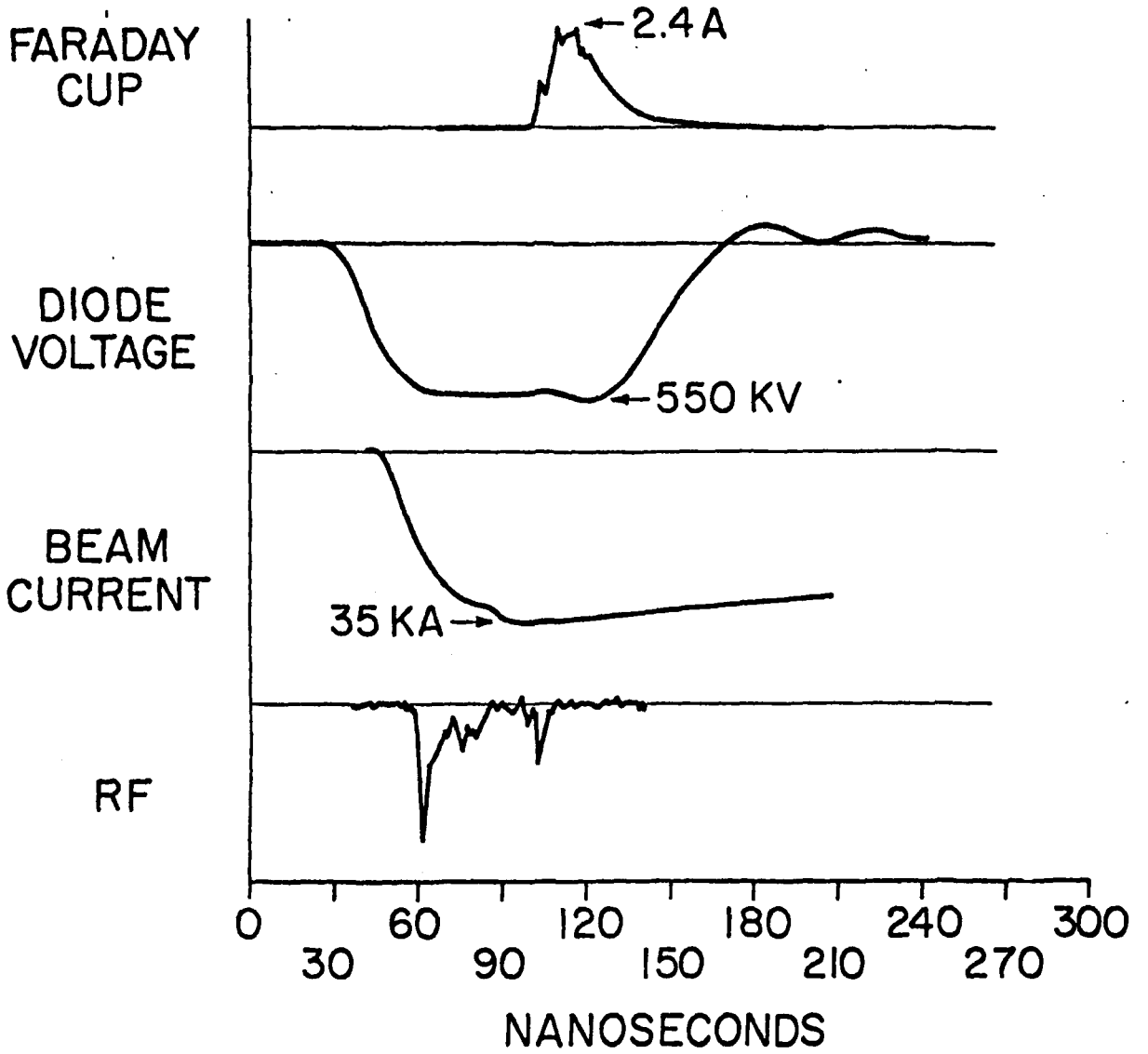
FARADAY CUP
2.4 A
DIODE VOLTAGE
550 KV
BEAM CURRENT
35 KA
RF
0
30
60
90
120
150
180
210
240
270
300
NANOSECONDS

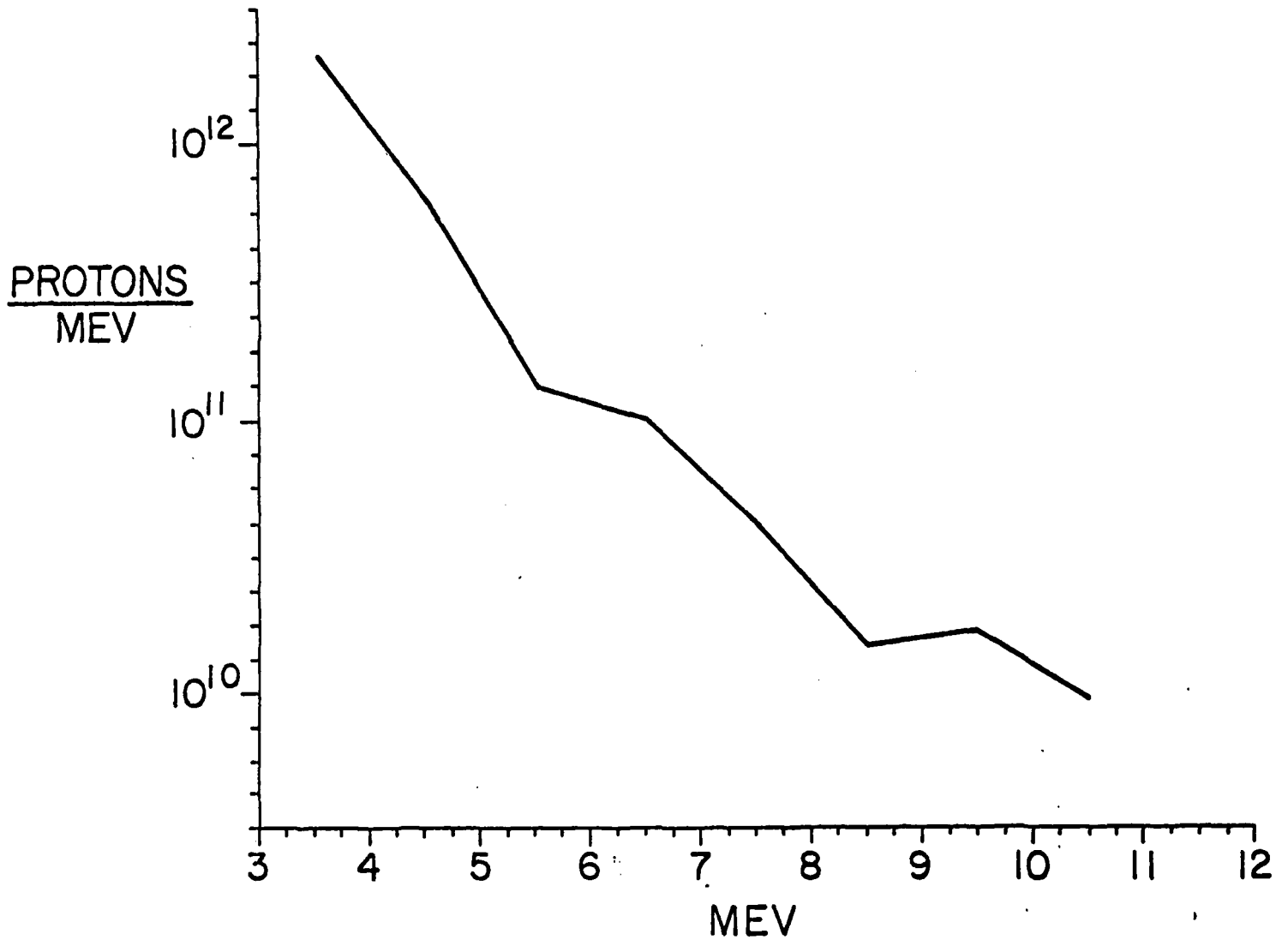
PROTONS
MEV
10^{12}
10^{11}
10^{10}
3
4
5
6
7
8
9
10
11
12
MEV

PROTON INJECTION INTO A LARGE AMPLITUDE SPACE CHARGE WAVE†

Richard J. Adler, George Gammel*, John A. Nation, James D. Ivers, George Providakes, Victor Serlin

Abstract

An account is presented of some aspects of recent progress in the Collective Ion Space Charge Accelerator (CISCA) program at Cornell University. The object of this program is to explore the potential of the slow space charge wave on an electron beam for use in an ion accelerator. We describe in this paper the results of a study of a Luce diode as an ion source and outline initial results obtained when the proton beam is injected into a space charge wave growth section. We find that it is possible to inject a beam of protons through a vacuum diode, used to generate the beam for wave growth, and for the conditions achieved to date to maintain the growth of a coherent wave.

Introduction

Previous reports[1-4] have described aspects of the use of a slow space charge wave for collective ion acceleration. Because the space charge wave can only propagate with zero phase velocity when the beam current is equal to the space charge limiting current, it is difficult to obtain and control the propagation of a wave capable of picking up an ion having a velocity of much less than 0.15 c. We have, therefore, chosen to study the Luce diode as a source of protons for injection into a demonstration wave accelerator. This device produces a continuous spectrum of protons up to an energy of about twenty times the energy of the electrons in the accelerating beam. For the purposes of demonstrating the space charge wave accelerator only the high energy protons in the tail of the ion distribution are relevant and we shall attempt to further accelerate them in the slow space charge wave.

It has proved convenient to generate the space charge wave by coupling the slow wave on a pencil electron beam to the TM modes of a periodic slow wave structure. In this configuration we have achieved wave growth and extracted waves with electric field strengths of 60 kV/cm without evidence of saturation. We have also observed wave coherence over lengths of more than one meter. Under the conditions used, the lowest phase velocity observed for the space charge wave has been about 0.25 c, a value in agreement with calculations using the measured beam operating conditions.

A central problem in the use of any wave accelerator is the injection of the protons into the wave for acceleration. The main purpose of the work described in this paper is to examine an experimental technique which will permit the nonadiabatic injection of a proton beam into the wave acceleration section. The results reported in this paper are preliminary and no effort has been made to achieve the conditions necessary for ion trapping. Rather we simply report on the technique used and on the results obtained with easily achievable ion fluxes.

Before discussing the results in the body of the paper it should be noted that we do not view the Luce diode system as a practical injector for a space charge wave accelerator. This device yields a proton flux which is restricted in its time duration and in the flux of useful ions that it yields. It does, however, serve the very useful purpose of providing an adequate source of high energy protons for injection into the wave accelerator for testing the principles involved in both the injection, loading, and acceleration. We presently believe that the most suitable wave accelerator injector system will probably be a proton Induction Linac. In this context we note that Induction Linacs have not yet been used for the acceleration of ions, although the acceleration of Cesium ions has been proposed as part of the Heavy Ion Fusion Program.[5] We are currently carrying out a design study of an ion injector system for use in a wave accelerator. The principle problem appears to be the control of the ion beam expansion, especially at low beam energies, by a combination of a partial space charge neutralization, and by magnetic guide fields. We conclude this section by noting that the injector problems, and the effects on the wave growth and wave acceleration can be adequately tested with the Luce diode as the ion injector.

Ion Source Developments

We now describe the results of our recent studies on the Luce diode as a source of high velocity protons for injection into the wave accelerator. The configuration used in these studies is shown in Fig. 1. In the results reported, which are representative of recent experiments, we have succeeded in obtaining protons with energies of more than twenty times the injection energy of the electron beam. The electron beam is generated from a Blumlein transmission line feeding a vacuum diode. The diode uses a conical

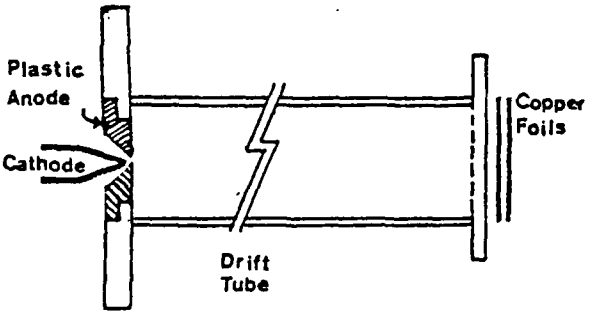

Figure 1. Experimental configuration used in the ion injector development.

aluminum or graphite cathode with a rounded tip having a radius of curvature of about 2.5 mm. The anode consists of a polyethylene disc with a thickness of 12.5 mm. It has a 45° full angle conical hole tapering at the drift tube side to 12.5 mm in diameter. A prepulse switch limits the prepulse, during the approximately 700 nsec duration charging of the line, to less than 15 kV. On a second pulse line, having a prepulse level of about 80 kV, it was not possible to obtain satisfactory diode operation. The experimental results for the ion energy spectrum, obtained using a nine ohm diode at 570 kV, less an inductive correction of order 100 kV, are shown in Fig. 2. Similar results have been obtained with higher electron beam injection energies.

To obtain this high multiple of the proton to electron energy it was necessary to operate at the impedance level stated. This occurred when the cathode tip penetrated about 6 mm into the polyethylene anode plate. The drift tube used had a 7.5 cm interior diameter and was about 1.3 m long. The ion energy spectrum was determined from copper activation of 25 micron foils located outside the drift tube. The drift

The authors are affiliated with the Laboratory of Plasma Studies and School of Electrical Engineering, Cornell University, Ithaca, New York 14853.
*Present address: Brookhaven National Laboratory, Upton, Long Island, New York 11973.

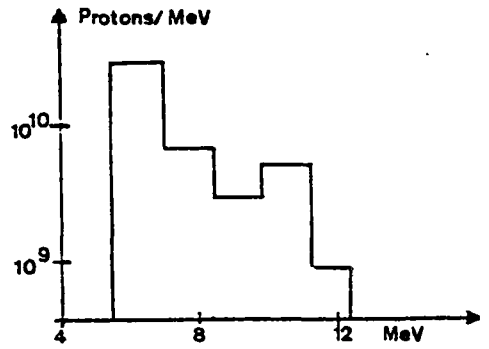

Figure 2. Proton energy spectrum from a 370 kV electron beam, obtained using a 'Luce' diode. Only that part of the spectrum above 5.3 MeV is shown.

tube was evacuated to a base pressure of approximately 10^{-4} Torr and the proton beam extracted, into the stacked copper foil system for activation analysis, through a 25 micron stainless steel foil. The results presented show an analysis of the ion spectrum taking the foils two at a time. Similar results were obtained (to within a factor of less than two) with the single foil analysis. In all cases where substantial acceleration of the protons occurred there was magnetic neutralization of the electron beam and substantially greater net currents than allowed in vacuum were monitored. The acceleration length for this experimental data was not measured, but based on previous data, was probably less than 10 cm. Autoradiographs,[6] obtained from the activated copper foils, showed that the high energy proton flux had a very low beam divergence. The spot size, after propagation of 1.3 m, was approximately 0.6 cm. This result, which is very encouraging for ion injection into wave experiments, is in contrast to the results obtained elsewhere, where a strong divergence of the high energy component of the ion beam was reported.[7] Part of this difference, as is the enhanced multiple of the proton to electron energy, is probably due to the relatively low beam diode impedance. The characteristic long high energy part of the distribution was enhanced as the beam impedance was decreased. The experiments reported here use lower beam impedances, and greater multiples of available electron current to the vacuum space charge limit,[8,9] than those reported elsewhere.

Ion Injection Into a Space Charge Wave

To test the concepts of the wave accelerator it is necessary to devise a scheme whereby the protons emitted from the Luce diode assembly can be injected into a wave growth and acceleration region. Since the injection must be nonadiabatic, we inject the proton beam into a second electron beam prior to growing the wave. Ions with the appropriate energies will be trapped in the wells of the space charge wave as it grows. In addition, since we have used for this demonstration experiment scheme one collective accelerator to produce the protons for injection into the second stage, we need to dump the hot electrons, generated in the Luce diode assembly, prior to their injection through the second diode. The dumping of the primary electron beam must be accomplished close to the second diode so that we do not lose the preaccelarated protons, prior to the space charge, re-neutralization in the second electron beam. These conditions are more severe than one might expect to encounter if an Induction Linac can be satisfactorily used as the ion source. The dumping of the remnants of the hot electrons in the first primary beam is required so that wave growth can be achieved with a second low energy, cool electron beam.

The above mentioned criteria have been satisfactorily met using the double diode configuration shown in Fig. 3.

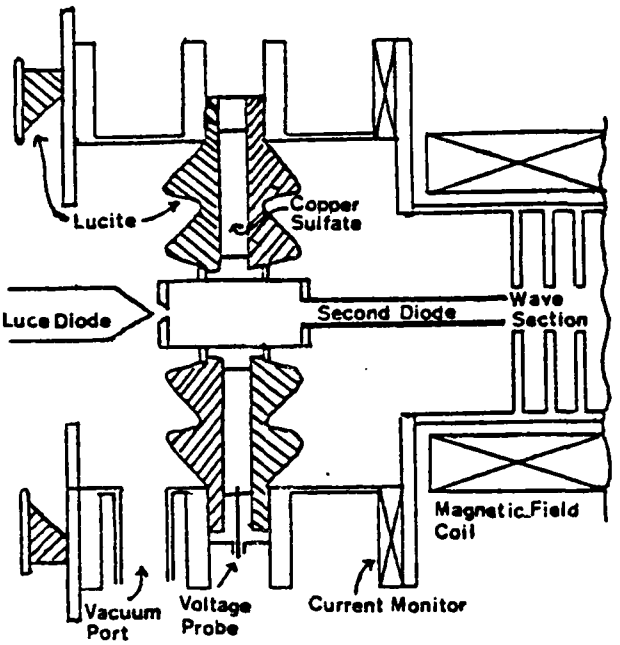

Figure 3. Schematic showing the double diode used for the injection of the proton beam into a wave growth section.

The dual diode assembly consists of a Luce diode, fed from a pulse line system, operated in series with a radial resistor. The potential drop across this .4 Ohm $CuSO_4$ resistor is used to feed the cathode of the second, low voltage diode. A pulsed magnetic field of up to about 12 kGauss is used to confine the low energy annular electron beam. The field spreads out radially close to the second cathode and does not extend into the proton acceleration region. The proton beam is accelerated from the first diode through a section of 7.5 cm diameter drift tube. The length of this section was about 10 cm in these experiments. Following the acceleration section, the three inch diameter tube changes discontinously to a 2.5 cm diameter stainless steel tube, in which is mounted the carbon cathode for the second beam. The carbon cathode is annular having a central hole of approximately 0.6 cm, through which the protons are injected into the wave growth region.

Experimental observations show that the primary electron beam current is reduced to less than 500 A, prior to exiting through the second cathode. This reduction is not due to the applied magnetic field. In fact, in the absence of the field the primary current drops to less than 50 Amps.

The protons, which are detected by the activation of Copper foils, or by time resolved Faraday cups, indicate that there are approximately 5×10^9 protons with energies between 5 and 7 MeV traversing the 1.7 meter length from the first diode to the end of the drift region. The current associated with this part of proton flux is approximately 0.1% of the electron current injected into the wave growth region. In addition to the higher energy ions there are also a number of ions with energies below the approximate 5.5 MeV energy

threshold for activation of the Copper foils, external to the drift tube (approximately 1 MeV is lost in traversing the 25 micron stainless steel vacuum seal). Figure 4 shows traces of various waveforms from the double diode system and the Faraday cup detector. The arrival of the higher energy ions follows the rise of the diode voltage pulse by about 60 nsec. There is also a comparable electron current reaching the cup. This precedes the positive ions so that the arrival time of the fastest ions may be over estimated. In addition, the time taken for the neutralized electron beam to detach from the anode of the Luce diode is of order 10 nsec. We, therefore, find that the Faraday cup observations are consistent with the observed activation data. The ion signal recorded by the Faraday cup lasts about 100 nsec corresponding to a range of proton velocities from 0.12 c to 0.03 c (energy range of 7 to about 0.25 MeV).

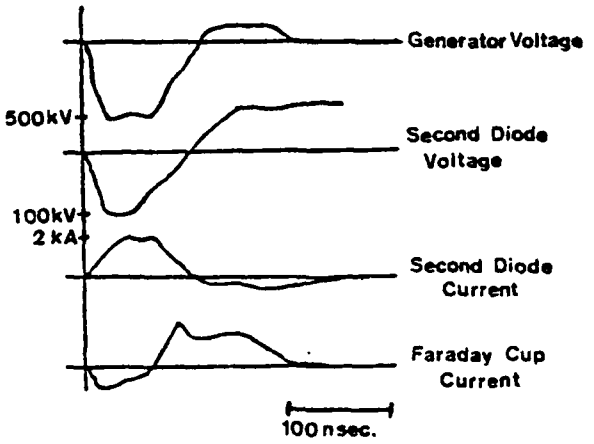

Figure 4. Double diode, and Faraday cup waveforms. The upper trace shows the generator output voltage and the second gives the lower energy diode voltage (also the primary diode current). The lower traces show the low voltage diode current and the response of the Faraday cup detector, 1.7 m from the 'Luce' diode.

Wavegrowth was recorded by a magnetic pick up loop located in the fifth of the six r.f. cavities used in the slow wave structure. This cavity was located approximately 65 cm from the Luce diode. Consequently, the proton flux traversed the measurement cavity at a time starting 20 to 30 nsec after the initiation of the diode pulse and continued throughout the remainder of the electron beam duration. r.f. emission was detected during the time interval when protons were present. There was no detectable degradation of the r.f. emission when the protons flux was present over that with no ions present. The r.f. emission was, in part, associated with the electron beam current from the first diode as evidenced by a reduction in the emission level when the hole through the second cathode was blocked. It is not clear, however, whether the contribution to the electron current arising from the primary beam has the full generator energy or only that of the low voltage diode. In these experiments the total line voltage was in the range 350-600 kV with a Luce diode current of about 25 kA. The second (low voltage) beam was therefore operated in the energy range 80-100 keV, and at a diode current level of 600-900 A.

In summary, we find that we can propagate high energy ions through a low voltage diode and maintain growth of a coherent wave. The operating conditions have not yet been optimized and it is possible to increase the ion and electron energies and the electron beam current. It is now possible to study, at interesting ion loading levels, the effects of resonant and nonresonant neutralizing background protons on wave growth and ion acceleration. These measurements will be carried out in the near future. The present measurements have confirmed the viability of the injection technique and give favorable first indications of the effects of ion loading on wave generation.

[*]This work supported by AFOSR, BMDATC, and NSF.

References

1. R. Adler, G. Gammel, J. A. Nation, M. E. Read, R. Williams, P. Sprangle, and A. Drobot, "A Wave Accelerator for Collective Ion Acceleration", Proc. 2nd Int. Conf. on High Power Electron and Ion Beam Research and Technology, Vol. II, 509-220, (Oct. 1977).

2. R. Adler, G. Gammel, J. A. Nation, G. Providakes, and R. Williams, "Space Charge Waves and Collective Ion Acceleration", to be published in Proc. 3rd Int. Conf. on Collective Methods of Acceleration, (June 1978). See also, Cornell University Laboratory of Plasma Studies Report 248 (July 1978).

3. R. Adler and J. A. Nation, "Ion Acceleration Mechanisms in Vacuum Diodes", Cornell University Laboratory of Plasma Studies Report 255 (Aug. 1978). To be published.

4. G. Gammel, J. A. Nation, and M. E. Read, "Slow Space Charge Wave Propagation on a Relativistic Electron Beam", Cornell University Laboratory of Plasma Studies Report 262 (Jan. 1979). To be published.

5. A. Faltens and D. Keefe, "Applications of Induction Linac Technology to Heavy Ion Fusion", Lawrence Berkeley Laboratory Report 6453 (July 1977).

6. R. Miller and D. Straw, "Scaling Studies of Collective Ion Acceleration with Intense Relativistic Electron Beams", IEEE Trans. Nucl. Sci. NS-22(3), 1022-1024, (June 1975).

7. J. Adamski, P. Wei, J. Beymer, R. L. Guay, and R. L. Copeland, "Collective Ion Acceleration in a Vacuum Diode", Proc. 2nd Int. Conf. on High Power Electron and Ion Beam Research and Technology, Vol. II, 497-507, (Oct. 1977).

8. J. S. Luce, "Neutrons and Radio Isotopes Produced by Collective Effect Acceleration", Annals of the N.Y. Acad. of Science 25, 217-233 (1975).

9. C. N. Boyer, W. W. Destler, and H. Kim, "Controlled Collective Field Propagation for Ion Acceleration Using a Slow Wave Structure", IEEE Trans. Nucl. Science NS-24, 1625-1628, (June 1977).

Published in Proc. 3rd Int. Conf. on High Power Electron and Ion Beam Research and Technology.

#12

STUDIES OF A SLOW SPACE CHARGE WAVE COLLECTIVE ION ACCELERATOR*

R. J. Adler, G. Gammel, T. Hughes, J. Ivers, J. A. Nation, E. Ott
G. Providakes, and V. Serlin
Laboratory of Plasma Studies and School of Electrical Engineering,
Cornell University, Ithaca, New York 14853 USA

I. INTRODUCTION

The collective ion acceleration program, at Cornell University, has as its objective a demonstration of the feasibility of using a slow space charge wave for the acceleration of protons.[1,2,3,4]

Due to the nature of space charge wave propagation in bounded media it is necessary, in order to achieve trapping, to inject moderately high energy ions into the wave. To accomplish this experimentally we have elected to use a second collective accelerator to generate the high energy ions required for the injection. The overall status of the program has reached the point where we have successfully injected high energy protons into a wave growth section, and have grown the wave in the presence of the ions. To date we have not achieved the conditions required for trapping of the ions in the space charge wave.

We shall in this paper review each of the elements of the program including an account of the "Luce" diode collective accelerator system to be used as the injector. We view this device as a convenient, and perhaps the only readily available device capable of producing an adequate number of ions for injection into the slow space charge wave. For the wave accelerator we are only interested in the high energy tail of the spectrum of the accelerated ions. We have experimentally achieved conditions where we have accelerated protons to energies up to about 25 times the electron beam injection energy. Wave studies are also reported in which we have achieved conditions where electric fields of up to about 60 kV/cm have been achieved at phase velocities of approximately 0.25 c. Present experimental work is aimed at monitoring the time history of the wave phase velocity on a 250 kV beam. Theoretical studies are also reported of large amplitude soliton propagation along a strong magnetic field. These studies show a substantial reduction in the soliton velocity as its amplitude is increased. Negative wave velocities have been observed at currents close to the limiting current for large amplitude waves. These results are important since they indicate that the conditions required for an injector may be relaxed when large amplitude waves are used. Finally, we shall describe experiments in which a proton beam from a "Luce" diode was injected through the cathode of an electron beam generator and wave growth monitored in the presence of the ion pulse. This latter experiment required that the electron beam used to collectively accelerate the protons be dumped prior to

*This work supported by U.S. AFOSR, BMDATC, and NSF.

ion injection into the wave growth region. This was accomplished satisfactorily without serious loss or enhanced divergence of the proton beam.

II. PROTON ACCELERATION IN VACUUM DIODES

Proton generation and acceleration in vacuum diodes has been reported in several laboratories.[5-7] Our studies have been mainly aimed at acquiring a high energy component in the tail of the distribution. In the configuration used in these experiments we have used a conical cathode inserted in a tapered hole cut into the polyethylene anode. The acceleration occurred in a 7.5 cm diameter tube immediately following the anode. The ion energy spectrum was determined from the activation of stacked copper foils mounted at the end of a 1.3 m long drift tube. A variety of additional diagnostics were employed to determine the acceleration mechanism. Figure 1 shows a spectrum of the accelerated protons obtained when a 700 kV, 60 kA beam was injected into the tube. Similar results have been obtained throughout the diode voltage range extending between about 500 kV and 750 kV, with the peak proton energy scaling approximately linearly with the injection conditions. Note that in the operating regime where high energy protons have been recorded it has been necessary to operate the generator at low impedance. In the case appropriate to the spectrum shown in Fig. 1 the corrected diode voltage is substantially lower than the monitored voltage. The corrected diode voltage for this event was less than 600 kV. The highest energy ions monitored have an energy corresponding to about 25 times the corrected diode voltage. Autoradiographs taken from the activated copper foils show that the ion beam has a size of about 2.5 cm after propagation through a drift tube about one meter long. In the experiments to be described later where an ion beam was injected into a wavegrowth structure followed by a 2.5 cm diameter tube, autoradiographs showed that the ion beam was better contained with the full spot size being about 0.6 cm after propagation through more than 1.5 m. In contrast to this observation we also note that there is a substantial radial loss of protons close to the anode plane. This is inferred from the detection of about 10^8 neutrons arising from

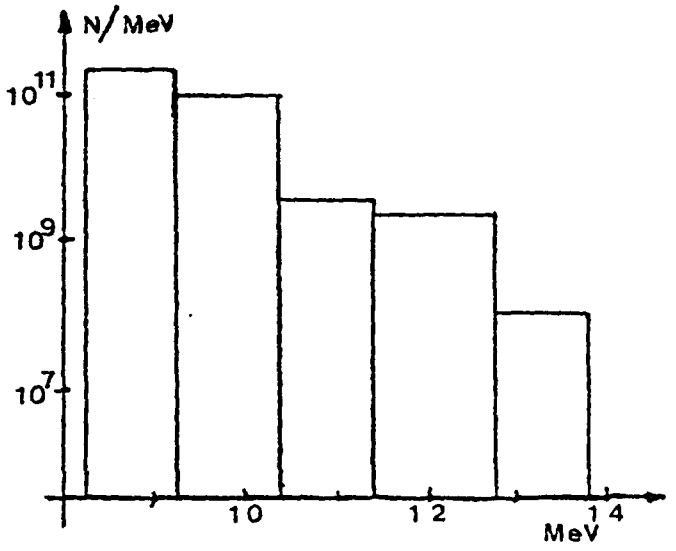

Fig. 1. Energy spectrum of collectively accelerated ions. Proton fluxes approaching 10^{10}/MeV may be obtained at high energies.

proton bombardment of the steel walls of the tube. The reaction forming the neutrons has a threshold energy of about 5.6 MeV. Generally the neutron detector output scaled fairly closely with the number of protons accelerated along the drift tube. It would seem that the acceleration close to the diode exhibits a strong two dimensional flow, while the axially accelerated protons only show a low divergence.

In other experiments we have attempted to measure the acceleration length for the protons by increasing the drift tube diameter non-adiabatically. At the discontinuity the space charge well at the beam head will change abruptly and it is reasonable to expect that the accelerated ions will be decoupled from the moving well. By varying the location of the discontinuity we find that acceleration continues over the first 15 cm of the drift tube at an average field strength of approximately 1 MV/cm. Close to the diode the accelerating field was somewhat stronger corresponding to about 2 MV/cm. A series of careful experiments have also been carried out to search for the existence of high energy electrons. These experiments are described in detail elsewhere.[8] They showed that there was no evidence for the existence of electrons having energies greater than about 80% of the uncorrected diode voltage. The failure to detect these electrons indicates that deep potential wells at the beam head are not present in our experiment and that they do not play a role in the acceleration. In these experiments additional evidence was also obtained for ion acceleration by moving wells from a comparison of the activations obtained in copper and mylar foils. The $C^{12}(d,n)N^{13}$ reaction contributes substantially to the activation of the carbon in the mylar, having an approximately equal yield to that arising from the $C^{13}(p,n)N^{13}$ reaction. This arises because of the greater abundance of C^{12} than that of C^{13} in the mylar. The deuteron activation in the copper is inconsequential as regards the yield of activated copper due to the small number of deuterons accelerated. A comparison of the activations of the two foils shows results consistent with the acceleration of a number of deuterons (having about the isotopic abundance relative to the protons in the plastic anode) to twice the energy of the protons.

Summarizing our present results we have obtained a proton spectrum extending out to about 25 times the corrected diode voltage. The velocity of the highest energy protons matches fairly closely the movement of the electron beam front as determined from Rogowski coil measurements of the net beam current. Net beam currents, measured 30 cm from the anode plane, show rapidly rising current waveforms to peak currents more than one order of magnitude greater than the vacuum limiting current. It would seem that the highest velocity protons recorded might well be limited by the inductively driven voltage developed at the beam head exceeding the driving voltage in the diode. A limit somewhat similar to this, but possibly less severe, has been examined by Putnam[9] and extended by Tsytovich and

Khodataev.[10] It should be noted that we have had to drive the electron beam source extremely hard (i.e., at low impedance) to obtain high multiples of the proton energy to the injection energy of the electrons. It was not possible in our experiments to obtain high energy components in the proton spectrum at the impedance levels reported elsewhere. This observation is consistent with the speculation offered above since the other experiments employed moderately high impedance beams in large diameter, short drift tubes.

III. WAVE PROPERTIES

The rapid dependence of the slow space charge wave phase velocity on the ratio of the beam to the limiting current indicates that the slow space charge wave accelerator may be best suited to the acceleration of ions from moderate energy to high energies. To achieve a practically useful accelerator, assuming the results of linear theory, we shall require an injector having an output energy of about 20 MeV. For our demonstration of the feasibility of the space charge wave accelerator we have decided to use a relatively low energy electron beam for the wave generation so that we can pick up ions having velocities of order of or slightly less than 0.2 c. Most of our work has been devoted to the development of techniques for the growth, control, and propagation of slow space charge waves on a 350 kV electron beam. These measurements have been time integrated over the duration of the pulse giving average phase velocities. Our present activities are concerned with the time evolution of the wave growth and its phase velocity, using a 250 kV beam. Figure 2 shows a calculated curve for the low amplitude wave phase

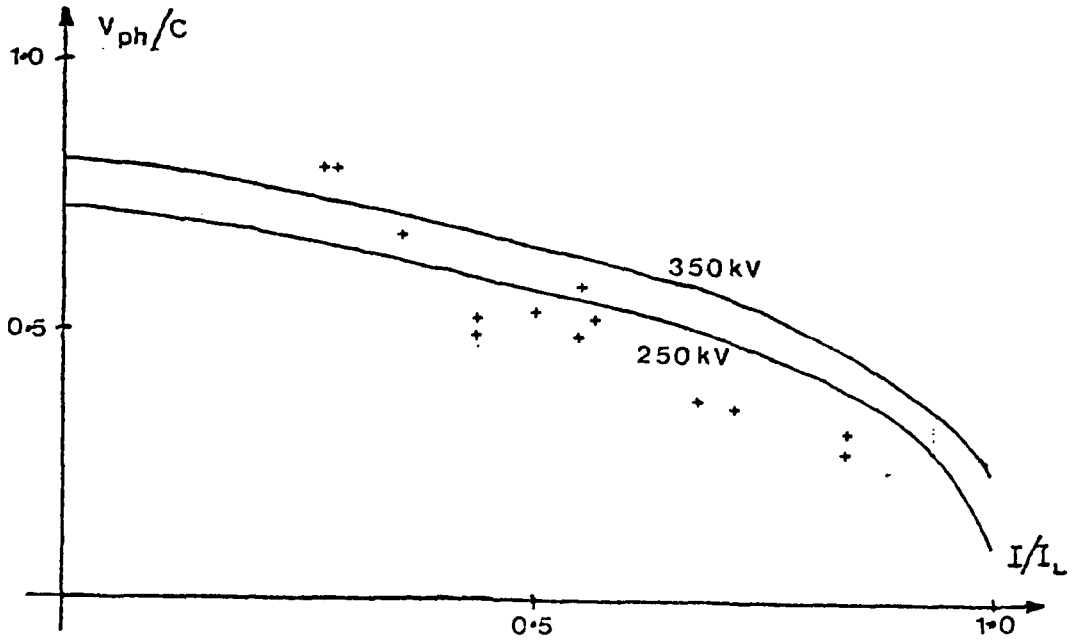

Fig. 2. Wave phase velocity at 1.1 GHz for a pencil beam in a drift tube. The solid lines represent the calculated velocities for 350 and 250 kV beams. The experimental points shown were obtained at an injection energy of 350 keV.

velocity as a function of the current to the limiting current. The two curves correspond to the cases of a 350 and a 250 kV pencil electron beam carrying 1.1 GHz space charge waves. The experimental points correspond to data obtained for the 350 kV beam case. The experimental data is appropriate to propagation of a 1.2 cm diameter beam in a 2.8 cm diameter drift tube. The experimental velocities, which were obtained for wave growth at 1.1 GHz are consistently lower than the expected values. The peak wave amplitude in these experiments corresponded to an accelerating electric field of 60 kV/cm. A feature of these experiments, and others in which the wave was carried on an electron beam in a diverging tube, was the onset of an instability in the beam propagation at currents close to the limiting current. In an experiment the space charge wave was grown on a beam having a current of 60% of the limiting value in the 2.8 cm tube. Following wave growth the tube size was increased to 7.5 cm in diameter. Measurements showed that the wave phase velocity first decreased as the tube expanded and subsequently increased in the latter half of the diverging section. Damage patterns showed that the beam had also expanded across the magnetic field lines. In these experiments the guide field was relatively weak having a value of about 6 kG so that some additional stabilization of the instability could probably have been obtained with a stronger field. The measured velocities were consistent with the measured beam size.

The generation and control of the wave growth is well understood. In this area we have measured the growth characteristics of the wave in the slow wave section of the tube and found growth rates of about 5 dB/cavity. The bandwidth of the signal was less than 40 MHz. Signals measured using pickup loops in the slow wave structure cavities showed well behaved wave trains. The growth rate of the instability was controlled by the use of dissipative material in the cavities. In these experiments we have reduced the growth rate to less than 1 dB/cavity by inserting resistive sheets in the cavities. With resistive damping present or absent we found that the signal was unsaturated after the end of the wave growth section. In the experiments mentioned above we used six cavities. Continued signal growth has been observed with up to nine cavities.

Figure 3 shows drawings of representative waveforms obtained in our present 250 kV experiments. The signals represent the outputs of two crystal detected signals from magnetic pick up loops, arranged to monitor the azimuthal magnetic field as a function of position along the drift tube. There is a common mode rejection of greater than 13 dB of the electrostatic fields of the pulse and wave. The second pulse gives the signal from the second pick up loop (a movable loop probe) and has been delayed by about 150 nsec from the first loop output. The third signal, which is delayed by a further 150 nsec, gives the interference signal obtained from combining the two signals. This technique has only just been

developed in our laboratory and has not yet been fully exploited under a variety of operating conditions. We have obtained a variety of beam characteristics during the hundred nanosecond beam pulse. The details of the waveforms depend on the detailed operating conditions. These variations are useful allowing us to monitor the change in the wave phase velocity corresponding to changes in the beam current to limiting current ratio during the pulse. The present technique will allow us to follow the evolution of the wave propagation during the pulse on a single shot basis. The system used has an approximate 500 MHz bandwidth. Note in Fig. 3 that the detected waveforms show two peaks and that the first peak

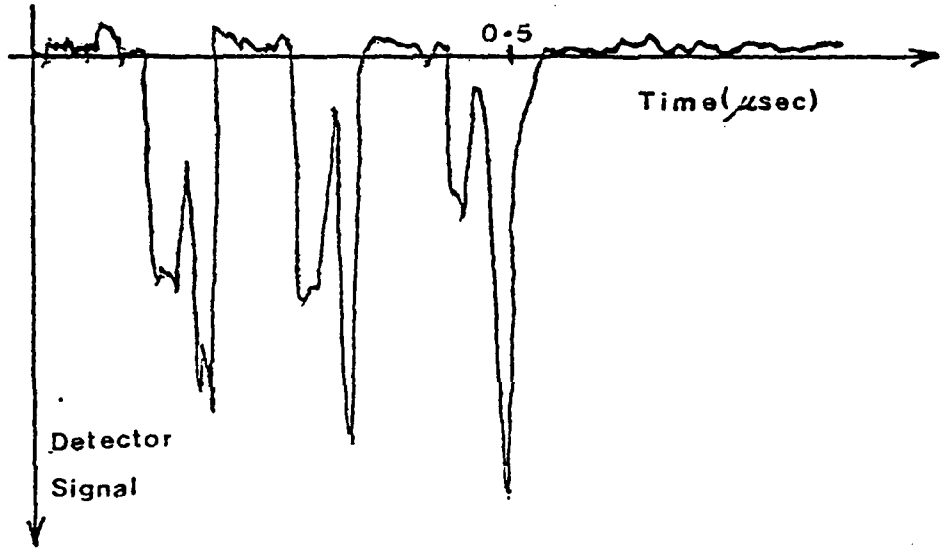

Fig. 3. Crystal detector outputs from two magnetic pickup loops located at different axial positions in the drift tube. The first two peaks represent the pickup signals and the third shows the interference pattern obtained by combining the two signals.

in each signal shows a destructive interference on combining the waveforms. In contrast, there is some reinforcement of the latter peak. The change in the interference pattern during the pulse corresponds to a change in the wave phase velocity as the net beam current changes during the pulse. A detailed analysis of the time variations has not yet been performed.

An interesting and important development for the space charge wave accelerator has arisen as a result of the study of the propagation of nonlinear solitons on a cold electron beam. In the wave frame of reference the use of the conservation of energy and particle flux in the Poisson equation gives

$$\nabla^2\phi = 4\pi e\Gamma(r)v^{-1} \quad ; \quad W + e\Phi = (\gamma - 1)mc^2 \ \ldots, \qquad (1)$$

where $\Gamma(r)$ and W are the particle flux and the electron energy. Numerical solutions of Eq. (1), for the case of a solid beam occupying 44% of the tube and for an electron injection energy of 250 keV, have been obtained. Figure 4 shows a

plot of the soliton velocity as a function of the perturbed potential on the tube axis at the center of the soliton. The velocity is given in the laboratory frame of reference and the potential well depth in the soliton is normalized to the equilibrium radial potential well depth Φ_o.

For the three cases shown, Φ_o has the values 160 kV, 177 kV and 185 kV, respectively. The upper point in each of the curves corresponds to the amplitudes at which the solitons break. As the amplitude of the wave is made larger the soliton profile sharpens, with the density profile spiking sharply close to the breaking amplitude. The characteristic axial width of the potential well varies with its amplitude and is somewhat less than the tube radius, close to the breaking amplitude.

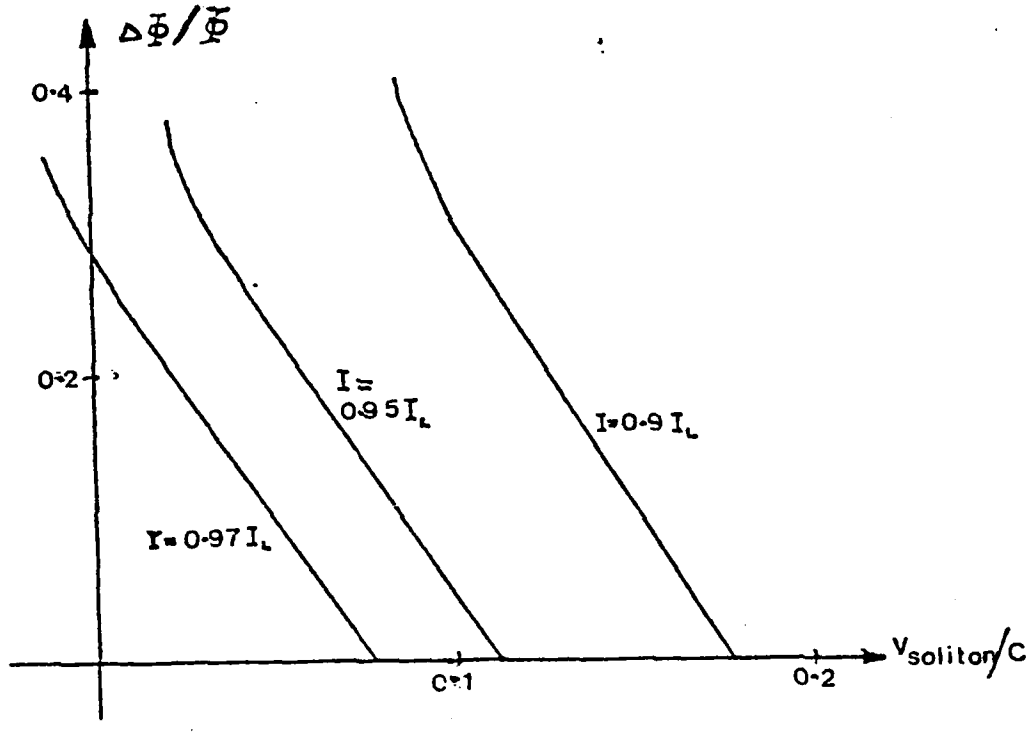

Fig. 4. Perturbed potential at r = 0, $\Delta\Phi = \Phi(z = 0) - \Phi(z = \infty)$ (where z = 0 corresponds to the peak of the soliton) normalized to the equilibrium radial well depth Φ_o, versus the soliton velocity in the laboratory frame. I_L denotes the limiting current.

The reduction in the velocity of the soliton as a function of its amplitude is substantial and can even result in negative velocities when the beam current is close to the limiting current. Although these results are appropriate to the propagation of a soliton it is not unreasonable to anticipate that similar results apply for periodic wave solutions. This result is important since it

suggests the injector requirements for a space charge wave accelerator may be considerably relaxed. Work is currently in progress on the amplitude effects on the propagation velocity of periodic space charge waves. It should also be noted that if large amplitude zero velocity periodic wave solutions exist then they may be excited in a nonuniform region, such as the injector location. The equilibrium would then be periodic rather than uniform.

IV. PROTON INJECTION INTO A SLOW SPACE CHARGE WAVE

We comment briefly here on the problems associated with the injection of a proton pulse into a space charge wave accelerator. To achieve trapping it is necessary to non-adiabatically inject the protons into the wave train. The experimental procedure envisioned considers injection of the proton pulse through a hollow cathode and subsequently growing the wave about the ion loaded beam. A similar procedure would be required for staging of the accelerator. i.e., it may be desirable to have several stages in an accelerator corresponding to given ranges of the wave phase velocity. In either the initial injector or in transfer between successive stages of an accelerator is necessary to transmit the accelerated protons into the new generator section while dumping the majority of the 'used' electrons. To test this concept we have injected a proton pulse from a "Luce" diode through a hollow cathode into a wavegrowth section and examined the effect of the ion loading on the wave growth. The proton pulse used had a maximum energy of about 7.5 MeV, and at the highest energies an ion flux of about 5×10^9 protons/MeV. This number was substantially higher at lower energies. The separation between the accelerator cathode tube (1.2 O.D., 0.6 cm I.D.) and the anode of the Luce diode was about 10 cm. The Luce diode current was 25 kA at a beam energy of 500 keV. Following the acceleration region the protons entered the 0.6 cm diameter hole in the cathode. This pipe was approximately 25 cm long. The cathode of the accelerator used for the wavegrowth was immersed in a strong axial magnetic field of 12 kG so that the injected particles had also to cross the fringing magnetic field lines prior to entering the diode which generated the beam used for the wavegrowth. The combination of the small pipe and the magnetic field led to a reduction in the injected electron beam from the Luce diode to less than 50 A. The injected protons were monitored after propagation through a total tube length of 1.7 m. The density of these protons compared to the electron beam density was close to 1% in the wavegrowth region. Wavegrowth was monitored by a pick up loop located in the fifth of the six cavities used for the wavegrowth. In these preliminary experiments there was no detectable effect on the wavegrowth or coherence due to the ion loading employed. It should be noted that the wave phase velocity was more than twice as large as the proton injection velocity so that there was no possibility of trapping of the ions. First attempts to achieve

trapping will be carried out in the future.

V. CONCLUSIONS

As stated previously the Cornell slow space charge wave accelerator study has now reached the point where all of the required elements to test the scientific feasibility have been tested, albeit not simultaneously for each of the required parameters. The recent results on the soliton wave velocity are especially encouraging in that they suggest there may be that a substantial relaxation in the requirements for an injector into the wave accelerator. Present data suggests that a reduction in the wave velocity may have been observed. With the current development of the phase velocity measurement techniques giving results on a single shot time resolved basis we now have the techniques needed to explore this effect further. Future work will be devoted to the study of wave amplitude effects on the phase velocity and on attempting to achieve proton trapping in the space charge wave train.

REFERENCES

1 ADLER, R., GAMMEL, G., NATION, J. A., READ, M. E., WILLIAMS, R., SPRANGLE, P., DROBOT, A., Proc. Second Int. Top. Conf. on High Power Electron and Ion Beam Research and Technology, (Ithaca, New York, 1977), Vol. II, p. 509.

2 GAMMEL, G., NATION, J. A., READ, M. E., accepted for publication in J. Appl. Phys. also Cornell University Laboratory of Plasma Studies Report 262 (1/79).

3 ADLER, R., GAMMEL, G., NATION, J. A., PROVIDAKES, G., WILLIAMS, R., Proc. 3rd Int. Top. Conf. on Collective Methods of Acceleration, (Laguna Beach, California, 1978), also Cornell University Laboratory of Plasma Studies Report 248 (7/78).

4 ADLER, R., GAMMEL, G., IVERS, J., NATION, J. A., PROVIDAKES, G., SERLIN, V., Particle Acceleration Conference, (San Francisco, California, 1979).

5 LUCE, J. S., Annals of the N.Y. Acad. of Sci. 25, 2171 (1975).

6 ADAMSKI, J., WEI, P., BEYMER, J., GUAY, R., COPELAND, R., Proc. Second Int. Top. Conf. on High Power Electron and Ion Beam Research and Technology, (Ithaca, New York, 1977), Vol. II, p. 497.

7 DESTLER, W., KIM, H., ZORN, G., HOEBERLING, R., Proc. 3rd Int. Top. Conf. on Collective Methods of Acceleration, (Laguna Beach, California, 1978).

8 ADLER, R., NATION, J. A., accepted for publication in J. Appl. Phys. (1979) also Cornell University Laboratory of Plasma Studies Report 255 (8/78).

9 PUTNAM, S., Phys. Rev. Letters 25, 1129 (1970).

10 TSYTOVICH, V. N., KHODATAEV, K. V., Comments on Plasma Physics and Controlled Fusion 3, 71 (1977).

Submitted for Publication

#13

COLLECTIVE ACCELERATION OF METALLIC IONS

Richard J. Adler and John A. Nation

Laboratory of Plasma Studies and
School of Electrical Engineering
Cornell University, Ithaca, New York

Preliminary results of collective acceleration of Aluminum and Iron ions from metal foils are presented. Aluminum ions of up to 15 MeV have been produced from a 0.6 MeV electron beam. Results also suggest that all particle species accelerated reach the same velocity (~.035c)

Experimental studies of Collective Ion Acceleration have been centered on proton acceleration in relativistic electron beams. The primary objective is to obtain a compact, high flux/MeV accelerator. A considerably smaller effort has been devoted to the acceleration of other ions, although experimenters have reported the successful acceleration of Helium, Carbon, Nitrogen, Argon, and Fluorine ions.[1,2] There is currently interest in the acceleration of heavy ions for pellet fusion applications and also for the development of new intermediate energy ion sources for Nuclear Physics, Nuclear Chemistry, and Medical applications.

The experiments previously reported have worked in two regimes: acceleration in low pressure gases and acceleration in vacuum of ions generated from dielectric anodes. In the former case all of the ions previously listed (except carbon and fluorine) have been accelerated and in the latter, carbon and fluorine. The peak ion energies obtained were up to about 15 times the beam energy for the low pressure gas case, and up to 7 MeV/nucleon or 60 times the beam energy in the fluorine case.

We report in this letter first observations of collectively accelerated ions (Aluminum and Iron) obtained from metallic foils. The experimental configuration used makes available many species previously inaccessible for collective acceleration. The same technique can clearly be used for the production of higher current heavy ion beams ~~at generator energies~~ from positive diodes[3] for applications such as implantation.

The experimental configuration used is shown in Figure 1. The electron beam is generated from a Blumlein transmission line operated at energies of up to 600 keV. The inhomogeneous magnetic field configuration was developed as a result of the desire to form the ions by reflexing the electrons many times through the anode foil (7μm Aluminum or 12μm stainless steel) and yet

still retain a field free region for the collective acceleration. Previous experiments, using a heated foil to drive off hydrogen impurities, in a homogeneous field had been successful in generating and collectively accelerating aluminum ions to about five times the beam injection energy. In the inhomogeneous field configuration used the electrons are confined radially by the external magnetic fields, and axially by the formation of a virtual cathode, and so must reflex through the foil. Fig. 2 shows a reproduction of the diode current, voltage and the net beam current measured 15 cm downstream of the anode. The voltage trace, which has been corrected for inductive effects, shows a double peak structure characteristic of 'bootstrapping' in reflex diodes.[4] The magnetic field at the anode plane increases with radius, such that the field at r=2 cm is almost twice that on axis. The field also decreases rapidly with distance from the foil, dropping to half its value at the anode plane in 1.5 cm.

A variety of techniques were used to monitor the accelerated ions. These included use of biased Faraday cups, dielectric track detectors, Secondary Ion Mass Spectrometry (SIMS), Nuclear Activation, and a magnetic spectrometer to facilitate momentum analysis. The spectrometer configuration used had a 7 cm long planar collimator located 63 cm from the anode plane. The width of the slit was continuously variable from 0 to 13 mm and was typically about 1.5 mm. Charged particles transmitted through the collimator were deflected by a transverse magnetic field having a peak value of 13 Kilogauss. Dielectric track detectors were located 15 cm from the collimator or, if the track detector was replaced by a Faraday cup, it was located 30 cm from the collimator. The ratio of the particle charge to momentum was established by monitoring the track displacements transverse to the magnetic field and the plane of the collimator. Information regarding the energy of

the ions and their charge state was obtained by the use of mylar absorbers of 0, 2, 4, 6, and 8 micron thickness located in front of the Lexan track detector.[5] The energy is determined from the range of Al ions in the mylar[6] and the charge state is inferred from the maximum deflection of the ions traversing any given foil. This identifies the velocity of those particles and hence permits the determination of the highest charge to mass ratio present. Experimentally, this yielded a mass/charge ratio of 14±3.5 corresponding to Al^{+2} or C^{+1} ions. The ion species accelerated and peak ion energy were confirmed using a SIMS measurement. In this experiment the accelerated ions were implanted into a Nickel target.

A typical SIMS result is shown in Fig. 3 for an aluminum anode foil. The carbon ions are believed to be due to impurities in the system. The peak Aluminum ion range in the Nickel is consistent with that found from the track detector results. Faraday cup measurements show that the acceleration of the highest energy ions commenced at the time of the dip in the voltage pulse. The acceleration of protons in the system (arising from hydrocarbon impurities) was investigated using the $C^{12}(p,\gamma)N^{13}$ reactions in stacked mylar foils. Results indicated that about 3×10^{12} protons were accelerated to energies in excess of 470 keV and that less than 10% of these reached energies of 1 MeV. Failure to detect neutrons from the $Cu^{65}(p,n)Zn^{65}$ reaction confirmed that there was no significant proton flux above 2.5 MeV. The proton contamination and its effect on the accelerated aluminum ions was much smaller than expected on the basis of prior results obtained with the homogeneous magnetic field system. In the homogeneous field peak Aluminum ion energies of 2 to 5 times the beam energy were obtained if the anode foil was preheated to drive off hydrocarbon impurities. We estimate an acceleration of about 6×10^{12} Aluminum Ions, in charge states +1 and +2, to energies in excess of the beam ~~current~~ Kinetic Energy. These

e ions and their charge state was obtained by the use of mylar absorbers of 0, 2, 4, 6, and 8 micron thickness located in front of the Lexan track detector.[5] The energy is determined from the range of Al ions in the mylar[6] and the charge state is inferred from the maximum deflection of the ions traversing any given foil. This identifies the velocity of those particles and hence permits the determination of the highest charge to mass ratio present. Experimentally, this yielded a mass/charge ratio of 14±3.5 corresponding to Al^{+2} or C^{+1} ions. The ion species accelerated and peak ion energy were confirmed using a SIMS measurement. In this experiment the accelerated ions were implanted into a Nickel target.

A typical SIMS result is shown in Fig. 3 for an aluminum anode foil. The carbon ions are believed to be due to impurities in the system. The peak Aluminum ion range in the Nickel is consistent with that found from the track detector results. Faraday cup measurements show that the acceleration of the highest energy ions commenced at the time of the dip in the voltage pulse. The acceleration of protons in the system (arising from hydrocarbon impurities) was investigated using the $C^{12}(p,\gamma)N^{13}$ reactions in stacked mylar foils. Results indicated that about 3×10^{12} protons were accelerated to energies in excess of 470 keV and that less than 10% of these reached energies of 1 MeV. Failure to detect neutrons from the $Cu^{65}(p,n)Zn^{65}$ reaction confirmed that there was no significant proton flux above 2.5 MeV. The proton contamination and its effect on the accelerated aluminum ions was much smaller than expected on the basis of prior results obtained with the homogeneous magnetic field system. In the homogeneous field peak Aluminum ion energies of 2 to 5 times the beam energy were obtained if the anode foil was preheated to drive off hydrocarbon impurities. We estimate an acceleration of about 6×10^{12} Aluminum Ions, in charge states +1 and +2, to energies in excess of the beam Kinetic Energy. These

results are similar to those predicted by Ryutov[7] who assumed a quasi-neutral plasma expansion driven by the effective pressure of the reflexing electrons. It is thought that the relatively low multiple of peak ion energy to electron beam energy was associated with the strong ($B \gtrsim 5$kGauss) field containing the beam, forcing early propagation, out of synchronism with the neutralizing heavy ions. For this reason the inhomogeneous field configuration described earlier was developed.

Heavy ion acceleration in the inhomogeneous field configuration described earlier was extensively studied using aluminum anode foils. The best results achieved to date were obtained at an axial magnetic field (at the anode plane) of 3.2 kGauss. A peak in ion energy as a function of field is to be expected since for weak fields no reflexing occurs, and at strong fields the electron beam will be constrained by the magnetic field and the beam will be transported to the wall. At least four transits of the electrons through the foil are needed to provide the aluminum ions.[8] Fig. 2 indicates that about 30% of the electron beam traverses the inhomogeneous field. The net beam current rises slowly reaching a peak well into the main pulse. The rise in the net beam current shown in Fig. 2, corresponds, based on time of flight, to the arrival of the highest energy ions at the Rogowski coil location.

The propagated current signals typically have a 30-60 nanosecond exponential decay at the end of the diode current pulse. This requires a fractional neutralization $f > 1/\gamma^2$, indicating that the number of neutralizing ions is greater than 10^{13}.

Peak Aluminum ion energies of 15 MeV (25 times the e beam energy) were determined from the ion range in the mylar foils. This result agrees with the result obtained from the SIMS range measurement. Based on the Faraday

cup signals we estimate that approximately 6×10^{12} aluminum ions were accelerated to energies in excess of the beam energy and from the stacked mylar foil observations, that about 10^{10} had energies in excess of 9 MeV.

The peak in track density, its lateral displacement, and its variation with absorber thickness indicates an average Aluminum ion energy of ~2.5 MeV with charge state +1. The SIMS results show the aluminum ions have greater ranges and energies than the carbon ions, and a limit on the proton energy has been established by activation. Within the limits of accuracy of the data available, all three ions species travel at essentially the same peak velocity, $\sim 10^9$ cm/sec. In the inhomogeneous field configuration proton contamination was not a major problem and ion acceleration was not degraded if the anode foil was unheated.

Preliminary SIMS results using a stainless steel anode show the successful acceleration of Iron ions to energies of several MeV. Track detection in Mica (which does not form tracks for ions having a mass less than 28 a.m.u.)[5] gives results consistent with the SIMS.

The results place several constraints on the acceleration mechanism. The similar H^+, C^+, and Al^{++} ion velocities indicate a moving well as the dominant mechanism. Two dimension flow effects were apparently important. In addition, due to the slow beam front velocities, we can rule out inductive field effects as being dominant in the acceleration.

The technique employed in these experiments has not yet been optimized, nor has it been applied to many different metallic foils. It shows considerable promise as a method for the generation and/or acceleration of many ion species.

The results of this experiment also have implications for conventional reflex triodes. In particular, one drawback of the triode is that ions are

produced in a strong magnetic field. This need not be the case with the inhomogeneous field system shown in Fig. 1. For an appropriately designed, large area triode, a ratio of anode field on axis to confining field on the boundary of 5 should be easily achievable.

The authors would like to thank George Ramsaer for performing the SIMS analysis, Jim Ivers and Frank Redder for technical and design assistance. One of the authors (R.J.A) would like to thank the National Research Council of Canada for providing a postgraduate scholarship during the course of this work. This work was supported by AFOSR and BMDATC.

References

1. Discussions of collective acceleration of heavy ions from gases appear in S.E. Graybill and J.R. Uglum, J. Appl. Phys. 41, 236 (1970); J. Rander, B. Ecker, G. Yonas, and D.J. Drickey, Phys. Rev. Lett. 24, 893 (1970).

2. Collective acceleration of heavy ions from dielectric (teflon) anodes as discussed in J.S. Luce, Ann. N.Y. Acad. Sci. 251, 217 (1975); W.W. Destler, R.F. Hoeberling, H. Kim, and W.H. Bostick, Appl. Phys. Lett. 35, 296 (1979).

3. S. Humphries, R.N. Sudan, and W. Condit, Appl. Phys. Lett. 26, 667 (1975).

4. D.S. Prono, J.M. Creedon, I. Smith, and N. Bergstrom, J. Appl. Phys. 46, 3310 (1975).

5. R.L. Fliescher, P.B. Price, and R.M. Walker, Ann. Rev. Nucl. Sci. 15, 1 (1965).

6. L.C. Northcliffe and R.F. Scilling, Nucl. Data Tables A7, 233 (1970).

7. D. Ryutov, G.V. Stupakov, Sov. J. Plasma Phys. 2, 427 (1976).

8. D. Swain, G. Goldstein, L. Mix, J. Kelley, G. Hadley, J. Appl. Phys. 48, 1085 (1977).

Figure Captions

Fig. 1. Schematic showing the experimental arrangement for the collective ion accelerator, and for the diagnostics used.

Fig. 2. Traces of diode voltage (corrected for inductive effects), diode current and the net beam current.

Fig. 3. SIMS analysis. The ordinate gives the detected counts appropriate to the ion designated. The vertical dashed line indicates the probable location of the Nickel surface. The 16 MeV ion energy is calculated for the range of 2.9 micron beyond the surface shown.

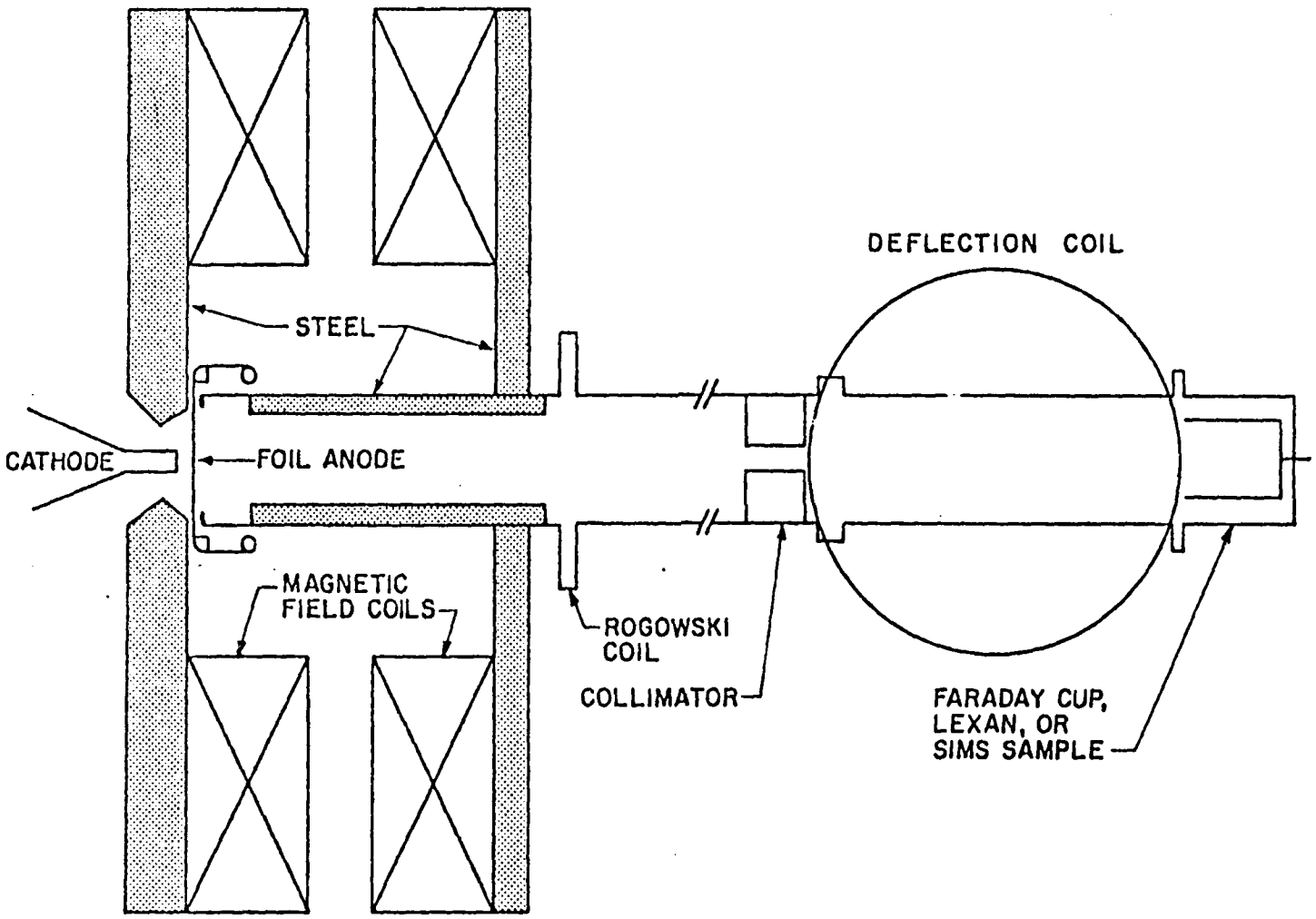
DEFLECTION COIL
STEEL
CATHODE
FOIL ANODE
MAGNETIC
FIELD COILS
ROGOWSKI
COIL
COLLIMATOR
FARADAY CUP,
LEXAN, OR
SIMS SAMPLE

Figure 1.

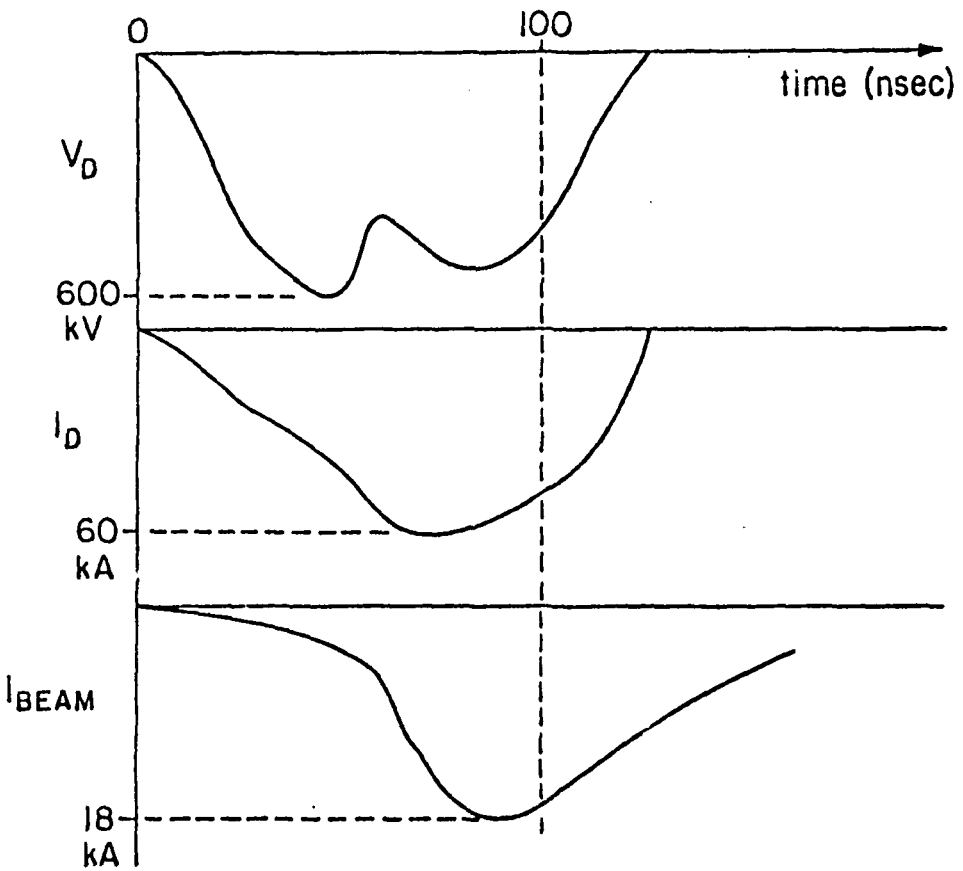

Figure 2.

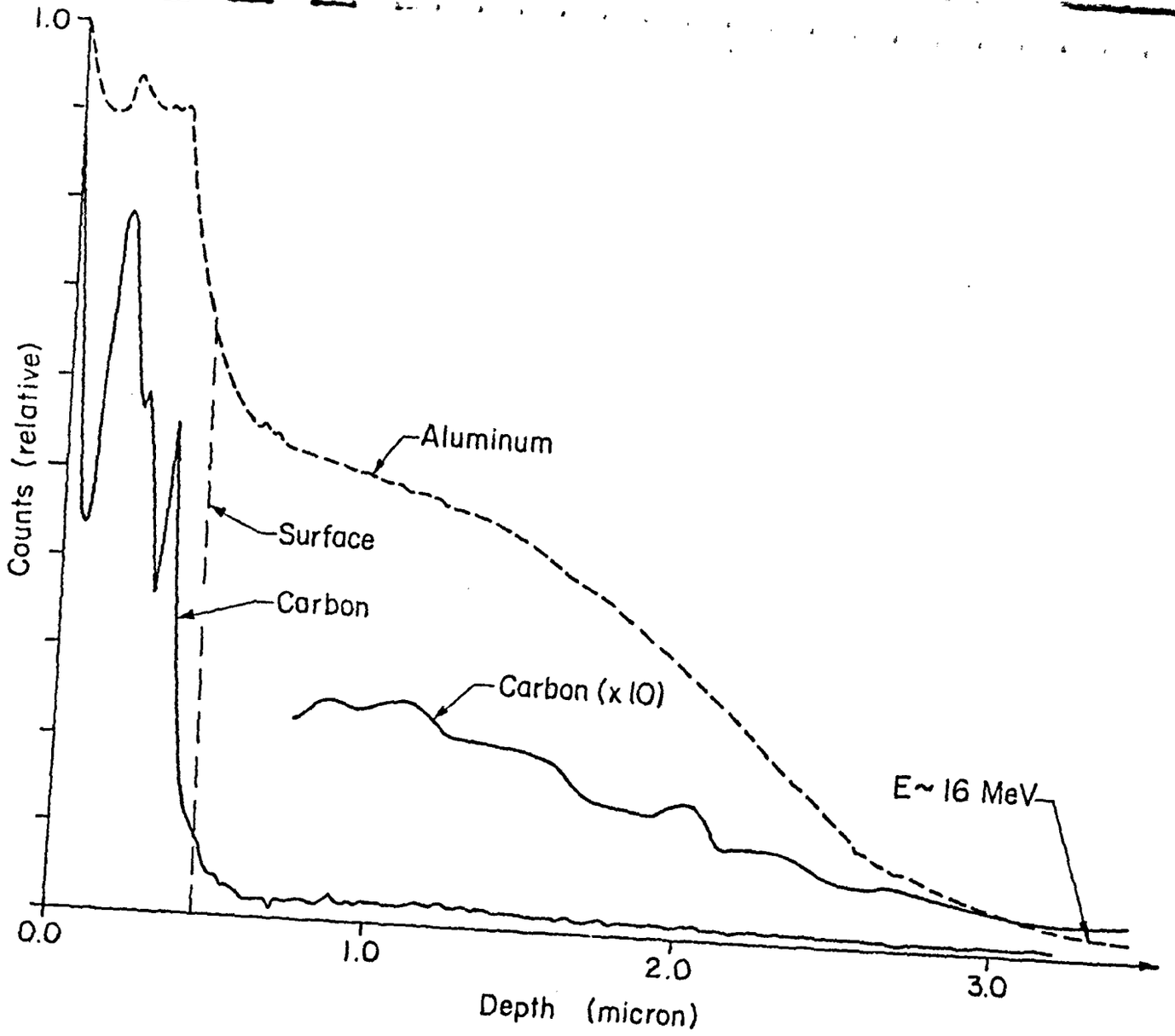
1.0
Counts (relative)
Aluminum
Surface
Carbon
Carbon (x 10)
E~ 16 MeV
0.0
1.0
2.0
3.0
Depth (micron)

Figure 3.

Particle Accelerators
1979, Vol. 10, pp. 1-30
0031-2460/79/1001-0001$04.50/0

HIGH-POWER ELECTRON AND ION BEAM GENERATION

JOHN A. NATION

Laboratory of Plasma Studies
and
School of Electrical Engineering
Cornell University, Ithaca, New York 14853

(Received January 29, 1979)

In this review we present an introduction to and summary of high-power electron and ion-beam technology. The research areas covered are diverse and have not all been previously summarized in a review. An effort has been made to include unpublished data on dielectric strengths and breakdown times in sufficient detail to be useful. Descriptions are presented of the essential machine components and their limitations from the design viewpoint. The physics of the electron and ion beam generating diodes are given, together with a summary of achieved beam characteristics. The review concludes with a brief summary of progress in the study of the collective ion acceleration, which may occur in high-current electron beams.

I. INTRODUCTION

There has been a rapid development since the early 1960's of new pulsed-power sources. These sources range from small 500-kV, 70-kA generators to large multi-terawatt sources such as the Aurora generator at the Harry Diamond Laboratories (14 MV, 1.6 MA). These generators, which were developed as devices for materials testing and as x-ray sources, typically produce high-power pulses for times of about 50–100 nsec. The generators, which can be operated in either polarity, have recently been utilized for a variety of other applications including controlled thermonuclear fusion,[1-6] and microwave generation.[7-8] In this review we shall describe the general characteristics of these beam devices, including the production of high-energy ion beams by collective processes,[9-11] but will not discuss applications other than to indicate the requirements they set on machine characteristics.

In the following sections we shall discuss the basic machine technology and illustrate this with reference to specific devices. The machines which have been constructed consist of three or more essential elements, an energy-storage device such as a Marx generator, a pulse-forming network, and a diode used for beam generation. The pulse line provides a fast-rise, short-duration pulse which is applied to the vacuum diode. The detailed design of the diode depends on whether the generator is to be operated in positive or negative polarity. For use as an ion-beam source it is necessary to suppress the electron flow, or at least to make the resistance to electron flow across the diode comparable to that for protons. We shall discuss the different configurations used for electron and ion beam generation and their relative efficiencies. In recent experiments ion beams have been generated at power levels approaching a terawatt.

Most of the work carried out to date has been aimed at producing ultra-high power electron beams at low impedance levels ($\gtrsim 1$ ohm). Although multi-terrawatt generators such as the Aurora machine (see Table I) have also been built, relatively little effort has been devoted to the production of modular, moderate-impedance, high-power, high-voltage pulses. A specific method of pulsed-power technology which has addressed this problem is the induction linac. In this device conventional pulsed-power systems are used to feed an inductive load. A particle beam in parallel with the ferrite load is accelerated by a changing magnetic field. Although little development has occurred in these systems in the last several years, the principle has been tested with the successful acceleration of several hundred amperes of electrons through a multi-stage system. This type of accelerator is currently being assessed as a 10-kA source of high-energy (50-MeV) electrons, and as an accelerator for use in heavy-ion fusion applications.

Since this review is concerned with the current research in high-power electron and ion accelerators, it is also appropriate to examine the present status of collective-ion acceleration in intense relativistic electron beams. There has been some resurgence of interest in this field in the last few years, as electron-beam technology has advanced, and

several groups are actively engaged in investigations of collective-acceleration processes. At present, most of the research has been concerned with the ion acceleration which can occur as the head of an electron beam propagates into a neutral gas, or into vacuum through a dielectric window. The most encouraging results show that proton energies of up to about 22 times the electron-beam energy have been achieved. There are also more recent efforts at controlled collective acceleration using either a wave train for the trapping and subsequent acceleration of the ions or an accelerating solitary wave. The present status of this work will also be examined.

II. MACHINE TECHNOLOGY

A. Introduction

High pulsed-power systems development was initiated at the Atomic Weapons Research Establishment in England in 1962. At that time, J. C. Martin successfully combined existing Marx-generator technology, which could be used to generate megavolt pulses with rise times of the order of microseconds, with transmission-line systems to produce short ($\simeq$ 50 nsec) duration, high-power pulses. This process required the solution to a number of technological problems ranging from interfacing compact Marx generators with pulse-forming lines to fast-switch development and finally to the coupling of sub-microsecond pulses from the pulse lines to vacuum diodes for the generation of high-power electron beams. Since that time, the development of this technology has proceeded rapidly to the point where multi-terawatt electron-beam generators are now available. The final system depends considerably on the application of the high-power pulse. Pellet fusion systems using electron or proton beams require pulse powers approaching 10^{14} watts at beam energies in the range of one to ten mega-electron volts.[12] In contrast to this, heavy-ion fusion systems require a beam energy of about 10–100 GeV in a 100-terawatt system.[13] Other applications, such as the generation of electron and ion rings for magnetic confinement of a fusion plasma,[14] show that higher energy beams will be needed than are required for electron-pellet fusion. Similarly flash x-ray sources may require, for maximum x-ray yield, higher-voltage operation to capitalize on the fact that the x-ray yield depends on the cube of the beam energy. For application to microwave generation, high-impedance machines are required, since these devices typically operate in vacuum where the electron-beam current is limited by space-charge considerations.[15–17] In summary, we find that the various applications of pulsed-power technology lead to beam requirements ranging from sub-ohm impedance, multi-terawatt systems to relatively modest megavolt generators having impedances of several hundred ohms. Table I lists the characteristics of several multi-terawatt generators. The basic technology of each of these generators is essentially identical. The development from the work of J. C. Martin and his group has occurred in a number of laboratories throughout the world and includes major programs in the U.S.A. and the U.S.S.R. In this paper we shall utilize developments in the U.S.A. to characterize machine systems. The study and development of the pulsed-power systems in the U.S.A. has occurred at several laboratories, including Cornell University, Ion Physics Co., Maxwell Laboratories, Naval Research Laboratories, Physics International Co., and Sandia Laboratories.

Figure 1 † shows a block diagram illustrating the principal components of a pulse generator. A Marx generator is used to impulse charge a pulse-forming line to high voltage. Charging is usually accomplished in less than a microsecond, so that the Marx must have a low inductance. The pulsed line is usually a Blumlein transmission line; it employs a water dielectric for low-impedance, moderate-voltage applications, or oil for high voltage use. The Blumlein has the advantage over a simple coaxial pulse line that it is capable of delivering the full charging voltage to a matched load. As shown in the figure, a transmission line couples the vacuum diode to the Blumlein. In some applications, the coupling line may also serve as a transformer to increase or decrease the characteristic impedance of the pulse. The vacuum diode is coupled to the electron-beam generation region through a solid-dielectric interface which may consist of a stacked, graded axial-ring assembly or a lower-inductance radial insulator. In pellet-fusion applications, an additional section is needed to provide the high ($\gtrsim 10^{11}$ W/cm^2) power densities required. This is provided by several long runs of magnetically insulated transmission line. We now discuss each of these components in more detail.

† Pulsed-power systems using Van de Graaff generators are also in use. They are less common, however, than the Marx Generator, pulse-line systems, and also less flexible. They do provide extremely stable sources with excellent repetition characteristics. They will not be discussed in this review.

TABLE I
Output characteristics of some multi-terawatt generators

Machine name	Voltage (MV)	Current (MA)	Pulse duration (nsec)	Power (TW)
Aurora	14	1.6	120	22
Hermes II	10	0.1	80	1
Proto II	1.5	6.0	24	9
Gamble II	1.0	1.0	50	1
Blackjack	1.3	1.1	50	1.4
Owl	1.5	0.75	110	1.2

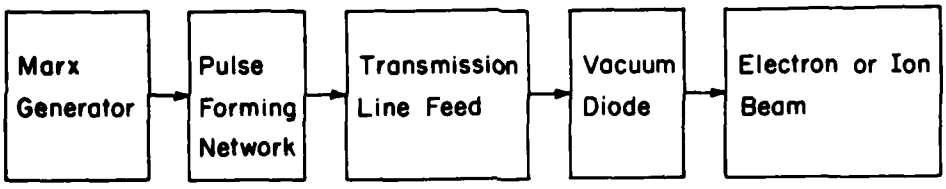

FIGURE 1 Block diagram of a typical high power pulse generator.

B. Marx Generators

A simplified schematic of a section of a Marx generator is given in Fig. 2. In the configuration shown, we have illustrated an $n = 2$ Marx. This arrangement is capable of erection, following the triggering of at least the first gap, at voltages approaching half the self-breakdown voltage of each individual gap. This configuration has been successfully used for the construction of a number of Marx generators with energies in the range of 100 kJ.

The system consists of a series of capacitors C_0 charged in parallel through the charging lines and ground returns. The system has stray capacitance C_g across each spark gap and is arranged so that there is a large C_c (compared to C_g) capacitance across every two spark gaps. To illustrate the rationale for the design, we consider the situation prevailing at the point A in the column. We assume that the previous $(p\text{-}1)$ spark gaps have closed so that the potential at the point A *is* pV_0, where V_0 is the charging voltage of each of the Marx capacitors. After erection of the column to the point A, the gap capacitor C_g and the coupling capacitor C_c act a voltage divider and the potential at the point B is

$$V_B = (p = 2)\,V_0 + 2V_0 \frac{C_g}{C_g + C_c} . \qquad (1)$$

Hence the potential difference across the gap V_{BA} is

$$V_{BA} = \frac{2V_0\,C_c}{(C_c + C_g)} . \qquad (2)$$

The coupling capacitor discharges through the charging resistor in a time of order RC_c and leaves the potential difference across the gap at twice the capacitor charging voltage, i.e., $V_{BA} = 2V_0$. The fact that the gap potential difference tends to $2V_0$ is characteristic of the $n = 2$ Marx configuration, in which the coupling capacitors C_c are made large across every two spark gaps, and because the charging and ground-return resistors also straddle two gaps. In an $n = 3$ configuration, the charging resistors couple three spark gaps and coupling capacitors C_c are made large across every third gap. For an $n = 3$ Marx, the gap voltage approaches $3V_0$ when the preceding two gaps have been triggered, and the Marx can erect, after triggering of the early gaps, with voltages of down to about one third of the self-break voltage of the individual gaps.

The high-n Marx configurations are relatively free from self-breakdown problems, but tend to erect more slowly than less complex configurations. It is not always best to use self-erecting Marx generators and in some cases it is preferable to trigger all the spark gaps. In such cases, trigger gaps may be coupled using a similar configuration in the trigger

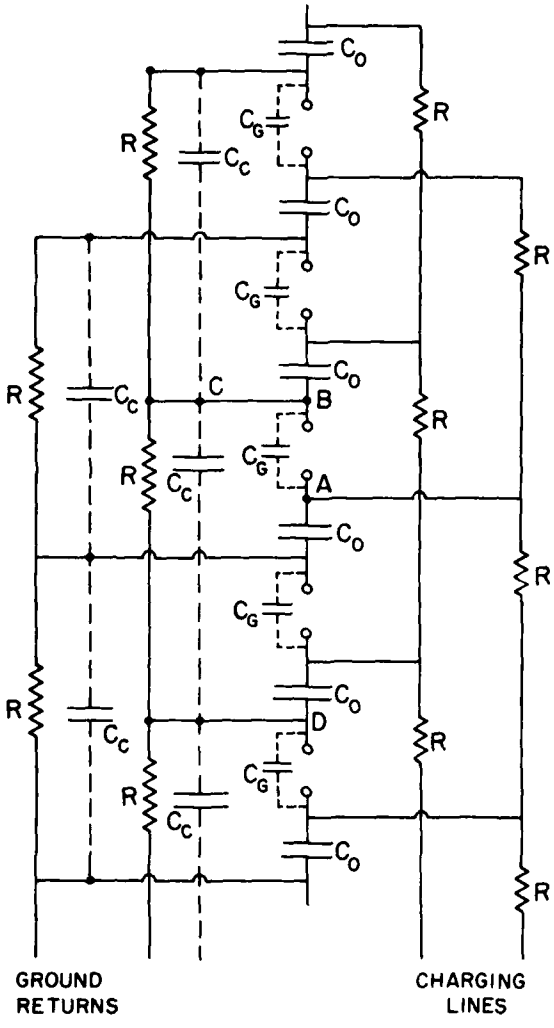

FIGURE 2 Simplified schematic of self triggered $n = 2$ Marx generator.

leads to that used for the charging columns and coupling capacitors in the self-erecting Marx. The use of plus-minus charging of alternate capacitors also enables one to reduce the number of switches required by a factor of two.

In most generators built, the charging and trigger resistors are made from copper-sulfate solution in flexible plastic tubing. These resistors are capable of high power dissipation and are also flexible enough that they can be contoured to suit the electrical stressing requirements of the generator.

In some large electron-beam generators designed to operate at low impedance, multiple Marx generators have been used as storage elements. For example, in the Proto II[18] generator at Sandia Laboratories, eight 112-kJ Marx generators are used in parallel to charge the fast line sections. This provides a lower-inductance and a faster rise-time system than could be achieved with a single large generator. Each Marx generator in this case consists of 32 0.7-μF, 100-kV capacitors. The equivalent circuit of the erected Marx generator has an output capacitance of 22 nF in series with an inductance of about 7 μH. The Marx has a series resistance of about 3 ohms and is shunted by 560 ohms.

One of the largest generators built to date, the Aurora facility,[19] has four Marx generators, each of which contains a 95 stage Marx generator with each stage consisting of four 1.85-μF, 60-kV capacitors wired as a 1.85-μF, 120-kV unit. The total energy storage in the generator is 5 MJ. The generator is a so-called hybrid Marx in which the coupling stray capacitors, and resistively coupled triggers are the dominant components in determining the column erection. The illustration of Fig. 2 shows an RC-coupled, self-erecting Marx.

A very low inductance variation of the Marx generator has been developed by Fitch and Howell.[20] This is called an LC Marx Generator and is shown in Fig. 3. In this configuration, alternate capacitors are charged with opposite polarities. On closing the switches, the column erects, reaching peak voltage in the half period of the resonant circuits. This circuit may be constructed with a low inductance, but is also prone to several different fault modes of operation, where, for example, not all of the gaps close at the proper time. Such faults may result in over-stressing, or ringing, of individual elements.

We conclude our discussion of Marx generators by noting that in certain applications the Marx generator has been directly coupled to a vacuum diode and has been used to produce a long-duration particle beam.[21,22] Beam durations of a few microseconds have been achieved and have been used for microwave generation and for electron and ion-beam production for plasma heating and containment systems. In this mode of operation, the beam rise time is much slower than that found with pulse lines and the generator impedance is relatively high, typically of the order of several tens of ohms. The shape of the pulse depends on the application but, if required, can be controlled using one or more stages of output filtering to give a 'square' pulse while

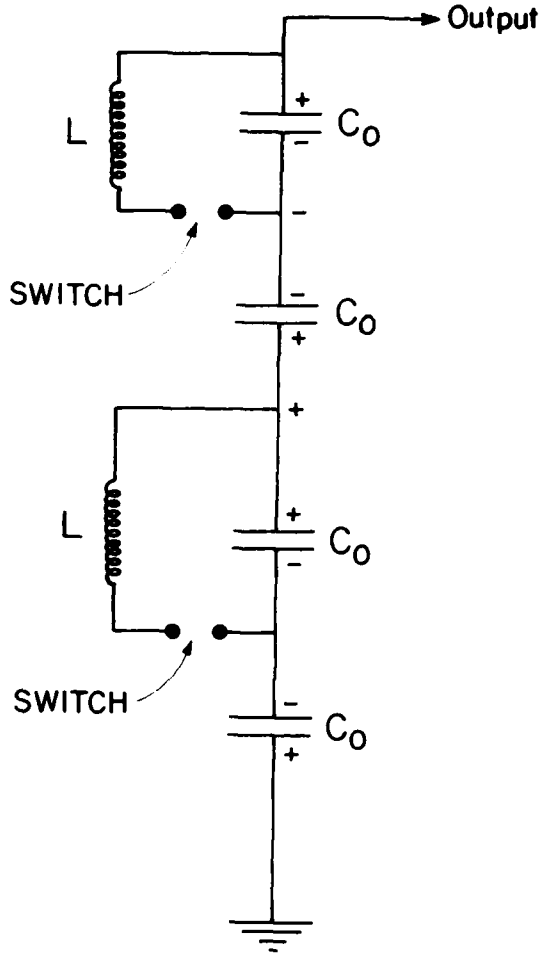

FIGURE 3 Simplified schematic of a four stage LC Marx generator. The capacitors are charged as shown. For simplicity the charging and triggering currents have been omitted.

maintaining an efficient transfer of energy from the primary Marx store to the beam.

C. *Pulse-Forming Network*

Marx generators are primary energy stores which can be used to energize a fast pulse-forming section in a time of order one microsecond. The fast section or pulse-forming network essentially consists of a transmission line that is charged from the Marx generator as a lumped capacitor, and is discharged in the transmission-line mode. The output pulse is fed to a vacuum diode which is used to generate the particle beam. The fast section typically produces an order of magnitude decrease in the pulse duration and a corresponding increase in the power output. Figure 4 shows schematically a Blumlein transmission-line system. This circuit, which was devised by A. D. Blumlein,[23] enables one to produce an output pulse into a matched load equal to the original charging voltage of the line. This is, of course, in contrast to the simple pulse line which delivers half of the charging voltage across a matched load.

In many instances, the Blumlein circuit consists of three coaxial cylinders with the intermediate cylinder charged from the Marx generator. There are also a number of refinements of this basic circuit which may be used to enhance the triggering capability or to modify the output characteristics. We shall discuss the basic principles first and subsequently outline specific modifications necessary for the special applications.

The intermediate conductor of the coaxial Blumlein is charged from the Marx generator in a time of the order of or less than one microsecond. Typical dielectrics used to insulate the conductors are deionized water or transformer oil. The RC discharge time for 10^4 Ωm water in cylindrical geometry is $\rho\varepsilon \sim 7$ μsec. Hence, submicrosecond charging times are adequate. The insulating interfaces are commonly made of lucite or some other plastic. These interfaces may also serve as supports for the conductors. The center conductor of the Blumlein is electrically connected to the outer grounded cylinder by a few microhenry inductor. The inductor ideally acts as a short circuit during the 1-μsec charging of the line and as an open circuit, compared to the characteristic impedance of the line, on the output-pulse duration time scale. The output impedance of the generator is equal to the sum of the characteristic impedances of the separate coaxial sections. The matched load impedance is therefore equal to the characteristic impedance of the section of coaxial line separating the Blumlein section from the load. This latter section is also helpful in reducing the prepulse voltage, which appears across the diode gap during the charging cycle, due to the unequal charging rates of the two halves of the Blumlein. The prepulse may be further reduced by the addition of a gas prepulse-suppression switch prior to the diode. Provided that the switch has a low capacitance compared to the diode assembly plus the feed section on the diode side of the switch, the switch will capacitively divide any prepulse voltage according to the capacitance distribution. As shown in the figure, the line is switched at one end and left

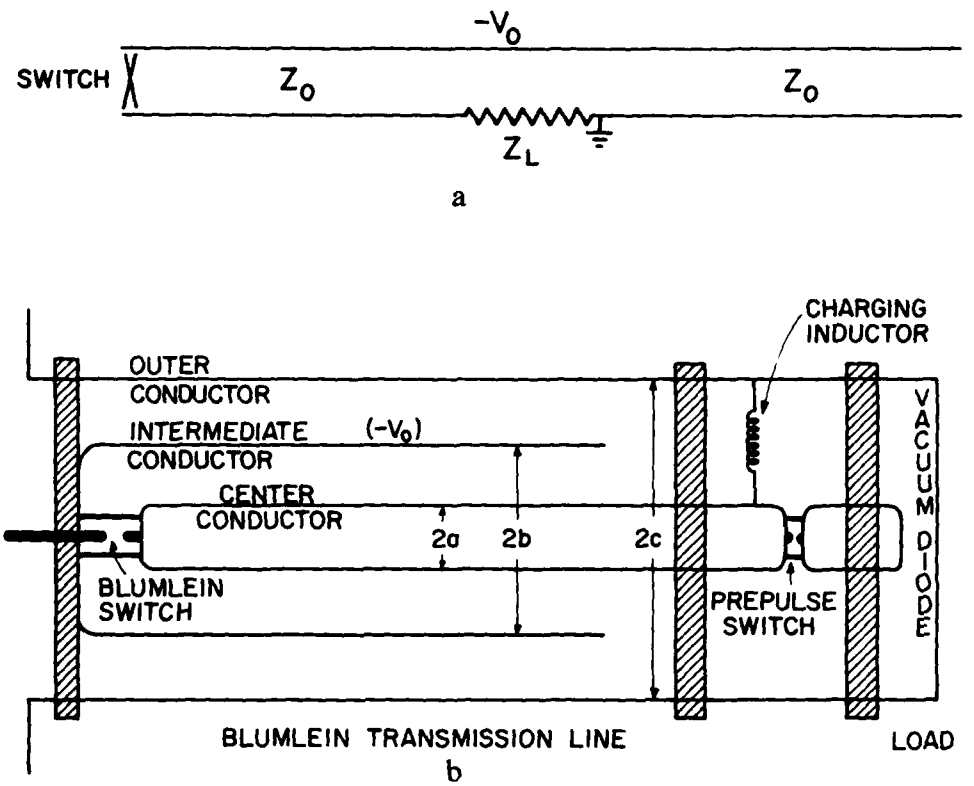

FIGURE 4 a) Blumlein transmission line. The line is charged to voltage V_0 on either side of the load, which in a matched configuration will have an impedance of $2Z_0$, twice the characteristic impedance of either section of the line. b) Cylindrical Blumlein transmission line.

open-circuit at the other. The load is located in the center (Fig. 4a) of the pulse-line system. The switch may be either a self-breaking liquid or gas switch or a triggered switch.

Almost all Blumlein configurations constructed to date have the geometry shown in Fig. 4b. In some cases, however, epecially where there is a need to synchronize the firing of many separate Blumleins, it may be useful to use the configuration sketched in Fig. 5, in which the switch is readily accessible. The high-voltage connection to the intermediate conductor is, however, less accessible. This latter configuration has been used in the Berkeley electron-ring accelerator pulse lines. It is electrically equivalent to the configuration illustrated in Fig. 4. Accounts describing the design and characteristics of several generators may be found in Refs. 24-34.

We now discuss some of the properties of different dielectrics and of different switching systems used in high-power pulse lines. Most of this data is based on the unpublished work of J. C. Martin[35] of Aldermaston.

D. Breakdown Characteristics of Insulators

We consider in this section the insulation properties of the common dielectrics used in pulse-forming networks. In cylindrical lines of the form previously described, the most commonly used dielectrics are water and transformer oil. Due to its high dielectric constant ($\varepsilon_r = 81$ at frequencies up to about 3 GHz), water provides a useful high energy-density storage medium, capable of storing energy at a density of about 160 kJ/m^3. In addition, the velocity of propagation of an electromagnetic wave through the water is c/9, so that water pulse-forming lines may be quite compact (~ 1 m long for a 50-nsec pulse). In contrast, the dielectric constant of oil is about 2.4, so

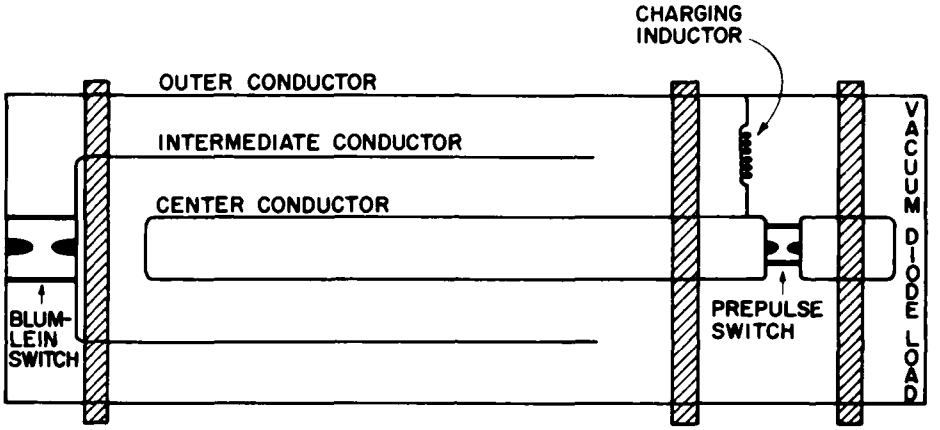

FIGURE 5 Cylindrical Blumlein with switching reversed.

that a 50-nsec Blumlein system would have a length of approximately 5.5 m. Oil may be used to store energy at a density of about 18 kJ/m^3.

J. C. Martin has shown that the dielectric strength of these liquids in uniform fields obeys a relation of the form

$$E_{BD} t^{1/3} A^{1/10} = k, \tag{3}$$

where E_{BD} is the breakdown electric-field strength of the liquid, A the electrode area and t the effective (submicrosecond) time duration of the high voltage. To compensate for rise time effects, in determining t we use only the time that the applied electric field exceeds 63% of its breakdown value. The constant k is polarity-dependent (denoted by the subscripts + and −). In mks units, k has the values given in Table II. Note that in water the breakdown is mainly determined by the positive-polarity electrode. For microsecond charging pulses, the breakdown strengths are about 15 MV/m for water and 25 MV/m for oil, where an electrode area of 0.1 m^2 has been assumed.

For short-duration (7–30 nsec), sub-megavolt pulses, VanDevender and Martin[36] have shown that the electric field at breakdown may be almost twice as large as predicted by Eq. (3). This result is important for electron-beam pellet-fusion systems, where the breakdown strength determines the current-handling capability of a vacuum diode [(Eq. (14)]. The breakdown field for these short-duration pulses is given by

$$E_{BD} = \frac{1.6 \times 10^6 \, d^{0.65}}{t^{0.39} A^{0.06}} . \tag{4}$$

In this case, as will be presented later for asymmetric electrode breakdown, it is not possible to describe the breakdown process without including an electrode separation factor d.

For the coaxial Blumlein configurations shown in Figs. 4 and 5, the electric field most likely to lead to breakdown is at the surface of the center conductor and has a value given by

$$E(a) = \frac{V \sqrt{\varepsilon_r Z_{ba}}}{60\, a} , \tag{5}$$

where V is the charging voltage, ε_r the relative permittivity of the dielectric and Z_{ba} the characteristic impedance of the coaxial section between the intermediate and center conductors. The breakdown criterion in water for electron-beam operation, i.e., in the negative-charge mode, is relatively worse than the positive-charge mode due to the polarity dif-

TABLE II

Values of constants k_+ and k_- used in determining the breakdown strength of water and oil

	k_+	k_-
Oil	2.0×10^5	2.0×10^5
Water	1.2×10^5	2.4×10^5

ference between the constants k. Following the closure of the switch, the center conductor becomes negative and is usually the most strongly stressed electrode. Due, however, to the short pulse duration compared with the charging time, the permitted electric field at the high-voltage conductor is much greater than that allowed during the charging phase.

In positive-polarity operation (i.e., for the generation of proton beams), the intermediate conductor has the greatest stress during the charging cycle, although the stressing obtained is weaker, due to the larger radius of the intermediate conductor. If a machine is required for use in both the electron and ion beam modes, then it may be a useful compromise to work with a system in which $Z_{CB}/Z_{BA} = b/a$.

In a coaxial system, the electric-field variation, at fixed potential difference between the conductors, has the form

$$E(r) = \frac{V}{r \ln\left(\frac{c}{r}\right)}, \tag{6}$$

where the outer conductor radius has been taken as c meters. It is straightforward to show that the electric field at radius r is a minimum when the logarithmic factor is unity. This result leads naturally to a preferred impedance range for a given dielectric. Water lines operate typically around 7 ohms, whereas oil is characteristically used in higher voltage applications at impedances of about 35 ohms.

A number of pulse-forming networks have utilized strip transmission lines for the fast section of the beam generator. In such a device, it is often possible to use a solid dielectric insulator such as Mylar. For uniform-field configurations, the breakdown field strength is volume-dependent, but essentially time-independent:

$$E_{BD}\,(V)^{1/10} = k, \tag{7}$$

where the constant k has a value of about 7.5×10^7 in mks units. The volume (V) dependence in the above relation and the area dependence in Eq. (3) for the breakdown of liquids are very similar. In the solid case, the volume is relevant since breakdown may originate anywhere in the insulating volume. In contrast, breakdown usually commences on the surface of a liquid. The exponents in both cases reflect the fact that the breakdown strength of a sample (liquid or solid) has intrinsic scatter corresponding to a standard deviation of about 10%. The mean value of the breakdown field strength is then sample-size dependent† and for the quoted standard deviation corresponds to a 1/10th power of the sample size. In gases, the intrinsic spread in the breakdown strength is an order of magnitude less and there is no significant volume effect, except in the largest of the Van de Graaff machines. The solid-dielectric systems employing plastic insulating sheets may be stressed to fields approaching 300 MV/m and are capable of storing energy at densities of greater than 1 MJ/m^3. We note in passing that the electric-field strength close to the edge of a strip-line conductor may be substantially greater than the average value between the plates. The stressing is usually relieved and the air voids between the dielectric sheets filled by immersing the whole line in a weakly conducting copper-sulfate solution. The solution serves as part of an RC network giving an effective radius of a few mm to the otherwise-sharp conductor boundaries.

The switching of a charged Blumlein into a load requires the reliable firing of a normally insulating gap. That is, we are interested in obtaining a failure of the insulation properties of the dielectric at a prescribed location, and at a predetermined time or voltage. This has been achieved by either using the self-breakdown of gaps or by deliberate triggering of the system. We deal in this review with the self-triggering situation. The breakdown of a switch follows similar laws to those given earlier for the breakdown of dielectric in a uniform field. In this case, however, breakdown is desired at a predetermined level and location. This is achieved by using nonuniform field configurations where the breakdown is required. Consider, for example, the self-breakdown of a Blumlein switch constructed of the same dielectric as is used to insulate the line. Table III gives phenomenological relations describing the breakdown characteristics for an edge-plane gap. As in the uniform field, there is a polarity effect, which for water continues to exhibit the preferential breakdown from the positive edge. At submegavolt voltages the oil breakdown is dominated by the negative edge. The breakdown fields given correspond to the average electric field across the gap and are typically in the range of about half the breakdown field strengths for the uniform gap

† The breakdown probability of a dielectric follows a Weibull distribution. Volume or area effects in determining dielectric strengths may be inferred from a knowledge of the breakdown statistics of a single (fixed volume or area) sample. For example, *N successive stressings of a volume V* is equivalent to a single stressing of a volume $N_1 V$.

TABLE III

Relationships describing the average electric field causing breakdown between an edge and a plane in water and oil. d is the gap between the electrodes and t is the time the field exceeds 63% of the breakdown field.

	Negative edge	Positive edge
Water ($0.1 < V < 1.0$ MV)	$E_{BD}t^{0.61}d^{0.09} = 1160$	$E_{BD}t^{0.83}d^{-0.67} = 610$
Water ($1.0 < V < 3.0$ MV)	$E_{BD}t^{0.5} = 1.3 \times 10^4$	$E_{BD}t^{0.4} = 4.38 \times 10^4$
Oil ($0.1 < V < 1.0$ MV)	$E_{BD}t^{0.78}d^{0.22} = 50$	$E_{BD}t^{0.57}d^{0.43} = 400$
Oil ($1.0 < V < 5.0$ MV)	$E_{BD}t^{0.63}d^{0.22} = 392$	$E_{BD}t^{0.63}d^{0.22} = 392$

stressing. The relatively rapid variation of the breakdown strength with time for the water case has been utilized in the development of fast low-jitter switches for the triggering of low-impedance, short-duration pulses. For short-duration charging times and rapidly rising pulses, standard deviations in gap triggering of 2 to 3% have been obtained. An important additional benefit is that the gaps break down simultaneously in multiple channels, leading to very low-inductance switches. The multiple breakdown can only occur when the channels are transit-time isolated.

The self-breaking of water switches has, for example, been used in the development of the multiple-source generator, Proto II. To achieve the multiple firing with sufficiently low jitter, the Marx generators are used to charge water-dielectric storage capacitors. These capacitors are switched, via triggered SF_6 gaps, into a water transmission line in about 300 nsec. The lines self-break, in over 100 channels each, transferring their energy into the feeds to the load. The intermediate capacitor and the water line both act to speed up the energy transfer time and hence permit consistent low-jitter firing of the final gaps. The charging time of the lines using this sequencing is a factor of three faster than could be achieved using the Marx generators alone, and the jitter in the firing an order of magnitude lower than could be obtained otherwise. The water transfer capacitor system has also been used in a number of other pulse-line facilities to enhance trigger reproducibility and also to reduce the trigger inductance. The latter effect arises due to the closure of multiple switching channels in the rapid-charging configuration.

Gas switching is in common use in a number of pulse-line systems, especially in cases where the line impedance is moderately high (several ohms or greater). Four gases are in common use in switch applications (or for insulation in low-voltage Marx generators). They are air, nitrogen, freon, or sulfur hexafluoride. In uniform fields, the breakdown of air or nitrogen has been shown to satisfy the relation

$$E_B = \frac{1}{F}\left[24.6p + 210\left(\frac{p}{d_{\text{eff}}}\right)^{\frac{1}{2}}\right], \tag{8}$$

where p is the pressure, and all quantities are given in mks units. The breakdown of sulfur hexafluoride or freon occurs at fields approximately two and a half and five times greater than that given above. Note that freon is not the preferred gas in switches because carbon is formed during discharges in freon. In the above relationship, the distance d_{eff} defines an effective gap separation for the electrodes and F represents a field enhancement factor for the switch geometry. In planar geometry d_{eff} equals the actual electrode separation and F is unity. Values of F have been given by Alston for cylindrical and spherical electrodes. Table IV defines d_{eff} and F for a gap with a spacing equal to the electrode diameter (d). Values of d_{eff}/d and F are given for other aspect ratios by Alston.[37]

Since avalanche breakdown and streamer formation in gaps take a finite time to develop, it is possible to apply greater stress across gaps for ultrashort pulse durations (< 10 nsec). The time dependence for the breakdown of asymmetric gaps, such as point-plane, has a polarity effect which may be adequately described by a relation of the form

$$E_{BD} = \frac{k_{\pm}\, p^n}{(dt)^{1/6}}, \tag{9}$$

TABLE IV

Effective gap length and field enhancement factors for typical switch geometries

Electrode shape	d_{eff}/d	F
Cylinders	0.115	1.3
Spheres	0.057	1.8

TABLE V
Values of the constants used in Eq. (9) for the determination of the time dependence of the breakdown of gas switches

	Air	Freon	Sulfur Hexafluoride
k_+	1.02	16.7	20.4
k_-	1.02	27.8	33.4
n	0.6	0.4	0.4

where the constants k and n have the values given in Table V. In a similar manner to the previous case for the breakdown of a solid or liquid, the time factor allows for the relatively unimportant low-voltage part of the applied voltage pulse by taking t as the time the voltage exceeds 89% of the breakdown voltage. E_{BD} is the average field across the gap. The relations for gas breakdown are limited to pressures of less than about five atmospheres, although in the case of sulfur hexafluoride they apply up to about ten atmospheres; the relations were also obtained with gap lengths greater than about 10 cm.

The performance of a switch is determined not only by its breakdown characteristics but also by its rise time. This is controlled by two factors, the switch inductance and the drop in resistance of the channel due to its expansion associated with ohmic plasma heating. The relative importance of these terms depends on the detailed switch conditions. The time for the inductive-current rise in a circuit or the voltage fall across a switch having an inductance L and being driven by a circuit having an impedance Z is

$$\tau_L = \frac{L}{Z} . \tag{10}$$

The corresponding term for the resistive phase has been shown to be

$$\tau_R = \frac{7.8\ \rho^{1/2}}{Z^{1/3}\ E^{4/3}} , \tag{11}$$

Note that these are e-folding times for the switch and that the actual 10–90% rise time is not simply related to the above times when the individual time constants τ_R and τ_L are comparable.

In low-impedance machines, where the rise-time effects may limit the useful pulse duration,† it is sometimes more useful to switch the pulse-forming network at higher impedance, and then transform the impedance to the lower value required using a tapered transmission line. Figure 6 shows schematically a pulse-line transformer. If Z_0 and Z_i represent the output and input impedances of the tapered section, then the output characteristics are related to the input parameters by the relations

$$\frac{V_0}{V_i} = \frac{I_i}{I_0} = \left(\frac{Z_0}{Z_i}\right)^{1/2} . \tag{13}$$

These relations assume that the change in line impedance is adiabatic, and that the tapered section has a length comparable to or greater than the length of the pulse. A step-down transformer has been used in the Naval Research Laboratory (NRL) generator Gamble II[29] to minimize the pulse rise time. Step-up transformers have been used, for example, on the VEBA facility at NRL[31] and on pulse lines at Cornell University. The radially converging feeds described previously in the Proto II generator[18] are also transformers.

E. Beam Diodes

In the previous sections we have outlined design criteria for the production of short-duration high-power pulses. To convert these pulses to particle beams requires the use of a high-voltage, low-inductance diode. Two diode arrangements are illustrated in Fig. 7. In the first of these figures we show a stacked-ring insulator in which the lucite insulating rings are alternated with annular aluminum discs. The lucite insulators are typically cut, on the vacuum side, at 45° to the axis of the diode and arranged so that electrons leaving the surface of the dielectric do not hit the plastic, causing secondary emission and a subsequent breakdown. The aluminum disks serve as grading rings, distributing the diode voltage uniformly along the length of the insulator. If the surrounding dielectric is water, this grading of the fields may be very effective. For oil insulation, the ring-to-ring capacitance is reduced and the field distribution is less uniform. In this case, the rings still serve the purpose of breaking the path of any incipient surface flashover. This type of diode has been satisfactorily used for a variety of electron-beam machines and can be safely stressed to about 150 kV/cm. A variation on the design is shown in Fig. 8. This variant is in use as a double-diode system for pellet-fusion applications. In such application, a very low diode inductance is required

† The switch rise time will be, for a given line impedance Z, greater in the geometry shown in Fig. 5, than for the arrangement in Fig. 4b. The arrangement in Fig. 4b may be preferable in low-impedance lines.

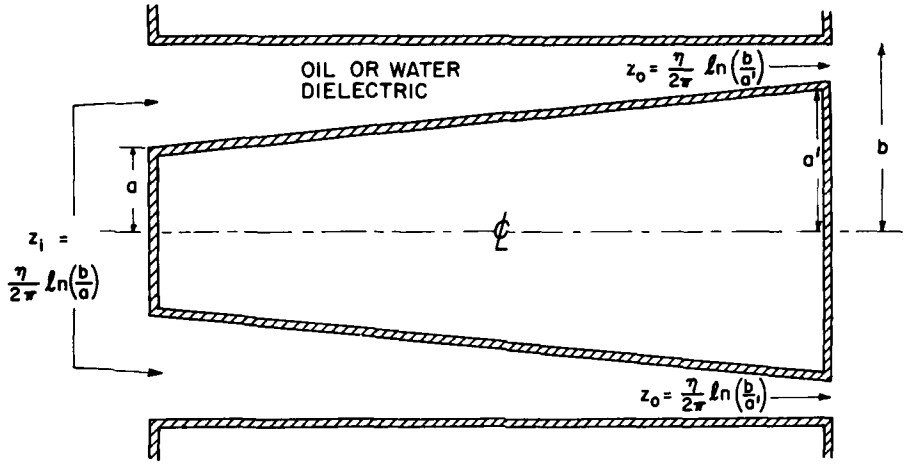

FIGURE 6 Section of a coaxial transformer. The line impedance varies adiabatically along the length of the system from Z_i at the input to Z_0 at the output.

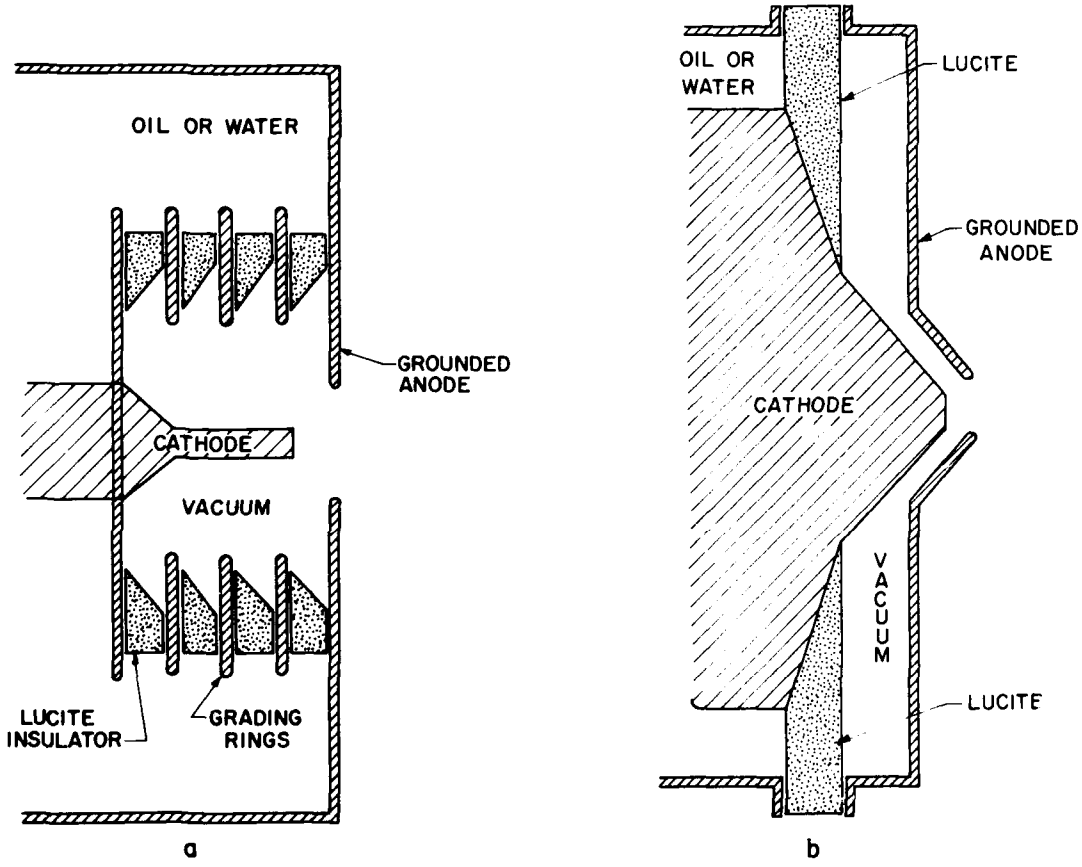

FIGURE 7 Vacuum diode assemblies using: a) a graded ring assembly, and b) a single radial insulator.

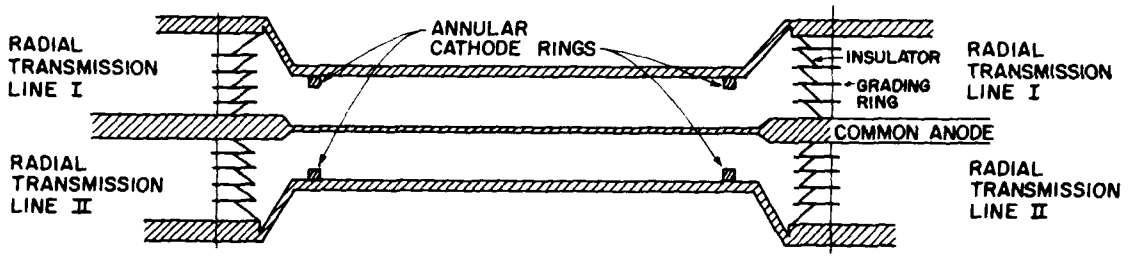

FIGURE 8 Two-sided diode used in pellet fusion experiments. High current electron beams emitted from the annular cathodes self pinch to the axis of the system. The system is fed from both sides by two similar transmission line systems.

and is achieved, using the geometry shown, with electron-beam emission occurring at large radii, close to the insulator rings. It is worth noting that the limiting electric-field stress at the diode rings, coupled with the radius of the rings, leads to a limitation on the generator current delivered to the load. In a uniform strip transmission line, the current flow per unit width of the line is given by

$$I = \frac{E\sqrt{\varepsilon_r}}{377} \; A/m. \tag{14}$$

For the lucite-ring assembly illustrated in the previous figure, the current capability of a two-sided 1-m radius diode, at a safe maximum stress, is about 0.75 MA, corresponding to a power flow density of about 0.1 GW/cm^2. The total power flux into the diode is too small for pellet-fusion applications[12] and it is necessary to go to magnetically insulated feeds to increase the power flow to the target. A promising approach to this problem is under investigation in both the U.S.A. and the U.S.S.R. It employs magnetic insulation of transmission lines.[38-41] This will be briefly indicated later, following the discussion of ion-beam generation.

A second diode configuration using a single insulating structure without grading has been extensively used at NRL and in other laboratories.[29,31] The insulator configuration is illustrated in Fig. 7b. In this design, considerable effort is devoted to forming the electric-field lines at large angles to the dielectric interface, so that any electron emitted cannot hit the insulator surface. Design figures of 315 kV/cm have been quoted for flashover on lucite at large angles, and the VEBA machine at Naval Research Laboratories has been operated at maximum field stresses of about 220 kV/cm. In addition to requiring that the electric-field lines make a large angle to the plastic interface, care is also taken to ensure that triple points, such as that occurring at the junction of a lucite wall with metallic wall and a vacuum are buried and not directly visible along the dielectric interface. The electrical stress is also minimized at these junctions. The detail of the buried junction is omitted in Fig. 7. The 'O' ring seals in metallic-dielectric interfaces are usually buried in the metal surface.

III. ELECTRON AND ION BEAM GENERATION

The diode configurations used in beam generators have been illustrated in Fig. 7. The beam generation depends, of course, on the polarity of the generator used in pulsing the diode. We describe initially the operation of a diode as an electron-beam generator, and subsequently outline the modifications used for the generation of ion beams. In both configurations, the vacuum used is quite modest and typically in the range of 10^{-5} to 10^{-3} Torr.

A. Electron-Beam Generation

The mechanisms associated with electron-beam generation in moderate-size electron-beam generators were studied in detail by Parker et al.[42] They operated an accelerator capable of generating an electron beam with an impedance of a few ohms at voltages in the three to four hundred kilovolt range. Typically, carbon cathodes were used as the electron source and the beams were extracted through a thin anode foil. With cathode diameters of about 5.0 cm, anode cathode gaps of a fraction of a centimeter were used to generate the beams. The applied voltage pulse was found to precede significant current flow by a few nanoseconds. During this phase, the current emission occurs through field emission from whiskers protruding from the cathode surface. The probable current density is limited to a few amperes per square centimeter during this phase, corresponding to field enhancements at the

whisker sites in excess of 100. As the enhanced field approaches a value of about 10^8 V/cm, the whisker current increases to provide sufficient energy to cause volatalization of the whisker tips. Subsequent emission comes from the plasma formed by the ionization of the vapor surrounding the cathode. This current may be quite large and is found following completion of the first phase of breakdown. The emission from the plasma approximately satisfies the Child-Langmuir relation for the diode geometry, provided that account is taken of the closure of the diode gap by the expanding cathode plasma. Observations made by Parker et al. and other groups[43] show that plasma-front velocities of one to four cm/μsec occur. As the beam current is increased, absorbed gases at the anode are released and ionized. A further plasma front originating from the anode starts to close the diode gap and the diode perveance increases further. The anode–plasma front velocity is less than that for the cathode plasma and usually about 1 cm/μsec. The flow is reasonably uniform from the diode unless significant field enhancements are present due to edge effects on the electrodes. The beam 'temperature' has been determined in a number of laboratories and found to be largely controlled by the scattering of the electrons in transit through the anode foil. Electron beams with energies in the range centered around 0.5 to 1.0 MeV have been obtained with mean scattering angles of a few degrees.

The presence of a preformed plasma in the diode, either from prepulse effects or due to plasma injection from an external source leads, in the case where the plasma density is high, to a rapid collapse of the diode impedance and to a shorting of the generator. Miller et al.[44] have shown that if the plasma density is limited to the 10^{13}–10^{14} cm^{-3} range, then the diode shorting does not occur and the diode behaviour can be well described by laminar bipolar flow. The current density is found to satisfy the equation

$$J_E = \sqrt{\frac{M_p}{m_e}}\, J_p, \tag{15}$$

where

$$J_p = 1.86 \left(\frac{4\varepsilon_0}{9}\right) \sqrt{\frac{2e}{M_p}}\, \frac{V^{3/2}}{x^2}, \tag{16}$$

and x is the thickness of the plasma sheath. The ion-current density is given by the usual bipolar flow limit, provided that proper account is taken of the expansion of the plasma sheath to allow for the provision of an adequately large flux of ions. This effect was important because the ion saturation current was typically less than that permitted by the space-charge-limited Child-Langmuir law.

Electron-beam generation has also been accomplished in foilless diodes. In cases where the electron beam is to be propagated in vacuum, such as in microwave-generation experiments or in some collective-acceleration systems, the practically obtainable beam impedance is high and can be achieved from a foilless diode. A beam propagating in vacuum along a strong magnetic guide field, has a space-charge limiting current given by[15,16]

$$I_L = \frac{17{,}000\,(\gamma^{2/3} - 1)^{3/2}}{1 + 2 \ln\left(\frac{b}{a}\right)}, \tag{17}$$

where a and b are the beam and tube radii respectively, and γ is the relativistic factor for the beam electrons at the anode plane. This value has been confirmed experimentally.[17] Other equilibria, in finite magnetic fields, in which the electrons rotate around the beam axis, have also been determined.[45,46] These also represent high-impedance beams.

Two foilless-diode configurations have been employed for the generation of electron beams. These configurations are sketched in Fig. 9. The first configuration[47] is essentially a magnetron type gun, in which the electrons are injected across the guide magnetic field. The magnetic field is sufficiently strong that the electrons do not cross the diode gap, but rather 'drift' into the experimental region following the curved magnetic-field lines. The second configuration is designed to inject the electrons approximately parallel to a uniform guide field.[14] In this configuration the electrons usually pass within a gyroradius or two of the anode plate. Both configurations are especially suited to high-impedance applications where a repetition rate or vacuum application is involved.

We now continue the discussion of foil-diode systems with a review of beam-pinching processes. As the diode current is increased, conditions develop which permit the beam to pinch as a result of the $J \times B$ interaction between the self magnetic field of the beam and the electron current. Pinching occurs when the current exceeds a critical current determined from the relations

$$\frac{I}{I_A} = \frac{\nu}{\gamma} \approx \frac{r}{2d}. \tag{18}$$

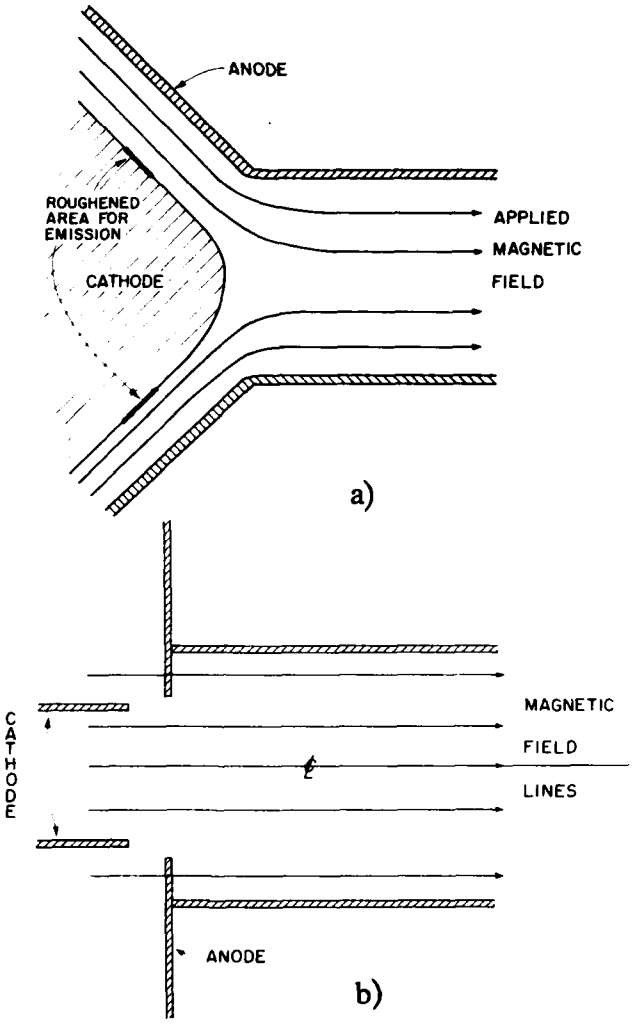

FIGURE 9 a) Foilless diode in which emission occurs orthogonal to the applied magnetic guide field. b) Foilless diode in which emission is parallel to the magnetic field lines.

In this relation ν is the number of electrons per classical electron-radius length of the beam and γ is the usual relativistic factor. The diode electrode gap is d and the cathode radius is r. The ratio ν/γ is also frequently designated as I/I_A, where

$$I_A = \frac{4\pi\varepsilon_0 m_e c^3}{e}\beta\gamma = 17{,}000\,\beta\gamma \quad (19)$$

is the Alfven-Lawson limiting current. The above relation [Eq. (18)] determines the value of the electron-beam current at which one expects non-laminar flow to develop.[48] Equation (18) may be simply derived by equating the gyroradius of an outermost electron in the beam to the diode-gap d. When these parameters are equal, one expects to find significant self-pinching of the electron beam. This result has been shown to give a reasonable account of the threshold for self-pinching, provided that one uses the actual diode spacing in the estimate, i.e., after allowance has been made for the gap closure of the plasma fronts from the cathode and anode plasma.[49]

Diode pinching is of considerable interest, since it has application to controlled-fusion pellet heating. Considerable analytic theory and simulation[50-54] have been carried out to determine optimum conditions for maximum compression of the electron beam. Qualitatively, it has been found that diode pinching always occurs when the diode current exceeds the value given in Eq. (18), although the pinch may not always be symmetric about the diode axis or always collapse to a very small radius. Important processes in determining the degree of the diode pinching and its control include the provision of a plasma on the axis of the diode (produced, for example, by an exploding wire) to neutralize the space charge of the beam in the late stages of collapse and, more importantly, the role of positive ions formed at the anode of the diode in determining the orbits of the electrons as they collapse to the axis. Other attempts to produce high current densities on the axis include the work of Morrow et al.,[55] who found that current densities in excess of 1 MA/cm^2 could be achieved on axis when a thin dielectric-rod cathode was used as the beam cathode. These results were subsequently confirmed by Condit et al.[56] and by Bradley and Kuswa.[57] The utility of this technique appears to be restricted to relatively high-impedance ($\lesssim$ 20 ohms) diodes; it did, however, stimulate the interest in electron-beam pellet fusion in pulsed-power generator diodes.

A satisfactory configuration used in the production of tightly pinched beams employs a hollow cathode which has a radius R much larger than the diode cathode–anode gap d. Simple theoretical models have been formulated for this configuration to describe the pinch characteristics. Both of the models presented predict that the diode current will have a magnitude given by a relation of the form

$$I = 8{,}500\, g\, \gamma \ln[\gamma + (\gamma^2 - 1)^{1/2}], \qquad (20)$$

where the parameter g depends on the details of the diode geometry. For the annular cathode $g = R/d$ in the parapotential flow model, and $g = R/d(\gamma)^{1/2}$ in the focused-flow model. The parapotential flow concept, which is originally due to dePackh[50] has been extended by Creedon.[51] In parapotential flow, one deals with a class of exact analytic solutions for the flow of electrons along equipotentials. In such a flow the rate of change of momentum of the electrons is zero and $\boldsymbol{E} = -\boldsymbol{v} \times \boldsymbol{B}$; the electrons then drift under the influence of the $\boldsymbol{E} \times \boldsymbol{B}$ force, with zero Larmor-radius orbits, along conical paths from the cathode to the anode. The parapotential flow model does not address the problem of the connection of the region of parapotential flow to the anode or cathode regions of the diode. Equation (20) describes the relation for saturated parapotential flow, in which the flow is focused along an equipotential terminating on the anode surface. The focused-flow model,[52] which exhibits an identical dependence (apart from the factor $\gamma^{1/2}$ in the relation for g) on the diode voltage to the parapotential flow, results from an integration of the cold-fluid electron model equations through the diode. In this model, the presence of a plasma at the anode and cathode surfaces plays an important role in determining the pinch. The flow may be represented largely as an $\vec{E} \times \vec{B}$ drift of the electrons through the vacuum region of the diode. The degree of pinching in this region is relatively weak. The final pinching is achieved in the charge- and current-free anode–plasma environment. Due to the similarity in the expressions for the current dependence on the diode voltage, many of the basic characteristics of both models have been confirmed.[58-60] For example, in the energy range extending from about 0.5 to 1.0 MeV, the diode impedance is essentially independent of the voltage, as has been observed experimentally. There are differences between the models, however, and their predictions do not coincide. An important difference is that the focused-flow model requires the presence of a plasma (or at least a counterstreaming ion flow) in order to produce the final stage of the pinch flow. This anode plasma has been shown to play an important role in determining the final stages of the compression. Cooperstein and Condon[60] have found that the empirical relationship

$$I = 8{,}500 \left(\frac{R}{D - \Delta}\right) \gamma^{1/2} \ln[\gamma + (\gamma^2 - 1)^{1/2}] \qquad (21)$$

provides a satisfactory description of the diode behavior. In their experiments, an effective diode-gap reduction Δ was identified as 0.15 cm, about 40% of the actual gap, and was independent of time. A possible explanation of this is associated with the large self magnetic field of the beam following the pinching, inhibiting the further expansion of the anode plasma. It should be noted, however, that the focused-flow model is strictly applicable for solid-cathode configurations and for a steady-state current flow following the pinch completion.

Subsequently detailed study of the time dependence of the pinch collapse in the annular-cathode configuration lead to an important realization, namely that the anode plasma sheath could not adequately account for the initial formation of the

pinch. Following application of the diode voltage pulse across the gap, an annular beam described by the Child–Langmuir equation is formed. As the current exceeds the critical current for pinching, a weak pinch is initiated. The impact of the beam electrons on the anode produces a plasma which expands towards the cathode with a velocity of about 2 to 4 cm/μsec. This expansion rate is insufficient for the formation of the plasma sheaths which are needed to obtain electron focusing on the axis. This realization resulted in a re-examination of the previous models and led to a new model in which the plasma at the anode served as an ion source for bipolar flow in the gap.[61–65] Once the critical current is exceeded and pinching starts, positive ions from the newly formed anode plasma stream towards the cathode. This flow enhances the diode electron current due to the redistribution of space charge in the gap. In its turn, the enhanced electron current helps augment the pinch compression. In this model, the radial pinch time is limited by the ion flow time through the gap. The characteristic ion velocity is more than two orders of magnitude greater than the corresponding plasma expansion rate; hence the diode pinch can develop rapidly. Radial collapse rates for the electron-beam pinch of up to 5 mm/nsec have been recorded experimentally. By varying the anode material, it has been shown that the radial collapse velocity of the pinch is dependent on the heating at the anode and hence on the release and subsequent ionization of the absorbed gases in the anode material.

B. Ion-Beam Generation

As noted in the previous section, bipolar ion and electron flow occurs in high-current beam diodes. Elementary calculations show that in space-charge-limited bipolar flow, the electron-beam current is enhanced by a factor of 1.86 over the pure electron flow. With allowance for relativistic effects, this enhancement may exceed a factor of two and has been calculated to rise to 2.14 at 5.0 MV.[66] Energy transfer to the ions (which unless otherwise stated will be taken to be protons) is limited, nonrelativistically, to the square root of the electron-to-ion mass ratio, namely 2.3% for protons.

Following the work of Humphries et al.,[67–69] a considerable effort has been devoted to developing proton sources with about 1-MeV energy, comparable to the high-current electron sources described previously.[70–73] This work has been largely motivated by the particle-beam pellet-fusion concept. High-current proton beams with energies in the one to ten megavolt range are particularly attractive for this application, since all energy deposition in the target is classical. In addition, ion-beam research is aimed at producing adequate proton fluxes to generate a field-reversed layer for magnetic confinement of thermonuclear plasmas.[3,14,74–76] To preview the following discussion we report that substantial progress has been made in this direction; sources available at present have achieved powers of about 0.7 TW at proton energies of about 1 MeV.

The principal effort in the production of high-current ion beams has been centered on the development of techniques for the suppression of the unwanted electron flow. Three main methods or devices have been developed to suppress the electron current, namely: a) the reflex triode and tetrode; b) magnetically insulating diodes; and c) pinched-beam configurations, in which the electron beam impedance is increased due to the long electron path in crossing the diode gap. We now examine these approaches in more detail.

The reflex triode was the original configuration used in the study of intense proton-beam generation by Humphries et al.[67,68] In this device, which is shown schematically in Fig. 10, the electron-current flow is suppressed and the ion current flow correspondingly enhanced by reflexing the electrons through the anode. In order to transfer energy efficiently to the protons, it is necessary to suppress the electron flow. In the reflex triode, the electrons emitted from the cathode traverse the diode gap and subsequently see a reverse field which tends to decelerate them. In practice, the center (anode) electrode is pulsed positively and hence the potential hill encountered by an electron, which has traversed the first part of the diode, is sufficiently large that the electron will be reflected at or close to the plane of the second cathode. In contrast to this, an ion formed at the anode plane will fall through the diode potential well, and, provided that the cathode is transparent, will emerge from the back of the cathode. The situation sketched in Fig. 10a is symmetric about the anode plane and hence the maximum efficiency which can be achieved in this configuration is limited to 50%. In practice, there is no need to use a second cathode electrode because the space charge beyond the anode will ensure the formation of a virtual cathode, and hence provide the reflexing of the electrons required to allow the ion flow to dominate.

There are a number of additional criteria that must be met before one can satisfactorily produce an ion beam from a reflex triode. The foremost of these

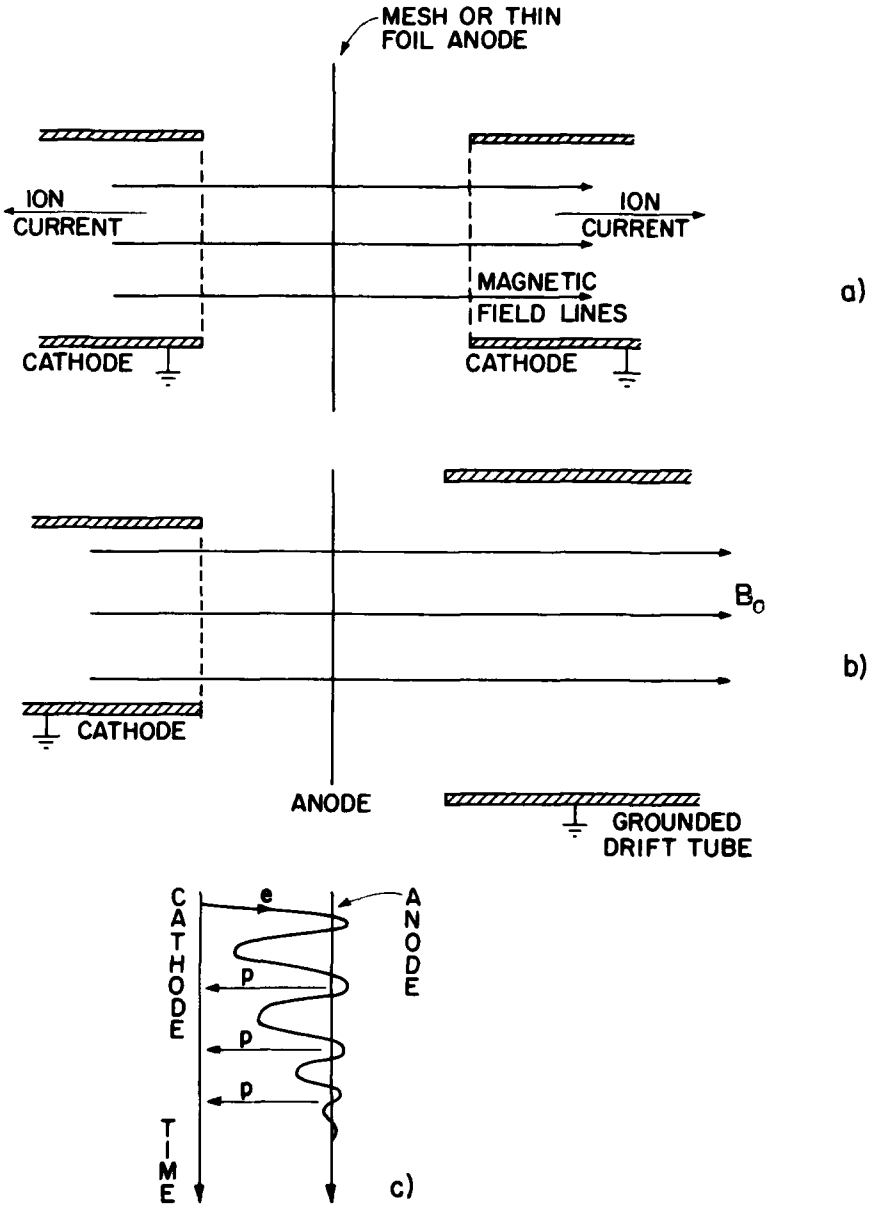

FIGURE 10 a) Reflex triode with two real cathodes. b) Reflex triode with one real and one virtual cathode. c) Trajectory of an electron through the reflex triode b. Energy loss in the anode foil leads to eventual loss of the particle in the foil. Protons only make a single traverse of the diode gap.

is concerned with the maintenance of at least a quasi one-dimensional configuration for the electron flow. The accumulation of negative space charge in the diode region will lead to the development of a radial electrostatic field which tends to expel the electrons from the diode region. This may be prohibited by a sufficiently strong axial guide magnetic field. Typically fields of order 10 kG are used in practice,

although several experiments have been satisfactorily carried out with the guide fields as low as about 1.6 kG.[71] An additional complication encountered with the reflex triode is the tendency of the diode gap to short due to gap closure arising from the plasma motion across the diode gap. We therefore find that diode gaps tend to be larger in ion-generation experiments than one would find in corresponding electron-beam generators. The Child–Langmuir space-charge-limited current flow from an evacuated diode, in which the electron current has been suppressed, is only slightly greater than two percent of the current obtained in the electron mode. Hence we find that large-area cathode configurations are appropriate for high-current applications.

The theoretical basis for the reflex-triode system was developed by Antonsen and Ott[78] and indepenently by Creedon, Smith, and Prono.[79] In both of these approaches a thin foil anode was considered. Multiple scattering of the electrons in the anode foil leads to an increase in the number density of the electrons close to the anode. The enhanced electron density in this region gives an increase in the ion emission from the hot anode plasma. A scaling study of the dependence of the ion current density on the diode voltage reported that current densities of up to 200 A/cm^2 were achieved, compared with the 30–50 A/cm^2 in the original mesh-anode studies. In addition, it was observed that the emitted current scaled much more rapidly with the diode voltage than the three-halves power law anticipated.[71,80] Ott and Antonsen showed in their analysis that the ion to electron current-density ratio could be described by a relation of the form

$$\frac{J_p}{J_e} = (1+\nu)\left[\frac{Z_m}{M_p}\right]^{1/2}, \qquad (22)$$

where ν is a constant given by

$$\nu = 2\,\frac{(1+\ln 4)}{3\langle\Delta\theta^2\rangle} \qquad (23)$$

In these relations Ze is the charge on the ion and $\langle\Delta\theta^2\rangle$ is the mean square scattering angle. Kapetanakos et al.[71] point out that the scattering angle term is approximately inversely proportional to the square of the diode voltage. Assuming a three-halves power law for the electron current density, we conclude that the ion current density should scale rapidly with the diode voltage. In this estimate the dependence is seen as a seven-halves power of the diode voltage. While the detail of the scaling is not clear, it is apparent that the ion current density does scale more rapidly than expected on the basis of the Child–Langmuir law and further that a thin foil anode leads to a greater ion current than one can achieve with a solid anode. The largest reported proton flux densities correspond to current densities of about 3 kA/cm^2.[72]

A recent development of the reflex triode has lead to a further increase in the available current density.[8] To achieve this, a second anode foil has been used. The reflex tetrode, which is sketched in Fig. 11, shows two anodes: the first, which is labeled A1, is constructed from Polycarbonate or aluminized Mylar. Previous experiments had established that both of these materials are poor proton emitters. The purpose of this configuration is to limit the proton flux towards the cathode, and to provide a good ion source at the second anode A2. The ion flux from the second anode must flow in the direction toward the virtual cathode, since the electrostatic field between the two anode planes is zero. The results obtained with this configuration show that an increase in the current densities obtained is consistent with single-direction ion flow. In these experiments a conversion efficiency, defined as the ratio of the extracted ion current to the total generator current, of up to 55% was achieved. To achieve this efficiency, it was necessary to use a thin foil (2 μ Polycarbonate) for the first anode and to optimize the anode separations. In the work described, the optimum separation was found to be about 0.5 cm. The results were insensitive to the guide-field strength in the range (2.7 to 7.6 kG) used.

The work on the reflex-triode system was closely followed by the study of magnetically insulating diodes.[82-93] The underlying principle of this device is

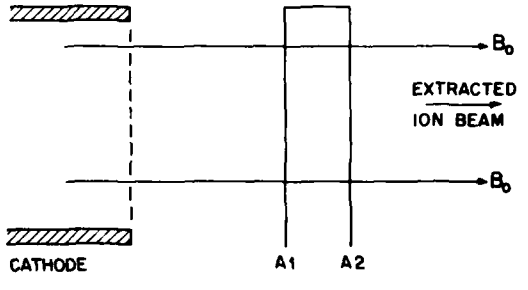

FIGURE 11 Schematic showing the principle of the reflex tetrode. The first foil A1 is a two micron polycarbonate sheet and is separated from the second anode A2 by about 0.5 cm.

shown in Fig. 12. A transverse magnetic field is applied across the diode. The field is sufficiently strong that the electrons will execute magnetron-like orbits and not be able to reach the anode plane. Calculations give the required field strength to produce magnetic insulation as approximately[77,88]

$$B_{cr} = \sqrt{\frac{2\,m_e V}{e}}\,\frac{1}{d}\left[1+\frac{eV}{2m_e c^2}\right]^{1/2}. \quad (24)$$

In crossing the diode gap, the protons are also deflected, but, due to their greater mass, their deflection is quite small and is readily shown to be of order

$$\bar{\theta} \sim \sqrt{\frac{m_e}{M_p}}\,\frac{B_0}{B_{cr}}, \quad (25)$$

where B_0 is the insulating magnetic field and B_{cr} is the critical field to achieve magnetic insulation. The angular deflection is of order one to two degrees and, if important, can be compensated by application of a magnetic field subsequent to proton extraction through the cathode plane.

A measure of the success of an insulating diode is the reduction in perveance of the diode as the field exceeds the critical field. Typical results,[93] with a copious source of plasma at the anode, are shown in Fig. 13. The perveance approaches the ion space-charge limiting value as shown by the dashed line, provided proper account is taken of the reduction in the diode gap spacing due to the space-charge neutralizing effect of the electrons emitted from the cathode.

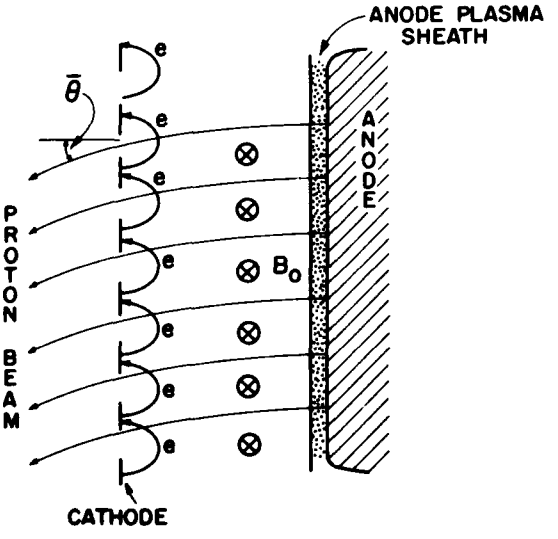

FIGURE 12 Schematic showing the principle of the magnetically insulated diode. Protons, emitted from the anode plasma, traverse the diode gap emerging through the cathode at a mean scattering angle θ to the diode axis. The electron motion is cycloidal along the cathode with electron flow inhibited by the traverse magnetic field B_0.

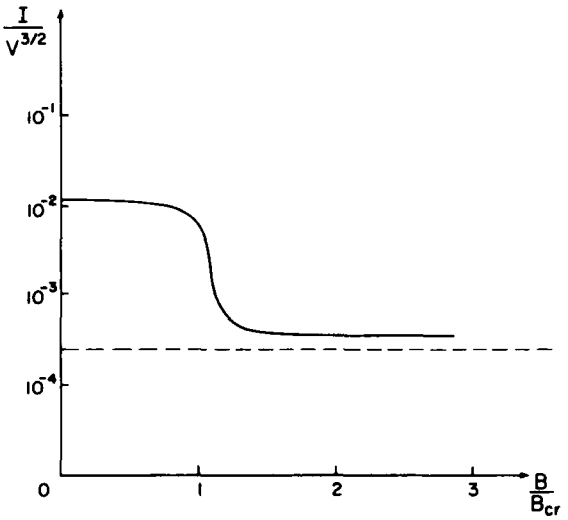

FIGURE 13 Reduction in diode perveance as a function of the magnetic field strength. This figure is based on data presented by Greenspan et al. [*Phys. Rev. Lett.* **39**, 24 (1977)].

There are two essential requirements for satisfactory operation of a magnetically insulating diode, a copious and prompt supply of ions at the anode plane, and a well-designed magnetic-field configuration. The former problem has been largely solved using surface-flashover techniques similar to those used for many years with plasma cathodes. In essence, a plasma is formed on the electrode, due to the electrostatic breakdown of the surface of a dielectric inclusion in an otherwise conducting plane. The rapid risetime of the applied potential requires the electric-field lines to follow the metallic anode surface. This results in the formation of electric fields along the surface of the dielectric inclusions. The breakdown along the dielectric surfaces produce the required ion-plasma source. Since most plastic dielectrics are hydrogen-rich, and since protons are the lightest of the ions, the preferential emission is protons.

The magnetic-field configuration required to produce the magnetic insulation is more complex, since one requires that the field lines do not cross the diode

gap. In practice, some field lines will almost always traverse the gap but their effect need not be too serious if the path length of the field lines in crossing from the cathode to the anode is much larger than the direct anode–cathode separation. Practically, this means that the field must not allow the electrons to easily traverse the gap so that they can absorb the generator power.

Various configurations have been used in magnetic-insulation experiments, although in much of the published work, two concentric cylinders with the cathode as the interior electrode have been employed. In these experiments, the ion beam is frequently extracted through holes in the cathode surface. In these experiments attempts have been made to focus these protons on to a line focus and current-density increases of an order of magnitude over the density at the cathode have been achieved. Similar studies have also been made recently using sections of a sphere for the anode and cathode to obtain a point focus for the ion beam.

Luckhardt and Fleischmann[85] have used magnetic insulation to produce long-duration proton pulses. In their experiments, a strong 20-kG magnetic field was used to insulate a 300-kV diode, consisting of two concentric cylinders, for times of up to 4 μsec. Two important results were noted; first in long-duration diodes the ion current achieved could exceed by a factor of order ten the predicted space-charge limiting emission based on the initial diode geometry, and secondly, high total numbers of ions could be generated. This latter result has application in the generation of field-reversing layers where the total number of particles generated is important. The ion yields reported are approximately ten times greater than those obtained with short-pulse machines operated under comparable diode-voltage conditions. Extension of this work[86] to megavolt energy has produced ion beam-current densities of up to 300 A/cm^2 for 1 μsec.

Magnetic insulation has been shown to provide a useful means for the generation of intense ion beams. The techniques developed have the additional advantage that they do not lead to a destruction of the anode with each event. The emitted current density is, however, still somewhat lower than that reported for reflex triodes. Typical peak current densities achieved to date are about 100 A/cm^2 with short-duration pulses and up to 300 A/cm^2 in long-pulse systems.

Although it is somewhat out of place to describe magnetically insulated transmission lines in the discussion of ion diodes, it is appropriate to point out that the same insulation process has been used to achieve the extremely high power-flow densities required for electron-pellet fusion. As pointed out earlier, the dielectric-strength properties of diode insulators limit the current and hence the power flow [see Eq. (14)] from the generator to the pellet. This limitation has been identified as a primary obstacle in the power-flow analysis. A successful solution to this problem has been found using the self magnetic insulation of vacuum transmission feeds.[38,41,94–99] At sufficiently high current levels, the self magnetic field of the transmission line wave is adquate to produce magnetic insulation. The best results achieved for power transfer have used a 7-m long triplate vacuum feed at electric-field strengths of up to 7 MV/cm.[99] This represents an increase of approximately 50 over the stress limits set by plastic diode insulating rings. About half of the power flow occurs in the vacuum fields along the vacuum line. The parapotential flow theory[51] is also relevant in this regime.

The final approach to be described in the generation of intense ion beams uses the self-pinch properties of electrons in vacuum diodes. This process has been extensively studied in various laboratories and also in computer simulation stud-

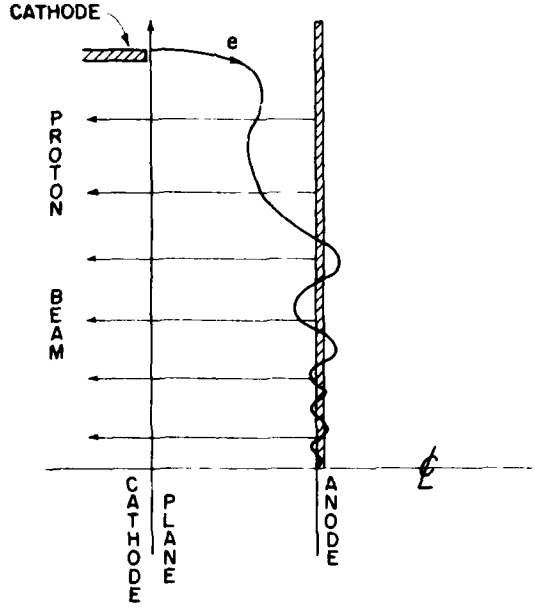

FIGURE 14 Ion and electron trajectories in a pinched electron beam diode. A thin anode foil is assumed.

ies.[64,100-107] The essential feature of the ion-beam generation is sketched in Fig. 14. Consider the production of a pinch beam using a large aspect-ratio diode with an annular cathode. The electron flow is initially laminar. As the current increases, the energy absorbed in the anode due to the electron-beam bombardment increases and eventually results in the release of gases and in the formation of a plasma in the anode material. The plasma formed drifts across the diode gap at a velocity of order 1 cm/μsec and is preceded by ion flow. The bipolar flow in the diode causes the electron-beam current to increase and beam pinching commences. At each stage of the compression, more plasma is released from the anode, ion emission from the plasma is established and the electron-beam pinch continues. When the electron beam reaches the axis of the diode, we achieve a quasi-steady state in which the electron current follows a long path from the cathode edge to the axis, while the ion emission follows an almost straight line path from the anode to the cathode. It has been shown that the difference in particle paths leads to a substantial increase in the energy transfer to the protons. The estimated ratio of ion to electron currents has a value[64]

$$\frac{I_p}{I_e} \gtrsim \tfrac{1}{2}\left(\frac{R}{v_e}\right)\left(\frac{v_p}{d}\right) = \frac{R}{2d}\left(\frac{2\text{ eV}}{M_p c^2}\right)^{\frac{1}{2}}, \quad (26)$$

where v_e *and* v_p are the final electron and ion velocities. For values of the aspect ratio $R/d \gg 1$, it is possible to achieve approximately equal ion and electron currents. More detailed numerical simulations have shown that this ratio can reach a value as high as three. Stephanakis et al.[102] have reported obtaining 4×10^{16} protons over 120 cm^2 from the Gamble generator. Of the 0.5 to 0.6 MA of current, about 150 to 200 kA was attributed to the protons.

A detailed study of the pinch process was carried out by Swain et al.[108] using a 200-kV, 50-kA generator. They observed that with a solid aluminum target 1 to 3 kJ/g of energy was required to generate the ions, and that with hydrocarbon anodes this figure could be reduced by about one order of magnitude. Irrespective of the anode material and its treatment, the primary ion found was either H^+ or H_2^+ and was presumably due to the rather poor vacuums usually used in high-power beam diodes ($\sim 10^{-4}$ Torr). In their investigation, they reported that all the ions observed had an energy approximately determined by the diode voltage and that ions with mass to charge ratio of 1, 2, 6, 12, and 16 were obtained. The maximum recorded current density for the protons was about 1 kA/cm^2. Unpublished studies at Cornell[109] have found that heating the anode foil, while under vacuum, to red heat causes an increase in the diode impedance by a factor of up to two. Presumably this is due to a reduction in the hydrocarbons absorbed on the foil from the pump oil and vacuum grease.

As might be anticipated from the discussion of the reflex triode work, the pinch process has been found to be helped by using thin anode foils[102,104] instead of solid targets. The reflexing of the electrons then results in an enhanced electron density close to the foil and a corresponding build up of the proton current. This is accompanied by a more rapid pinching of the electron beam. It is worth noting that the rise time of the ion beam is comparable to the collapse time of the electron pinch and that occurs on a time scale much shorter than the electron-beam rise time. Efforts to aid diode pinching by the use of an externally driven axial[110] diode current did not lead to an improvement of the diode pinch process, which seems to be primarily controlled by the proton emission from the anode surface. Exploding wires have also been used to produce a plasma on axis for space-charge neutralization and to aid focusing.[111]

D. Repetition Rate

Primary interest in high-power electron and ion beam generators has been centered on low-impedance, very high power devices. To date, none of these devices has been operated with a repetition rate greater than a few pulses per hour. To demonstrate the feasibility of such an accelerator, work has been carried out at Sandia on the use of a modest accelerator in a repetition-rate mode.[112] A 350-kV, 300-J accelerator has been pulsed at a repetition rate of 40 pulses per second for over a million successive shots. For a short period operation was maintained at 100 Hz.

IV. INDUCTION ACCELERATORS

As stated early in this review, relatively little work has been done on utilizing pulsed-power technology to obtain very high-energy, medium-current relativistic beams.

The first devices used for this purpose were the electron linear-induction accelerators built at LBL,[113] LLL,[114] and NBS.[115] The essential features of an induction linac are shown in Fig. 15. In this device, the center conductor is pulsed negatively from a pulse or Blumlein transmission line. The

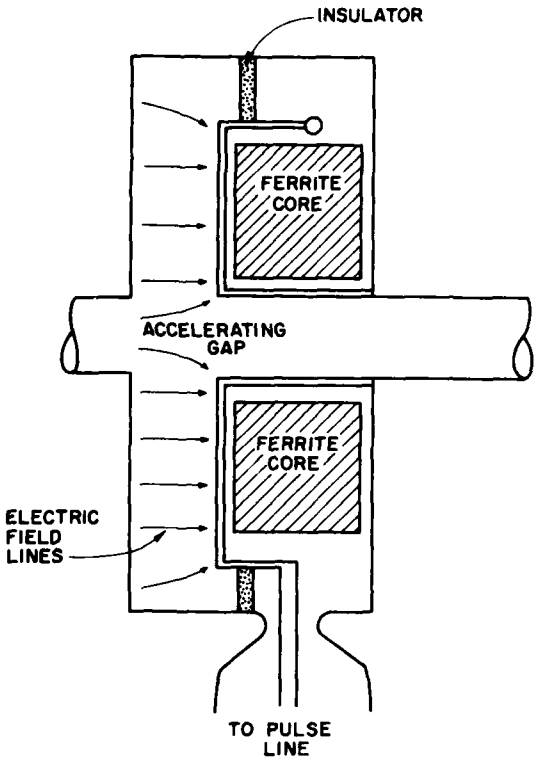

FIGURE 15 Induction assembly acceleration module. The field lines are appropriate for positive ion acceleration from the left to the right.

incoming wave divides between the two halves of the system with each half feeding a section of a cylindrical ferrite core which surrounds the beam channel. The induction field appears concentrated across the accelerator gap. Following acceleration of the electrons through the gap, they are buried inside a hollow pipe in which the electric field is zero. Following a drift section, approximately 1-m long in the LBL system, the electrons enter a further gap fed from a separate pulse line. Since the accelerator is driven by the rate of change of the magnetic field in the ferrite loop, the final electron energy achieved is equal to the energy acquired in a single gap multiplied by the number of gaps in use. In the LBL system each acceleration gap produced an electron energy gain of 0.25 MeV through the induction fields. The output energy of the electrons was 2.5 MeV, which was achieved with a repetition rate of about 5 pulses per second. In these experiments an electrostatic injector was used to provide a 1-MeV source for the electron beam. A new induction accelerator of this type is currently under construction at LLL.[116]

A variety of other devices that depend on the rate of change of flux through a circuit encircling the beam path have been described in the literature. These include the radial transmission pulse lines described by Pavlovskij et al.[117] and the Auto-accelerator described by Friedman and Lockner.[118] In both of these devices, which are shown in Figs. 16 and 17, the rate of change of flux is achieved through use of the distributed circuits illustrated, i.e., the

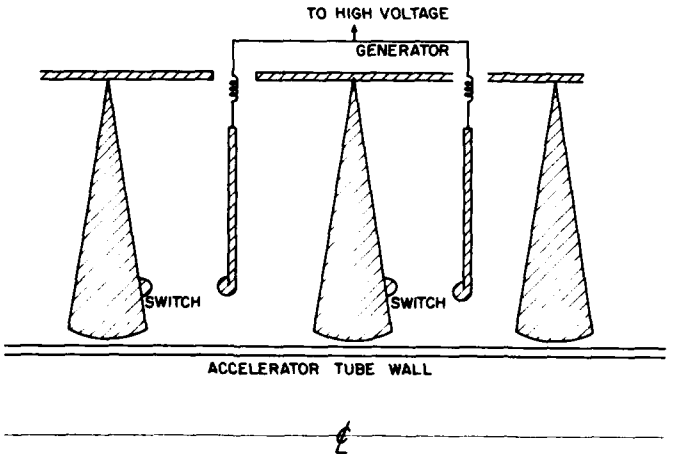

FIGURE 16 Section of an accelerator using radial transmission lines. The switches are closed, discharging the lines at times phased with the charged particle acceleration in the accelerator tube.

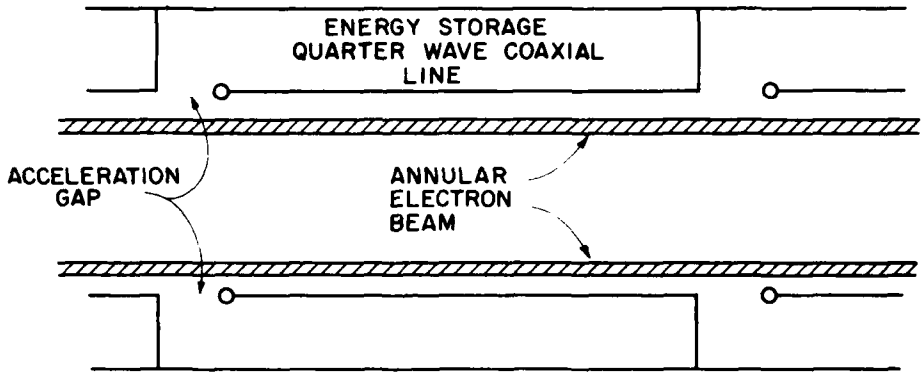

FIGURE 17 Section of an electron autoacceleration device.

change is produced by the propagation of an electromagnetic wave through an extended line, rather than through the lumped-parameter characteristics of the ferrite core of the LBL system. In Fig. 16 we show two sections of a radial-line induction accelerator. In this device, the electrons are accelerated by the fringing fields of the radial line. A series of appropriately sequenced switches short one side of each of the lines, so that the wave shorts out the voltage on the line in its initial transit. The wave is reflected from the open circut of the unloaded accelerating gap. Throughout the period that the wave propagates from the open circuit to the switch and is reflected back, the flux linked by the loop closed by the open circut gap on one side and the switch on the other, increases linearly in time. This rate of change of magnetic flux drives the electric field accelerating the charged particles across the gap. The acceleration achieved in each gap is cumulative as a result of the induction nature of the fields. Pavlovski projects that an accelerator of this type could be used to obtain electron beams with energies of order 10^5 J in the energy range of 10^6 to 10^7 eV.

The autoaccelerator system works on a different principle, but is of the same generic type as the induction accelerator. In this device, a slowly rising potential, applied to a vacuum diode, is used to produce a magnetically confined electron beam. After buildup of the beam to the required level, the beam is switched off rapidly by diverting the applied voltage from the gap through an auxilliary path. As a result of the beam propagation through the drift space, magnetic energy is stored in the concentric cavities. The beam current rapidly drops to about 20% of its peak level in about 5 nsec. Following the reduction in beam current the energy originally stored in the cavities cannot be maintained. The excess energy is transferred to the beam electrons as they cross the gaps and they are further accelerated. In this system, there is an automatic phase matching for the successive accelerating fields, since the cavity length equals the separation of the successive cavities and the electron velocity is essentially equal to the speed of light. This system, which has been successfully used with two cavities, is driven by the rate of change of flux in the cavities and hence belongs to the induction-linac family. Interstage cavity coupling appears to present some problems in the extension of this acceleration scheme to an arbitrarily large number of cavities.

An analysis of energy transfer in such devices has recently been reported by Eccelshall and Temperley.[119]

There has been a recent resurgence of interest in acceleration of moderate current beams to high energies, as a result of the heavy-ion fusion program. An approach to this problem being considered entails the use of linear induction accelerators for acceleration of high atomic number ($A \gtrsim 100$) materials to energies in the range of several GeV.[120] This approach and a separate program on intermediate atomic-number accelerators[121] have recently been initiated. In these systems, electrostatic acceleration will be used in the low-energy stages. Ions will be accelerated through a magnetically insulated diode, transported through an electrostatically neutralized section, and when all of the earlier-stage acceleration is complete, the tube in which the ions are buried will be pulsed so that the ions may be reaccelerated by a further magnetically insulated section. The final stages of the accelerator will use

induction acceleration. A variant of these schemes has been proposed by Winterberg.[122] Present induction accelerators have only been used for electron acceleration.

V. COLLECTIVE ACCELERATION

We conclude this report with a brief summary of progress and a report of current directions in collective acceleration. A number of previous reviews summarize this area,[123-129] so that only recent developments will be discussed. In collective ion accelerators, a high-power relativistic electron beam is used to accelerate a beam of positive ions to high energy. This process is achieved through the use of the collective fields of the primary electron beam. Work on this process was originated in the United States when Graybill and Uglam[130] first observed high-energy ions occurring when a high-current relativistic electron beam was injected into a low-pressure gas. Subsequent work has confirmed that it is relatively easy to achieve collective acceleration of the ions to energies corresponding to about three times the electron-beam energy, but that it has not been clear that this process can be scaled, for example, to achieve the high-energy (several hundred MeV) protons needed for electronuclear breeding. In addition to studies of collective acceleration of protons in electron beams, there has been additional work devoted to the acceleration of heavy ions. This work may have application to heavy-ion fusion sources and also to radio chemistry. Presently, achieved results indicate that collective accelerators may be competitive with cyclotrons for the generation of heavy ions in the 100 to 200 MeV range, and considerably cheaper. In the following section we shall present an account of the general results obtained and, in particular indicate directions presently being investigated for extension of this work to the high energies and fluxes required for projected applications.

Most of the research carried out to date has been centered on one of two areas, acceleration occurring when a high-current beam is injected into a low-pressure gas or into an evacuated tube through a dielectric anode. In the low-pressure gas case, the basis of the acceleration is at least qualitatively clear. A deep electrostatic potential well exists external to the anode and is separated from it by a distance of order c/ω_p.[131,132] The well is formed because the time taken to neutralize the beam space charge is long compared to the time taken for well formation and also because the current that can propagate in the unneutralized state is usually much smaller than the injected current. The well depth may, on a transient basis, exceed the diode accelerating potential and has been estimated to reach depths of between two and three times the diode potential difference. This potential well is in the sense that will accelerate ions from the vicinity of the anode parallel to the direction of the electron-beam propagation. The accelerated ions tend to neutralize the electron space charge and permit the beam to move from the diode region with a velocity approximately equal to the velocity acquired by the ions in falling through the potential well towards the virtual cathode. The correspondence between ion energy and the drift velocity of the beam has been verified experimentally.[133]

Generally most of the features observed in low-pressure gas acceleration are reasonably described by Olsen's detailed theory.[131] The observations which are reasonably accounted for include the cut-off in ion energy at about three times the beam energy, the short duration of the acceleration, the acceleration length scale and also the observed high-pressure cut off of the acceleration. At the higher pressures, one finds that the time scale to achieve a neutralized beam is comparable to or less than the acceleration time scale and hence acceleration ceases. Other models of the acceleration process have also been proposed, including the localized-pinch model.[134]

Consideration of energy balance[127,135] in propagating electron beams, coupled with an assumed beam-head acceleration, shows that conservation laws may impose serious limits on the achievable energies. This analysis also provides a description of the observed ion scaling with injection current and tube size. These scaling processes are not satisfactorily accounted for in the Olsen model. With the exception of ion acceleration occurring in high ν/γ beams, the observed acceleration has been limited to about three times the electron-beam energy. Of course, multiply charged ions have been detected and in these cases ion energies are scaled with the charge state. In the high ν/γ regime, the investment in reactive energy associated with beam transport is substantial, and the beam-head velocity is much less than the injection velocity of the electrons. Under such conditions, a high-energy contribution to the ion spectrum has been observed extending to about an order of magnitude greater energy than the beam electron energy.[136]

Much of the phenomenology described above is

AD-A085 312 CORNELL UNIV ITHACA NY LAB OF PLASMA STUDIES F/G 20/7
COLLECTIVE ION ACCELERATION.(U)
1980 J A NATION F44620-75-C-0054
UNCLASSIFIED AFOSR-TR-80-0440 NL

3 OF 3
AD A085312

END
DATE FILMED
7-80
DTIC

equally applicable to the acceleration observed when a high-current electron beam is injected into an evacuated tube through a hole in a plastic anode. This configuration, which was first investigated by Luce et al.,[137,138] does, however, have a significant ion spectrum extending out to about twenty times the electron-beam energy. The phenomenon is once again related to the formation of virtual cathodes and deep potential wells. Ion acceleration has only been observed when the injected beam current exceeds the space-charge limit. Measurements with Rogowski coils also show that the propagating net beam current may exceed the space-charge limit and that magnetic neutralization occurs.[133] In fact, ion acceleration only appears to be important when magnetic neutralization of the beam is present. The high-energy tail is tacitly associated with the propagation of the well associated with the virtual cathode. Experiments have shown that in at least certain conditions the ion energy acquired is controlled by the velocity of the ions, i.e., deuterons have twice the energy of protons. The acceleration achieved appears to be limited by the available electron-beam momentum and will probably only be increased substantially by more efficient use of the electron momentum, either by reflexing of the electrons or by limiting the number of ions available, especially those at the low-energy end of the spectrum.[139] A variation on the Luce system[140,141] was recently investigated in which an attempt was made to control the beam propagation by injection into a dielectric-wall tube. In this configuration, proton acceleration up to about ten times the beam energy was achieved with a characteristic distribution function similar to that found in the Luce diode. In both the neutral-gas acceleration and the vacuum acceleration, the accelerating fields obtained exceed 1 MV/cm.

It should be noted that the dielectric-anode configuration has also been used for the acceleration of heavier ions. For example, the use of a teflon anode has resulted in the acceleration of fluorine ions to energies in excess of 135 MeV from a 2-MeV electron-beam generator.[137] Other experiments have been carried out in which the ions have been separately generated, using a laser beam or a puff valve, for provision of a localized ionized-gas region.[138] It may well be that the first useful application of collective accelerators is in the generation of medium-energy (a few hundred MeV) heavy ions.

Before discussing schemes presently being explored to attempt to control the ion acceleration, we point out a few of the observed limitations of the present schemes, and observations relevant to the theories of ion acceleration. For example, the deep potential well model implies the existence of wells with depths of up to three times the diode potential difference. Such wells should expel electrons. Efforts to search for high-energy electrons having energies up to three times the beam energy have failed,[139,142] the highest energy electrons being detected having only about 1.2 times the beam injection energy. Part of this may be accounted for by the fact that the wells are inherently transient in nature and can only exist dynamically. Electrons leaving the well will sample several oscillation periods of the well; hence we anticipate seeing only electrons with energies up to the average well depth. This appears to be the case in these experiments. One must therefore question the validity of the deep potential-well acceleration model, since the ion acceleration time is much greater than the well oscillation period.

Perhaps the most revealing information relating to the acceleration mechanism is the apparent failure to accelerate ions in the presence of a uniform magnetic guide field. Only two published observations have been reported in which acceleration occurred with magnetic guide fields.[143,144] In the first case the acceleration occurred when the electron beam was made to rotate by injection through a cusp field; the second occurred following the nonadiabatic expansion of the beam drift tube. In both cases, ion spectra extending to about or slightly greater than three times the beam energy were reported.

A number of experiments are currently in progress to control the ion acceleration. We shall describe briefly some of these efforts. Beam-head control is reported in two experiments (other experiments using pressure gradients to control beam-head velocity have been reported previously). The first of these uses a helix to surround the beam channel.[145] In this experiment, the pitch of the helix is changed so as to increase the velocity of the potential well at the beam head. The change in pitch of the helix has been selected to match the expected electric field causing the acceleration. It is too early to comment on the success of this experiment, but it is at least apparent that the beam-head acceleration is affected by the presence of the helix and that acceleration is only observed when the helix pitch is changed in the correct sense. The results obtained do not yet, however, yield any enhancement of the ion energy. The second experiment, which has not been in progress for a few years, provides active

control of the beam-head velocity. In this experiment a high-power laser is used, in conjuction with fiber optics, to externally spatially ionize a cesium channel at a predetermined rate. Accelerated ions will be generated from trace gases maintained in the acceleration chamber at densities too low to allow neutralization of the beam. Present progress has reached the point where control of the beam propagation has been demonstrated over a 10-cm channel. Acceleration rates corresponding to beam-head electric fields in the range of 0.1 to 1.0 MV/cm have been demonstrated.[146]

The second technique being investigated for the controlled collective acceleration of protons uses a negative-energy wave train grown on the electron beam propagating in vacuum. There are two experiments currently in progress to investigate the potential of variable phase-velocity wave trains to collective acceleration. The former, which has been extensively investigated theoretically,[147] uses a slow cyclotron wave on the electron beam. The wave is to be grown using either self-excitation in a helical structure surrounding the beam, or by imposing the desired wave frequency and wave number on the beam by propagation through a series of appropriately spaced resonant loop drives. In this experiment it is planned to accelerate protons to about 30 MeV using a 3-MeV electron beam.

The second system being used for acceleration in wave trains employs a slow space-charge wave grown on the beam during its propagation through a slow-wave structure.[143,149] In this experiment, wave growth, propagation, and coherence over a meter length of drift space has been demonstrated experimentally. Wave electric fields of about 50 kV/cm have been reported without evidence of saturation. In contrast to the cyclotron wave, the space-charge wave can only propagate at zero phase velocity at low frequency and at the space-charge limiting current. Present experiments indicate that useful velocities of as low as 0.2 c can be achieved and that this might go lower still with appropriate system design. In addition to investigating the variation of the phase velocity of the wave with the ratio of the current to limiting current, a preliminary experiment has been carried out to demonstrate the variation of the wave phase velocity in a drift tube. In this experiment, the demonstration of the principle entails accelerating protons from about 20 to 25 MeV in a meter or so of drift tube. Present experiments are devoted to injecting ions into a wave-growth region to establish the effect of the ion loading on the wave growth. It would seem that a linear-induction proton accelerator would be the most likely injection source for a practical accelerator.

It should be pointed out that the latter devices will, if they are successful, generate a reasonably monoenergetic ion beam with an energy spread limited to the well depth used for ion trapping. In scaling to multi-hundred MeV systems this would correspond to ion energy spectral widths of less than 0.25%.

Finally, we observe that other groups are now addressing wave acceleration experimentally[149,150,151] and that there are efforts under way to extend ion energies into the hundred megavolt range. These efforts include attempts to stage existing accelerator systems,[152] to proposed experiments where the high-energy ions can be produced through the adiabatic compression of proton rings.[153] As stated in the introduction, work on the electron-ring accelerator is proceeding but has not been discussed in this review. It should be noted, however, that recent results have demonstrated the acceleration of nitrogen ions to about 28 MeV.[154]

CONCLUSIONS

This review has been written with the object of outlining the current status of high-power electron and ion beam generation. By virtue of the breadth of the field the account is, of necessity, somewhat cursory.

We summarize the preceding sections by noting a few of the accomplishments in this rapidly developing area:

1. Electron and ion beam generators have been constructed and run at power levels of about one terawatt.
2. Diode and accelerator technology have advanced to the point where system behavior can be fairly confidently predicted.
3. Techniques have been established for the generation of ultrashort and also for moderate-length (few-microsecond) duration beams.
4. Devices have now been built with repetition rates as high as one hundred pulses per second.
5. A substantial number of applications of high-power beams have been identified and in some cases, e.g., high-power microwave generation, have been exploited to practical conclusions. Other applications include materials testing, x-ray generation, electron and ion beam fusion, and with the use of collective acceleration such diverse areas as

electro-nuclear breeding and radio-chemistry technology may become economically accessible.

6. Collective acceleration has reached a milestone in that people are now carrying out experiments to control the ion acceleration process instead of allowing nature to control the acceleration. Basic acceleration mechanisms are qualitatively understood, and equally importantly, heavy-ion collective acceleration is developing rapidly. It is presently at a stage where output ion energies competitive with those obtainable with cyclotrons have been produced.

ACKNOWLEDGEMENTS

I am grateful to my colleagues who have sent me reprints of their published work, and hence simplified the task of preparing this report. I am especially grateful to Richard Adler, David Hammer, Jim Ivers, Edward Ott, George Providakes, Victor Serlin, and Charles Wharton for their comments on the draft of this paper.

This work has been supported in part by AFOSR, BMDATC, and NSF.

REFERENCES

1. G. Yonas, J. W. Poukey, J. R. Freeman, K. R. Prestwich, A. J. Toepfer, M. J. Clauser, and E. H. Beckner, *Proceedings of Sixth European Conference on Controlled Fusion and Plasma Physics,* (Moscow, 1973), p. 483.
2. L. I. Rudakov, A. A. Samarsky, *Proceedings of Sixth European Conference on Controlled Fusion and Plasma Physics,* (Moscow, 1973), p. 487.
3. R. N. Sudan, *Proceedings of Sixth European Conference on Controlled Fusion and Plasma Physics,* (Moscow, 1973), p. 184.
4. L. S. Levine and I. M. Vitkovitsky, *IEEE Trans. Nucl. Sci.* **NS-18**, 255 (1971).
5. F. Winterberg, *Phys. Rev. 174*, 212 (1968).
6. H. H. Fleischmann, *Phys. Today* **28**(5), 35 (1975).
7. J. A.. Nation, *Appl. Phys. Lett.* **21**, 491 (1970).
8. M. Friedman and M. Herndon, *Phys. Rev. Lett.* **28**, 210 (1972).
9. S. E. Graybill and J. R. Uglum, *J. Appl. Phys.* **41**, 236 (1970).
10. J. Rander, B. Ecker, G. Yonas, and D. J. Drickey, *Phys. Rev. Lett.* **24**, 283 (1970).
11. V.I. Veksler, *Proceedings of CERN Symposium on High Energy Acceleration and Ion Physics,* (1956), Vol. I, p. 80.
12. T. H. Martin, *Proceedings of the International Pulsed Power Conference,* (Lubbock, Texas, 1976), ID1-1.
13. J. H. Nuckolls, *ERDA Summer Study of Heavy Ions for Inertial Fusion,* LBL-5543, p. 1, (1976).
14. N. C. Christofilos, *Proceedings of the 2nd United Nations International Conference on the Peaceful Uses of Atomic Energy,* **32**, 279 (1958).
15. L. S. Bogdankevitch, A. A. Rukhadze, *Soviet Phys. Uspekhi* **14**, 163 (1971).
16. J. A. Nation and M. E. Read, *Appl. Phys Lett.* **23**, 429 (1973).
17. M. E. Read and J. A. Nation, *J. Plasma Phys.* **13**, 127 (1975).
18. T. H. Martin, J. P. VanDevender, D. L. Johnson, D. H. McDaniel, and M. Aker, *Proceedings of the International Topical Conference on E-Beam Research and Technology,* (Albuquerque, New Mexico, 1975), p. 450.
19. B. Bernstein and I. Smith, *IEEE Trans. Nucl. Sci.* **NS-18**, 294 (1971).
20. R. A. Fitch and V. T. S. Howell, *Proceedings IEE,* (1964), Vol. III, p. 4.
21. T. H. Martin and R. S. Clark, *Rev. Sci. Instrum.* **47**, 460 (1976).
22. S. P. Bugaev, G. M. Kassirov, B. M. Kovalchuk, and G. A. Mesyats, *Zh. Eksp. Teor. Fiz. Pis'ma Red.* **18**(2), 92 (1973).
23. A. D. Blumlein, U.S. Patent No. 2,465,840 (March 29, 1948).
24. W. T. Link, *IEEE Trans. Nucl. Sci.* **NS-14**, 777 (1967).
25. S. E. Graybill and S. V. Nablo, *IEEE Trans. Nucl. Sci.* **NS-14**, 782 (1967).
26. K. R. Prestwich, *IEEE Trans. Nucl. Sci.* **NS-18**, 493 (1971).
27. T. H. Martin, *IEEE Trans. Nucl. Sci.* **NS-16**(3), 59 (1969).
28. F. M. Charbonnier, J. P. Barbour, J. L. Brewster, W. P. Dyke, and F. J. Grundhauser, *IEEE Trans. Nucl. Sci.* **NS-14**, 789 (1967).
29. J. D. Shipman, *IEEE Trans. Nucl. Sci.* **NS-18**, 294 (1971).
30. T. H. Martin, *IEEE Trans. Nucl. Sci.* **NS-22**, 289 (1975).
31. R. K. Parker, M. Ury, *IEEE Trans. Nucl. Sci.* **NS-22**, 983, (1975).
32. L. N. Kazansky, *Atomaya Energia* **42**(2), 113 (1977).
33. E. A. Abramyan, B. A. Altercop, and G. D. Kuleshov, *Proceedings of the Second International Topical Conference on High Power Electron and Ion Beam Research and Technology,* (Ithaca, New York, 1977), Vol. II, p. 743.
34. B. A. Demidov, M. V. Ivkin, V. A. Petrov, E. A. Smirnova, and S. P. Fanchenko, *Proceedings of the Second International Topical Conference on High Power Electron and Ion Beam Research and Technology,* (Ithaca, New York, 1977), Vol. II, p. 771.
35. J. C. Martin, *Internal Report SSWA/JCM/704/49,* AWRE, Aldermaston, England (1970).
36. J. P. VanDevender and T. H. Martin, *IEEE Trans. Nucl. Sci.* **NS-22**, 979 (1975).
37. *High Voltage Technology,* L. L. Alston, Ed., Oxford University Press (1968).
38. E. I. Baranchikov, A. V. Gordeev, V. D. Korolev, and V. P. Smirnov, *Proceedings of the Second International Topical Conference on High Power Electron and Ion Beam Research and Technology,* (Ithaca, New York, 1977), Vol. I, p. 3.
39. M. S. DiCapua, D. Pellinen, and P. D. Champney, *Proceedings of the Second International Topical Conference on High Power Electron and Ion Beam Research and Technology,* (Ithaca, New York, 1977), Vol. II, p. 781.

40. D. H. McDaniel, J. W. Poukey, K. D. Bergeron, J. P. VanDevender, and D. L. Johnson, *Proceedings of the Second International Topical Conference on High Power Electron and Ion Beam Research and Technology,* (Ithaca, New York,1977), Vol. II, p. 819.
41. A. A. Kolomensky, *Pis'ma JTP* **3**, 775 (1977).
42. R. K. Parker, R. E. Anderson, C. U. Duncan, *J. Appl. Phys.* **45**, 2463 (1976).
43. J. J. Clark, M. Ury, M. L. Andrews, D. A. Hammer, and S. Linke, *Record of the 10th Symposium on Electron, Ion, and Laser Beam Technology,* San Francisco Press, (1969), p. 117.
44. P. A. Miller, J. W. Poukey, and T. P. Wright, *Phys. Rev. Lett.* **35**, 940 (1975).
45. P. Diament, *Phys. Rev. Lett.* **37**, 168 (1976).
46. M. Reiser, *Phys. Fluids* **20**, 477 (1977).
47. M. Friedman and M. Ury, *Rev. Sci. Instrum.* **41**, 1334 (1970).
48. F. Friedlander, R. Hechtel, H. Jory, and C. Mosher, *Varian Associates Report* DASA-2173 (1968), unpublished.
49. G. Yonas, J. W. Poukey, K. R. Prestwich, J. R. Freeman, A. J. Toepfer, and M. J. Clauser, *Nucl. Fusion* **14**, 731 (1974).
50. D. dePackh, *NRL Radiation Progress Report* 5 (1968), unpublished; D. dePackh, *NRL Radiation Progress Report* 17 (1969), unpublished.
51. J. M. Creedon, *J. Appl. Phys.* **46**, 2946 (1975).
52. S. A. Goldstein, R. C. Davidson, J. G. Siambis, and R. Lee, *Phys. Rev. Lett.* **33**, 1471 (1974).
53. J. Poukey, J. W. Freeman, and G. Yonas, *J. Vac. Sci. Technol.* **10**, 954 (1973).
54. J. Poukey and A. J. Toepfer, *Phys. Fluids* **17**, 1582 (1974).
55. D. L. Morrow, J. D. Phillips, R. M. Stringfield, W. O. Doggett, W. H. Bennett, *Appl. Phys. Lett.* **19**, 444 (1971).
56. W. C. Condit, D. O. Trimble, G. A. Metzger, D. G. Pellinen, S. Heurlin, and P. Creely, *Phys. Rev. Lett.* **30**, 123 (1973).
57. L. P. Bradley, G. W. Kuswa, *Phys. Rev. Lett.* **29**, 1441 (1972).
58. M. DiCapua, J. Creedon, and R. Huff, *J. Appl. Phys.* **47**, 1887 (1976).
59. A. Blaugrund, G. Cooperstein, and S. Goldstein, *Phys. Fluids* **20**, 1185 (1977).
60. G. Cooperstein and J. J. Condon, *J. Appl. Phys.* **46**, 1535 (1975).
61. A. E. Blaugrund and G. Cooperstein, *Phys. Rev. Lett.* **34**, 461 (1975).
62. J. W. Poukey, *Appl. Phys. Lett.* **26**, 145 (1975).
63. J. W. Poukey, *J. Vac. Sci. Technol.* **12**, 1214 (1975).
64. S. A. Goldstein and R. Lee, *Phys. Rev. Lett.* **35**, **1079** (1975).
65. A. E. Blaugrund, G. Cooperstein, and S. Goldstein, *Proceedings of the International Conference on Electron Beam Research and Technology,* (Albuquerque, New Mexico, 1975), p. 223.
66. J. Poukey, *Appl. Phys. Lett.* **26**, 145 (1975).
67. S. Humphries, J. J. Lee, and R. N. Sudan, *Appl. Phys. Lett.* **25**, 20 (1976).
68. S. Humphries, J. J. Lee, and R. N. Sudan, *J. Appl. Phys.* **46**, 187 (1975).
69. S. Humphries, R. N. Sudan, and W. Condit, *Appl. Phys. Lett.* **26**, 667 (1975).
70. J. Golden, C. A. Kapetanakos, S. J. Marsh, and S. Stephanakis, *Phys. Rev. Lett.* **38**, 130 (1977).
71. C. A. Kapetankos, J. Golden, W. M. Black, *Phys. Rev. Lett.* **37**, 1236 (1977).
72. D. S. Prono, J. W. Shearer, and R. J. Briggs, *Phys. Rev. Lett.* **37**, 21 (1976).
73. D. S. Prono, J. M. Creedon, I. Smith, and N. Bergstrom, *J. Appl. Phys.* **46**, 3310 (1975).
74. H. H. Fleischmann, *Proceedings of Conference on Electrostatic and Electromagnetic Confinement of Plasmas and Phenomenology of Relativistic Electron Beams,* (N.Y. Academy of Science, 1974), p. 472.
75. H. H. Fleischmann and T. Kammash, *Nucl. Fusion* **15**, 1143 (1975).
76. C. A. Kapetanakos and R. Parker, *Appl. Phys. Lett.* **26**, 284 (1975).
77. T. Antonsen and E. Ott, *Phys Fluids* **19**, 52 (1976).
78. T. Antonsen and E. Ott, *Appl. Phys. Lett.* **28**, 424 (1976).
79. J. M. Creedon, I. D. Smith, and D. S. Prono, *Phys. Rev. Lett.* **35**, 91 (1975).
80. J. Golden, C. A. Kapetanakos, R. Lee, and S. Goldstein, *Proceedings of the International Topical Conference on Electron Beam Research and Technology,* (Albuquerque, New Mexico, 1975), p. 635.
81. J. A. Pasour, R. A. Mahaffey, J. Golden, and C. A. Kapetanakos, *Phys. Rev. Lett.* **40**, 448 (1978).
82. P. Drieke, C. Eichenberger, S. Humphries, and R. N. Sudan, *J Appl. Phys,* **47**, 85 (1976).
83. S. Humphries, R. N. Sudan, and L. Wiley, *J. Appl. Phys.* **47**, 2382 (1976).
84. T. J. Orzechowski and G. Bekefi, *Phys. Fluids* **19**, 43 (1976).
85. S. C. Luckhardt and H. H. Fleischmann, *Appl. Phys. Lett.* **30**, 192 (1977).
86. S. Luckhardt, H. H. Fleischmann, and R. Kribel, to be pulished, see also, *Bull. Am. Phys. Soc.* **23**(7), 816 (1978).
87. R. N. Sudan and R. V. Lovelace, *Phys. Rev. Lett.* **31**, 1174 (1973).
88. R. V. Lovelace and E. Ott, *Phys. Fluids* **17**, 1263 (1974).
89. A. Ron, A. A. Mondelli, and N. Rostoker, *IEEE Trans. Plasma Sci.* **PS-1**, 85 (1973).
90. K. Bergeron and J. Poukey, *Appl. Phys. Lett.* **27**, 58 (1975).
91. K. Bergeron, *Phys. Fluids* **20**, 688 (1977).
92. G. Kuswa, S. Humphries, D. Johnson, R. Leeper, and J. Freeman, *Proceedings of the Second International Topical Conference on High Power Electron and Ion Beam Research and Technology,* (Ithaca, New York, 1977), Vol. I, p. 99.
93. M. Greenspan, S. Humphries, J. Maenchen, and R. N. Sudan, *Phys. Rev. Lett.* **39**, 24 (1977).
94. J. Creedon, *J. Appl. Phys.* **48**, 1070 (1977).
95. K. Bergeron, *J. Appl. Phys.* **48**, 3065 (1977).
96. J. Poukey and K. Bergeron, *Appl. Phys. Lett.* **32**, 8 (1978).
97. I. Smith, P. Champney, and J. Creedon, *Proceedings of the International IEEE Pulsed Power Conference,* (New York, 1976), Vol. II, C-8.
98. M. DiCapua, D. Pellinen, P. Champney, and D. McDaniel, *Proceedings of the Second International Topical Conference on High Power Electron and Ion Beam Research and Technology,* (Ithaca, New York, 1977), Vol. II, p. 781.
99. D. McDaniel, J. Poukey, K. Bergeron, J. VanDevender,

and D. Johnson, *Proceedings of the Second International Topical Conference on High Power Electron and Ion Beam Research and Technology,* (Ithaca, New York, 1977), Vol. II, p. 819.
100. J. Poukey, J. Freeman, M. Clauser, and G. Yonas, *Phys. Rev. Lett.* **35**, 1806 (1975).
101. J. Poukey, *J. Vac. Sci. Technol.* **12**, 1214 (1975).
102. S. Stephanakis, D. Mosher, G. Cooperstein, J. Boller, J. Golden, and S. Goldstein, *Phys. Rev. Lett.* **37**, 1543 (1976).
103. P. Gilad and Z. Zinamon, *Phys. Rev. Lett.* **37**, 697 (1976).
104. P. Gilad, S. Miller, and Z. Zinamon, *Appl. Phys. Lett.* **31**, 151 (1977).
105. S. Miller and Z. Zinamon, *Phys. Rev. Lett.* **36**, 1303 (1976).
106. D. Mosher, G. Cooperstein, S. J. Stephanakis, S. Goldstein, D. Colombant, and R. Lee, *Proceedings of the Second International Topical Conference on High Power Electron and Ion Beam Research and Technology,* (Ithaca, New York, 1977), Vol. I, p. 257.
107. P. Gilad, Z. Kaplan, S. Miller, J. Wachtel, N. Zeiberg, and Z. Zinamon, *Proceedings of the Second International Topical Conference on High Power Electron and Ion Beam Research and Technology,* (Ithaca, New York, 1977), Vol. I, p. 219.
108. D. Swain, S. Goldstein, L. Mix, J. Kelley, G. Hadley, *J. Appl. Phys.* **48**, 1085 (1977).
109. R. Adler and J. Nation, unpublished.
110. M. Read and J. Nation, *J. Appl. Phys* **47**, 5236 (1976).
111. G. Yonas, K. Prestwich, J. Poukey, and J. Freeman, *Phys. Rev. Lett.* **30**, 164 (1973).
112. G. J. Rohwein, M. Buttram, and T. Prestwich, *Proceedings of the Second International Topical Conference on High Power Electron and Ion Beam Research and Technology,* (Ithaca, New York, 1977), Vol. II, p. 845.
113. R. Faltens and D. Keefe, (1970), unpublished; R. T. Avery et al., *Proceedings of the IEEE Accelerator Conference,* (1971), **NS-18**, p. 479.
114. J. Beal, N. Christofilos, and R. Hester, *Proceedings of the IEEE Accelerator Conference,* (1969), p. 294.
115. J. F. Leiss, *Proceedings of the Proton Linac Conference,* (1972), p. 197.
116. R. Hester, L. Reginato, A. Chesterman, and A. Faltens, to be presented at the IEEE Accelerator Conference, (San Francisco, 1979).
117. A. I. Pavlovskij, V. S. Bosamykin, G. Kuleshov, A. Gerasimov, V. Tenanakin, and A. Klement'ev, *Dokl. Akad. Nauk SSSR* **222**, 817 (1975).
118. T. Lockner, J. Siambis, and M. Friedman, *Proceedings of the Second International Topical Conference on High Power Electron and Ion Beam Research and Technology,* (Ithaca, New York, 1977), Vol. II, p. 585.
119. D. Eccleshall and J. Temperley, *J. Appl. Phys.* **49**, 3669 (1978).
120. A. Faltens and D. Keefe, *LBL Report* 6453 (1977).
121. S. Humphries, *J. Appl. Phys.* **49**, 501 (1978).
122. F. Winterberg, *Z. Physik A.* **280**, 359 (1977).
123. G. Yonas, *Particle Accelerators* **5**, 81 (1973).
124. M. Rabinovich and V. N. Tsytovich, *Particle Accelerators* **5**, 99 (1973).
125. A. Kolomensky, *Particle Accelerators* **5**, 73 (1973).
126. C. Olsen, *Particle Accelerators* **6**, 107 (1974).
127. S. Putnam, Presented at 2nd Symposium on Collective Methods of Acceleration, (Dubna, USSR, 1976), *Physics International Report* PIIR-7-76.
128. Ya. B. Fainberg, *Particle Accelerators* **6**, 95 (1976).
129. C. Olsen, *Sov. J. Plasma Phys.* **3**(3), 259 (1978).
130. S. Graybill and J. Uglam, *J. Appl. Phys.* **41**, 236 (1970).
131. C. Olsen, *Phys. Fluids* **18**, 585 (1975); C. Olsen, *Phys. Fluids* **18**, 598 (1975).
132. J. Poukey and N. Rostoker, *Plasma Phys.* **13**, 897 (1971).
133. R. Miller and D. Straw, *J. Appl. Phys.* **47**, 1897 (1976).
134. S. Putnam, *Phys. Rev. Lett.* **25**, 1129 (1970).
135. V. N. Tsytovich and K. V. Khodataev, *Comments on Plasma Physics and Controlled Fusion* **3**, 71 (1977).
136. B. Ecker and S. Putnam, *IEEE Trans. Nucl. Sci.* **NS-24**, 1665 (1977).
137. J. S. Luce, *Annals of the N.Y. Acad. of Sci.* **25**, 2171 (1975).
138. W. Destler and H. Kim, *Proceedings of the Second International Topical Conference on High Power Electron and Ion Beam Research and Technology,* (Ithaca, New York, 1977), Vol. II, p. 521.
139. R. Adler and J. Nation, *Cornell University Laboratory of Plasma Studies Report* 225 (1978), to be published.
140. A. Greenwald and R. Little, *Proceedings of the Second International Topical Conference on High Power Electron and Ion Beam Research and Technology,* (Ithaca, New York, 1977), Vol. II, p. 553.
141. J. A. Pasour, R. Parker, W. Doggett, D. Pershing, and R. Gullickson, *Proceedings of the Second International Topical Conference on High Power Electron and Ion Beam Reseach and Technology,* (Ithaca, New York, 1977), Vol. II, p. 623.
142. R. Adler, G. Gammel, J. Nation, G. Providakes, and R. Williams, *Proceedings of the Third International Conference on Collective Methods of Acceleration,* (Laguna, Beach, 1978), to be published. Also, *Cornell University LPS Report* 248 (1978).
143. C. W. Roberson, S. Eckhouse, A. Fisher, S. Robertson, and N. Rostoker, *Phys. Rev. Lett.* **36**, 1457 (1976).
144. S. Eckhouse, A. Fisher, R. Mako, C. W. Roberson, S. Robertson, and N. Rostoker, *Proceedings of the Second International Conference on Collective Methods of Acceleration,* (Dubna, 1976), p. 9i.
145. W. Destler, H. Kim, G. Zorn, and R. Hoeberling, presented at Third International Conference on Collective Methods of Acceleration, (Laguna Beach, 1978), to be published.
146. C. Olsen, presented at Third International Conference on Collective Methods of Acceleration, (Laguna Beach, 1978), to be published.
147. M. Sloan and W. Drummond, *Phys. Rev. Lett.* **31**, 1234 (1973).
148. R. Adler, G. Gammel, J. A. Nation, M. E. Read, R. Williams, P. Sprangle, and A. Drobot, in *Proceedings of the Second International Topical Conference on High Power Electron and Ion Beam Research and Technology,* (Ithaca, New York, 1977), Vol. II, p. 509.
149. P. Sprangle, A. Drobot, and W. Manheimer, *Phys. Rev. Lett.* **36**, 1180 (1976).
150. S. Yadavelli, *Appl. Phys. Lett.* **29**, 272 (1976).
151. P. Sprangle, private communication.
152. J. Adamski, P. Wei, J. Beymer, R. Guay, and R. Copeland, in *Proceedings of the Second International Topical Conference on High Power Electron and Ion Beam Research and Technology,* (Ithaca, New York, 1977), Vol. II, p. 497.
153. H. H. Fleischmann, *Proceedings of Conference on Elec-*

trostatic and Electromagnetic Confinement of Plasma's and Phenomenology of Relativistic Electron Beams, (N.Y. Acad. Sci., 1974), p. 472.

154. V. P. Sarantsev, *Proceedings of the Third International Conference on Collective Methods of Acceleration,* (Laguna Beach, 1978), to be published.